2014

MULTISCALE MODELING OF THE MINE VENTILATION SYSTEM AND FLOW THROUGH THE GOB

William Chad Wedding
University of Kentucky, chad.wedding@uky.edu
Digital Object Identifier: https://doi.org/10.13023/etd.2014.001

STUDENT AGREEMENT:

I represent that my thesis or dissertation and abstract are my original work. Proper attribution has been given to all outside sources. I understand that I am solely responsible for obtaining any needed copyright permissions. I have obtained needed written permission statement(s) from the owner(s) of each third-party copyrighted matter to be included in my work, allowing electronic distribution (if such use is not permitted by the fair use doctrine) which will be submitted to UKnowledge as Additional File.

I hereby grant to The University of Kentucky and its agents the irrevocable, non-exclusive, and royalty-free license to archive and make accessible my work in whole or in part in all forms of media, now or hereafter known. I agree that the document mentioned above may be made available immediately for worldwide access unless an embargo applies.

I retain all other ownership rights to the copyright of my work. I also retain the right to use in future works (such as articles or books) all or part of my work. I understand that I am free to register the copyright to my work.

REVIEW, APPROVAL AND ACCEPTANCE

The document mentioned above has been reviewed and accepted by the student's advisor, on behalf of the advisory committee, and by the Director of Graduate Studies (DGS), on behalf of the program; we verify that this is the final, approved version of the student's thesis including all changes required by the advisory committee. The undersigned agree to abide by the statements above.

William Chad Wedding, Student

Dr. Andrzej M. Wala, Major Professor

Dr. Thomas Novak, Director of Graduate Studies

MULTISCALE MODELING OF THE MINE VENTILATION SYSTEM AND FLOW THROUGH THE GOB

DISSERTATION

A dissertation submitted in partial fulfillment of the
Requirements for the degree of Doctor of Philosophy in the
College of Engineering
At the University of Kentucky

By

William Chad Wedding

Lexington, Kentucky

Co-directors: Dr. Andrzej M. Wala, Professor of Mining Engineering
Co-directors: Dr. Alexandre Martin, Assistant Professor of Mechanical Engineering

Lexington, Kentucky

ABSTRACT OF DISSERTATION

MULTISCALE MODELING OF THE MINE VENTILATION SYSTEM AND FLOW THROUGH THE GOB

The following dissertation introduces the hazard of methane buildup in the gob zone, a caved region behind a retreating longwall face. This region serves as a reservoir for methane that can bleed into the mine workings. As this methane mixes with air delivered to the longwall panel, explosive concentrations of methane will be reached.

Computational fluid dynamics (CFD) is one of the many approaches to study the gob environment. Several studies in the past have researched this topic and a general approach has been developed that addresses much of the complexity of the problem. The topic of research herein presents an improvement to the method developed by others. This dissertation details a multi-scale approach that includes the entire mine ventilation network in the computational domain. This allows one to describe these transient, difficult to describe boundaries. The gob region was represented in a conventional CFD model using techniques consistent with past efforts. The boundary conditions, however, were cross coupled with a transient network model of the balance of the ventilation airways. This allows the simulation of complex, time dependent boundary conditions for the model of the gob, including the influence of the mine ventilation system (MVS).

The scenario modeled in this dissertation was a property in south western Pennsylvania, working in the Pittsburgh seam. A calibrated ventilation model was available as a result of a ventilation survey and tracer gas study conducted by NIOSH. The permeability distribution within the gob was based upon FLAC3d modeling results drawn from the literature. Using the multi-scale approach, a total of 22 kilometers of entryway were included in the computational domain, in addition to the three dimensional model of the gob.

The steady state solution to the problem, modeling using this multi-scale approach, was validated against the results from the calibrated ventilation model. Close agreement

between the two models was observed, with an average percent difference of less than two percent observed at points scattered throughout the MVS. Transient scenarios, including roof falls at key points in the MVS, were modeling to illustrate the impact on the gob environment.

KEYWORDS: Multi-Scale CFD, Gob Environment, Longwall Mining, Methane Mitigation, Explosive Contours

William Chad Wedding

Student's Signature

4/23/2014

Date

MULTISCALE MODELING OF THE MINE VENTILATION SYSTEM AND FLOW THROUGH THE GOB

By

William Chad Wedding

Dr. Andrzej M. Wala

Co-Directors of Dissertation

Dr. Alexandre Martin

Co-Directors of Dissertation

Dr. Thomas Novak

Director of Graduate Studies

4/23/2014

Date

DEDICATION

This dissertation is dedicated to my wife Kathy, and to my family and friends. I've been very fortunate to have received their love, support, and sacrifice while I pursued the opportunity before me. I know my wife will always be there for me.

Finally, I like to give special thanks to my late Grandfather Gough, who set a wonderful example for me to follow.

ACKNOWLEDGEMENT

I would like to offer my humble gratitude to Dr. Andzrej Wala for his wisdom and guidance through this process. I also extend my thanks to Dr. Alexandre Martin, Dr. Thomas Novak, and Dr. Braden Lusk for their time and energy for this research effort.

I would like to acknowledge the researchers at NIOSH (The National Institute for Occupational Safety and Health) including Lilly Zhou, Gerrit Goodman, and Jack Trackemas for sponsoring this research effort.

I sincerely appreciate the contributions of those both within and outside the department. This includes Dr. Rick Honaker, Dr. Kyle Perry, Dr. Saito, Dr. Jhon Silva, Dr. Joe Sottile, and Dr. Kot Unrug. Their guidance was invaluable. I'd like to give thanks for the wonderful staff members for their help, including Megan Doyle, Kathy Kotora, and Ed Thompson. I offer my thanks for my fellow graduate students on the project, Sampurna Arya and Todor Petrov, and all the other graduate students in the department. Finally, I'd like to thank my wife, Kathy, for her unwavering support.

TABLE OF CONTENTS

LIST OF TABLES

LIST OF FIGURES

1 Introduction

1.1 Historical Significance of Problem

Miners have dealt with the hazard of methane liberated into the workings of coal mines for a long time. Early accounts discuss the dangers of firedamp, as it is known in 19th century English coal mines. A complete understanding of the dangers of methane buildup was not known at this time, as exemplified by the practice of sending miners into the workings with long torches to burn away the accumulation of the day. Figure 1-1 shows an artist rendering of the role of a "penitent", the miner responsible for burning away the methane wearing a heavy protective robe, so named for his resemblance to a monk. They failed to comprehend the hazardous nature of methane buildup which becomes explosive in air when the concentration falls between five and fifteen percent. As a result, the mining industry, and especially coal mining, has endured a tragic history and maintains a reputation for being a dangerous profession.

Figure 1-1 Artist rendering of a 19th century coal miner igniting accumulated firedamp, originally published in Mines and Miners by L. Simonin, 1868 (Source: Terry 2012)

As safety practices in coal mines matured, new technologies and protocols were implemented to deal with methane explosions. These included split ventilation systems, safety fuse, and the Davy lamp. Modern mining techniques, with well-designed ventilation systems and permissible electrical equipment, greatly reduce the potential for methane explosions. The improvements are evident in the industry statistics, where fires and explosions attributable to methane in underground coal mines have not been the leading cause of injury and fatality, on average (MSHA 2012a), in the United States. Encounters with powered haulage, mobile equipment, or rock falls are leading hazards in the mining environment. Coal mine fatality statistics can be seen in Figure 1-2, comparing methane with powered haulage and other sources of hazard. Methane explosions remain a serious concern because they still occur at irregular intervals. When they occur, they usually cause multiple fatalities and are devastating to the community and the company responsible for the safety of its workers.

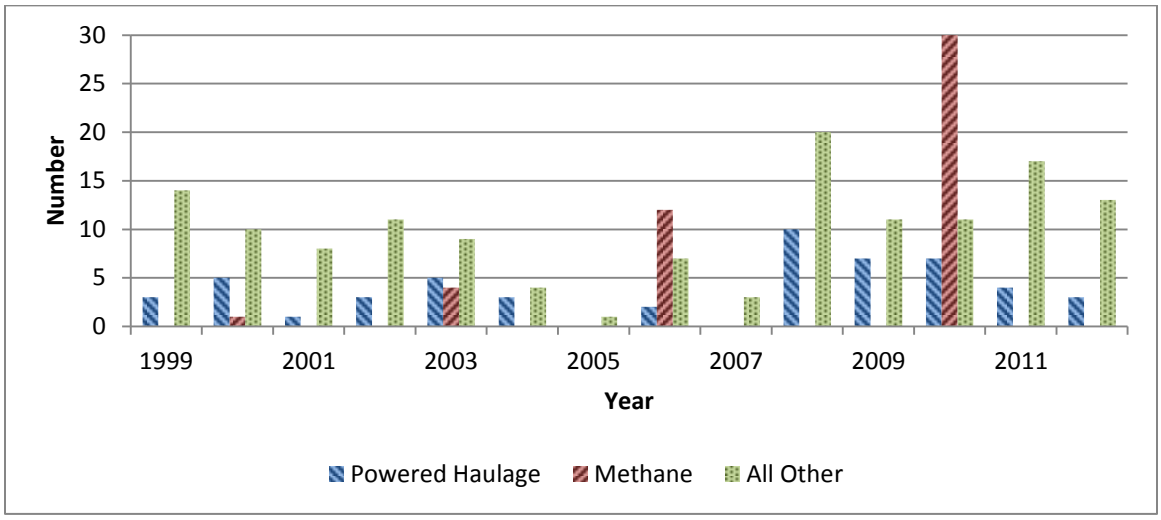

Figure 1-2 United States coal mine fatality statistics by type since 1999 (Source: MSHA Fatality Statistics 2012)

There have been dramatic examples of coal mine explosions in recent history. The Upper Big Branch Mine in Rayleigh County, West Virginia, was the most recent in US history. In total, 29 miners were killed in an explosion on April 5, 2010, making it the most devastating mine disaster since 1970 (Bluestein, Smith 2010). The probable cause

was a methane ignition that transitioned to a coal dust explosion, killing all but two miners underground on that day (MSHA, 2012b). The Sago Mine disaster occurred in January of 2006, which resulted in 12 deaths (MSHA, 2012a). The Darby Mine explosion followed in May of 2006, a loss of 5 more miners (MSHA, 2012a). Additional examples can be found around the globe in all the coal producing regions. On February 22, 2009, a methane explosion at the Tunlan coal mine in the Shanxi province of China killed 74 people and injured many more (Yinan and Ke, 2009). Russia experienced its largest coal mine disaster at the Ulyanovsk Mine in the Kemerovo region. A methane explosion killed more than 100 people on March 19, 2007 (BBC, 2007). Poland suffered a coal mine methane explosion on September 18, 2009 at the Wujek Slask Mine that killed 17 miners (Cienski, 2009). The Bhatdih Coal Mine in eastern India experienced an explosion that claimed 54 lives. It occurred on September 8, 2006 (Ravi, 2006).

1.2 Research Goals

More research is needed to develop a better understanding of the causes of these types of mine disasters. Computational fluid dynamics, as a tool to improve safety in mining, has progressed rapidly, but the challenges of modeling the mine environment are not insubstantial. Ren and Balusu discussed this topic in 2005. Common areas of research include the control of methane and spontaneous heating in the gob area, gob inertisation strategies, and dust and method control at the working face. The quality of this work has been improved by adopting a multi-scale approach from other disciplines. This multi-scale approach allows one to include the entire mine network within the computational domain, with reduced complexity at areas removed from the immediate area of interest.

The multi-scale approach to CFD modeling provides a practical means to include the entire mine ventilation system (MVS) and the gob region in the computational domain. This leads to improved understanding of the gob environment and its influence on mine workings, specifically under transient conditions.

The project was broken down into five key tasks for the development of a multi-scale model of the entire system. A brief description of these tasks follows.

1.2.1 Network Model of the MVS

The first task was the development of the network model of the mine ventilation system. The one-dimensional network model imports the network topology, geometry, and initial conditions from VnetPC, during the initial creation of the network. VnetPC is one of the industry leading network simulation tools that employs the Hardy Cross technique to solve network problems. The import procedure was developed to rapidly incorporate the ventilation models that are maintained by mine operators. Once imported, the 1D model of the MVS network was solved using a finite difference approach with explicit time marching

1.2.2 Integration of Network Model with Cradle CFD

With the network model finished, the coupling routine was developed in Cradle CFD. A user defined function was written to pass data back and forth from the one-dimensional network to the three-dimensional domain. Pressure boundary conditions are asserted upon the three-dimensional domain where it interfaces the network. Inflow conditions for species concentration, turbulence and turbulence energy are also defined. Pressure and species concentration are determined from the network model, while empirical relationships are used to approximate the turbulent kinetic energy k and turbulent dissipation rate ε. The mass flow through the boundaries of the three-dimensional domain along with the species concentration establishes the boundary conditions for the one-dimensional network.

1.2.3 Gob Modeling

User define functions were required to develop the model of the influence of the gob. The porous media model was used to determine the pressure drop through the gob as per Darcy's law. During the development two models of varying complexity were used. The first was a zoned model which included an inner and outer region; regions with uniform permeability representing an average value experienced in the region. The

second was a continuous anisotropic model based upon a surface fit of the calculated permeability distribution within the whole gob zone. This followed the technique developed by Esterhuizen and Karacan (2007), and improved by Wachel(2012). Porosity was utilized to calculate the permeability using the well-known Kozeny-Carman equation.

1.2.4 Steady State Analysis of Gob and MVS

Modeling the gob environment began with a steady state scenario. The purpose was to develop a validated model of the gob environment with its influence on the ventilation network. Ventilation surveys of the mine site were needed to provide the necessary validation data. This was accomplished with a detailed pressure and quantity surveys, performed during the course of a tracer gas study at the mine by researchers at NIOSH. The significant result of the study to this effort was a validated network model which included the influence of the gob.

The results from the tracer gas study were combined with the FLAC3D modeling results to build the multi-scale model of the gob region along with the ventilation network. It was then used as the basis for a series of sensitivity studies to garner additional insight into the behavior of the gob environment's response to model parameters. Sensitivity studies included the following.

- *Mesh Independence:* Mesh independence was tested to ensure the solution to the problem was free from error due the chosen mesh size.
- *Turbulence Modeling:* A total of 13 turbulence models are available for use in Cradle SC/Tetra, including Standard $k-\varepsilon$, and its extensions such as RNG $k-\varepsilon$, MP $k-\varepsilon$, and Realizable $k-\varepsilon$, a number of Linear Low Reynolds Number models, and others. The applicability of six of these models to the problem was investigated.
- *Gob Permeability:* The results of the gob permeability modeling had a large impact on the gob environment. The sensitivity of the model to changes in permeability was investigated.

- *Coupling Region Count:* The number of coupled regions in the real world scenario differs from the presented MSVM. Along the longwall face and the start up room, there was a nearly continuous connection between the two regions in reality. Along the gateroad entries, there are connections at every crosscut. These connections were simplified to a limited number of connections between the network model and the CFD domain. The number of coupling regions was varied to investigate the impact on the results of the MSVM calculation.
- *Methane Emissions:* The methane emission rate into the gob region was based upon measurements taken along with the experience of the mine operator at the mine site. As a significant portion of the methane was released by the action of the longwall shearer, methane was introduced into the network model to simulate this influence. Variations in this release rate and location were tested to see the impact upon the conditions at the face and in the bleeder entries.

The sensitivity studies provided guidance to select a baseline model for comparison to the transient models. This incorporated the most appropriate choices for modeling assumptions, such as mesh size and turbulence model.

1.2.5 Transient Analysis of Gob and MVS

With the completion of the steady state modeling, the project then progressed to exploring a transient scenario that was thought to influence the gob environment, longwall face, and entries. Changes to the validated multi-scale model were implemented in the 1D domain to mimic scenarios that mine operators may face. The goal of this task was to provide recommendations to industry for ways to they can guard against these potential hazards. The transient scenarios included the following.

- *Roof Falls:* Roof falls introduce regions of relatively high resistance in the mine ventilation network. This caused changes in the pressure and flow distribution in the mine with an accompanying change to the flow through the gob.

- *Bleeder Fan Malfunction:* This scenario included a stoppage of the bleeder fan. This resulted in a very pervasive change to the pressure and flow distribution in the mine network, and a drastic change in the flow pattern through the gob.

1.3 Organization of the Dissertation

This dissertation is composed of six chapters. The first chapter introduces the subject and its historical context. Upon establishing the need for this work, it lists the research approach used to advance the understanding of this problem, along with specific goals.

Chapter two includes a survey of the literature concerning gob modeling and the mine ventilation network. The background information pertaining to the problem of methane within the coal seam is covered, including the influence of mining and subsequent release of methane into the mine workings. It then summarizes past and present gob modeling efforts. It concludes with an introduction to the multi-scale technique that is practiced in other areas of research.

Numerical modeling of the problem is detailed in chapter three. This covers the concept behind computational fluid dynamics, such as the principle governing equations, turbulence modeling, and the idea of control volume discretization. This continues with the formulation of the 1D network model, including a justification for its need and the necessary governing equations. It concludes with an overview of the user defined function developed in SC/Tetra to support this dissertation.

Chapter four describes steady state MSVM simulation of the selected longwall mine. It includes the parameters used during the modeling exercise, beginning with the parameters used for the CFD portion. This includes geometry, gob permeability parameters for two different gob models, and inflow turbulence properties. The details provided for the network portion of the MSVM are included, such as geometry and friction factors. The coupling scheme for the model is presented. The chapter also includes model sensitivity studies for grid independence, turbulence modeling, and others. Validation results against the original, calibrated VNetPC model are presented.

Details of the transient model are presented in chapter five. Three scenarios are addressed. Two are roof falls in key branches in the bleeder portion of the mine ventilation network. The MSVM model responds by moving from one equilibrium point to the next. Flow and pressure distributions are recorded in both the gob model and the network model. The final scenario is a malfunction of the bleeder fan. Flow through the bleeder shaft is allowed to come to a near halt. The pressure and flow through the network and gob were examined.

The last chapter details the conclusions drawn from this work. It highlights the novel contribution to the field of mining engineering that this work represents. Finally, it offers recommendations for future work.

2 Literature Review

2.1 Overview

The review of the literature has concentrated on three areas. The first portion is an overview in the nature of coal bed methane. This includes a look at the source of methane, as well as means to quantify the amount of methane associated with a particular mine property. Next, the influence of mining activity on the coal bed methane is discussed. This identifies the key contributors to the inflow of methane from the gob and near layers of the surrounding strata. The latter portion discusses the modeling techniques that have been employed to study this problem, along with an introduction to the multi-scale approach that was employed in this study.

2.2 Coal Bed Methane

Coal bed methane is one of the names given to the gas associated with a seam of coal. It has been referred to by a number of different names, such as coal seam gas, coal seam methane, etc. For our purposes, these are the same. It is not exclusively methane, but rather a mixture of methane, carbon dioxide, and possibly smaller fractions of ethane, nitrogen, hydrogen sulfide, and other gases (Rice, 1993). The predominant gas is methane, CH_4, whose hazard within the mining environment is now widely known.

H.F. Coward wrote about the dangers of methane accumulation behind stoppings in 1929. In this paper, he presented what came to be known as the Coward Triangle, which is a graphical representation of the explosive range of methane when mixed with air. A version of it can be seen in Figure 2-1. Methane can be found at a high concentration within the coal, sometimes approaching 100%. Methane, in concentrations between 5% and 15% when mixed with air, is explosive. The most energetic mixture is one that is stoichiometrically balanced, or 9.8% methane in air. During the process of dilution, the air and methane mixture must pass through this explosive range to the low levels prescribed by regulation and engineering prudence as shown in Figure 2-2 (Kissell, 2006). It is important that this dilution happens as quickly as possible or is contained to a region that is largely inaccessible to minimize the risk.

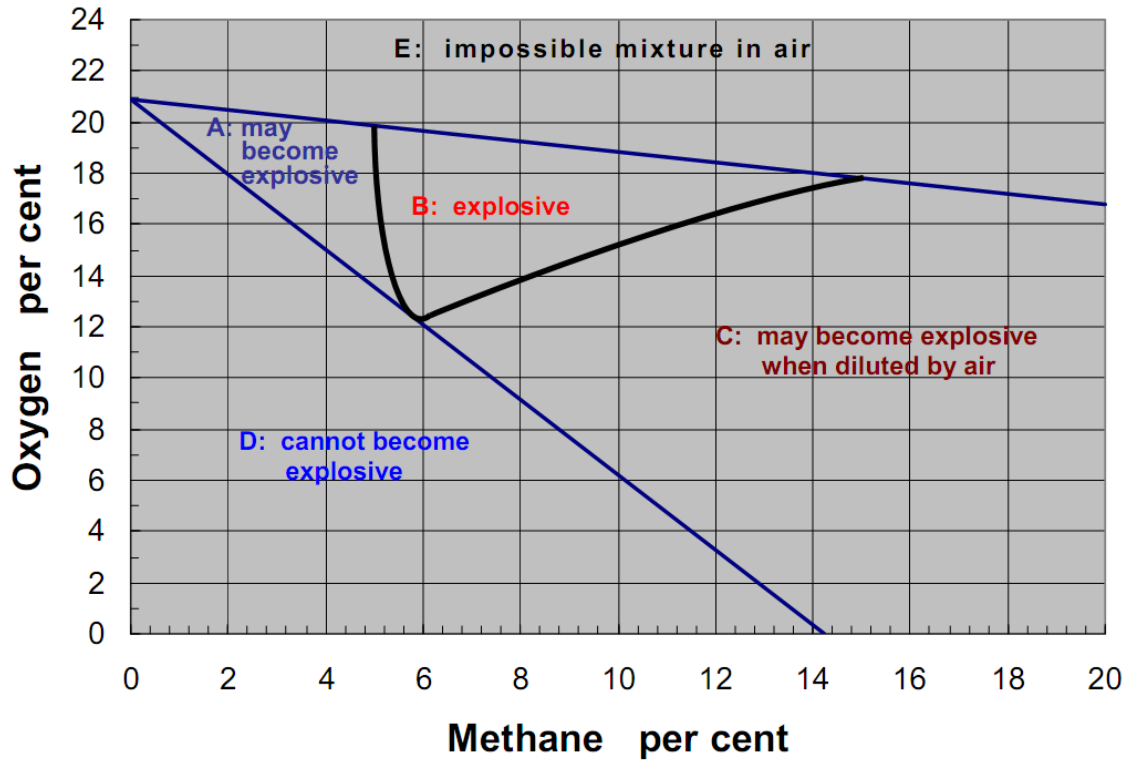

Figure 2-1 Coward Triangle for methane, carbon monoxide, and hydrogen (Adapted: McPherson, 2009)

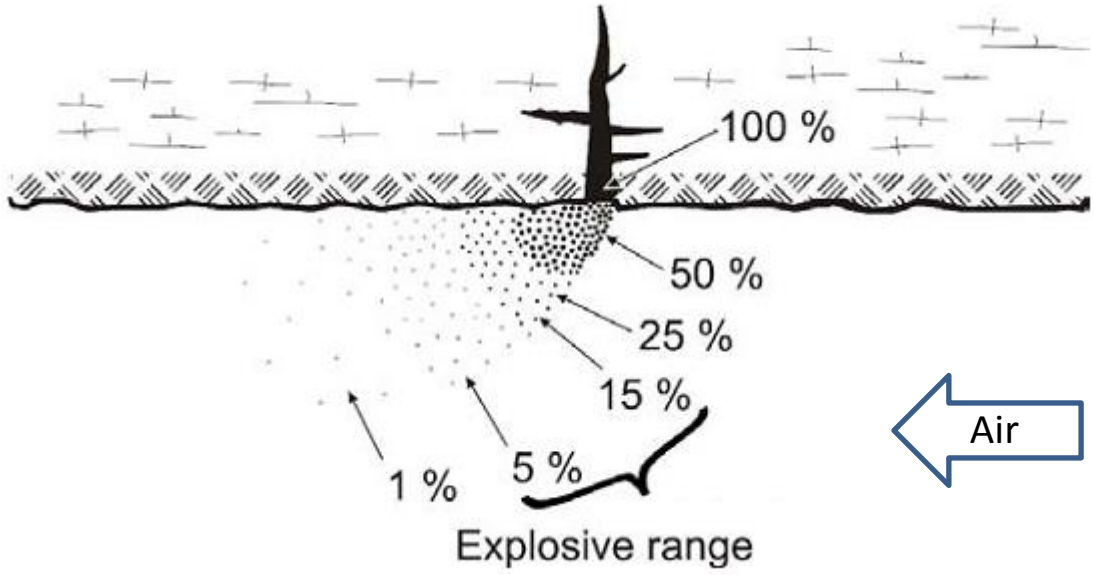

Figure 2-2 Diagram of methane inflow from a fracture and the progressive dilution due to airflow in the entry (Adapted: Kissell, 2006)

2.2.1 The Source of Coal Bed Methane

Methane within the coal bed is generated during the coalification process (Levine, 1993). This is the process by which plant material is progressively converted to coal. The progression from the early stages of coalification, peat and lignite, to later stages of coalification, anthracite, is due to geophysical and chemical processes in an irreversible process (Levine, 1993) (Rice, 1993) (Moore, 2012). A visual representation of the coalification process can be seen in Figure 2-3. From left to right are some common ranks of coal recognized by ASTM specification number D388-12 from 2012 titled "*Standard Classification of Coals by Rank*" (ASTM, 2012). A coal's rank can be determined by its fixed carbon yield, volatile matter yield, and gross calorific value. The measure of vitrinite reflectance is shown at the top, which is a favored measurement for ranking coal.

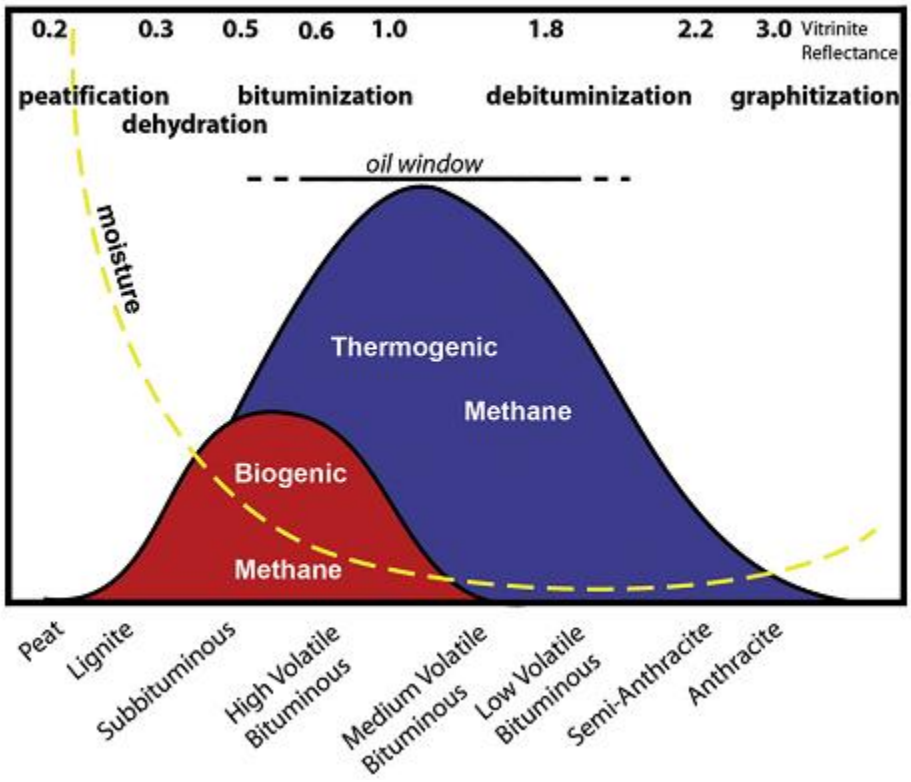

Figure 2-3 The progression of methane generation due to the coalification process and attendant increase rank of coal (Source: Moore, 2012)

The five steps that Levine used to describe the process of coalification are shown in Figure 2-3 below the vitrinite reflectance. These steps are peatification, dehydration, bituminization, debituminization, and graphitization. As the coal matures through this five step process, methane is generated in a combination of two ways, biogenesis, and thermogenesis.

During the beginning phases of coalification, nearly all of the methane generated is biogenic in nature. There are literally hundreds of taxa of microorganisms living under the ground, within the coal seams that metabolise methane (Strapoc et al., 2008). These organisms are termed methanogens and are from the bacterial and archaeal domains. These organisms, working in concert, break the low rank coal macro-molecules down into simpler components through two main pathways: fermentation and anaerobic oxidation (Green et al., 2008). A generalized process for the production of biogenic methane can be seen in Figure 2-4. Gas content in low rank coals are rarely above 4 to 6 m^3/ton (Moore, 2012).

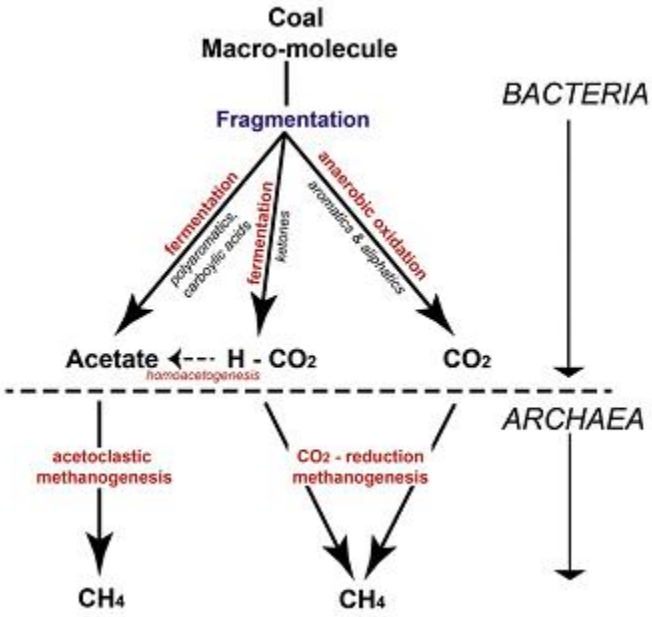

Figure 2-4 Generalized biogenic methane production process (Source: Moore, 2012)

As the coal matures in rank, the generation of thermogenic gas begins. This occurs when the coal reaches the high volatile bituminous classification and continues through the remainder of the coalification process (Clayton, 1998). A combination of time, heat and pressure causes devolatilization and production of methane, carbon dioxide, nitrogen, hydrogen sulphide, and larger hydrocarbon gases, such as ethane and propane (Moore, 2012). Thermogenic methane production has a higher potential for methane content, with values in excess of 20 m^3/ton documented in the field (Moore, 2012). The other major products from this process are water and carbon dioxide. Carbon dioxide, being water soluble, typically migrates away from the coal seam, leaving the methane selectively locked within the coal.

Coal serves as both a source and a reservoir for the methane. The methane produced through the biogenic and thermogenic processes is, for the most part, locked away onto the surface of the coal. One of the unique characteristics of coal is its high degree of porosity. Researchers have reported surface areas as high as 115 square meters in a single gram of coal (Şenel et al., 2001). Due to its porosity, coal has an incredible capacity to store methane adsorbed onto the surface area of its pores (Rice, 1993).

2.2.2 Coal Bed Methane Content Estimation

The methods to characterize the quantity of coal bed methane are divided into two basic categories. There are indirect methods and direct methods. The indirect methods of gas content estimation include methods based upon sorption isotherm data (Kim, 1977), or empirical relations to other variables such as coal bed depth and coal rank (Diamond et al., 1976) (McFall et al., 1986). Examples of this technique can be seen in Figure 2-5 and Figure 2-6. The relation detailed by Kim is based upon adsorption analysis of different coal samples from various depths (1977). The data put forth by McFall and colleagues provides a similar relationship for a specific region, namely the Black Warrior Basin in Alabama (1986). It should be noted that the literature recommends only using this technique for providing an initial estimate.

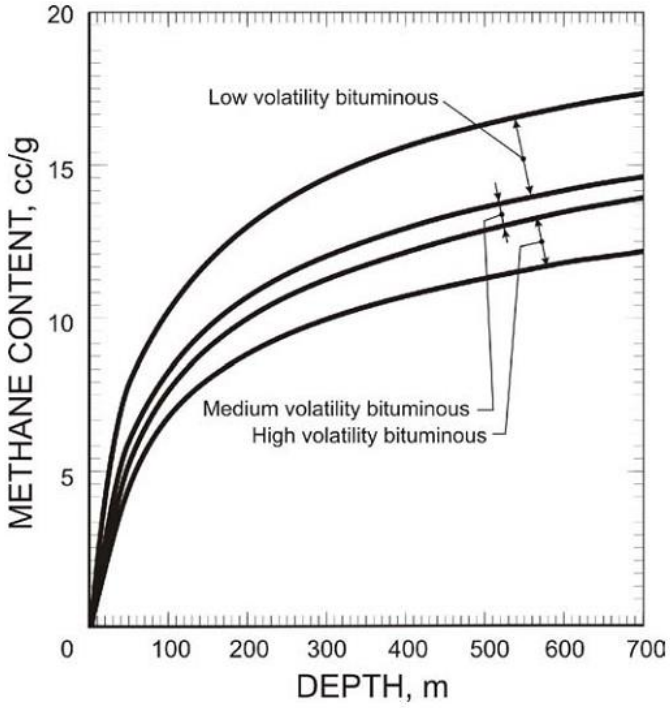

Figure 2-5 Predicted coal bed methane content as a function of overburden depth and coal rank (Source: Kim, 1977)

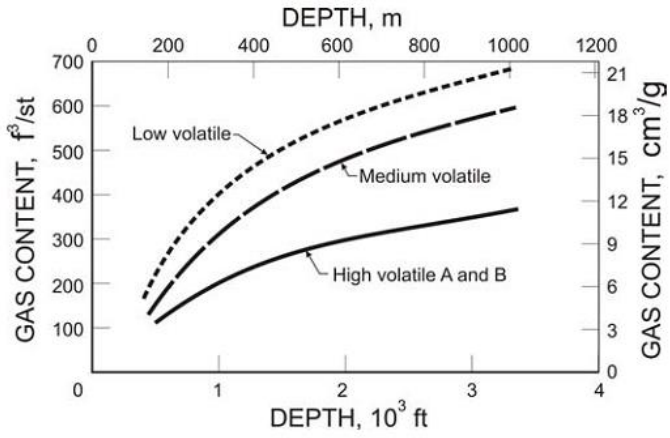

Figure 2-6 Predicted coal bed methane content as a function of overburden depth and coal rank in the Black Warrior Basin, Alabama (Source: McFall et al., 1986)

The preferred method to estimate the amount of gas in the coal bed is through the use of a direct measurement technique introduced by Bertrand in 1970 (Bertard et al., 1970). The technique is described in the ASTM standard number D7569-10 from 2010

titled "*Determination of Gas Content of Coal – Direct Desorption Method*" (ASTM, 2010). It represents an evolution of the work at the US Bureau of Mines in the 1970s and 1980s (Diamond, 1978) (Diamond and Levine, 1981) (Kim, 1973) (Kim, 1977). Improvements have since been made, but the essential steps remain the same.

The direct method of coal bed methane content measurement requires the following steps. A sample of coal is taken from the bed being characterized via a wire-line coring system. This core sample is then brought to the surface. Upon being exposed to the atmosphere, the hydrostatic head due to the weight of the overburden is relieved. Lacking this pressure to keep the methane adsorbed onto the surface, the desorption process begins. Once the core sample is on the surface, it is secured in an airtight canister, such as the one shown in Figure 2-7.

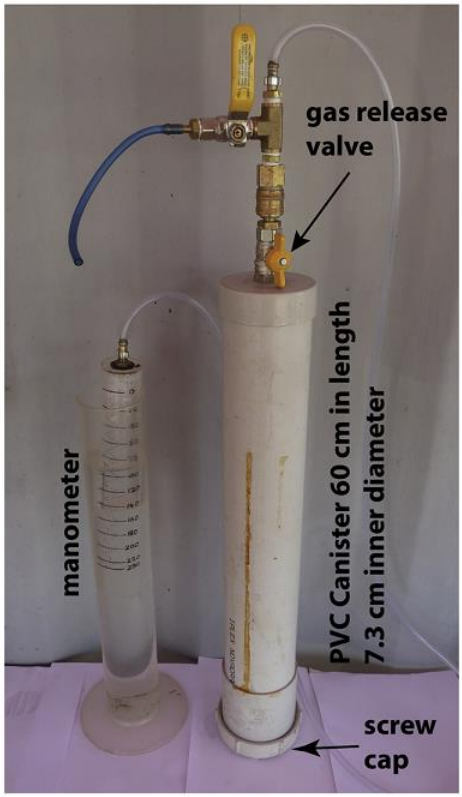

Figure 2-7 Typical gas desorption canister for determining desorbed gas content from core samples (Source: Moore, 2012)

An example of the results from a direct desorption test can be seen in Figure 2-8. As recommended by Bertrand, the data is plotted with measure gas content versus the square root of desorption time (1970). Three values found during this testing are important. The amount of gas during the test is known as the measured gas. Testing continues until a low amount of gas is recorded, on average. Suggested cutoff values for ending the desorption test by Diamond and Levine is an average of 10 cm^3 of gas desorption per day for one week (1981). Gas remaining in the coal is termed residual gas and must be characterized via a different test procedure. This residual gas is of little consequence for this study.

As mentioned before, there is a delay before the sample can be secured in an airtight canister. The gas lost in this window is known as lost gas. The US Bureau of Mines method of estimating the amount of lost gas is shown graphically in Figure 2-9. A linear regression, including the first few data points is performed and the line is extrapolated to time zero, when the desorption process began (Diamond and Schatzel, 1998). In this manner, an estimate of the lost gas can be obtained.

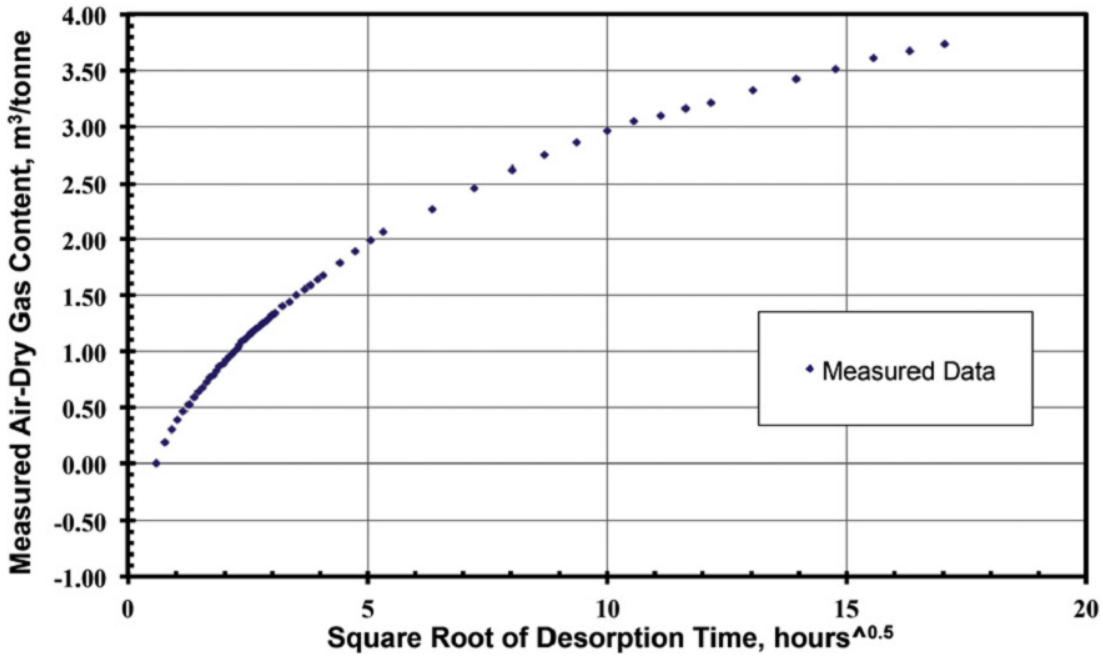

Figure 2-8 Example of direct desorption test data (Source: Moore, 2012)

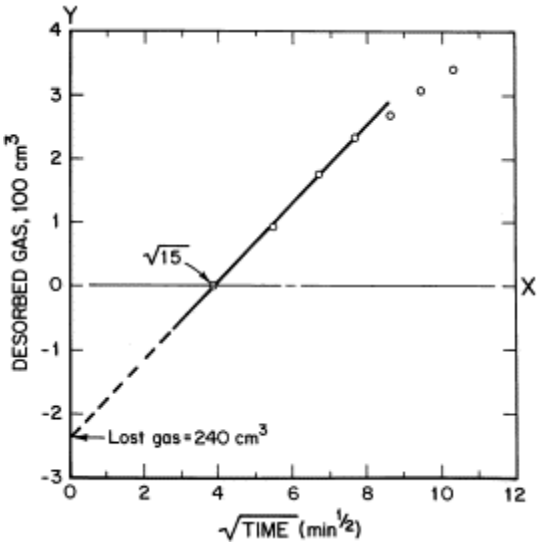

Figure 2-9 USBM method of determined the amount of gas lost during retrieval (Source: Diamond and Schatzel 1998)

Results of comprehensive coal bed methane surveys can be seen in Figure 2-10. Notable coal basins are the Black Warrior, San Juan, and Powder River Basins. The Black Warrior and San Juan Basins are high rank coals, while the Powder River Basin is a massive low rank coal bed. These exceptionally gassy regions have proven to be profitable sources of natural gas. Coal bed methane production data for these three coal basins can be seen in Figure 2-11.

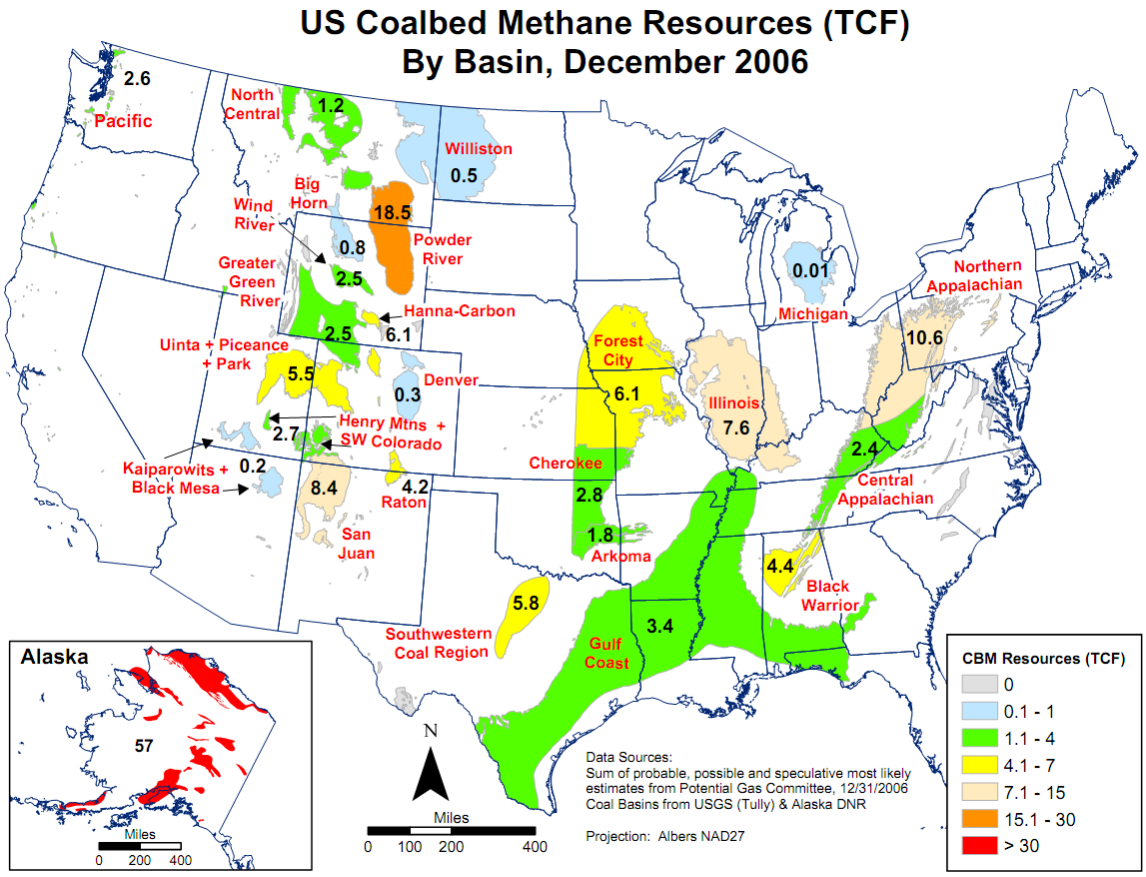

Figure 2-10 Map detailing principal coal basins in the United States along with estimated coal bed methane quantities (Source: EIA, 2006)

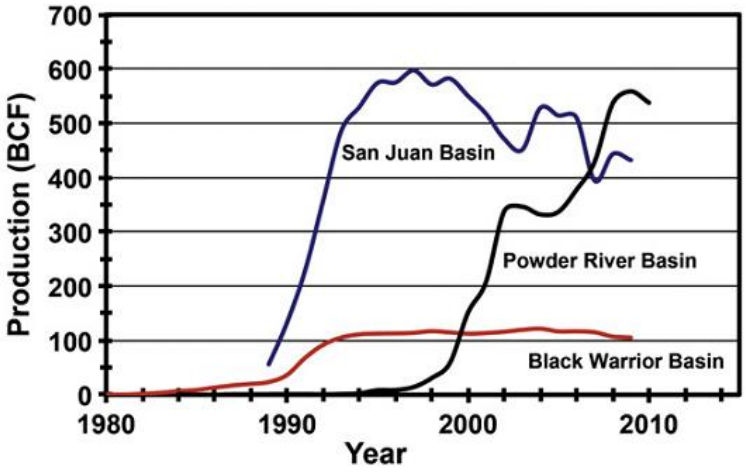

Figure 2-11 Coal bed methane production data for three prominent basins in the United States, from 1980 to 2010 (Source: Moore, 2012)

2.3 Consequences of Mining Activity

According to statistics provided by the National Mining Association, during 2011, 31% of the coal mined in the United States comes from underground production (2012). Of these underground mines, just over half employ longwall mining equipment, the alternative technique being room-and-pillar mining. A longwall system is an engineering marvel that fully extracts large panels of an underground coal seam. A representation of a longwall system can be seen in Figure 2-12. The shearer translates from end to end of the panel, breaking the coal free from the face where it falls onto an armored chain conveyor. The coal is transported via a series of conveyor belts to the surface for processing in the preparation plant. The equipment is self-advancing with its built in multitude of shields that serve to support the roof. As it advances, the roof is allowed to collapse behind the shields. A longwall mining section has a reputation for high productivity while requiring fewer workers as compared to the alternative. It also has a higher recovery rate. The primary drawback is the high capital cost of the equipment.

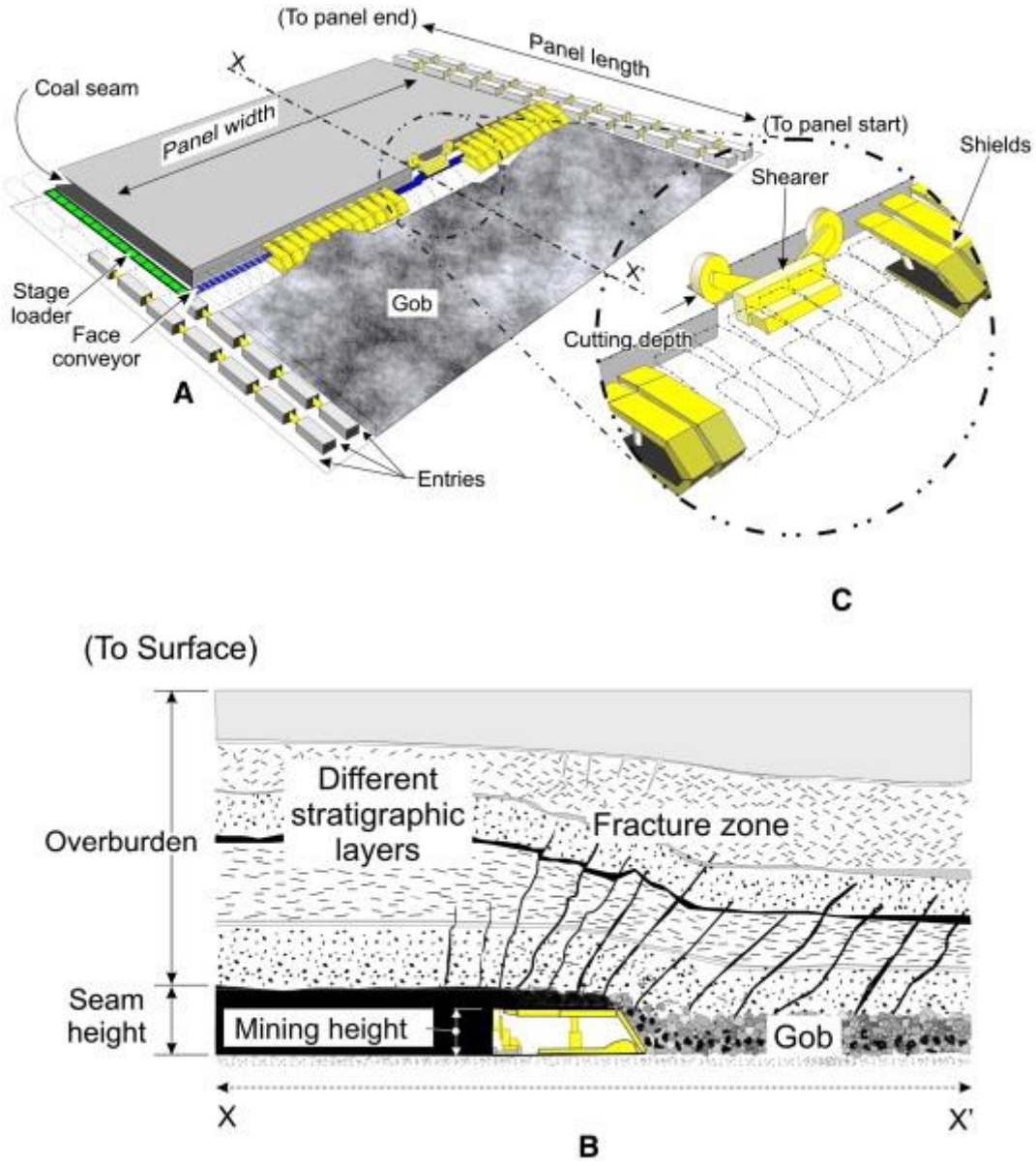

Figure 2-12 Representations of an active longwall panel and the formation of gob as the longwall retreats (Source: Karacan, 2008)

The gob area resulting from the extraction of the coal is a critical area of concern for the mine ventilation system. Strata permeability is a principal factor controlling gas emission into the mine workings (Ren and Edwards, 2000) (Guo et al., 2008), along with production rates, extents of the panel, and the presence of rider coal seams in the surrounding strata (Kissell, 2006). Two key changes within the gob area occur as the

longwall advances, disturbance to the surrounding strata and the release of overburden pressure.

The first major change is the significant disturbance to the surrounding strata, as seen in Figure 2-12 and Figure 2-13. Researchers describe this disturbance in terms of four distinct deformation zones in the overburden (Singh and Kendorski, 1981) (Kapp and Williams, 1972) (Galvin, 1987). They are, in order of increasing height above the mined out coal, as follows.

1) The first zone is the caving zone where rocks from the overlying strata collapse into the void left from the mining activity. It ranges from 5 to no more than 10 times the mining height.
2) The next is a disturbed zone where sagging rocks exhibit bed separation, fracturing, and joint opening. This extends to a height approximately 15 to 40 times the mining height.
3) Above the region with bed separation, there is a zone with minimal disturbance.
4) At the surface, there is a tensile fracture zone that can be up to 20 meters thick.

The actual extent of each of these zones is variable and dependent upon the local geology. The importance of this upheaval is the accompanying increase in permeability. Researchers commonly cite permeability increases up to three orders of magnitude. (Forster and Enever, 1992) (Reid et al., 1996) (Zhang, 2005) (Esterhuizen and Karacan, 2007)

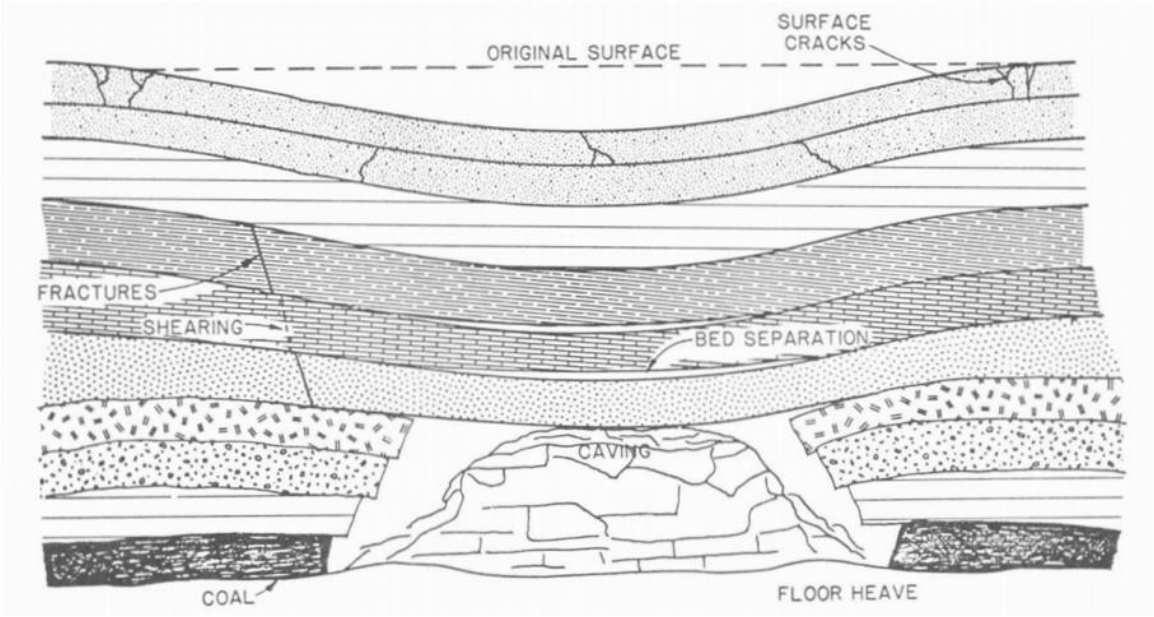

Figure 2-13 Expected strata disturbance and subsidence development as a result of coal extraction in a longwall panel (Source: Singh and Kendorski, 1983)

The second major change within the gob area is the radical change in pore pressure experienced by the strata. The pressure from the overburden is relieved in the caved zone, and significantly lessened in the fractured zone. This is then given a path to communicate with the atmosphere through the mine workings. The methane adsorbed onto the surface of the coal is now free to flow into the mine workings. The change in permeability within the mostly intact strata also comes into play as well as the relatively large fractures open pathways to the mine workings. The extent of the area from which the gas emission develops can be seen in Figure 2-14. By these estimates, the majority of the gas comes from within 20 meters of the floor and 60 meters of the roof.

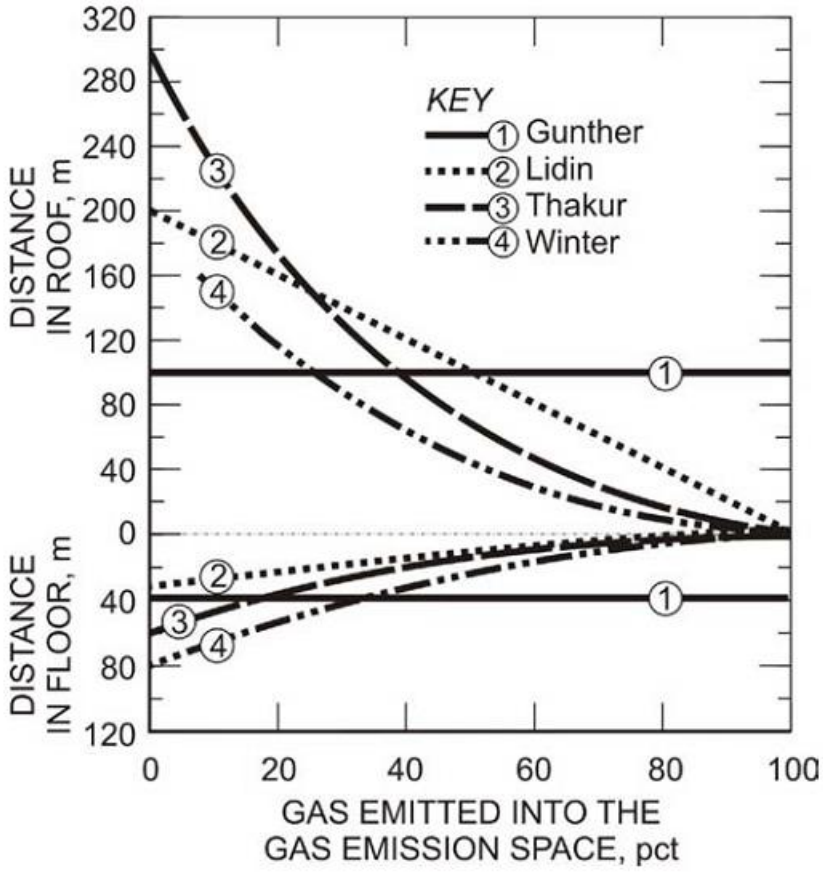

Figure 2-14 Extent of gas emission space within the gob as presented by four different authors: Lidin, 1961; Thakur, 1981; Winter, 1975; and Gunther and Bélin, 1967 (Source: Kissell, 2006)

An additional consideration for the modeling of methane ingress into the mine workings is the use of gob drainage schemes. There are techniques for pre-mining methane drainage, as well as post-mining methane drainage. Pre-mining methane drainage, in the United States, would typically be hydraulically fractured vertical wells that draw the methane from the coal bed to the surface (Kissell, 2006). These are outside the scope of the research, but are worth mentioning.

The influence of post-mining methane drainage is important to the efforts of this research. The typical method for managing methane in mines is through dilution via the

action of the main fan or fans to levels below federally mandated thresholds. Fresh air is forced to the face and used to dilute the methane seeping into the face and along the roadways. For some mines, the rate of gas release makes the economic prospects of diluting the inflow of methane infeasible. In these cases, the most common solution is the application of vertical gob wells to drain the methane before it has a chance to enter the mine workings (Kissell, 2006). This can be seen in Figure 2-15. Other types of degasification systems include vertical pre-mine wells, horizontal boreholes, and cross-measure boreholes. Karacan found that many mines still employ horizontal boreholes drilled from inside the mine into the coalbed prior to mining. In either case, the drainage efficiency is reported to be up to 50% (Karacan, 2009).

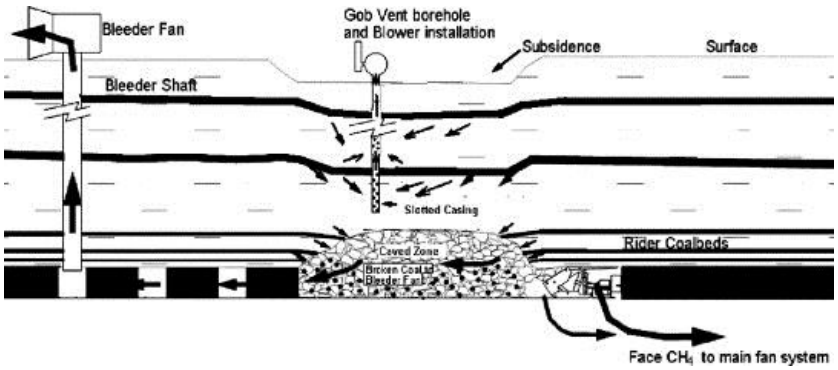

Figure 2-15 Example gob vent borehole arrangement (Source: Karacan et al., 2007)

2.4 Previous Modeling Efforts

Previous modeling efforts have focused on the control of methane and spontaneous heating in the gob area, gob inertization strategies, and dust and methane control at the working face. The modeling efforts can be divided into three basic techniques, depending upon the computational approach taken. These three techniques include network based approaches, reservoir simulation, and the use of computational fluid dynamics (CFD). The first step to each of these techniques is the development of a permeability model for the gob region.

2.4.1 Permeability Modeling

The earliest attempts to model the permeability distribution within the gob were the works of Ren and Edwards (2000). They developed a model using finite element techniques to determine the distribution of stress within the caved area. Extreme values for the permeability were found in the literature and these were mapped to the values of stress computed via the finite element model (Ren and Edwards, 2000). The resulting distribution of permeability can be seen in Figure 2-16.

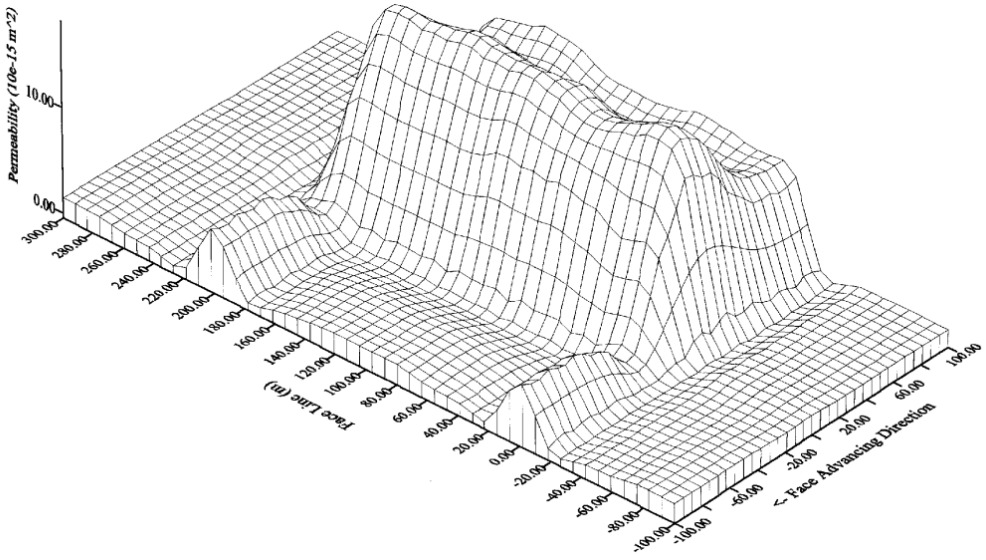

Figure 2-16 Early attempts at permeability modeling using the finite element method (Source: Ren and Edwards, 2000)

Esterhuizen and Karacan developed a new methodology for determining gob permeability distribution in 2005 utilizing geomechanical modeling (2005). The model used empirical relationships between fracture permeability and stress to calculate the change in permeability around the longwall face. The model was set to adjust the permeability by one order of magnitude for every 10 MPa the stress in the strata changed. Changes were applied independently in the horizontal and vertical directions, to account for the anisotropic nature of rock masses, via the following formulas.

$$K_h = K_{h_0} e^{-0.25(\sigma_{yy} - \sigma_{yy_0})} \quad (2.1)$$

$$K_v = K_{v_0} e^{-0.25(\sigma_{xx} - \sigma_{xx_0})} \quad (2.2)$$

The results of the modeling effort, using FLAC3D a commercial geotechnical modeling package to determine the permeability, were promising. The model was calibrated against field data for vertical gob bore vent wells.

Esterhuizen and Karacan further refined their model for permeability within the gob in 2007. FLAC3D was used to calculate both the stress distribution, along with the fracture and compaction character of the strata. This allows one to calculate the permeability distribution based on initial permeability and porosity via the well-known Carman-Kozeny equation, as seen in Equation 2.3. Results from the modeling exercise can be seen in Figure 2-17, which shows permeability distribution within the fully caved gob region.

$$K = \frac{K_0}{0.241}\left(\frac{n^3}{(1-n)^2}\right) \quad (2.3)$$

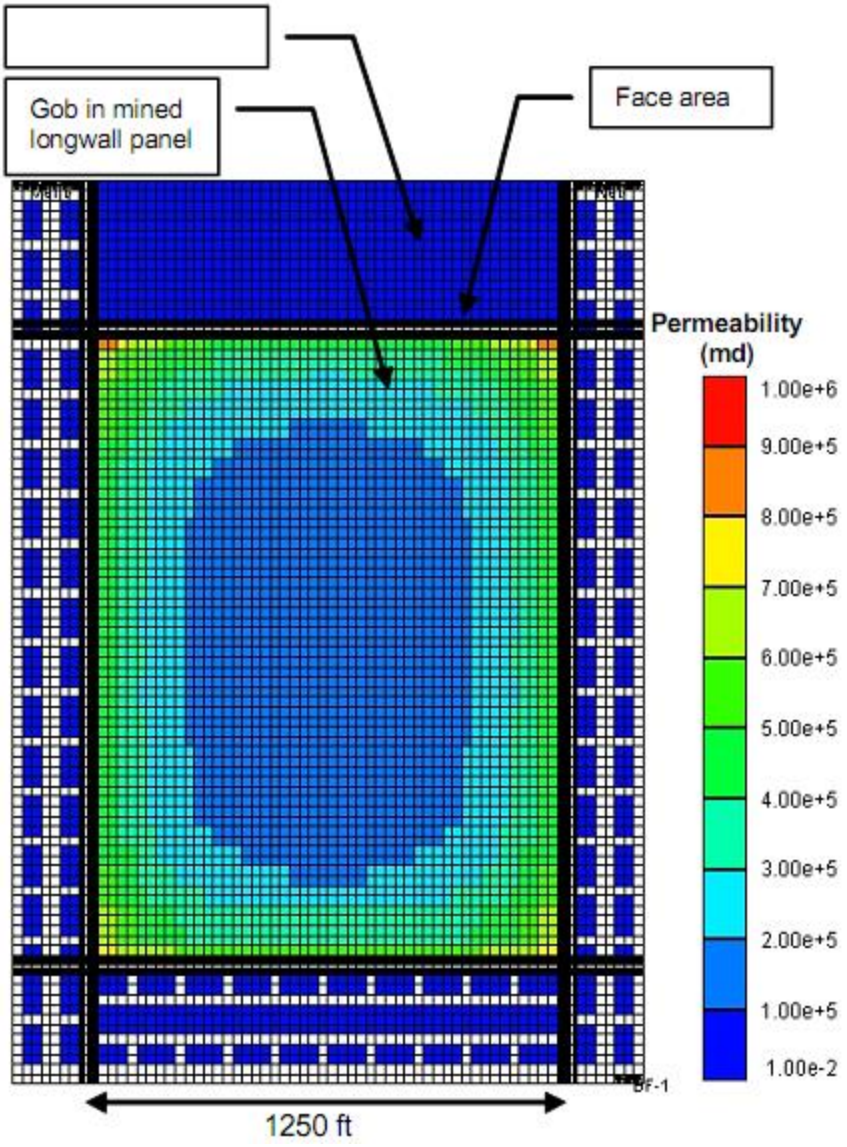

Figure 2-17 Plan view of gob permeability distribution within the caved gob area via FLAC3D modeling (Source: Esterhuizen and Karacan, 2007)

Wachel continued this line of FLAC3D modeling in 2012. In this work, a geomechanical model of a mine site was developed based upon a stratigraphic data provided by the mine operators. The work advanced upon the contributions of Esterhuizen and Karacan by modeling the formation of the gob through a progressive series of steps mimicking the mining process. In essence, 10 meter width sections were removed from the model representing the ongoing advance of the longwall face, in sequence. This resulted in a

permeability distribution that more accurately shows the influence of time on the state of the gob. This can be seen in Figure 2-18.

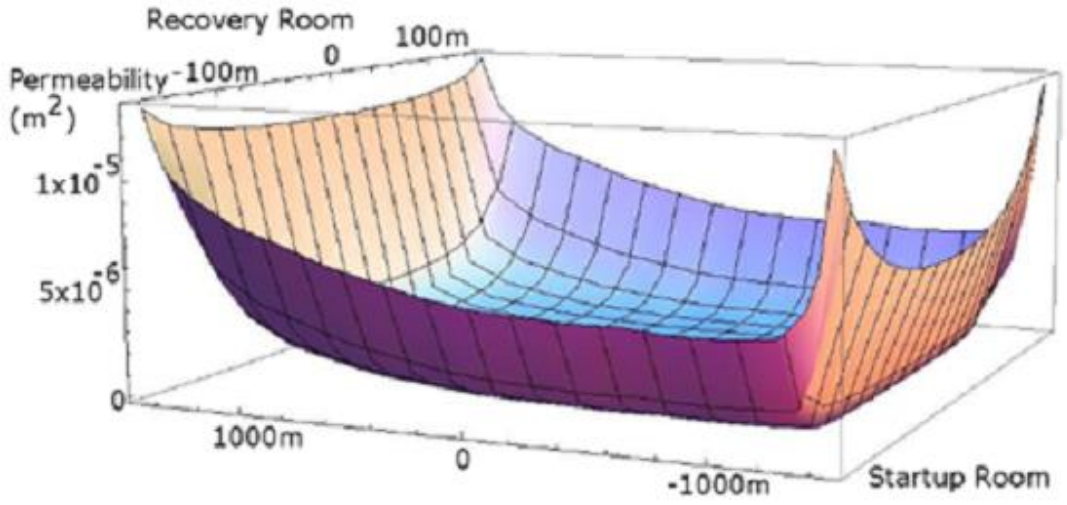

Figure 2-18 Permeability predictions via FLAC3D modeling (Source: Wachel, 2012)

The permeability distribution provides an input to flow through porous media, as described by Darcy's law. This is an empirically derived relation between flow, permeability, viscosity, and pressure. Darcy's law is commonly formulated as shown in Equation 2.4. This equation provides the commonly accepted description of flow through the irregular, broken, porous gob.

$$Q = \frac{-kA}{\mu}\left(\frac{P_b - P_a}{L}\right) \qquad 2.4$$

2.4.2 Network Based Modeling Approach

Dziurzynski and Wasilewski presented recent work with the network modeling package, VentZroby an add-on module to VentGraph, in 2012. In this network based model, the gob is discretized into a series of regularly connected pathways. Resistances to flows are defined based upon numerical and empirical methods. The entire gob regions is represented by a two dimensional plane with source conditions to introduce methane at

points spread through the gob. It includes the appropriate connections to the ventilation network. Figure 2-19 demonstrates the capability of the system to predict methane concentrations. These efforts have been supported with close cooperation between the research and mining communities, thus affording the researchers the highest quality of data for calibration and model validation. The primary advantage for such a tool is its low computational requirements.

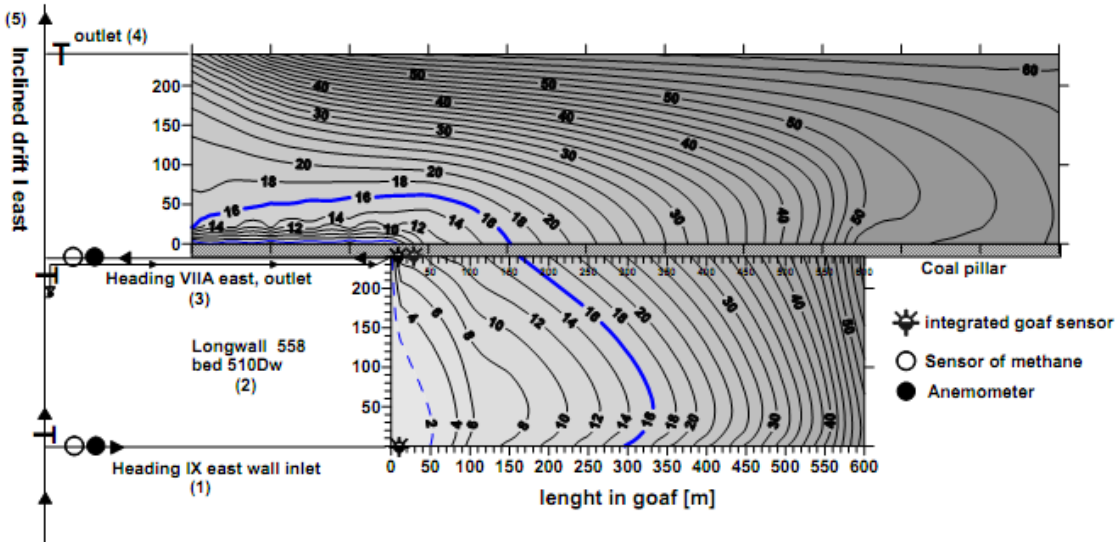

Figure 2-19 Isolines of methane concentration within the gob via VentZroby network modeling (Source: Dziurzynski and Wasilewski, 2012)

2.4.3 Reservoir Based Modeling Approach

The reservoir based modeling approach adapts techniques developed by the petroleum and natural gas industries. Their focus is modeling recovery processes through wells with advanced multi-phase and multi-component fluid models combined with relatively advanced heterogeneous models of the strata. Esterhuizen and Karacan published results from a study of gob vent borehole (GVB) production using GEM, a reservoir modeling tool, in 2005. As one would expect, the technique closely predicted GVB production as shown in Figure 2-20. One of the main advantages to using a reservoir based modeling tool is the means by which it predicts methane release rates. It employs a non-equilibrium desorption simulator to better quantify the methane release

rate from the strata, taking into account diffusion across the surface of the coal cleats. (Saulsberry et al., 1996).

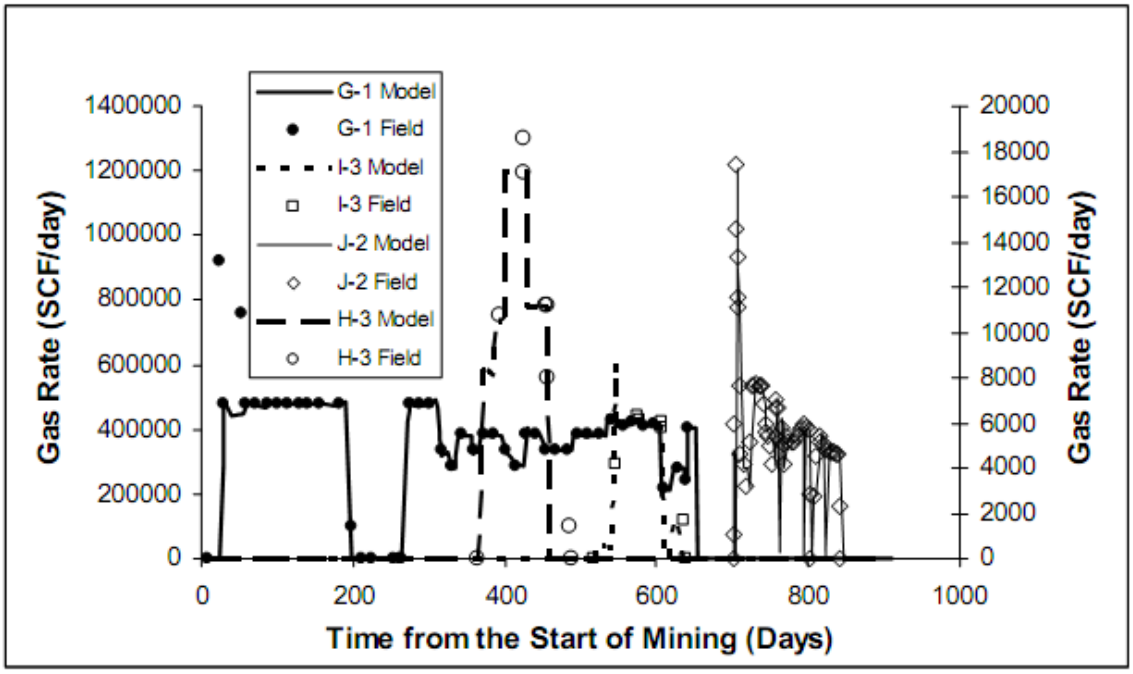

Figure 2-20 Comparison between gob vent borehole well production for observed versus simulated data (Source: Esterhuizen and Karacan, 2005)

2.4.4 Computational Fluid Dynamics Modeling Approach

Ren and Edwards began applying computational fluid dynamics to the problem of modeling the gob environment in 2000. They began with a model detailing methane migration around a longwall face. Ren continued improving their early model and by 2005 had developed a model to help control spontaneous combustion in the longwall gob. The ventilation model was improved and shows the characteristic geometry now associated with gob modeling, as seen in Figure 2-21. As shown in this figure, a significant portion of the computational domain is dedicated to the gob and overlying strata. Scenarios were run with an eye towards determining the extent of oxygen penetration into the gob, since oxygen ingress is a primary concern when dealing with spontaneous combustion. Careful examination of a number of scenarios for gob gas inertization via injection of nitrogen gas revealed a definite advantage to injecting the

gas at a point 200 m behind the face. The typical practice was to introduce the inert gas directly at the face. The optimum inertization strategy was implemented at the Newlands Colliery and was highly successful (Ren and Balusu, 2005).

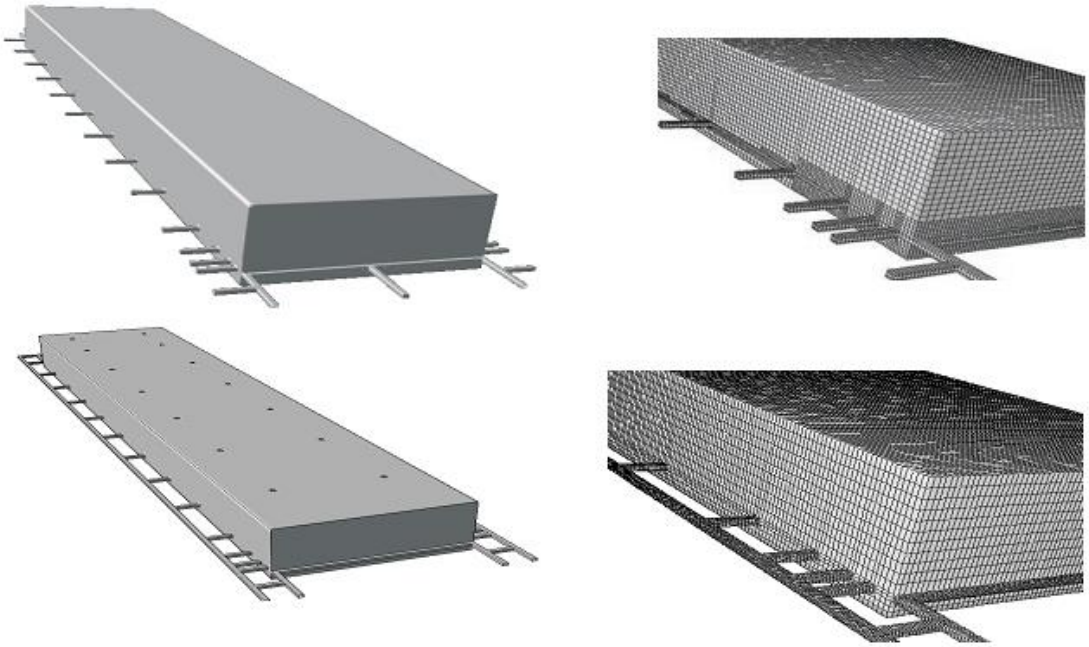

Figure 2-21 Typical geometry used in CFD models of gob gas migration (Source: Ren and Balusu, 2005)

Based upon their contributions to permeability modeling, Esterhuizen and Karacan developed an excellent model of the flow contours within the gob area (2007). As expected, flow was highest immediately behind the shields where the gob is very loose, likely open in spots. They reported that the simulation was consisted with observations at the mine being modeled.

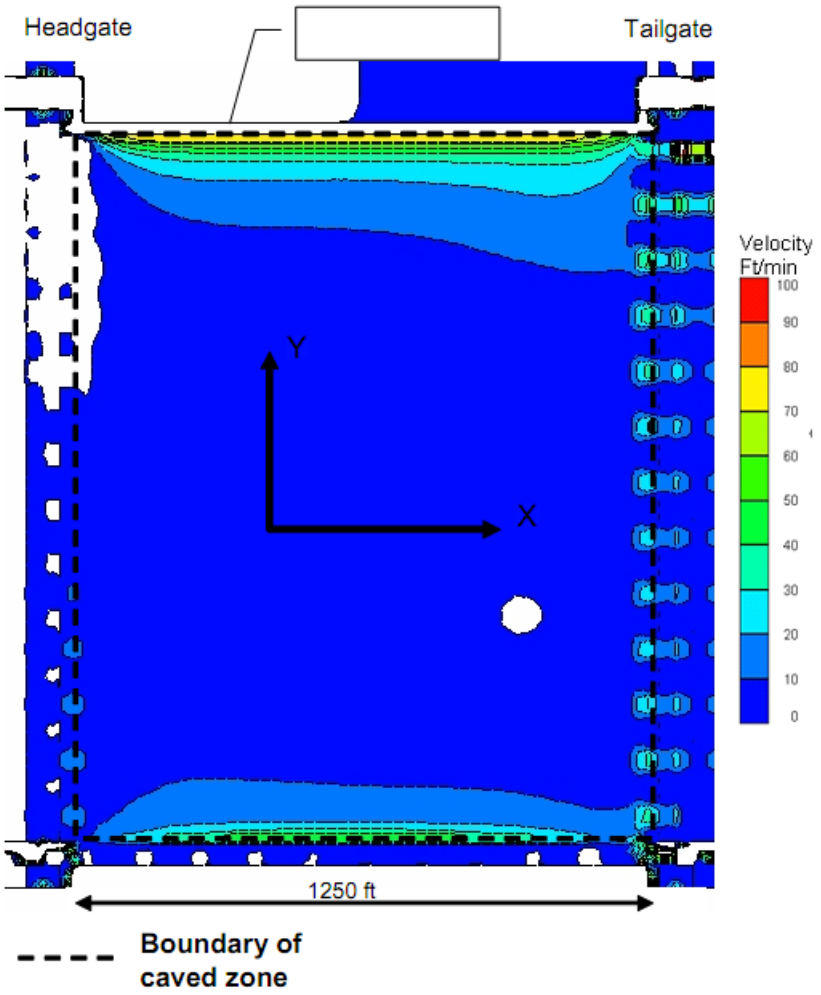

Figure 2-22 Simulated velocity contours within the fully caved gob zone (Source: Esterhuizen and Karacan, 2007)

Using the permeability model developed by Esterhuizen and Karacan, Yuan and Smith developed a model of the spontaneous heating that can occur within the gob area (2007). They considered a simplified chemical reaction where coal combined with oxygen to release heat and carbon monoxide. The reaction was governed by an Arrhenius type rate equation. They successfully determined temperature profiles for the gob area. The key finding in the study was a confirmation of a critical velocity zone for potential spontaneous combustion. There is a balance between providing sufficient oxygen to support self-heating, while not cooling the gob through convection due to high air velocities. Results from their findings can be seen in Figure 2-23. They were

also the first to develop a CFD model that included both a completely mined out panel alongside an active mining zone.

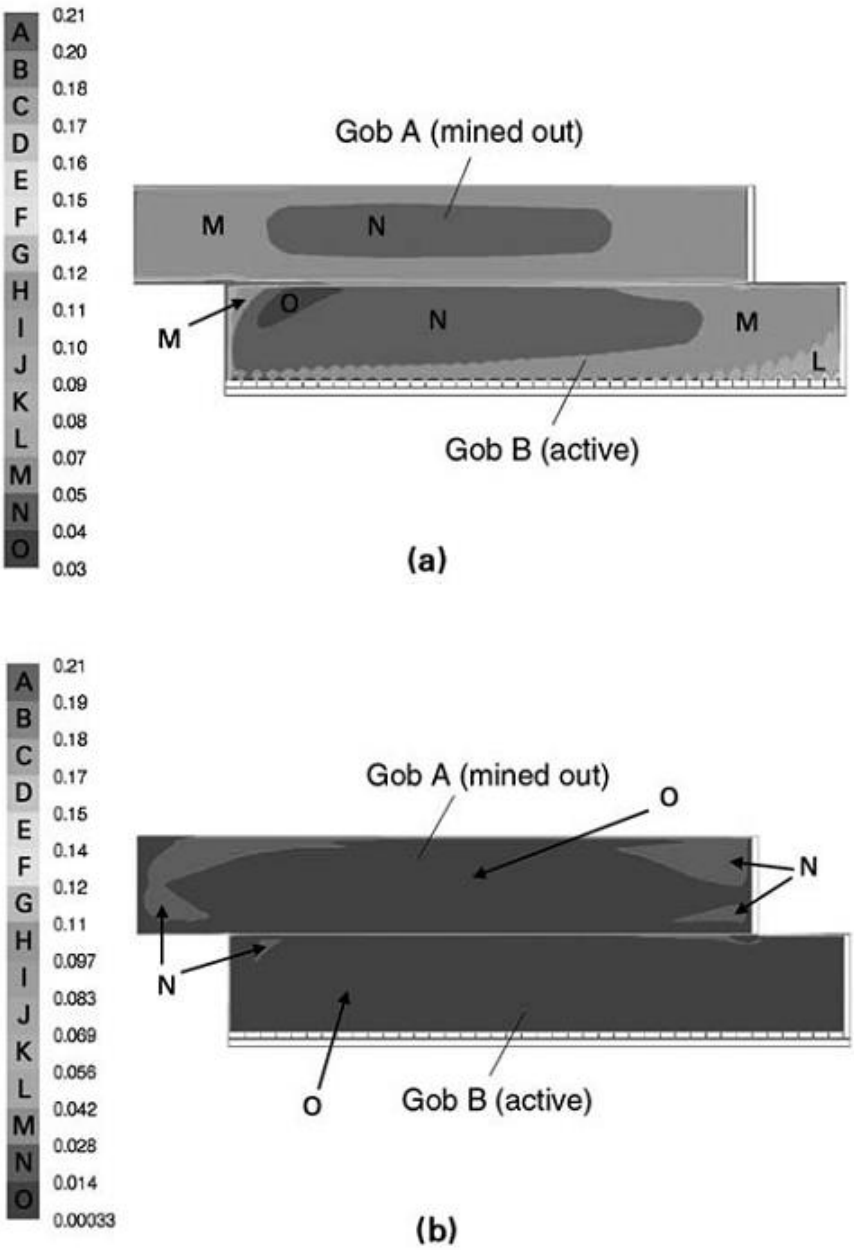

Figure 2-23 Simulated contours displaying oxygen concentration within two adjacent gob zones (Source: Yuan and Smith, 2007)

Ren and Balusa continued their work with inertization of the gob area via inert gas injection (2009). Results from their work can be seen in Figure 2-24. They reported

continued success with their efforts to optimize inertization of the gob area, supported by field data at several more mine sites.

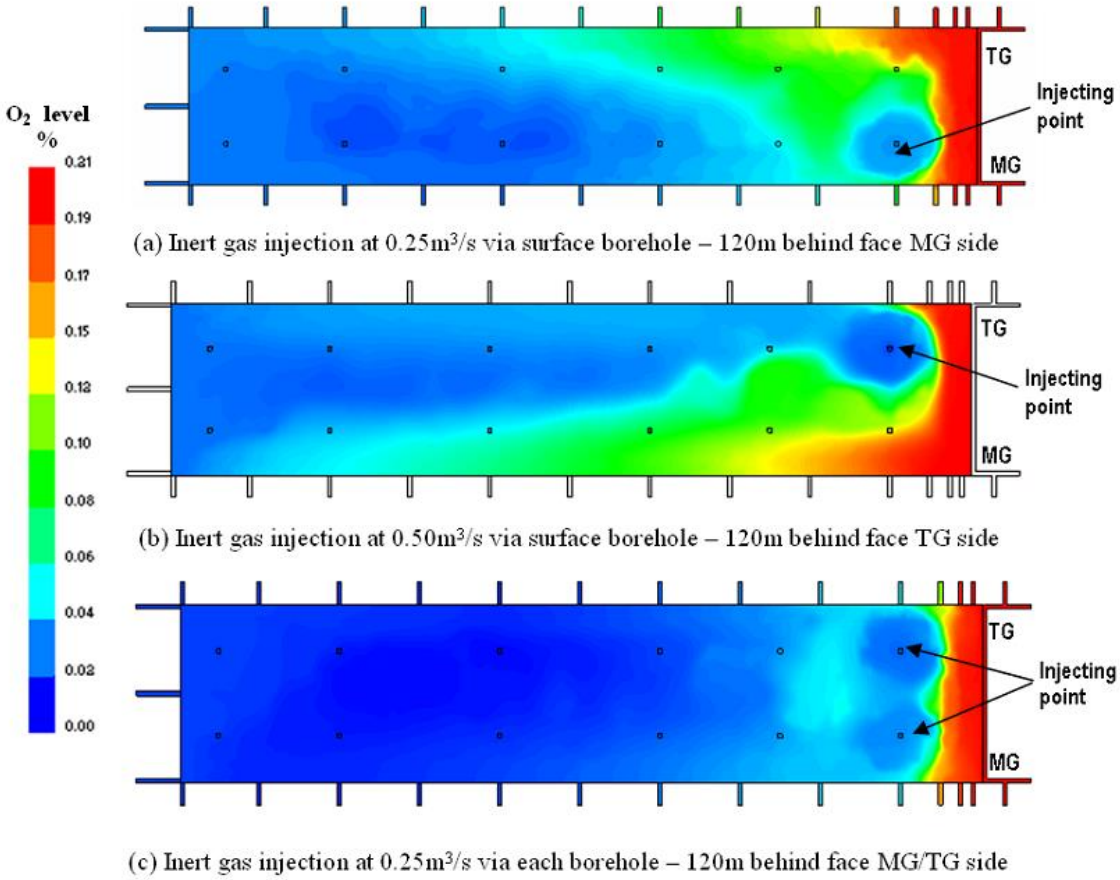

Figure 2-24 Simulated contours displaying oxygen concentration within a sealed longwall panel under the influence of inert gas injection (Source: Ren and Balusa, 2009)

The most recent effort at CFD modeling of the gob environment was completed by Dan Worrall, Jr. in 2012. His work concentrated on developing explosive potential contours within the longwall gob. The mine that was modeled used a bleederless, U-type ventilation arrangement, with gob isolation stoppings, to reduce the potential for spontaneous combustion. This made the problem well suited for CFD studies, as the boundary conditions for the computational domain were well defined. A good portion of the work was concentrated on a longwall equipment recovery scenario. A mesh of that region of interest can be seen in Figure 2-25. Several steps during that recovery

process were modeled with their attendant changes to the ventilation scheme. The aim was to develop a set of recommendations for the ventilation parameters to reduce the explosive potential. Studies of the entire panel were also conducted.

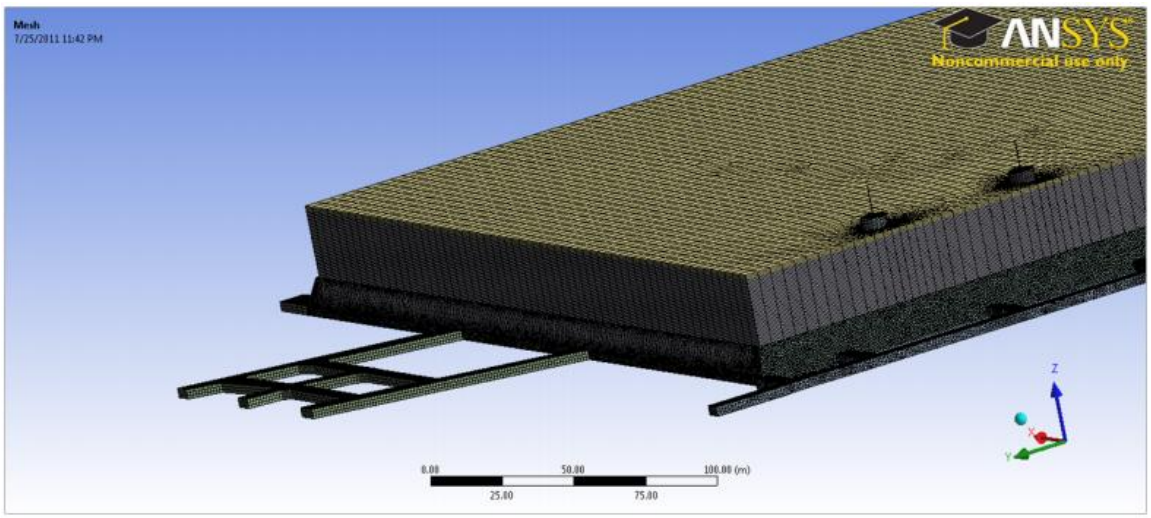

Figure 2-25 Mesh of region of interest at end of longwall panel prior to equipment recovery (Source: Worrall, 2012)

The modeling effort included a number of features consistent with past efforts. The gob environment was modeled in FLAC3D, with stratigraphic data provided by the mine operator. The results of which were seen in Figure 2-18. Geometry for the scenario was developed from mine maps. The gob region included layers for the caved gob, the fractured strata above the gob, and a rider seam which served as the methane source for this simulation (Worrall, 2012). A void directly above the longwall shield was modeled to account for the open space observed at the mine site. GVBs were added at the appropriate location as detailed by the mine map. Nitrogen injection points were added to the headgate and tailgate entries, consistent with the ventilation arrangement during the longwall recovery process. A cross section of the model can be seen in Figure 2-26.

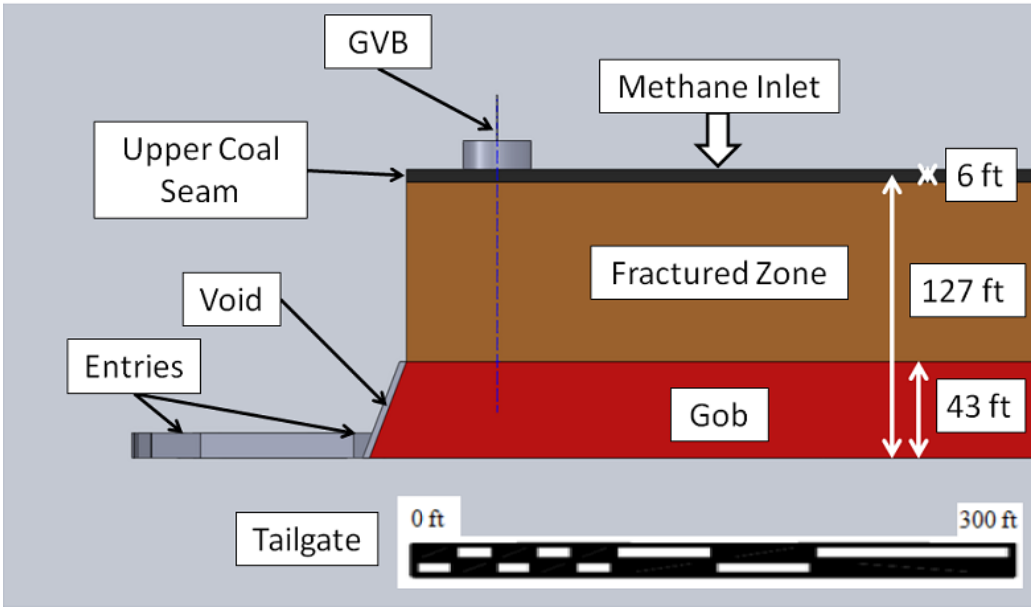

Figure 2-26 Model cross section of longwall recovery operation (Source: Worrall, 2012)

A key advancement introduced in this work was the adaptation of Coward's Triangle, see Figure 2-1, to color code the CFD results. This allows one to easily visualize the gob environment's explosive potential. This summary graph has been previously used in network simulation packages and now brought forward to CFD. An example of these results can be seen in Figure 2-27

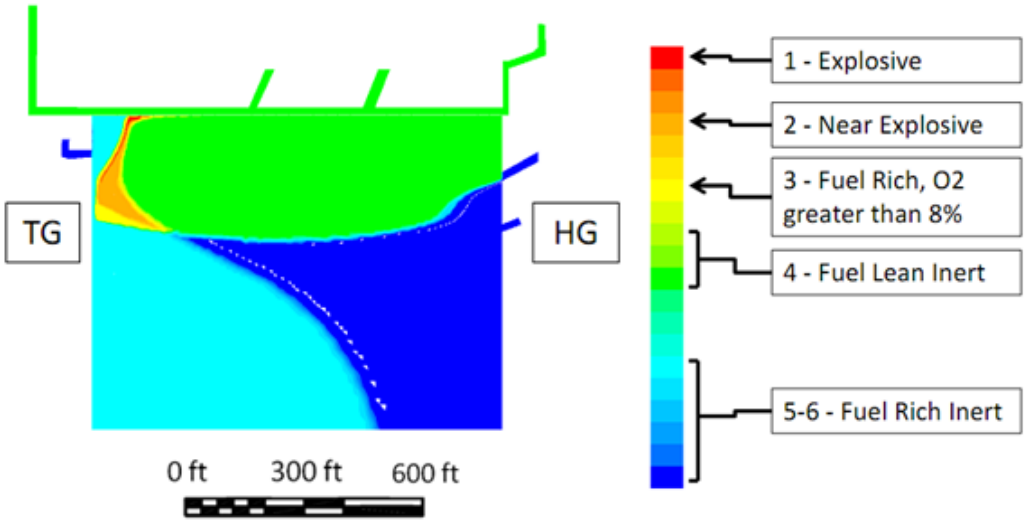

Figure 2-27 Contours of explosive potential within the gob (Source: Worrall, 2012)

The utility of the explosive potential contour plots can be easily seen in Figure 2-28. Changes to the gob environment can be seen as it reacts to varying levels of ventilation delivered to the longwall face.

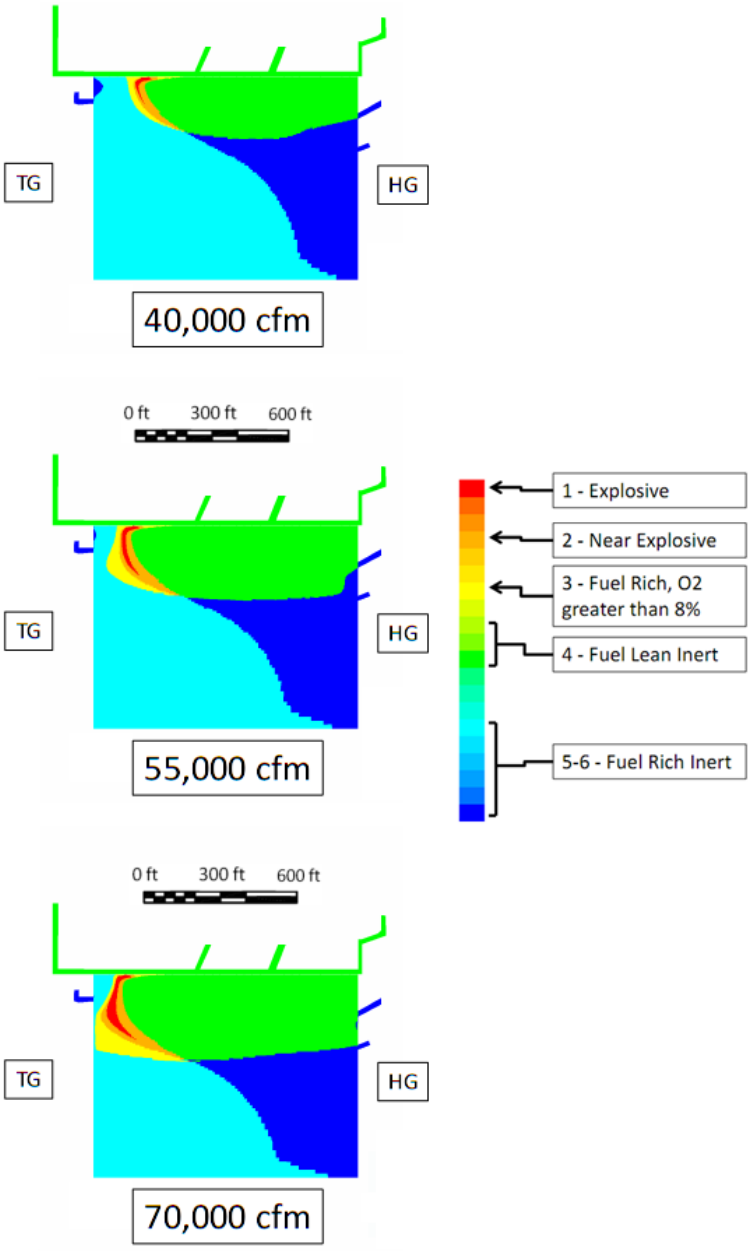

Figure 2-28 Contours of explosive potential as influenced by quantity of air delivered to the longwall face (Source: Worrall, 2012)

2.5 Multi-scale Analysis as Applied to Other Disciplines

A number of researchers have demonstrated the viability of multi-scale approaches to difficult problems. Flowmaster is a commercial CFD package that specializes in the analysis of pipe systems. It includes the ability to include both one-dimensional and three-dimensional elements in the same domain. Critical parts of the network can be modeled in full 3D, while the balance of the system is composed of 1D elements.

2.5.1 Multi-scale Modeling of Tunnel Ventilation Flows and Fires

Colella and colleagues have had great success modeling tunnel ventilation flows and the influence of fires (2011). Their approach was to use a multi-scale model of the traffic tunnel and its attendant ventilation ducts. Much like mine networks, representing the entire tunnel in the three dimensional domain becomes too computationally costly, so the ventilation network and portions of the transit tunnel were represented with a one-dimensional model. The region near the fire was represented in CFD. An example of the result can be seen in Figure 2-29.

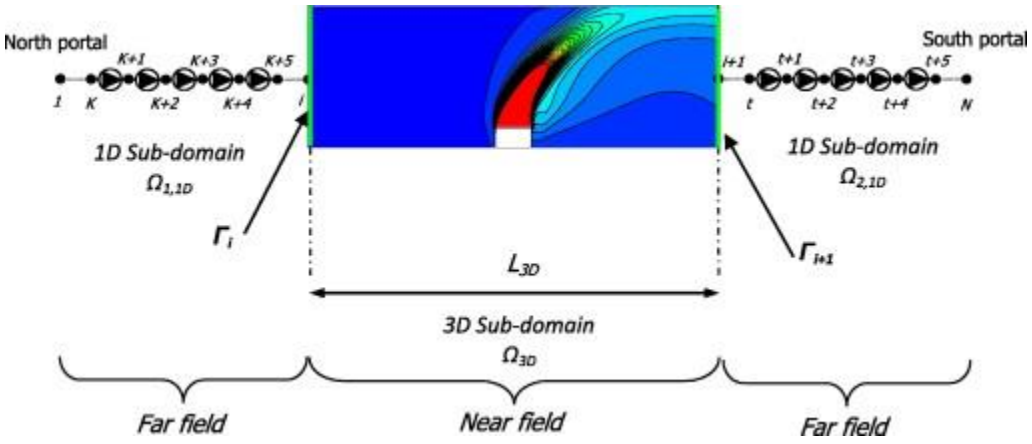

Figure 2-29 Multi-scale approach to modeling fires in tunnels (Source: Colella et al., 2011)

Colella reported a reduction in computing time by a factor of 40 with no loss in accuracy over the entire domain (2011). The approach used invokes the SIMPLE algorithm to solve a one-dimensional model of the tunnel which is then bi-directionally coupled to

the three dimensional domain, as shown in Figure 2-30. It did not attempt to model the propagation of pollutants through the network model.

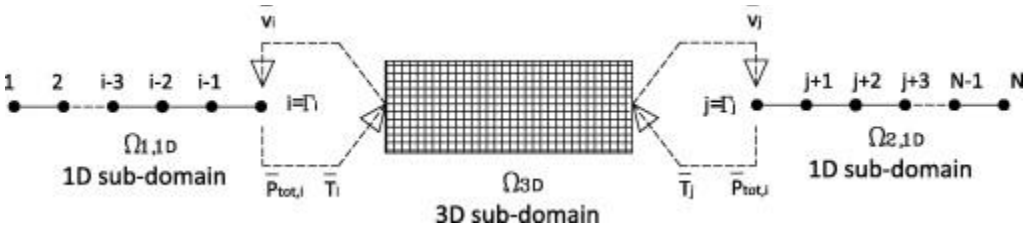

Figure 2-30 Bi-direction coupling strategy employed in multi-scale tunnel fire study (Source: Colella et al., 2011)

2.5.2 Multi-scale Respiratory Modeling

Another area of success with multi-scale techniques is in the arena of respiratory modeling. The numerous pathways within the lungs become exceedingly small. Generating a three-dimensional mesh that accurately captured the behavior of the flow would be computationally prohibitive.

Choi and Lin developed a multi-scale CFD model of the human lungs based upon a computed tomography scan. The largest airways were reconstructed from the CT scan data, while the smaller airways were represented as one dimensional branches. The bidirectional coupling strategy allowed Choi to predict detailed flows with the central airways, along with physiologically consistent regional ventilation throughout the lungs. The technique was used to simulate a breathing lung, complete with elastic deformation of the airways (2011).

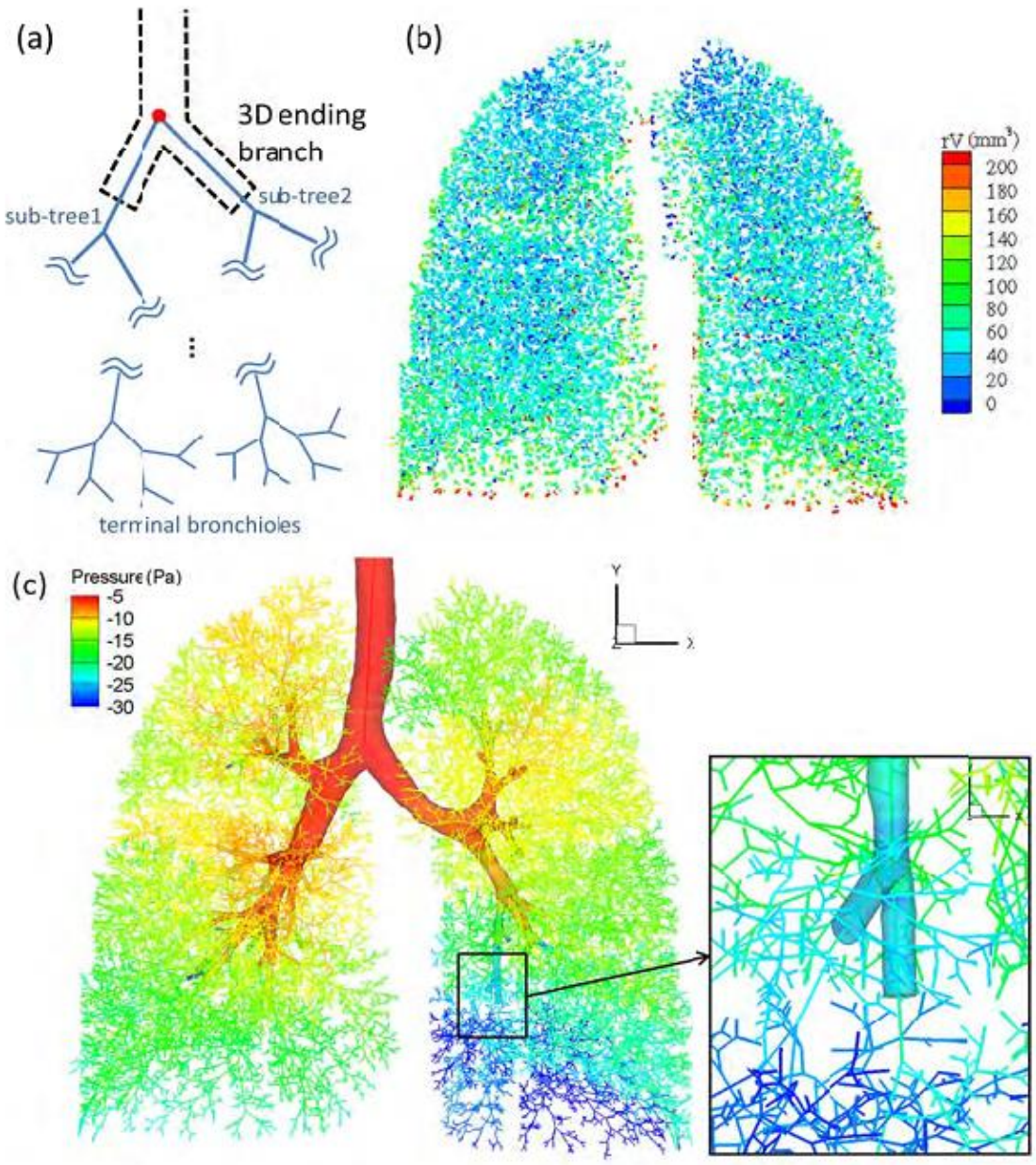

Figure 2-31 Schematic of coupling between 3D and 1D regime within a human pulmonary system (Source: Choi and Lin, 2011)

Kuprat and colleagues presented a novel multi-scale approach to model the upper pulmonary airways in three dimensions, bi-directionally coupled to one-dimensional models of the distal lung mechanics (2012). In this way, the researchers were able to resolve the spatial nature of chronic lung disease, in a computationally efficient manner. An example of the results obtained from this approach can be seen in Figure 2-32.

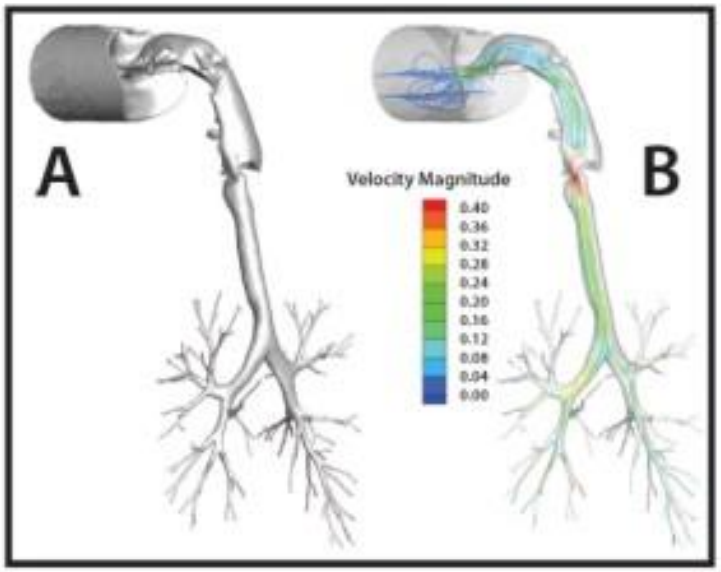

Figure 2-32 Multi-scale approach to modeling the human respiratory system (Kuprat et al., 2012)

2.6 Summary

The literature review revealed several important findings that guided the efforts that went into this dissertation. When combined with the discussion between the author, other researchers, and other professionals in the industry, a few conclusions can be drawn. These conclusions are summarized below.

- *Hazards of CoalBed Methane*
  The dangers of methane in coal mines, while commonly known, remain a significant threat to the lives of miners and the productivity of mines throughout the world. Varying levels of sophistication are employed in the design and monitoring of mine ventilation systems, but there are no risk free operations. Greater emphasis, in the United States, needs to be placed upon atmospheric monitoring tools.
- *Regulatory Pressures*
  There is significant pressure in the mining sector due to heightening regulatory oversight. A change in the regulatory environment has tempered some mine operator's willingness to cooperate with research efforts, perhaps due to their desire to avoid additional external visibility or general desire to absorb no further changes to their current business practices.
- *Gob Permeability*
  The current state of gob permeability knowledge is sufficiently advanced to allow the

modeling of the gob environment. Additional work is sorely needed to further validate this difficult environment. Researchers in the past have used scale models of subsiding gob regions in 2D and 3D models. The difficulty of characterizing this environment presents a good opportunity to employ scale modeling techniques and it should be investigated further.

- *CFD Modeling of Gob Environments*
  Researchers have demonstrated the successful use of computational fluid dynamics to characterize the gob environment. This has directly translated to improvements in inertization strategies by optimizing nitrogen injection amounts and/or gob vent borehole placement and well production. The geometry used to model the gob has been largely unchanged in ten years with a vast increase in computing power during the same time.
- *Other Gob Modeling Techniques*
  VentZroby seems to be the most practical tool for modeling the gob environment. It is a module within VentGraph designed specifically for use at mines. It is capable of transient simulations of the mine and incorporates feedback from atmospheric monitoring within the mine. With its close connection to industry, it seems to be the next evolution in network modeling tools in use by the mine industry. The US coal industry is ill prepared to adopt such a tool due to a lack of dedicated ventilation engineers and staff at US mines. This technique currently lacks the capability to model reactive gobs, those with the potential for spontaneous heating. This process may be more readily represented with a CFD model, due to the complexity of the scenario.
- *Multi – Scale Simulation Techniques*
  From transit tunnels to pulmonary systems, the multi-scale simulation approach has been used in numerous courses of study. There are consistent parallels between the nature of those studies and the simulation of mine ventilation systems. In each, the complexity of the system has prevented direct application of the CFD approach. By employing the multi-scale technique, the researchers can extend the computational boundary to include the entire problem, only at reduced complexity. Likewise, in mine ventilation systems, there is an inherent complexity that prevents including the entire mine in a single CFD model. For some classes of problems, the multi-scale approach shows promise.

3 Numerical Modeling Techniques

3.1 Overview

This section provides details concerning the numerical modeling used to develop the multi-scale ventilation model of a longwall gob. The first section offers a brief overview of the theories used to develop a 3D CFD model. The second section includes the development of the 1D network model. These will be referred to as the gob model and the network model. The final section details the user defined functions developed to assist with the multi-scale technique and gob post-processing. This includes the coupling algorithm used to initiate the multi-scale approach, the function to establish the gob permeability, and the details of the gob explosibility analysis.

3.2 Gob Model

The following work is closely based upon the work of Versteeg and Malalasekera (2007) along with details provided by *SC/Tetra Version 10 User's Guide: Basics of CFD Analysis* (2012). The governing equations for thermofluid analysis are those fundamental equations that describe the physics that best explain the flow of fluid and transfer of heat. SC/Tetra utilizes the finite volume method to numerically solve these equations. This method converts the governing equations into an integral conservation form that is formulated over a multitude of control volumes.

The basic governing equations are the conservation of mass, momentum, and energy. The first states that the overall mass can be neither created nor destroyed. The second is a statement that the change in momentum over time must be equal to the sum of the forces on a fluid. The last is a statement of the first law of thermodynamics. Energy must be conserved. Within the context of fluid flow, energy conservation means that the change in energy of a system is equal to the heat added to it, plus the net work performed on the system. The next equation to consider is the turbulence model.

As the characteristic Reynolds number of a fluid flow increases, it eventually becomes unstable. These flows are said to be turbulent, marked by the chaotic motion of swirls and eddies along with significant fluctuations in velocity. These fluctuations in velocity

induce additional stresses in the fluid flow, called Reynolds stresses. The influence of turbulence most certainly cannot be neglected, but the direct description of the motion of the particles would be too computationally intensive due to their random nature, for nearly all practical problems. A technique called Reynolds decomposition is employed to describe the flow in terms of an average value for velocities, along with statistics describing the intensity of the fluctuations. This allows a turbulence model to be applied to the simulation to account for the influence of this random chaotic flow. This appears as an additional set of equations, such as the standard κ-ε model.

The final governing equation of importance is the equation of state. Three thermodynamic variables that can be linked to an equation of state are in play during thermofluid analysis. They are density, pressure, and temperature. By assuming thermodynamic equilibrium throughout the flow, the ideal gas equation of state provides a link between them. This assumption remains valid in most cases, due to the effectively instantaneous adjustment that fluid particles make to their surroundings.

3.2.1 Governing Equations

The governing equations used in SC/Tetra are as follows, in compressible form:

- *Conservation of Mass Equation*

$$\frac{\partial \rho}{\partial t} + \frac{\partial}{\partial x_i} \rho \, u_i = 0 \tag{3.1}$$

- *Conservation of Momentum Equations*
  The Navier-Stokes Equations

$$\frac{\partial \rho u_i}{\partial t} + \frac{\partial u_j \rho \, u_i}{\partial x_j} = -\frac{\partial \sigma_{ij}}{\partial x_j} + \rho g_i \tag{3.2}$$

- *Conservation of Energy Equation*

$$\frac{\partial \rho H}{\partial t} + \frac{\partial u_j \rho \, H}{\partial x_j} = \frac{\partial p}{\partial t} + \frac{\partial u_j p}{\partial x_j} + \sigma_{ij} \frac{\partial u_i}{\partial x_j} + \frac{\partial}{\partial x_j} K \frac{\partial T}{\partial x_j} + \dot{q} \tag{3.3}$$

❖ *Turbulence Model Equations*
Standard κ-ε Model

$$\frac{\partial \rho \kappa}{\partial t} + \frac{\partial u_i \rho\, \kappa}{\partial x_i} = \frac{\partial}{\partial x_i}\left(\frac{\mu_t}{\sigma_\kappa}\frac{\partial \kappa}{\partial x_i}\right) + \rho(G_S - G_{S1} - G_{S2} - G_{S3} - \varepsilon) \quad 3.4$$

$$\frac{\partial \rho \varepsilon}{\partial t} + \frac{\partial u_i \rho\, \varepsilon}{\partial x_i} = \frac{\partial}{\partial x_i}\left(\frac{\mu_t}{\sigma_\varepsilon}\frac{\partial \varepsilon}{\partial x_i}\right) + C_1\frac{\varepsilon}{\kappa}(G_S - G_{S1} - G_{S2} - G_{S3} - \varepsilon) - C_2\frac{\rho\varepsilon^2}{\kappa} \quad 3.5$$

❖ *Diffusive Species Equations*

$$\frac{\partial \rho C}{\partial t} + \frac{\partial u_j \rho C}{\partial x_j} = \frac{\partial}{\partial x_j}\rho D_m \frac{\partial C}{\partial x_j} + \rho \dot{d} \quad 3.6$$

❖ *Equation of State*
Ideal Gas Law

$$p = \rho R T \quad 3.7$$

3.2.2 Solving Conservation Equations

With the exception of the equation of state, each of these differential equations is a statement of a different conservation principle. There is an underlying symmetry amongst these equations. There is an implicit balance between the processes that are influencing the dependent variables in the equation. The dependent variables are the physical quantities, represented with Φ. It is possible to cast these in a general form as in Equation 3.8, which allows one to solve them with a similar process.

$$\frac{\partial}{\partial t}(\rho\Phi) + \nabla \cdot (\rho \boldsymbol{u}\Phi) = \nabla \cdot (\Gamma_\Phi \nabla i) + S_\Phi \quad 3.8$$

The four terms in the general equation are the unsteady term, the convection term, the diffusion term, and the source term. The variable Φ can represent any number of physical properties. For each physical property, a different form of the diffusion coefficient Γ and of the source term S will be required. The determination of these forms is the result of the manipulating the particular differential equation until it matches this form. The coefficient of the gradient of Φ in the resulting diffusion term will be Γ, while the remaining terms will be S.

The advantage of using the general form of the equation will reveal itself during the solution procedure. With every conservation equation cast as a unique case of the general form, the techniques used to solve the equation numerically will be similar. Once a solution technique for Equation 3.8 is developed, it can be applied to each in turn. The dependent variable Φ is a function of space and time as shown in Equation 3.9.

$$\Phi = \Phi(x, y, z, t) \tag{3.9}$$

The values $x, y, z,$ and t are independent variables for which values of Φ is calculated. These are three dimensions in space and one in time. For the network model being developed, the goal is to reduce the number of dimensions in space to one, simply x. The dependence on time t determines whether a problem is steady or unsteady. Steady problems are those independent of time, thus the unsteady component of the general Equation 3.8 would be neglected. The solution to unsteady problems will have a time-dependent component.

As mentioned earlier, three conservation equations are necessary to describe the transient flow field of interest. For these three equations, the variable Φ represents mass fraction, velocity, and enthalpy, respectively. In the conservation of mass equation, or continuity equation, the mass fraction will be equal to unity when there is only one fluid in the problem domain.

The crux of the numerical technique used to solve Equation 3.9 involves approximating the values of the dependent, continuous variable Φ at a discrete number of points. With the value of Φ known at these points, the distribution of Φ can be readily determined. These points are known as grid points. The process of replacing the continuous distribution of Φ with its approximation is known as discretization. There are various methods to perform the discretization, with the control volume method discussed here. The goal of the discretization is to develop a scheme that is both physically realistic and maintain overall balance.

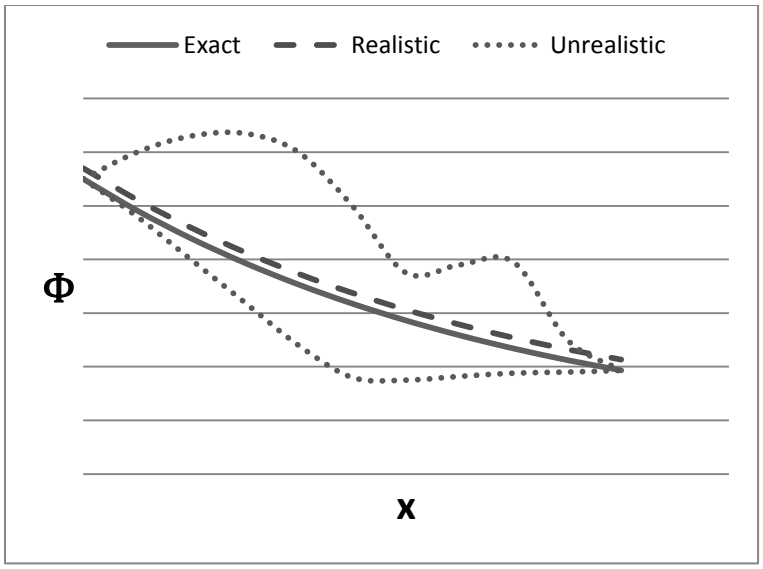

Figure 3-1 Example of Physically Realistic Behavior (Adapted: Patankar, 1980)

The concept of a physically realistic solution is best illustrated by Figure 3-1. The unrealistic approximations are not following the general trend of the variance of the exact solution with x. They demonstrate either slopes trending counter to the exact solution, or values beyond a reasonable range. For example, if the total pressure in a duct is known to decrease monotonically from 100 Pa to 50 Pa, it would be unrealistic to see a value of 200 Pa in the approximation.

An approximation that maintains overall balance is equally important to having a physically realistic solution. As these are approximations of conservation equations, it is reasonable to say that balance should be maintained over every portion of the problem domain, including the boundaries. If one visualizes a scenario as in Figure 3-2, the flux F_w between volumes *i-1* and *i* must be equal and opposite. The extensive property $\rho\Phi$ exiting a volume is equal to that entering the next volume. The same is true for the flux F_e between volumes *i* and *i+1*. In this manner, balance is maintained.

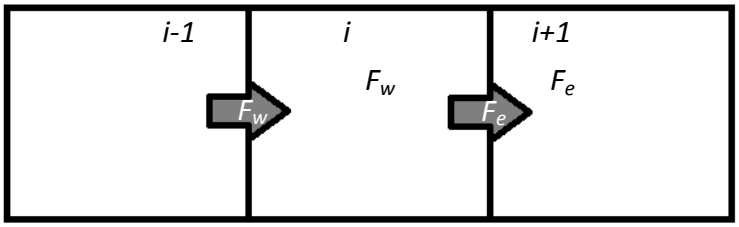

Figure 3-2 Balanced treatment of fluxes (Adapted: Versteeg and Malalasekera, 2007)

Patankar states that there are four basic rules for the formulation of the discretization equations (1980). These are the natural extension of the two previous guidelines discussed earlier. The rules are as follows:

- *Consistency at Control-Volume Faces*

  Faces that are shared by two neighboring control volumes will have the same expression in the discretization equations for both control volumes.
- *Positive Coefficients*

  Coefficients of the neighboring points shall have the same sign to indicate that an increase in a point will tend to increase the value of nearby points.
- *Negative Slope Linearization of the Source Term*

  When it becomes necessary to linearize a Φ dependent source term, a negative slope shall be used.
- *Sum of the Neighbor Coefficients*

  The coefficient of a point is equal to the sum of the neighboring coefficients.

3.2.3 Porous Media Model

SC/Tetra provides a number of porous media models to represent a variety of conditions. Of the models provided, two are of interest. The first is the basic isotropic porous medium, an implementation of Darcy's law. The second is a packed bed porous medium model that implements Kozeny-Carman equation, a more elaborate formulation of Darcy's law that depends upon the porosity of the packed bed and the general size and shape of the particles filling the bed. Either would be sufficient to implement the pressure drop experience in the gob with one exception. Neither

implementation is flexible enough to implement a continuously variable permeability as shown in Figure 2-18. Beyond that, there are only certain functions within SC/Tetra that support the creation of user defined function. Instead, a more general pressure loss model was applied, of a form to match the Kozeny-Carman equation, which had the capability to use a user defined function.

The pressure loss function in SC/Tetra takes the following form and is linked to a formula for the necessary body force to be applied.

$$\Delta P = au^2 + b|u| \tag{3.10}$$

$$F = -sign(\Phi - V) \cdot \{C(\Phi - V)^2 + B|\Phi - V|\} \cdot SCL \tag{3.11}$$

Where

$sign$	Sign function
Φ	Flow velocity at specified control volume
SCL	Volume or area of specified control volume
C	$\frac{\mathrm{a}}{\mathrm{L}}$
V	0.0
B	$\frac{\mathrm{b}}{\mathrm{L}}$

The form of Darcy's law must be converted to fit the above interpretation of a pressure loss function. Darcy's law provides for no inertial loss component, so the value of a in Equation 3.10 must be zero. The value of b, with some rearranging of Darcy's law, becomes the ratio of dynamic viscosity multiplied by a length to permeability. The length is dependent upon the path the flow takes through the gob. Flow is generally oriented from headgate to tailgate, but in the case of the longwall face, it doesn't necessarily travel the entire width of the gob. Considering this, the value of L must be some fraction of the width of the gob. This was part of the need for conducting a sensitivity study of the input to the porous media model. The permeability values come from the surface fit of the output of the FLAC modeling.

3.3 Network Model

3.3.1 Network Model Rationalization

The desire to use a 1D network model of branches was established early in the course of the research for this topic. An effort was undertaken to develop a rubric for meshing branches of the ventilation system in Cradle. The focus of the effort was to establish the minimum number of elements needed, that would support the range of velocities one would normally encounter in the mine. The predominant influence of the branches of the system is to provide resistance to flow at the walls, the dominant momentum sink in the system.

The roughness of the wall and sheer size of the mine precludes directly modeling the geometry. In CFD, this would be implemented with an application of the Log Law of the Wall, with the rough surface amendment available in SC/Tetra. The log law of the wall imposes a velocity profile upon the flow near the wall based upon the roughness characteristics of the wall. The key to applying this model is assuring correct dimensionless wall distance (y^+) values are achieved at elements near the wall. The value for y^+ should be at least above 10.8 and ideally in the logarithmic region shown in Figure 3-3. The equation for the log law of the wall for rough surfaces is as follows.

$$\frac{u}{u^*} = \frac{1}{k} ln\left(\frac{y}{k_S}\right) + B \qquad 3.12$$

Where

u	Velocity of the flow
u^*	Frictional velocity of the flow
k, B	Von Kármán constants, 0.41 and 8.5 respectively
y	Distance to the wall
k_S	Roughness of the wall

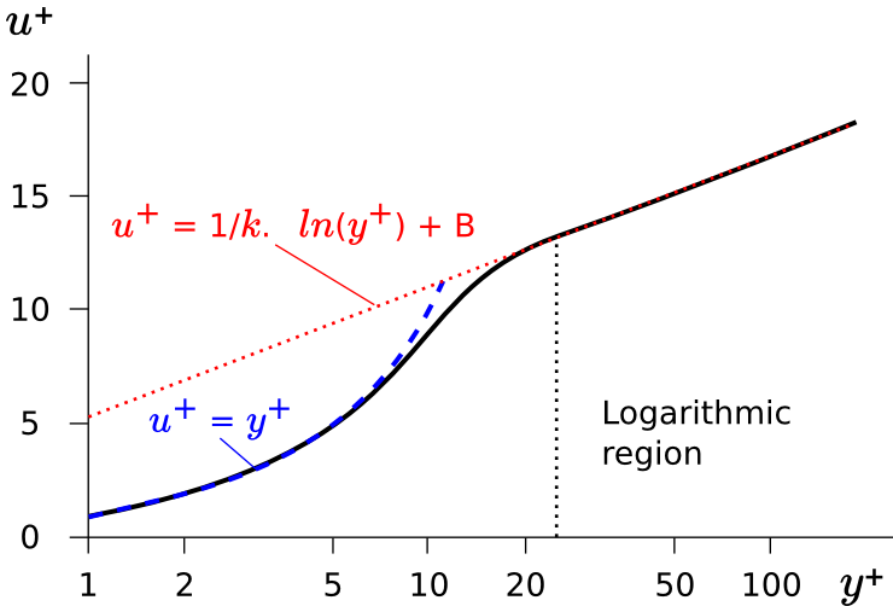

Figure 3-3 Log law of the wall (Source: Creative Commons, 2012)

The roughness of a wall or conduit is commonly characterized by the Moody Friction Factor. The roughness of the surface in mines in characterized with Atkinson's Friction Factor. Atkinson's work experimenting with flows through mine ventilation circuits predates the work of Darcy, Reynolds, Stanton, Prandtl, and Nikurandse, and was limited to shallow workings. He never established the importance of density. His friction factor is related to the Moody Friction Factor by a factor of the density divided by 8. This provides a means to compare values found in mining literature to the more common Moody Diagram.

A series of calculations were completed in CFD to find pressure drop based upon meshing choices and the inputs to the rough log law of the wall. PERL scripts were prepared that automated the mesh generation and data collection process. Mesh choices were tested over a range of roughness values and velocities one would reasonably expect to encounter in mine. An example of summary results can be seen in Table 3-1. Appendix I gives greater detail about the derivation of this relationship.

Table 3-1 Example summary results from one mesh and roughness combination

Roughness	150	mm	0.050	Length	120	m	
Differential Pressure (Pa)	Area (m^2)	Hydraulic Diameter (m)	Volume Flux (m^3/s)	Mean Velocity (m/s)	Reynold's Number	Moody Friction Factor	Atkinson's Friction Factor (Ns^2/m^4)
0.00625	12	3	0.708	0.06	11678	0.074507	0.011232
0.025	12	3	1.432	0.12	23630	0.072794	0.010974
0.1	12	3	2.881	0.24	47537	0.071947	0.010846
0.4	12	3	5.778	0.48	95351	0.071531	0.010783
1.6	12	3	11.573	0.96	190986	0.071318	0.010751
6.4	12	3	23.164	1.93	382260	0.071211	0.010735
25.6	12	3	46.343	3.86	764767	0.071165	0.010728
102.4	12	3	92.704	7.73	1529843	0.071136	0.010724
409.6	12	3	185.428	15.45	3060019	0.071120	0.010721

The automated testing narrowed the choices for mesh generation down to a manageable set of values for representative coal mine entries. The preferred mesh parameters, rounded to reasonable numbers, were found to be the following.

- *Entry Size:* 6 meter by 2 meter, typical of US coal mines
- *Element Size:* 0.4 meter octant size
- *Prism Layer Thickness:* 0.04 meters
- *Prism Count:* 3 layers

The results of the testing were compared to the expected results found through the application of the Colebrook-White Equation. For convenience, the results have been summarized in Figure 3-4, to a Moody Diagram. The calculated RMS error for the scenarios was found be less than 0.7% for all cases tested, which covered the range of roughness values and velocities. An example of the y^+ verification can be seen in Figure 3-5. It clearly shows the reason the chosen mesh was successful as the minimum normalized wall distance was maintained over the range of velocities tested.

While the development of a rubric of meshing coal mine entries was wholly successful, it also highlighted the cost of doing so. For every meter of entryway, approximately 1,000 elements are needed to resolve flow and pressure. The mine scenario examined later in the dissertation, a significant portion but not complete set of mine entryways, had a combined length exceeding 22,000 meters. This would require 22 million elements before including the gob.

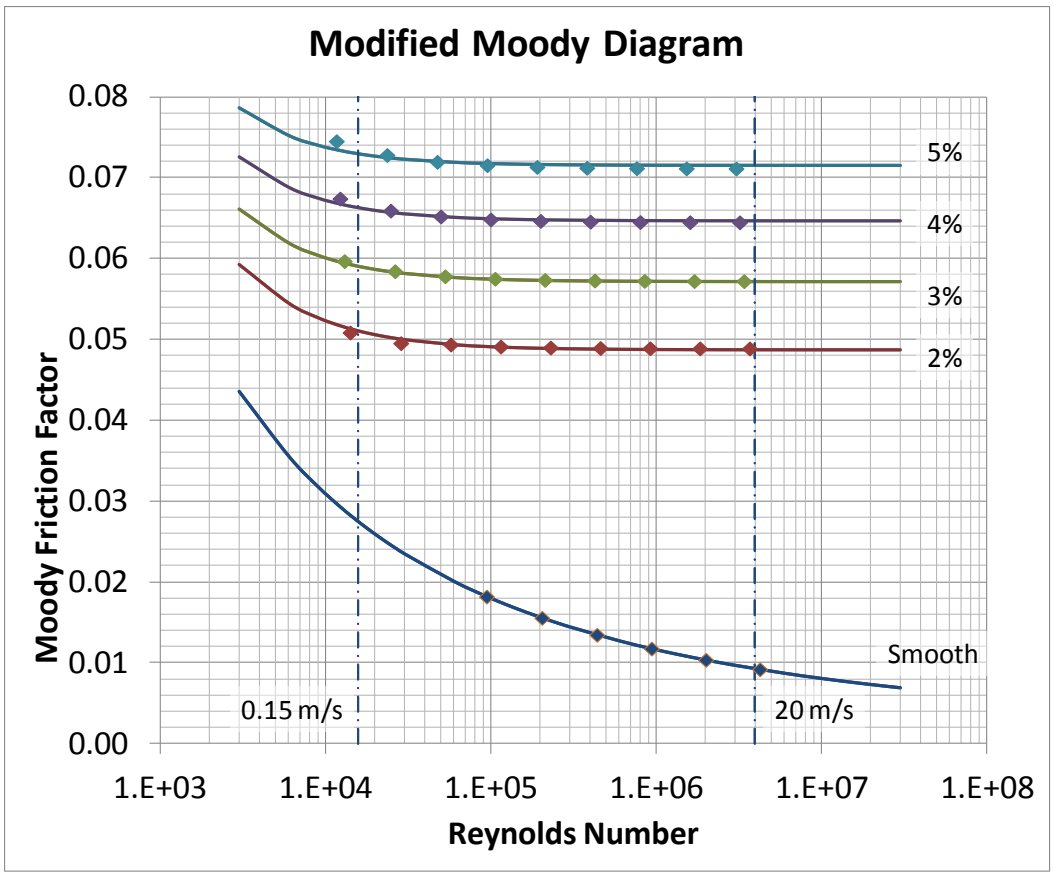

Figure 3-4 Comparison between achieved results and the Colebrook-White Equation

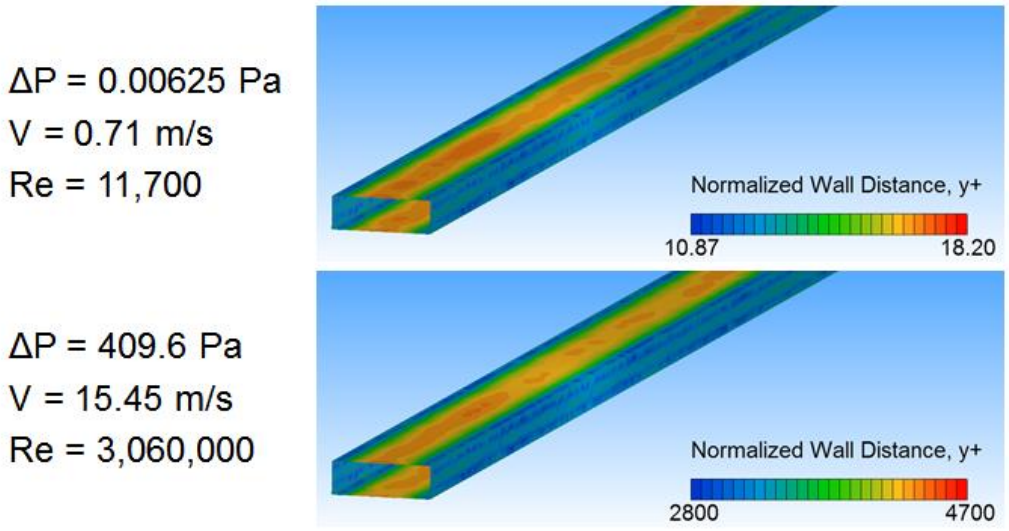

Figure 3-5 Example y^+ Verification

3.3.2 Network Model Development

Mine ventilation systems lend themselves to being represented by network models. Branches typically have regular entry dimensions, whether they are shafts from the surface, slopes, or entryways dedicated to ventilation. They often have high aspect ratios, with lengths often much greater than their heights, widths, or diameters. The high aspect ratios allow flows to become fully established in the entryways reinforcing the applicability of 1D models for flow and pressure. Along their lengths, opportunities for leakages are generally present where nodes would naturally be located. A simple representation of a portion of a MVS can be seen in Figure 3-6.

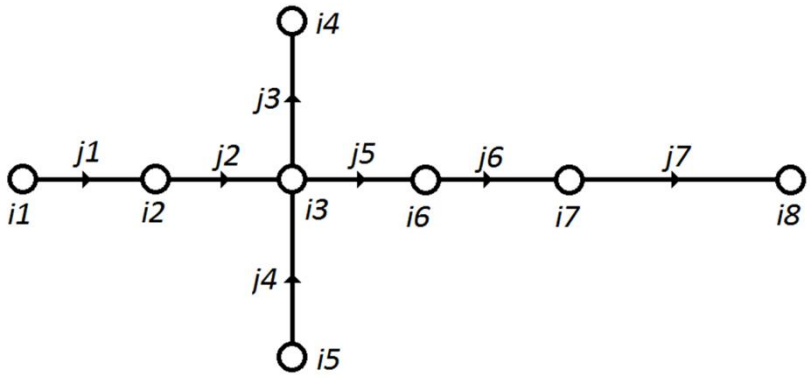

Figure 3-6 MVS as series of nodes and branches

The topology of the MVS can be readily represented with a directed incidence matrix as demonstrated in Figure 3-7. Within the incidence matrix, elements are defined as either 0 or ±1, depending upon details of the network topology. Each branch, *j*, has two connections, an inlet marked with +1 and outlet marked -1. Initial branch orientation is assumed from the design intent. Zeroes are used to denote no connection. Each node, *I*, has one or more connections for each branch connected at the point. From the directed incidence matrix, one can see that branch j_2 is connected to nodes i_2 and i_3, while node i_3 has four branches connected to it.

$$
\begin{array}{c} \\ i_1 \\ i_2 \\ i_3 \\ i_4 \\ i_5 \\ i_6 \\ i_7 \\ i_8 \end{array}
\begin{array}{c}
\begin{array}{ccccccc} j_1 & j_2 & j_3 & j_4 & j_5 & j_6 & j_7 \end{array} \\
\begin{bmatrix}
+1 & 0 & 0 & 0 & 0 & 0 & 0 \\
-1 & +1 & 0 & 0 & 0 & 0 & 0 \\
0 & -1 & +1 & -1 & +1 & 0 & 0 \\
0 & 0 & -1 & 0 & 0 & 0 & 0 \\
0 & 0 & 0 & +1 & 0 & 0 & 0 \\
0 & 0 & 0 & 0 & -1 & +1 & 0 \\
0 & 0 & 0 & 0 & 0 & -1 & +1 \\
0 & 0 & 0 & 0 & 0 & 0 & -1
\end{bmatrix}
\end{array}
$$

Figure 3-7 Directed incidence matrix corresponding to preceding figure

The solution algorithm for the network model was developed with certain goals in mind. A key goal of the effort was to develop time dependent boundary conditions for the CFD domain while in turn updating conditions in the network model. For this reason, it was necessary to develop a transient model to add value to the multi-scale approach. It was also necessary to track pollutant dispersion through the model to identify hazards and/or health issues that may arise due to methane, carbon monoxide, or other pollutant. While it was desirable to consider heat transfer between the flows and the walls and implement a compressible model for a certain class of problems, this was deemed outside the scope of this dissertation. This led to a number of simplifying assumptions.

- *Constant Density*
  For the purpose of this work, an incompressible model was implemented. The model included the necessary provisions to support a compressible mode of operation. For flow through the gob, there was no compelling reason to implement this feature.
- *Isothermal*
  The flow was modeled as an isothermal flow with no heat exchange to the walls.
- *Fully Turbulent*
  The flows are assumed to be fully allowing the use of the Atkinson equation to determine frictional pressure losses.
- *Dry Air*
  There is no water vapor exchange at the wall and flow interface.

- *Mixing at the Nodes*
  In the case of species concentration, perfect mixing occurs at the union between branches.
- *Advection Dominated Flows*
  With the flows assumed fully turbulent, the transport of species occurs primarily through bulk motion of the fluid. Diffusion is not considered.
- *Average Values*
  The values stored in branch locations are average values that prevail over the entire branch volume.

Using the directed incidence matrix, the continuity equations can be written in a compact matrix form. Furthermore, the implementation within Matlab was straightforward due to the way in which it handles matrices. The continuity of mass equation can be written as follows. Mass flows at the boundaries are introduced in the nodes, for both external boundary conditions such as the main intake or return shaft, as well as the coupled boundary conditions.

$$[A^T]\{\dot{m}\} + \{\dot{m_B}\} + \{\dot{m_{CP}}\} = 0 \qquad 3.13$$

Where

$[A^T]$	Transpose of directed incidence matrix
$\{\dot{m}\}$	Mass flow rate through branches
$\{\dot{m_B}\}$	Mass flow rate due external boundary conditions
$\{\dot{m_{CP}}\}$	Mass flow rate due coupled boundary conditions

In a similar fashion, the pressure drop through the branches in the MVS can be represented with the following form. The pressure drop occurs in the same direction as the flow.

$$\{\Delta p\} = [A]\{p\} \qquad 3.14$$

Where

$[A]$	Directed incidence matrix
$\{p\}$	Pressure at the nodes
$\{\Delta p\}$	Pressure drop across branch

The continuity of momentum equation was expressed as a finite difference in time. Likewise, the pressure loss due to friction was expressed as function of previous values for branch mass flows, using the Atkinson equation.

$$\left\{\frac{\dot{m}-\dot{m}^{o}}{\Delta t}\right\}=\left\{\frac{a'\rho}{L}\left(\Delta p+\rho\Delta Z+p_f-p_L\right)\right\} \quad 3.15$$

$$\{p_f\}=\left\{\rho R_t\left(\frac{\dot{m}^{o}}{\rho}\right)\cdot\left|\frac{\dot{m}^{o}}{\rho}\right|\right\} \quad 3.16$$

Where

$\dot{m}^{o}$	Mass flow rate through a branch at the previous time step
Δt	Time increment
a'	Cross-sectional area
ρ	Density
L	Length of the branch
ΔZ	Change in elevation between branch inlet and outlet
p_f	Change in pressure due to a fan source
p_L	Frictional pressure loss
R_t	Atkinson's Friction Factor in rational turbulent form

In order to solve the system of equations established for the network model, a set of recursive equations were established. First, the mass flow rate through the branches in Equation 3.15 was isolated with the following substitution.

$$\{\gamma\}=\left\{\frac{a'\rho\Delta t}{L}\right\} \quad 3.17$$

$$\{\dot{m}\}=\{\dot{m}^{o}\}+\{\gamma\Delta p+\gamma\rho\Delta Z+\gamma p_f-\gamma p_L\} \quad 3.18$$

At this point, Equation 3.14 may be substituted into Equation 3.18, which was then inserted into equation 3.13. This allows one to solve the resulting equation for the unknown nodal pressures, $\{p\}$, using values of branch mass flow at the previous time step. Since the equation for the unknown nodal pressure is now in terms of known values, the pressure at the nodes may be directly calculated.

$$[A^T]\{\dot{m}^o\} + [A^T][\gamma][A]\{p\} + [A^T]\{\gamma\Delta p + \gamma\rho\Delta Z + \gamma p_f - \gamma p_L\} + \{\dot{m}_B\} + \{\dot{m_{CP}}\} = 0 \quad 3.19$$

$$\{p\} = [M]^{-1}[A^T]\{-\gamma\Delta p - \gamma\rho\Delta Z - \gamma p_f + \gamma p_L - \dot{m}^o\} - [M]^{-1}\{\dot{m}_B + \dot{m}_{CP}\} \quad 3.20$$

Where

$[\gamma]$ Diagonal matrix containing elements from $\{\gamma\}$

$$[M] = [A^T][\gamma][A]$$

In order to solve the system of equations, a sufficiently small time step was chosen. Initial values for the problem take the form of branch mass flow rates that satisfy the continuity of mass equation. Equations 3.20, 3.14, and 3.18 are then applied in a loop, with the present value of the mass branch flows being updated at every cycle. When performing a steady state analysis, the system is considered to have converged when the changes become smaller than the allowable residual. The residual, as defined in Equation 3.21, is the sum of the absolute value of the change in branch mass flow from successive time steps.

$$Residual = \sum \left|\{\dot{m}\} - \{\dot{m}^o\}\right| \quad 3.21$$

A converged steady state solution provides the initial values for a transient solution. For such a problem, the same sets of equations are applied in nearly the same manner. Instead of continuing until convergence is reached, the solution proceeds with time-marching until the desired time is reached using successive iterations at the small time increment used previously.

Species concentrations values are stored within the branches. It is necessary to compute the concentrations at the nodes to determine the change in concentration within the branch. The average concentration in the node must take into account the directionality in the network; that is fluid flows in only one direction. The concentration in the node is only influence by those values in the upstream direction of the node and the average is weighted against the flow through the branches. The mass flow through the branch was previously solved, so this new value for mass flow is used to update the

species concentration to the same point in time. The finite difference formulation for species concentration is shown in Equation 3.22.

$$\left\{\frac{C - C^o}{\Delta t}\right\} = \left\{\frac{\dot{m}({C_N}^o - C^o)}{\rho V}\right\} \quad 3.22$$

Where

C	Species concentration
C^o	Species concentration of the previous time step
Δt	Time increment
$\dot{m}$	Mass flow rate through a branch at the current time step
${C_N}^o$	Average concentration at the branch inlet based on the previous time step, weighted by flow directed into the node
ρ	Density
V	Volume of a branch

Since the equation is in terms of all known values, the unknown branch species concentration can be solved. The equation to iteratively determine branch concentration is shown in Equation 3.23.

$$\{C\} = \{C^o\} + \left\{\frac{\dot{m}\Delta t({C_N}^o - C^o)}{\rho V}\right\} \quad 3.23$$

3.4 Coupling Scheme

The early design process for the coupling scheme included a set of trials with manual coupling between the network model and the gob model. The network code was modified to generate new input files to the gob model. While the CFD code generated coupling output data for import into the network model as per normal. The gob model was allowed to run to convergence before generating the input for the network model. These values were then used by the network model to produce the next set of input files for the gob model. An example of the data generated during this model can be

seen in Figure 3-8. Pressure data was generated by the network code while the flow data was produced by the gob model.

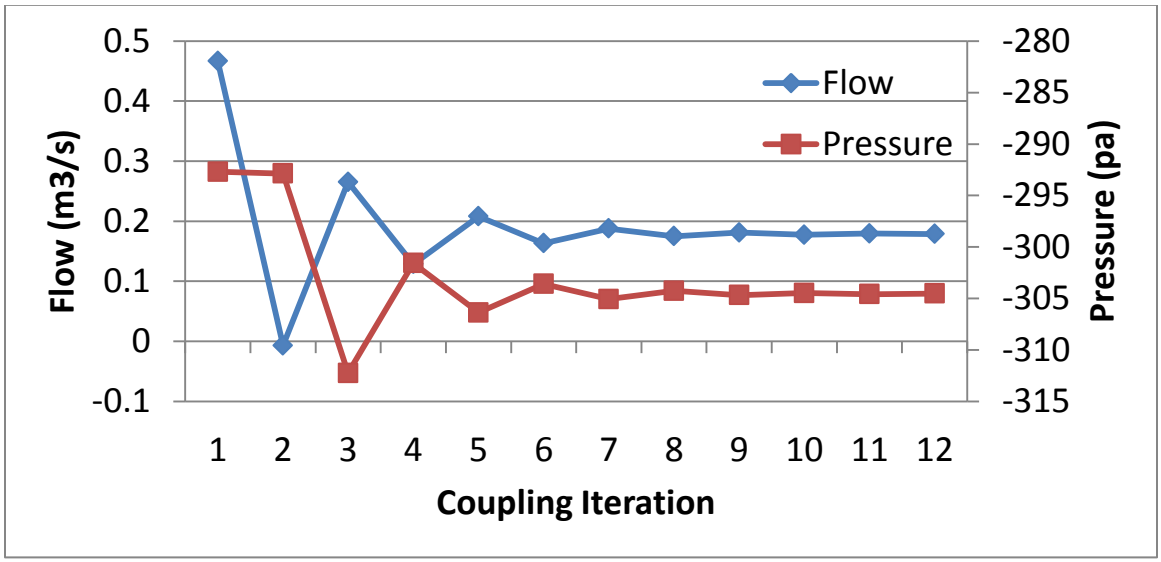

Figure 3-8 Manual exchange of variables at the headgate 1 coupling region

Convergence of the coupled model was judged by the exchange of flow from the Gob model to the network model. Equation 3.21 was used to calculate the unscaled residual for the model. The convergence was judged sufficient when the residual fell below 10^{-3} m^3/s. For this particular problem, the coupling proceeded smoothly to convergence after 13 iterations.

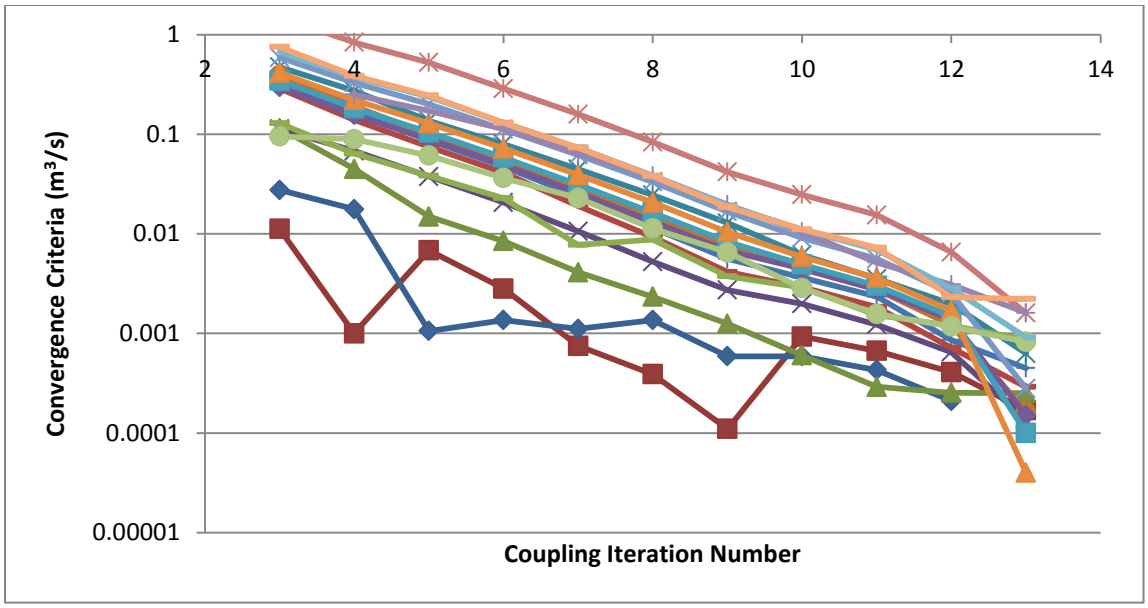

Figure 3-9 Iteration to steady state convergence with manual exchange of coupling information between network and gob models.

SC/Tetra does not provide user defined functions to manipulate the details of convergence criteria. Furthermore, only limited information from previous cycles can be retrieved with the available user defined functions. For this reason, the design of the coupling scheme was limited to either cycle number of elapsed time as a condition for exchanging information from SC/Tetra. Coupling by cycle number occurs when a steady state solution is sought. The elapsed time criterion is used for transient simulations.

3.5 User Defined Functions

SC/Tetra provides numerous user defined functions (UDFs) to enhance its capabilities. The standard user interface cannot anticipate every conceivable, detailed time or space dependent arrangement of physical properties and boundary conditions. SC/Tetra provides a range of user defined functions to support these cases. The vendor has supplied documentation and sufficient examples to aid the process of creating user defined functions. The UDFs were written in the C language and tested first on a Windows platform. The functions were later recompiled for Linux, with minor changes due to the manner in which the two systems handle file structures and handling text

and binary files. In each case, the complete listing of the code is included in the appendix, while a brief summary of the function appears in the following sections.

3.5.1 Coupled Boundary Condition

The coupled boundary condition UDF was developed to allow SC/Tetra to read in boundary conditions from the network model. The results of the CFD calculations are then used to generate new boundary conditions for the network model. The network model was developed in Matlab, so a neutral format for exchanging data had to be designed. It was also necessary to have a system that would operate independent of platform. The most direct route was the exchange of flat text files, in comma separated value format. This served the purpose of exchanging data, but also provided a record of the exchange for documentation.

The loose connection between the two models was implemented as a pair of producer – consumer loops. The Matlab loop would run, producing and consuming coupling data at its rate, while the SC/Tetra loop did the same. A token text file was passed back and forth to guard against race conditions. The Matlab loop would look for the presence of the CFD token file which signaled that new coupling data was available. It would then consume the data and produce a new set of boundary conditions for the SC/Tetra loop. Once the files were written, a Matlab token file was generated, and the Matlab loop would await a new CFD token file.

The Matlab token file signaled to SC/Tetra that data was available for import. SC/Tetra would import the data, but not apply it until the appropriate coupling criteria, either cycle number of elapsed time, had been met. Further, the SC/Tetra progress would not be interrupted in the event new Matlab data was unavailable. This was to ensure that the system could achieve steady state convergence after a prescribed number of coupling exchanges. As the Matlab loop runs more rapidly for steady state solutions, this proved a good solution to the problem of race conditions.

The implementation of the coupling boundary exchange presented a problem for transient solutions. There was some inherent overhead when dealing with reading and

writing files between two separate systems, Matlab and SC/Tetra. For this reason, the time penalty for conducting a perfectly synchronized coupled calculation was deemed too large. Instead, the solution for transient problems, was accomplished with asynchronous coupling, where a prescribed time interval, such as 30 seconds, was used to set the criteria for exchanging boundary information. Other time intervals were possible and were tested, extending down to 0.3 seconds.

The coupling UDF was spread over several user functions in SC/Tetra. In general, the coupling UDF performed tasks one time during the initialization phase and at the end of the final cycle. It also completed tasks during the beginning and end of every cycle. During the usu_init() function, the upfront memory management for the suite of UDFs was performed. Memory was allocated to the variables for pressure and species boundary conditions. Files for the output from SC/Tetra to Matlab were opened with headers printed to them.

During the calculation, tasks were performed at the beginning and end of every cycle with a call from the usu_cycle_start() function. Specifically during the very first cycle and at every cycle meeting the coupling criteria, the coupling UDF would raise a flag signaling that a coupling exchange should be performed. At the same time, the coupling UDF checked for the presence of the token file from Matlab. With both conditions true, the coupling UDF would then read in the coupling data from the appropriate files for pressure and species concentration. Error handling and condition monitoring were established and reporting occurred to the SC/Tetra log file. Before the function call finished, additional details were written to the SC/Tetra output coupling files, including cycle number, timestep and elapsed time.

The data written to the SC/Tetra output coupling files were generated with reporting functions. Data would only be recorded to the coupling files when the coupling flag was set to true. The first was usl_chkf_flxio(). This reported the mass flux through particular surfaces mentioned in the CHKF command in the SC/Tetra input file, in the same order in which they are listed in that input file. The concentration of species at the coupling

boundaries was reported with the usl_chkc_flxio() function. This command records the mass flux of a particular species across a control polygon, using the CHKC command in the SC/Tetra input file. Control polygons had to be generated for every coupling boundary. Care was taken to ensure that the control polygon was properly directed to the boundary and completely encompassed the cross sectional area of the coupling boundary. In the next chapter, one will observe the small extrusions added to the gob geometry. This control polygon implementation necessitated the addition of those features.

The usu_cycle_end() function was called at the end of every cycle. Provided the coupling flag was found to be true, the function would then append a newline character to the file and lower the coupling flag. A CFD token file was generated to inform the Matloop that data was available. During this cycle, the function would also then raise a flag signaling that the Matlab token file was ready to be destroyed at the very beginning of the next cycle. Because SC/Tetra is an MPI enabled program allowing large scale parallel activity, each of the threads would arrive at cycle start and end at different times. Any interaction with the file system had to be limited to the root process, prl_root equal to 0, thus the need for strict protocols for file creation, destruction, and text output.

Memory was managed during usu_final(). Allocated memory was freed to prevent memory leakage.

3.5.2 Gob Permeability

The gob permeability UDF was developed to implement the pressure loss function modeled by Darcy's law with variable permeability throughout the gob. Due to limitations in the porous media model in SC/Tetra, Darcy's law was implemented with a general body force. The UDF was implemented with a combination of the usr_forc() reading function and the use_forc() setting function in SC/Tetra. The first function is called once during the solution routine, prior to initialization of the problem. The

second function is called at every cycle, for every element in the domain. For this reason, care was taken to minimize computation time.

The first portion of the UDF reads in the details of the surface fit from Matlab, such as the surface seen in Figure 3-10. The example shown is a poly55 fit from the Matlab Curve Fitting Toolbox. It models the permeability data as a fifth order polynomial in the following form.

$$\text{poly55: } Z = p00 + p10x + p01y + p20x^2 + p11xy \ldots p14xy^4 + p05y^5 \qquad 3.24$$

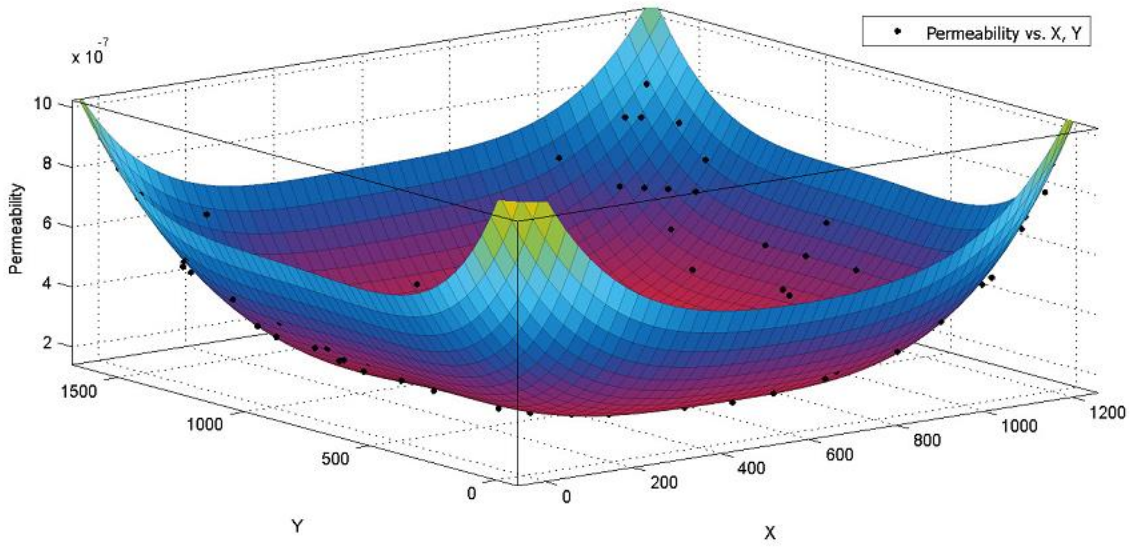

Figure 3-10 Gob permeability surface fit

With the UDF as designed, the permeability varied along the length and width of the panel. It was unchanging along its height. The results from the FLAC3D models that generated this data were not capable of predicting changes in permeability in the vertical direction.

After reading in the coefficients of the surface fit using usr_forc(), the values were used in the use_forc() function. During the first cycle, the coefficient for the body force was calculated for every element. The results of this calculation are retained for subsequent cycles since the values do not change during the simulation. This prevented needless

computation and a waste of CPU time, as the values can be merely applied at every subsequent cycle.

3.5.3 Gob Explosibility

The gob explosibility UDF was developed to provide a way to identify the hazard due to the current composition of the gob. It involved assigning values to the nodes in the gob region according to the colors in the Coward's Triangle as shown in Figure 3-11. The values were chosen from 0 to 1, and correspond to a specially selected "reverse" colorbar available in SC/Tetra.

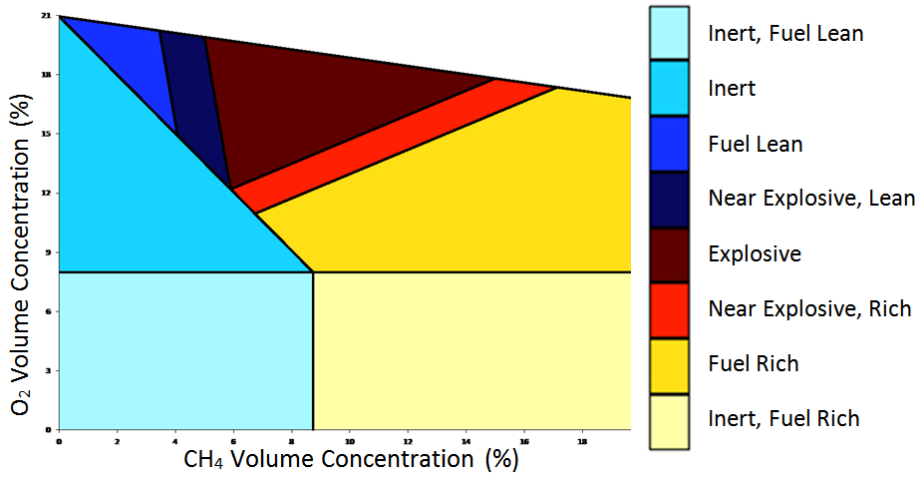

Figure 3-11 Gob explosibility color coding using Coward's Triangle

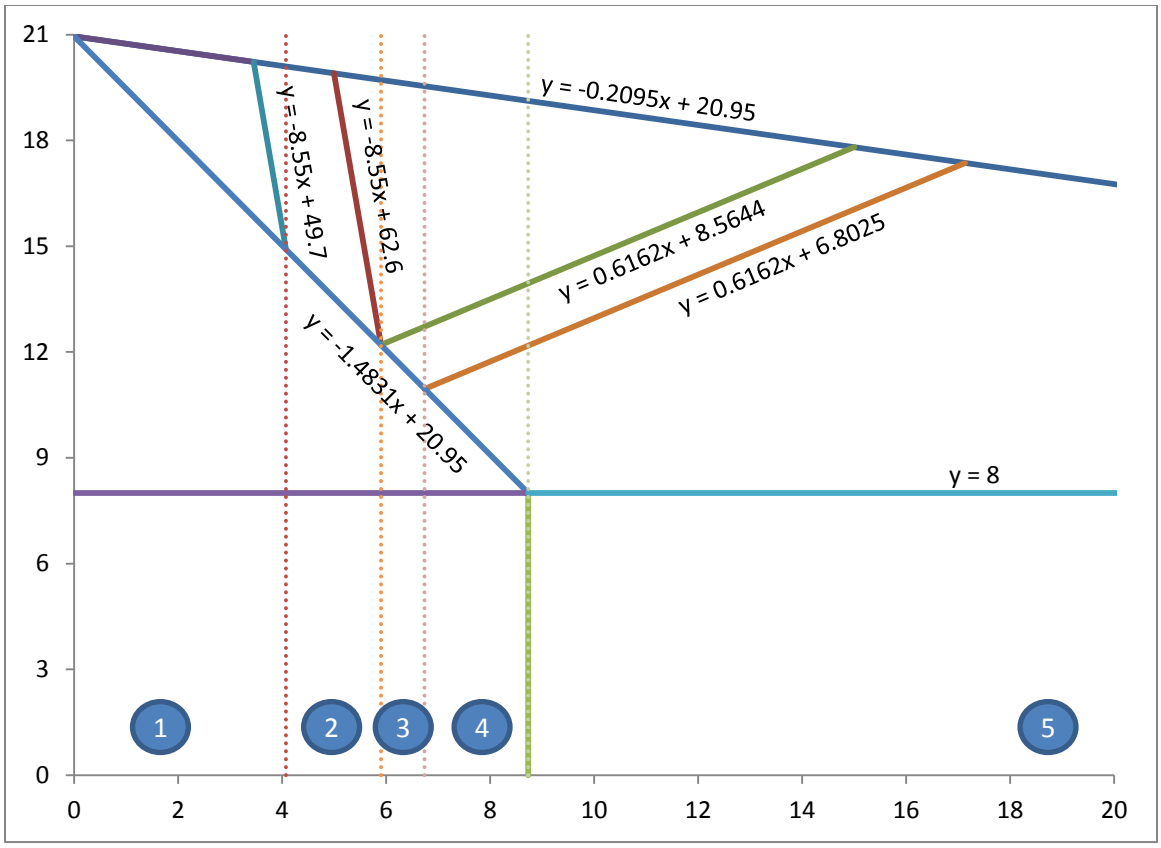

Figure 3-12 Details of gob explosibility color determination based on threshold operations

The calculation of the gob explosibility UDF was handled with the usu_fld_scalar_out() user function, which was called at the end of every completed cycle. In a loop that spans the number of nodes in the CFD domain, it began by determining the volume concentration of O_2 and CH_4 at a node. These values were used to find exactly which color the node should be assigned. The methane concentration determined which region of the chart in Figure 3-12 should be used, regions 1 through 5. Depending upon the region of the chart, appropriate thresholds values were calculated for that zone. Comparing the oxygen concentration level to the thresholds determined which color to assign. The gob explosibility UDF was calculated at the completion of every cycle in SC/Tetra. In this way, the evolution of hazard in the gob was evaluated during transient simulations. An example of the output of the gob explosibility can be seen in Figure 3-13.

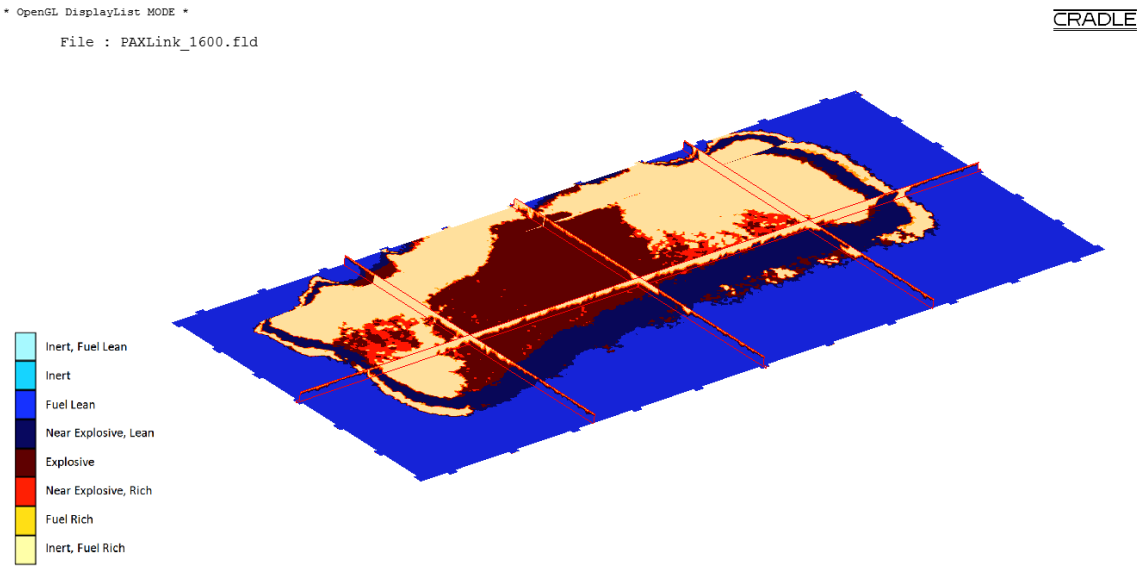

Figure 3-13 Example of the output of the gob explosibility UDF identifying regions containing potentially explosive mixes of air.

4 Steady State Modeling

4.1 Longwall Mine

The longwall mine used for this study is a property located in south western Pennsylvania which is working in the Pittsburgh seam. It was the site of comprehensive examination of the ventilation network in 2010 by a research team from NIOSH. Tracer gas studies were conducted to determine airflow rates through the inaccessible gateroads that make up the bleeder system surrounding the mined out portion of the longwall panel. The bleeder areas were characterized by unstable roof conditions which pose too great a hazard to miners and researchers. This prevented direct measurements in these locations. A tube sampling system was established in the bleeder system to allow indirect sampling through the use of the tracer gas, sulfur hexafluoride (SF_6) (Krog, Schatzel, and Dougherty, 2011). The mine map can be seen in Figure 4-1. The study was chosen due to the accuracy of the resulting network model of the longwall panel.

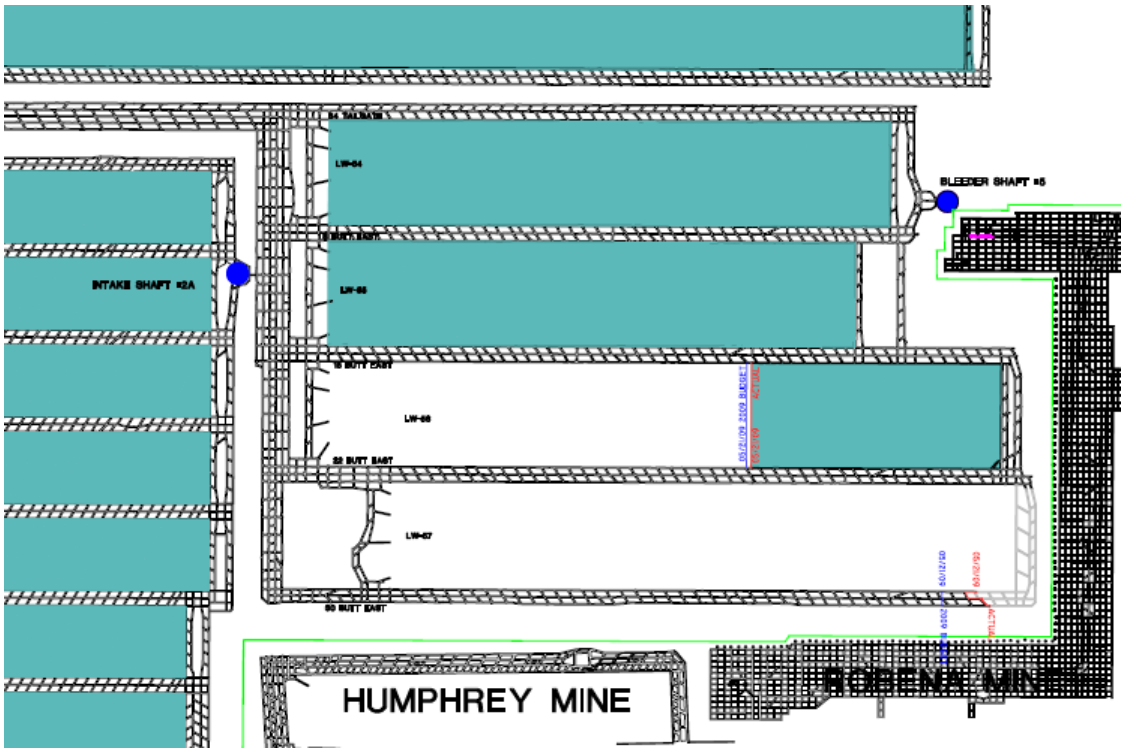

Figure 4-1 Longwall district layout for the gob modeled (Source: Trackemas, 2014)

With the results of the tracer gas study, a network model of the longwall panel was prepared. In addition to the entries dedicated to intake, neutral, and return entries, it included branches dedicated to flow through the gob and the surrounding bleeder entries. This network model was calibrated against measurements taken during the tracer gas study along with ventilation surveys through the accessible portion of the mine as shown in Figure 4-2. A CFD model of the gob was prepared by the same authors that conducted the tracer gas study. It included the gob and branches immediately adjacent to the gob. The model used a two zone model for the gob with estimates for the gob permeability drawn from literature.

Conversations with the researchers at NIOSH yielded additional information about the mine. A portion of the network model was provided to serve as a starting point for the development of a multi-scale ventilation model as seen in Figure 4-3. Methane liberation rates to the longwall district were also provided. At this mine, the bleeder fan liberated between 1.4 and 1.6 million cubic feet of methane per day. The mine also employed gob vent boreholes to provide post mining drainage. The first borehole was generally offset 500 feet from the setup room and spaced every 2,000 feet afterwards. The row of boreholes typically fell between 250 and 300 feet from the tailgate entries.

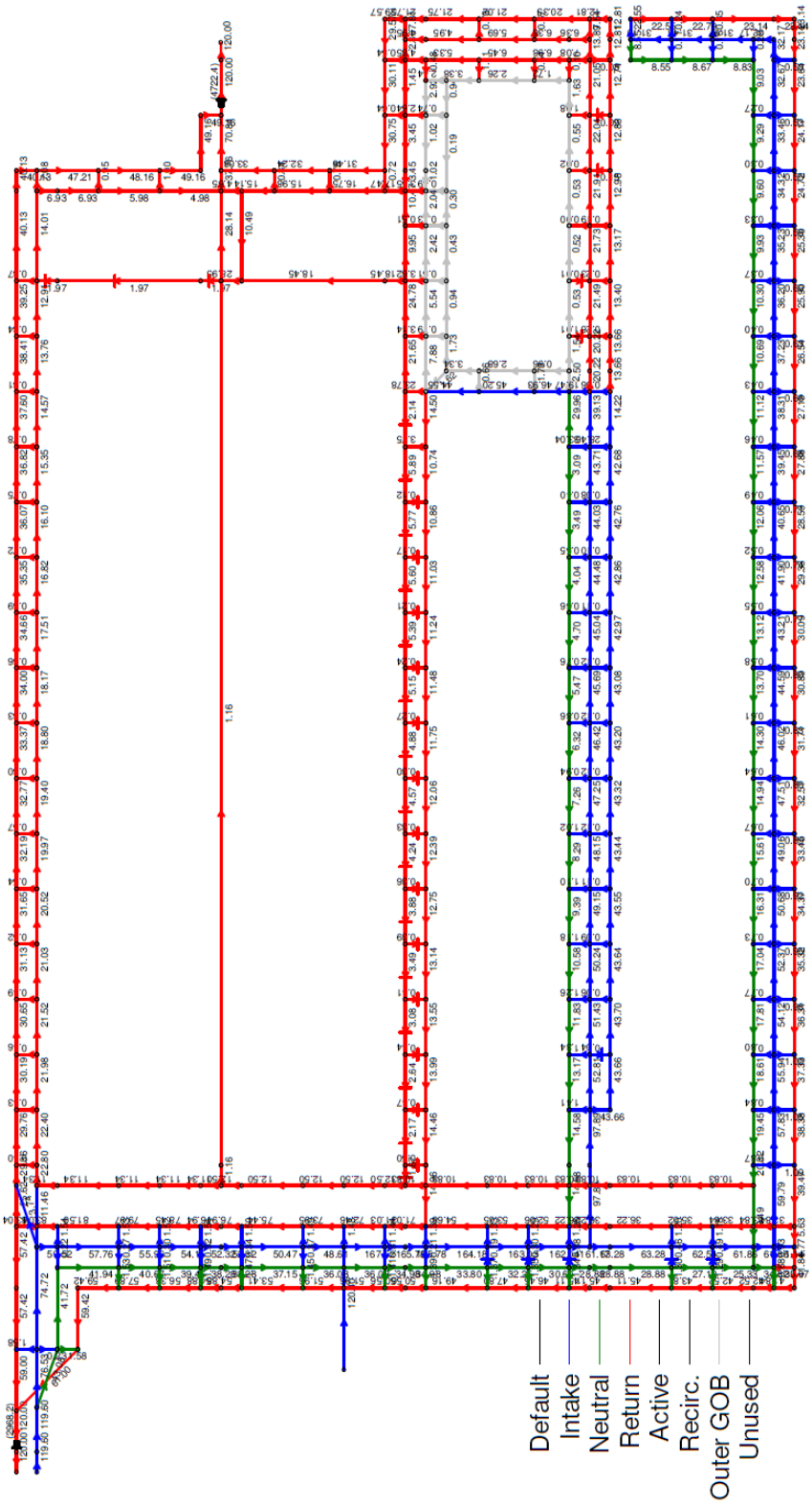

Figure 4-2 Longwall district network ventilation model (Source: Krog, 2014)

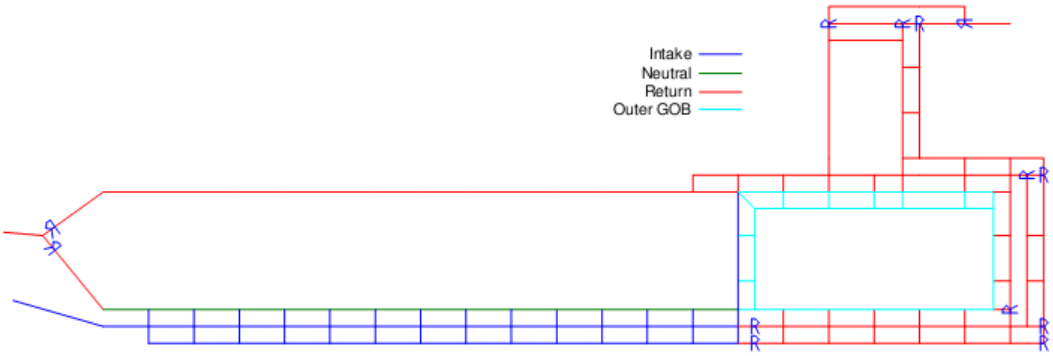

Figure 4-3 Longwall panel network ventilation model (Source: Krog, 2014)

4.2 Multi-Scale Ventilation Model

4.2.1 Gob model

Geometry for the Gob model was prepared in the Pro/ENGINEER CAD package. The panel width for this study was 420 meters with a planned length of 2,650 meters when completely mined out. At the time of the tracer gas study, the gob portion was approximately 1,035 meters in length. The height of the model was set at 12.5 meters, based on the expected caving height and previous gob modeling efforts in the literature. This yielded a volume of 5.4 million cubic meters. The geometry included protrusions representing the connection between the gob and the surrounding bleeder entries. These connections served two important roles later in the modeling. First, they established a clear section through which the coupling exchange of air could occur. Control polygons were required to monitor the passing of diffusive species. These entries served to isolate the polygons from the body of the gob. The second major purpose is to aid meshing. Prism layers are generally expected at the boundary of porous media and aid in the convergence of the model. By introducing these entryways, the SC/Tetra meshing routine was consistently able to add high quality prism layers at this boundary between the network model, and the porous region representing the gob.

The entries were 12.5 meters wide by 2.5 meters high and extended 5 meters normal to the surface to which they were attached, as seen in Figure 4-4.

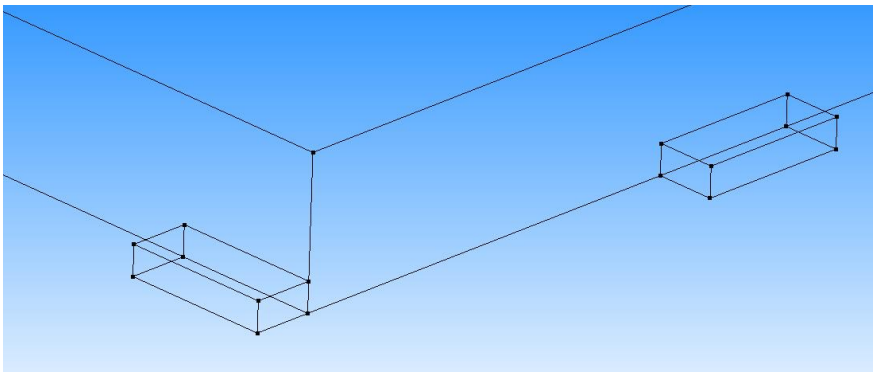

Figure 4-4 Wireframe detail of coupling entryways

Methane inflow was introduced as a uniform volumetric flow into the gob region from the upper surface. The quantity of methane was established from the details provided by the mine operator along with knowledge of typical mining practices. According to the mine operator, the bleeder fan liberated between 1.4 and 1.6 million cubic feet of methane per day, which equals 0.492 m^3/s and a resulting methane concentration in the bleeder shaft of 0.8%. Not all of the methane reporting to the bleeder fan comes from the gob, much of the methane is liberated at the face. Methane generation at the face is limited to concentrations below 1.0%. Production is interrupted if this threshold is passed. Assuming that the operator maintains an average concentration just below this threshold at 0.7%, 0.262 m^3/s would come from the action of the longwall shearer and from the coal on the face conveyor. Of this amount of methane, 24% reports to the return airways and should not be included in the quantity of methane reporting the bleeder shaft. The remaining 0.293 m^3/s of methane was assumed to be distributed equally by area across the two worked out panels in the district and the area of the active gob. The result was a conservative value of 0.122 m^3/s of methane introduced into the active gob.

The permeability in the gob was modeled in two different ways. The first model included an elementary two zone gob model, an inner and outer gob. The outer gob

represents the more loosely compacted material at the perimeter of the gob, near the pillars. The interior, in the case for supercritical panel widths, supports the weight of the overburden causing it to suffer greater compaction. The permeability of the inner gob was higher relative to the outer gob. The outer gob consisted of the first 50 meters of gob around the perimeter. This two zone model can be seen in Figure 4-5.

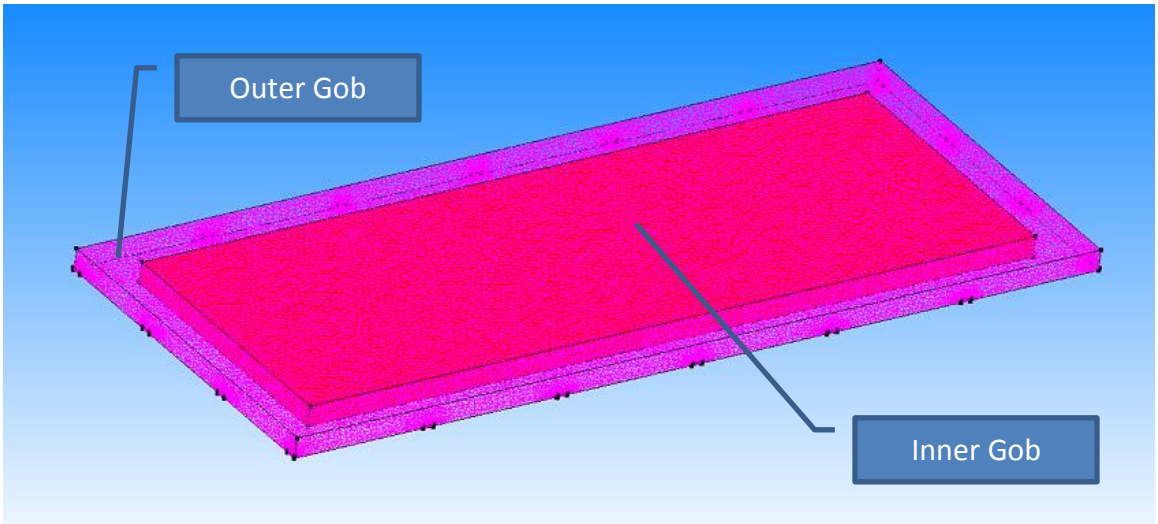

Figure 4-5 3D Gob model using 2 zone to represent the permeability distribution within the gob

The second manner in which permeability was implemented consisted of applying a continuously varying surface to the gob zone. Permeability data was drawn from literature and imported into Matlab. The built in curve fitting tool was applied to the data to achieve a polynomial surface fit. The resulting equation was then used to calculate the permeability at the various locations in the gob. As discussed during the section concerning UDFs, the permeability is invariant along the vertical direction. A contour plot used in the model can be seen in Figure 4-6.

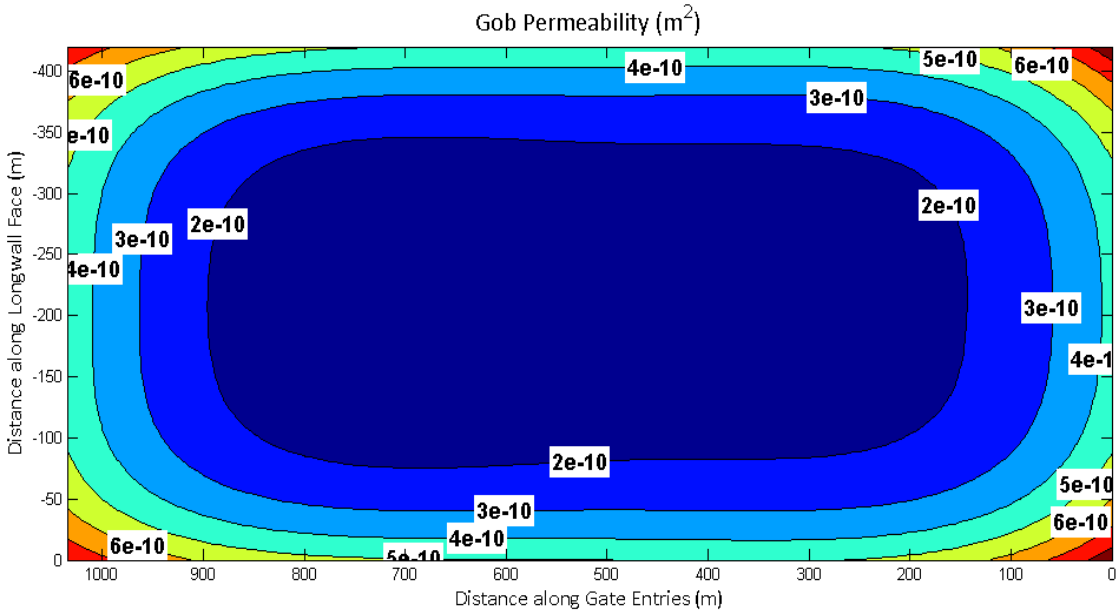

Figure 4-6 Gob permeability contour plot of the surface fit obtained (Adapted from: Esterhuizen and Karacan, 2007)

The output from the Matlab Curve Fitting Toolbox can be seen below, in Table 4-1. It is a fit of permeability versus x and y location within the gob. The goodness of fit statistics are presented there as well. The model had an R-square value of 0.9835 and a standard error of regression of 2.507e-11, which was judged sufficient for the model. The quality of this fit can be attributed to the source. It was based upon the output of FLAC3d numerical modeling with inputs that were homogenous. The result is the smooth contour seen in Figure 4-6.

Table 4-1 Output from the Matlab Curve Fitting Tool showing the resulting equation for the gob permeability surface fit

Linear model Poly55

$$f(x,y) = p00 + p10*x + p01*y + p20*x^2 + p11*x*y + p02*y^2 + p30*x^3 + p21*x^2*y + p12*x*y^2 + p03*y^3 + p40*x^4 + p31*x^3*y + p22*x^2*y^2 + p13*x*y^3 + p04*y^4 + p50*x^5 + p41*x^4*y + p32*x^3*y^2 + p23*x^2*y^3 + p14*x*y^4 + p05*y^5$$

where *x* is normalized by mean -205.6 and std 162.3
and where *y* is normalized by mean 485.3 and std 379.3
Coefficients (with 95% confidence bounds):

p00 =	1.37e-10	(1.105e-10, 1.635e-10)
p10 =	8.676e-12	(-2.849e-11, 4.585e-11)
p01 =	-3.962e-11	(-7.639e-11, -2.845e-12)
p20 =	2.729e-11	(-1.118e-11, 6.575e-11)
p11 =	1.11e-12	(-1.734e-11, 1.956e-11)
p02 =	-5.58e-11	(-8.895e-11, -2.266e-11)
p30 =	3.236e-12	(-5.685e-11, 6.333e-11)
p21 =	4.282e-11	(6.685e-12, 7.895e-11)
p12 =	-3.749e-12	(-3.48e-11, 2.73e-11)
p03 =	2.14e-11	(-2.754e-11, 7.034e-11)
p40 =	1.127e-10	(9.47e-11, 1.307e-10)
p31 =	6.156e-13	(-1.04e-11, 1.163e-11)
p22 =	1.634e-11	(-1.023e-13, 3.278e-11)
p13 =	-1.448e-12	(-1.118e-11, 8.281e-12)
p04 =	1.208e-10	(1.051e-10, 1.366e-10)
p50 =	3.373e-12	(-2.343e-11, 3.017e-11)
p41 =	-4.161e-12	(-2.191e-11, 1.359e-11)
p32 =	4.016e-12	(-1.396e-11, 2.199e-11)
p23 =	-3.494e-11	(-5.642e-11, -1.346e-11)
p14 =	-1.55e-12	(-1.36e-11, 1.05e-11)
p05 =	-1.468e-11	(-3.528e-11, 5.92e-12)

Goodness of fit:

SSE: 4.27e-20
R-square: 0.9897
Adjusted R-square: 0.9875
RMSE: 2.143e-11

With the boundary conditions for pressure and species inflow concentration set by the coupled boundary, the remaining inlet condition to the Gob model was the turbulence condition. SC/Tetra allows two options for setting turbulence properties at boundaries. The values of κ and ε, or ω where appropriate, can be set directly. The other manner is

to set a turbulence intensity and turbulent viscosity ratio, which was the chosen method. Turbulence intensity is the ratio of the root mean square value of the turbulent velocity fluctuations to the free stream velocity as a percent while the turbulent viscosity ratio is the ratio of turbulent to laminar viscosity.

$$T_u = \frac{u'}{\bar{u}} \quad [\%] \tag{4.1}$$

$$\beta = \frac{\mu_t}{\mu} \tag{4.2}$$

Values for the turbulent inflow properties were unavailable from the network model. The estimations were based upon the suspected conditions at those coupled boundaries. They are generally very low speed ventilation flows approximating pipe flow with a Reynolds number ranging from 1,850 to 7,000, so a turbulent intensity of 0.5% with a turbulent viscosity ratio of 50, were selected.

4.2.2 Network Model

The network model was provided by the research team at NIOSH. The choices for friction factors for the entryways can be seen in Table 4-2. These values are typical for coal mine entryways and were drawn from the Harman ventilation text (1997). The resistance for stopping was set to 5,000 Ns^2/m^8. Along the gateroads, crosscuts were grouped in threes to sensibly reduce the number of branches in the model. The gob portion was modeled as a branch with large cross sectional area, but with a very high friction factor. Values for the regulator resistances were based upon survey data. Most importantly, the model was validated against the tracer gas study, as well as a ventilation survey of the areas that were accessible.

Table 4-2 Friction factors used in network model

Friction Factors	kg/m^3	$lbf \cdot min^2/ft^4 \times 10^{-10}$
Intake Entries	0.0075	40
Return Entries	0.0087	47
Belt Entries	0.0106	57
Longwall Face	0.0180	97
Cribbed Tailgate Entries	0.0680	367
Gob Zone	1.0000	5391

4.2.3 Coupling Scheme

The next step was to choose the regions for the coupled exchange of boundary conditions. Initial choices for the boundaries were based upon the existing structure of the network. There were nodes present in the network already connected to its simplified gob branches. These nodes were the initial choices for the coupling regions, as seen in Figure 4-7. Coupled regions along the longwall face were prefaced with LW. Those along the headgate entries were labeled with HG, likewise with the tailgate entries and those along the start-up room. Numbering of the regions started from the headgate side, increasing to tailgate side and from longwall to start-up room. A total of 18 regions were identified to exchange coupling data.

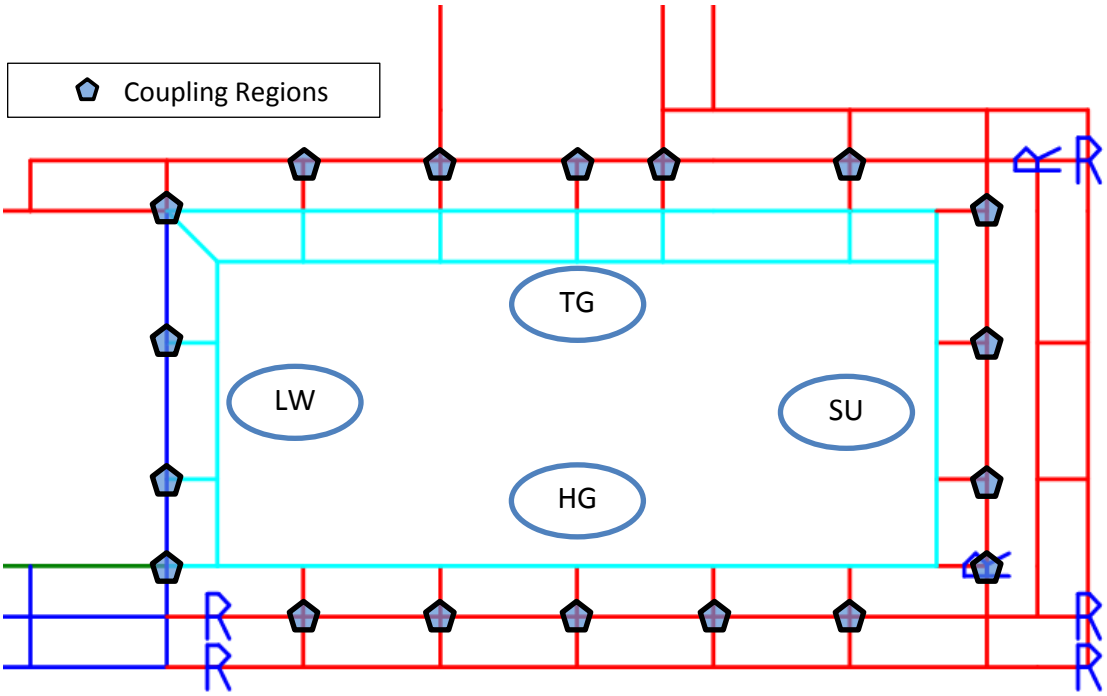

Figure 4-7 Locations for the 1D network coupling regions

Complementary coupling regions were added to the 3D model. The coupling regions are represented in the 3D model as short protrusions from the body of the gob. This was necessitated by the need for clear control polygons to measure the flux of species through the coupled boundaries. A free slip wall condition was applied to the walls of these coupling regions. A detail of this can be seen in Figure 4-8.

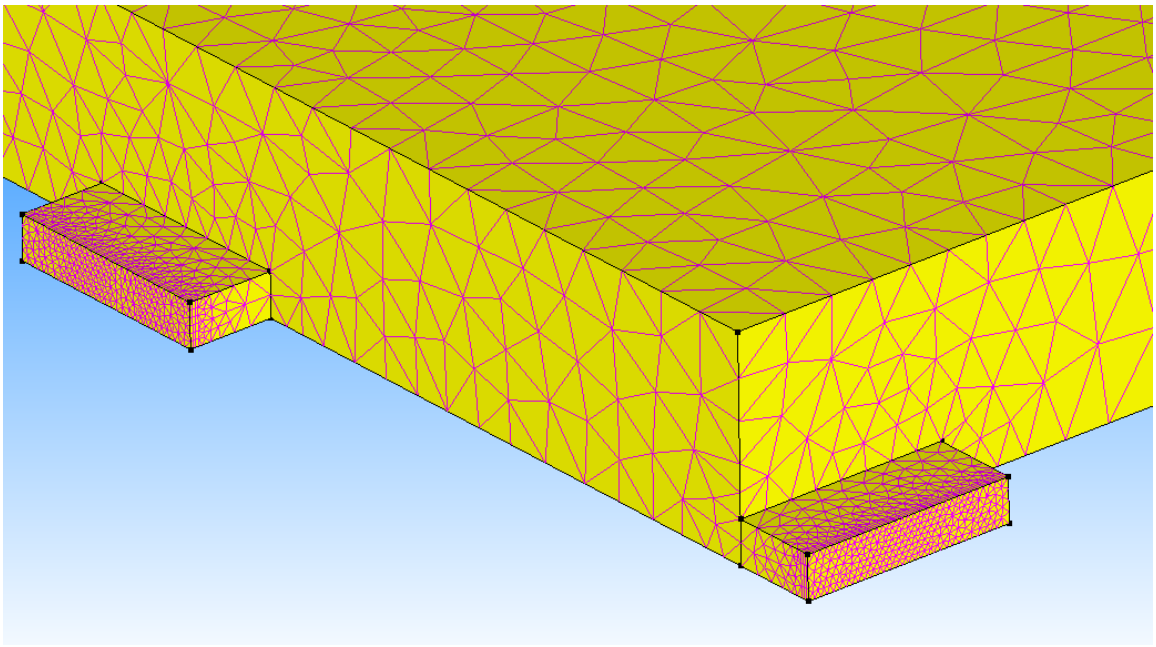

Figure 4-8 Protrusion representing the 3D coupling region in the gob model

4.3 Results and Discussion

4.3.1 Mesh Independence Results

A study to establish mesh independence was completed early in the research. This provided the guidance for meshing choices in later studies. Details such as base octant size and prism layer selections were varied to determine the influence of the mesh upon the final solution. The desired result is to establish a set of guidelines that would result in a mesh that did not influence the final solution commonly referred to as grid independence. During the course of the study, element quality was monitored to ensure an appropriate average h-ratio was achieved. The h-ratio, a measure of mesh quality, is the ratio of the radii of the inscribed sphere and the circumscribed sphere of a tetrahedral element. The maximum h-ratio is 0.33, for a regular tetrahedron. The minimum target h-ratio was greater than 0.27. The mesh independence study began with a relatively coarse mesh and continuing refining until the solution was found to be independent of the mesh. Details of the meshes examined are summarized in Table 4-3.

Table 4-3 Levels of mesh refinement used for mesh independence study

		Mesh Independence Levels				
		1	2	3	4	5
Maximum Octant Size	(m)	5	4	3	2.5	2
Inlet Region Octant Size	(m)	0.5	0.4	0.3	0.25	0.2
Inlet Prism Layer Size	(m)	0.25	0.2	0.15	0.125	0.1
Inlet Prism Layer Count		3	3	3	3	3
2 Zone Gob Prism Layer Size	(m)	1	0.8	0.6	0.5	0.4
2 Zone Gob Prism Layer Count		2	2	2	2	2
Total Element Count		373,769	527,988	800,385	1,475,053	2,391,270
Total Node Count		94,295	130,617	205,664	354,556	570,953
Average h-Ratio		0.2733	0.2758	0.2712	0.2752	0.276
Computation Time (1,100 Cycles)	(s)	555	822	1,359	2,487	4,773

The response variables for the mesh independence study were based on the desirable parameters of a gob bleeder system. The principle factor was termed the gob participation value. This represents the volumetric flow into the gob, which is useful for bleeding the gob area. This was further broken down in the four sides of the model, showing participation across the longwall face, gate entries, and start up room. The results from this are summarized in Table 4-4.

Table 4-4 Flow response to mesh independence study

		Flow Response to Mesh Independence Levels				
		1	2	3	4	5
Gob Participation	(m^3/s)	5.08	4.04	3.94	3.69	3.61
Gob Participation	% *diff*	33.8%	11.2%	8.7%	2.2%	
Longwall Face Participation	(m^3/s)	2.45	2.37	2.49	2.35	2.30
Longwall Face Participation	% *diff*	6.3%	3.0%	7.9%	2.2%	
HeadGate Participation	(m^3/s)	1.65	1.34	1.40	1.29	1.27
HeadGate Participation	% *diff*	26.0%	5.4%	9.7%	1.6%	
Tailgate Participation	(m^3/s)	2.17	2.03	2.10	2.07	2.05
Tailgate Participation	% *diff*	5.7%	-1.0%	2.4%	1.0%	
Start Up Room Participation	(m^3/s)	3.90	2.34	1.89	1.66	1.61
Start Up Room Participation	% *diff*	83.1%	37.0%	16.0%	3.1%	

The performance of the mesh for levels one and two were deemed unacceptable. The percent difference from the level five fine mesh was too significant to consider, with participation values varying by as much as 80% from the fine mesh results. The level three mesh was marginal. Results, with the exception of the start-up room boundaries,

were within 10% of the fine mesh results, while needing only 28% of the computation time. The fourth mesh was chosen from this study. Results were, on average, within 2% of the fine mesh results in roughly half the time to complete the same number of cycles.

The resulting methane distribution within the gob was the next criteria for gaging the performance of the meshes. The distribution of methane for the level 4 and level 5 meshes can be seen in Figure 4-9 and Figure 4-10, which demonstrated only minor observable differences.

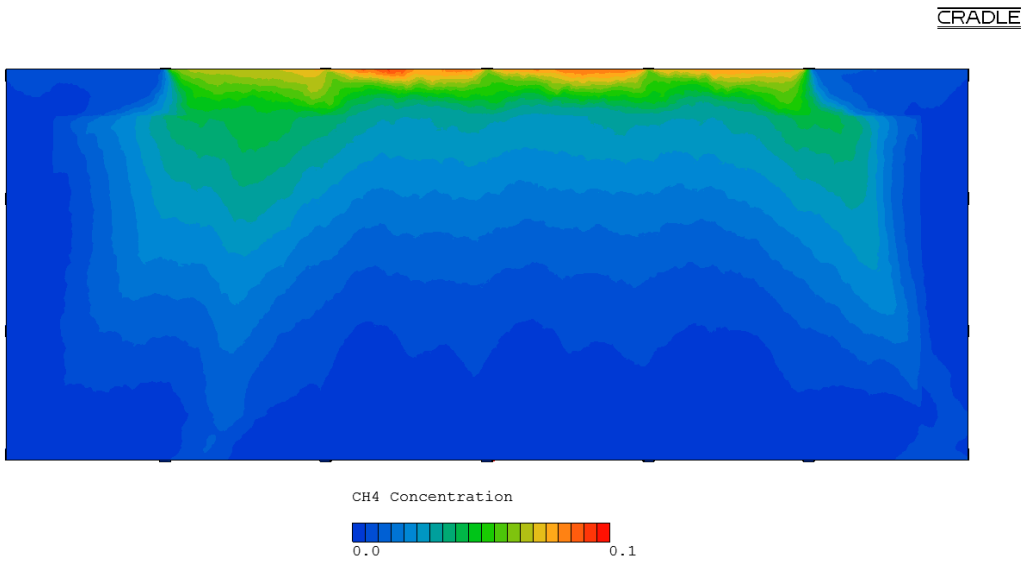

Figure 4-9 Methane concentration within the gob at a 1 meter height for the level 4 mesh

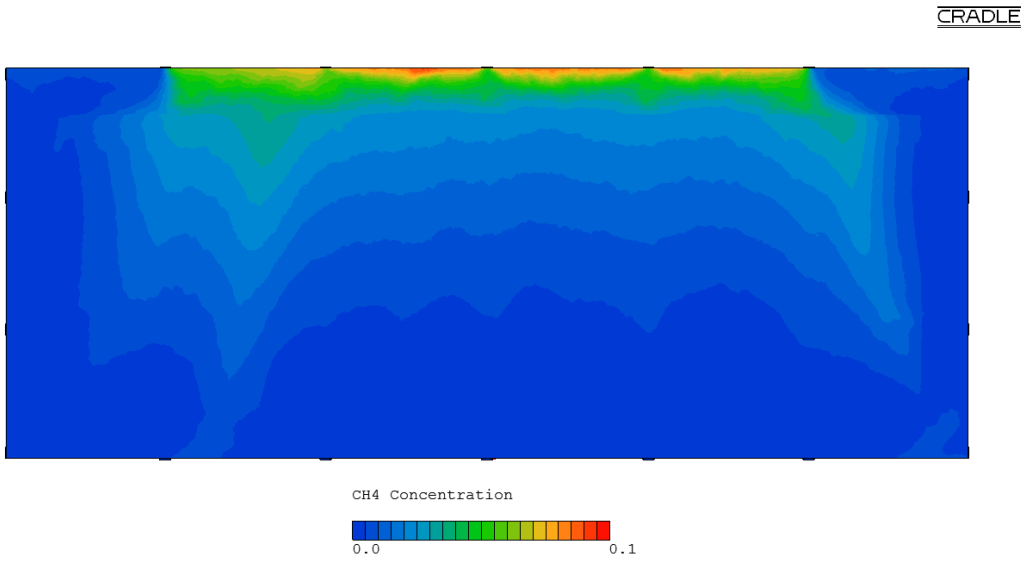

Figure 4-10 Methane concentration within the gob at a 1 meter height for the level 5 mesh

The final selection for meshing parameters was selected as the level 4 mesh from the grid independence study. This was deemed the appropriate balance between accuracy and computation time. For the majority of subsequent studies, the level 4 meshing parameters were used, unless stated otherwise. The level 4 mesh can be seen in Figure 4-11 along with the element quality distribution in Figure 4-12.

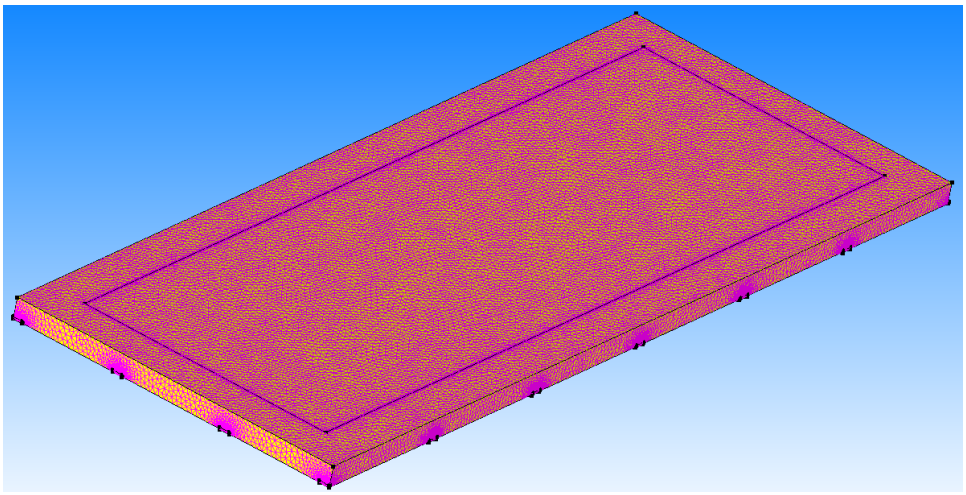

Figure 4-11 Level 4 mesh chosen from the mesh independence study for the 2 zone gob model

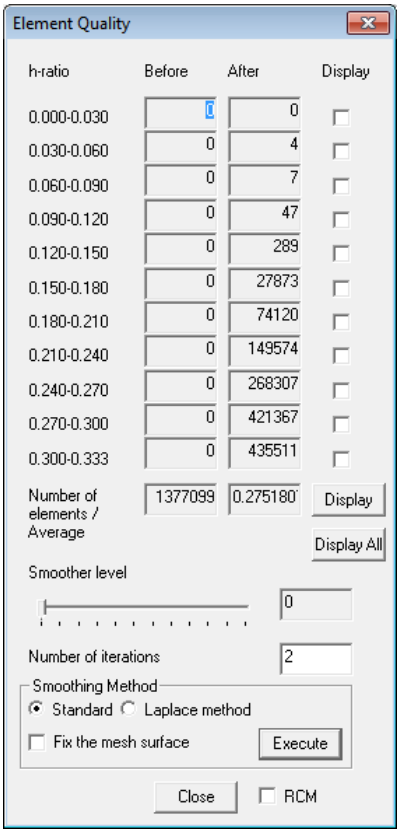

Figure 4-12 Mesh quality distribution for the Level 4 mesh chosen from the mesh independence study for the 2 zone gob model as reported by SC/Tetra

4.3.2 MSVM Coupling Performance

The grid independence study was also used to judge the performance of the coupling boundary convergence. The coupled model was run past the point when SC/Tetra considered the model to have converged. With uncoupled or standard pressure boundary conditions, the model would tend converge after approximately 220 cycles. The model was instead run for 20 iterations of coupling, at an interval of 50 cycles, with an additional 100 cycles for the Gob model to come to convergence after completing the coupling routine. This means the Gob model ran for a total of 1,100 cycles in each trial. To prevent early convergence, the criterion for one of the species concentrations was set unrealistically stringent. Final convergence of the Gob model was judged manually by examining the steady state status, to ensure that the convergence was met.

The network model ran for a total of 20 times; each time convergence was achieved before generating new coupling data for the Gob model. The data exchanged at the coupling boundary for pressure, total flow, and methane flow residuals are displayed in Figure 4-13, Figure 4-14, and Figure 4-15. Pressure residuals were normalized against the average pressure value in the gob, -408 Pa, while the flow residuals were normalized against the gob participation factor, 3.61 m^3/s. Normalized pressure values rapidly settled below a threshold of 10^{-3} after 9 coupling iterations. Normalized total flow residuals never achieved the threshold of 10^{-3}, but instead settled below a value of $1.7x10^{-3}$ after 20 coupling iterations. Methane flow residuals varied significantly during early iterations as the initial conditions for the atmosphere within the network and Gob models did not reflect the eventual steady state values. The residuals settled below the 10^{-3} threshold after 9 coupling iterations. Relaxing the threshold to $2x10^{-3}$ had the pressure residual meeting it after 6 coupling iterations, the total flow residual after 14 iterations, and the methane flow residual after 7 coupling iterations.

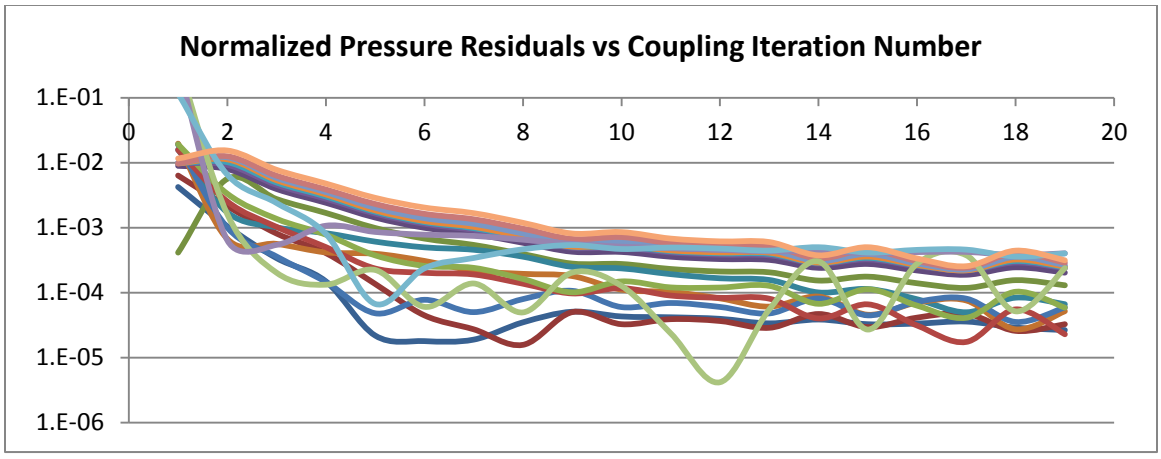

Figure 4-13 Normalized pressure from coupling data from mesh level 5

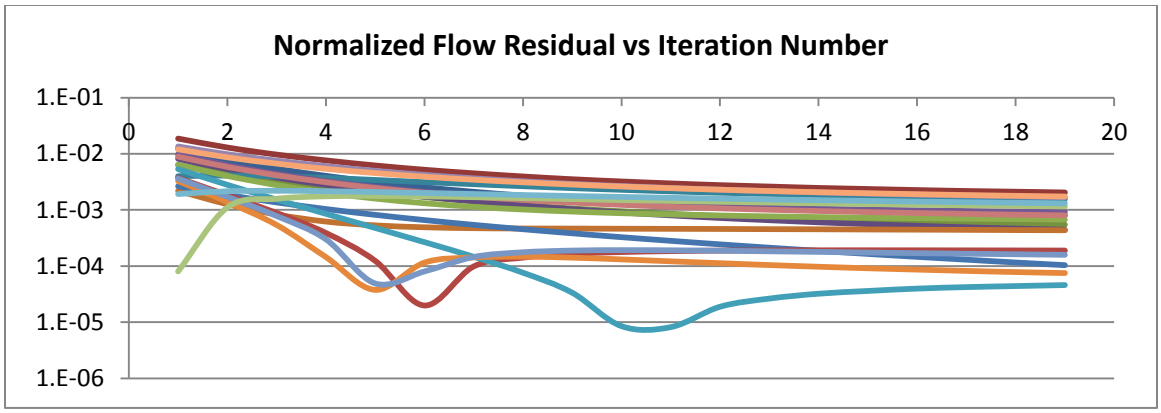

Figure 4-14 Normalized flow residual from coupling data from mesh level 5

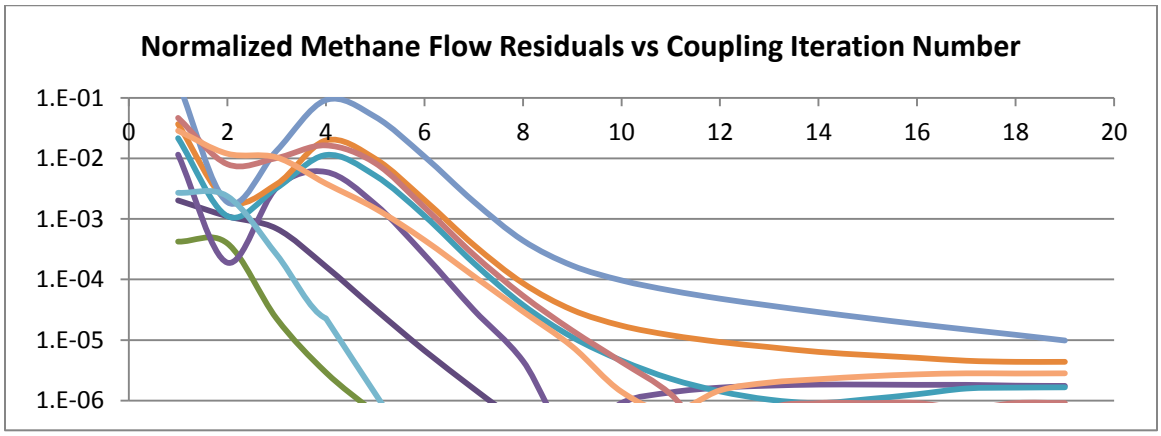

Figure 4-15 Normalized methane flow residual from coupling data from mesh level 5

4.3.3 MSVM Validation against Original VNetPC Model

Details from the network model can be seen in the following three images. The distribution of pressure around the network can be seen in Figure 4-16. Flow is in Figure 4-17, while the steady state methane concentration can be seen in Figure 4-18. Comparison between the performance of the network model and the original VNetPC model can be seen in Table 4-5. A total of 32 data points spread about the network were examined. The data points were spread across all regions of the mine ventilation system, including intake, longwall, headgate, bleeder, tailgate, return, and belt entries. The average percent difference for flow between the present MSVM study and the original calibrated VNetPC model was 1.92%, and 1.22% for pressure data points. The only significant difference was found in a branch in the tailgate entries, which had a

percent difference of 27%, but an absolute difference of 0.054 m^3/s. This was below the convergence criteria for VNetPC, which is 10^{-1} m^3/s. In summary, there was excellent agreement between the two models for pressure and flow.

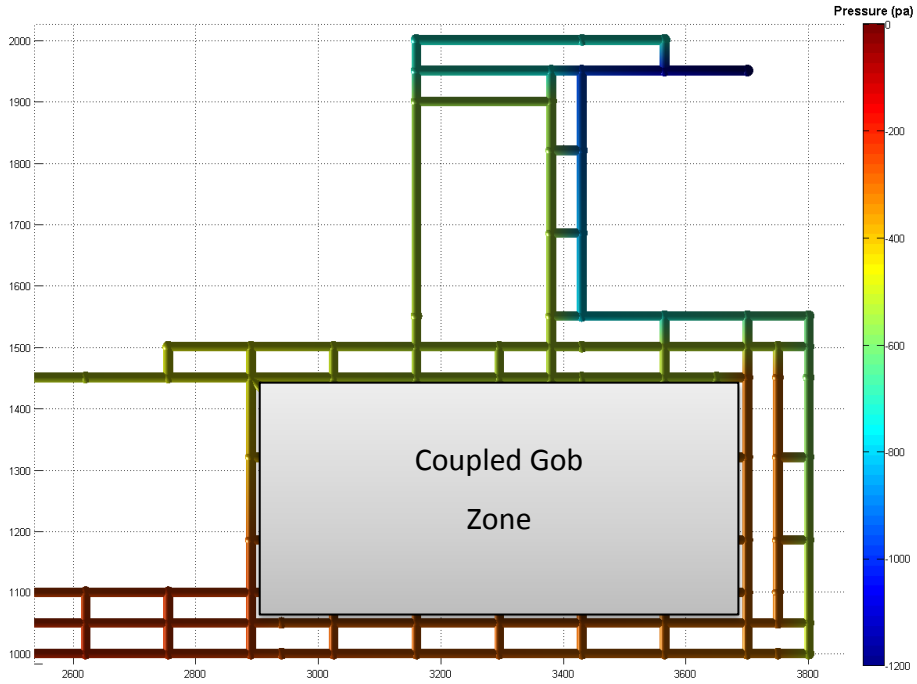

Figure 4-16 Pressure through the network when coupled with the level 5 mesh

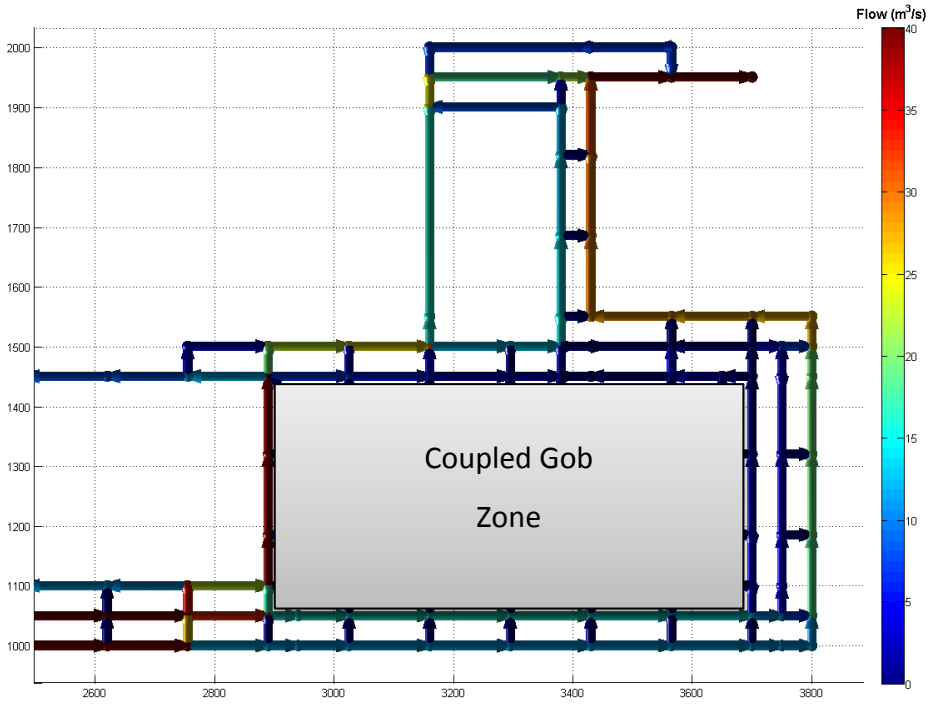

Figure 4-17 Flow through the network when coupled with the level 5 mesh

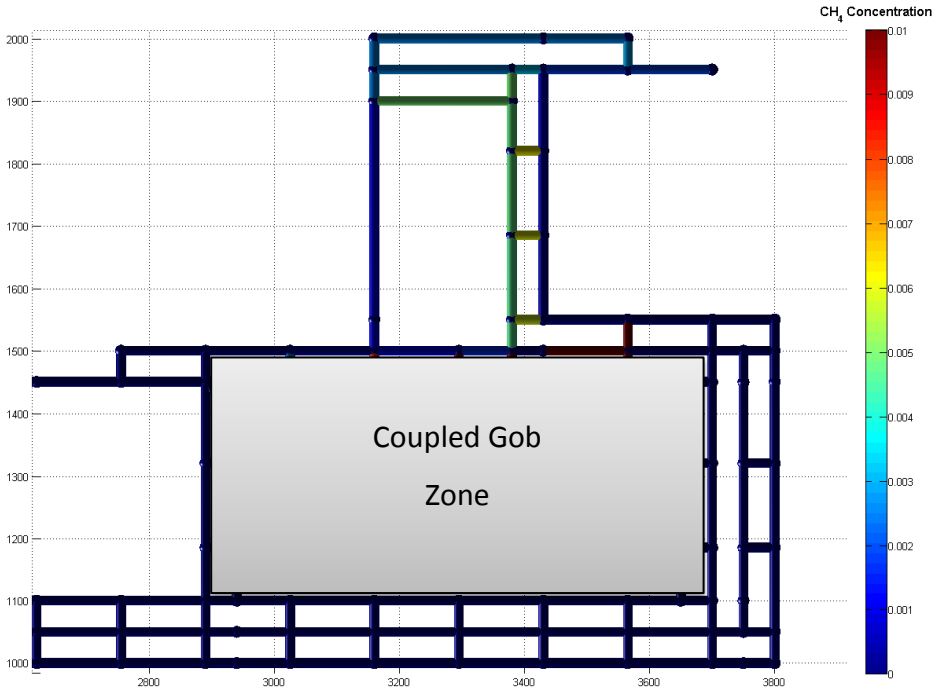

Figure 4-18 Methane concentration through the network when coupled with the level 5 mesh

Table 4-5 Comparison between MSVM network results and original VNetPC results

Comparison Between MSVM Network Results and Original VNetPC Results								
		Flow (m^3/s)				*Pressure (Pa)*		
Region	ID	MSVM	Original	% diff	ID	MSVM	Original	% diff
Intake	43	48.56	48.63	-0.15%	42	-81.288	-81.7	-0.51%
	23	39.93	39.99	-0.15%	22	-81.831	-82.3	-0.57%
	51	41.05	41.10	-0.12%	50	-200.07	-201.7	-0.81%
	31	39.27	39.31	-0.09%	30	-194.78	-195.8	-0.52%
Longwall	510	39.34	39.58	-0.62%	183	-292.79	-296.4	-1.23%
	632	38.28	38.41	-0.35%	160	-404.12	-410.1	-1.47%
	629	38.61	37.86	1.96%	94	-472.06	-476.9	-1.02%
Headgate	57	15.47	16.03	-3.57%	56	-302.06	-294.6	2.50%
	37	11.17	11.55	-3.31%	36	-287.45	-287.7	-0.09%
	61	14.31	14.87	-3.85%	60	-313.8	-301.9	3.87%
	41	11.30	11.35	-0.46%	40	-323.93	-322.7	0.38%
Bleeder	430	11.15	11.48	-2.88%	332	-313.84	-302.3	3.75%
	420	11.50	11.49	0.06%	2	-502.85	-501.3	0.31%
	424	19.72	19.90	-0.93%	161	-599.97	-604.2	-0.70%
	501	2.94	3.07	-4.47%	7	-508.51	-515.4	-1.35%
	141	28.53	28.59	-0.21%	138	-772.03	-776.5	-0.58%
	120	-1.54	-1.52	1.31%	118	-506.79	-514.5	-1.51%
	455	29.96	30.01	-0.17%	171	-895.76	-900.4	-0.52%
	439	13.22	13.22	0.00%	167	-538.57	-546.2	-1.41%
	480	15.82	15.77	0.32%	157	-554.71	-561.5	-1.22%
Tailgate	496	7.3413	7.33	0.15%	95	-491.36	-497.1	-1.16%
	116	23.102	23.07	0.14%	115	-491.49	-497.3	-1.18%
	494	2.9778	2.97	0.26%	97	-505.23	-512.5	-1.43%
	119	13.193	13.05	1.09%	169	-506.9	-514.6	-1.51%
	493	2.8851	2.73	5.52%	168	-506.67	-514.3	-1.49%
	492	-0.2235	-0.17	27.19%	99	-505.54	-514.2	-1.70%
Return	115	3.2274	3.22	0.23%	113	-482.08	-487	-1.02%
	95	11.949	11.94	0.08%	93	-482.06	-487	-1.02%
	94	8.7213	8.72	0.01%	92	-487.45	-492.4	-1.01%
Belt	75	22.794	23.07	-1.20%	73	-240.89	-242.8	-0.79%
	71	12.751	12.69	0.48%	69	-246.84	-249.1	-0.91%
	64	19.622	19.6	0.11%	62	-265.86	-269.9	-1.51%

4.3.4 Turbulence Model Selection

SC/Tetra has a total of thirteen turbulence models available for use. These are spread amongst two different turbulent flow formulations. The first is Reynolds-Averaged Navier-Stokes (RANS) and the second is Large Eddy Simulation (LES). The RANS

formulation was chosen due to the availability of low Reynolds number turbulence models. Further, LES formulations generally have higher computational costs due to the greater need for small elements and higher-order difference schemes for the advective term in the Navier-Stokes equation. The ones examined in this study were as follows:

- *Standard κ-ε Model*
- *Re-Normalization Group (RNG) κ-ε Model*
- *Abe-Nagano-Kondoh (AKN) κ-ε Model*
- *Goldberg Peroomian Chakravarthy (GPC) κ-ε Model*
- *Shear Stress Transport (SST) κ-ω Model*
- *Spalart-Allmaras (S-A) 1Equation Model*

The standard κ-ε model and the RNG κ-ε model are common starting points for CFD studies and thus were included. The AKN and GPC κ-ε model were chosen because they are classified as linear low Reynolds number turbulence models. The standard model and its derivatives contain several empirical constants based upon experiments with generally high Reynolds number flows, at least high compared to the present study. The SST model was included as they are unique from the κ-ε model. The SST model is a κ-ω model that replaces the turbulence dissipation variable, ε, with a dissipation rate per unit turbulence energy, $\omega \sim \varepsilon/\kappa$, that has been noted as applicable for general CFD work. The Spalart-Allmaras one equation model is a variation that solves for the eddy viscosity directly instead of relying on the two equation approach adopted in the other models.

According the SC/Tetra User's Guide, the AKN κ-ε model offers a number of advantages that are suited to this study. Of particular importance is its ability to accurately model a wide range of flows with Reynolds number varying from low to high. It also has the capability to model the flows that transition from turbulent to laminar and from laminar to turbulent. The model accomplishes this by introducing a damping function that incorporates wall effects into the formulation for eddy viscosity.

The GPC κ-ε model is another low Reynolds number turbulence model. While the AKN κ-ε model requires a calculation of wall distance, the damping function in this model is

independent of wall distance and introduces more substantial changes to the formulation of the turbulence dissipation rate.

The turbulence study was conducted in a similar fashion to the grid independence study. Coupling between the network model and the Gob model was active. A total of 1100 cycles were completed, with 20 exchanges of coupling information on 50 cycle intervals. Excepting the turbulence model, all other variables remained unchanged. Default values for each of the model were used. The standard κ-ε model and the RNG κ-ε model failed to converge. For these two models the condition of the turbulent energy matrix degraded rapidly leading to a floating-point exception within the first thirty five cycles. The accuracy of the standard κ-ε model for low Reynolds number flows has been identified as one of the drawbacks of that model According to Versteeg and Malalasekera, the root of the problem is the inaccuracy of the wall function for low Reynolds number flows (2007). There are two recommended solutions. The first is to add sufficient elements to the wall to resolve the change in velocity and subsequent change in turbulence energy and dissipation rate, which is computationally prohibitive over such a large volume. The second is to add damping to the turbulence model, which is the case with the AKN κ-ε model. The remaining models all progressed for the requested 1,100 cycles. Since there was little expected turbulence in the interior of the gob, the model for turbulence was expected to have little influence on the problem. It is essentially laminar on the interior. A laminar model though, failed to converge. It is suspected that this fails for similar reasons to the standard κ-ε model, with the problem due to the lack of refinement in the mesh as it tends to the wall. The results from the turbulence study are listed in Table 4-6, which demonstrated virtually identical results for gob participation across the four models that ran successfully. For subsequent studies, the AKN κ-ε model was included.

Table 4-6 Flow Response to Turbulence Models at the Coupling Interface

Flow Response to Turbulence Models						
		AKN κ-ε	GPC κ-ε	SST	S-A	Average
Gob Participation	(m^3/s)	3.68533	3.68532	3.68532	3.68530	3.68532
Gob Participation	% *diff*	0.00033%	0.00006%	0.00014%	-0.00054%	
Longwall Face Participation	(m^3/s)	2.35146	2.35160	2.35160	2.35157	2.35156
Longwall Face Participation	% *diff*	-0.00414%	0.00178%	0.00195%	0.00041%	
HeadGate Participation	(m^3/s)	1.29242	1.29244	1.29244	1.29243	1.29243
HeadGate Participation	% *diff*	-0.00103%	0.00068%	0.00075%	-0.00041%	
Tailgate Participation	(m^3/s)	2.07038	2.07038	2.07038	2.07038	2.07038
Tailgate Participation	% *diff*	0.00001%	0.00001%	-0.00004%	0.00001%	
Start Up Room Participation	(m^3/s)	1.65622	1.65622	1.65622	1.65622	1.65622
Start Up Room Participation	% *diff*	0.00005%	-0.00002%	-0.00002%	-0.00002%	

4.3.5 Gob Models

As discussed previously, two gob models were implemented in this study. The first was a two zone gob model, while the second included continuously variable permeability along the length and width of the panel. The geometry remained consistent between the two models with the exception of the surfaces that divided the gob into the two zones. This unnecessary feature was removed from the smooth gob, and the model was remeshed according the level 4 meshing guidelines.

The following images were drawn from the two gob models under the same initial conditions at a plane 1 meter from the floor. As with the mesh independence study, the MSVM models are run to 1,100 CFD cycles over 20 coupling iterations. Convergence was manually verified after each run due to setting the CN02 convergence criteria artificially high, to ensure completing the coupling routine. Convergence values can be seen in Table 4-7 and Table 4-8.

Table 4-7 Two Zone Gob Model Scaled Residuals as reported by SC/Tetra

Steady State Check - Two Zone Gob Model					
U	6.83E-06	V	2.61E-06	W	4.23E-06
P	2.15E-06	TK	6.95E-05	TE	4.05E-05
CN01	4.22E-05	CN02	4.09E-03	CN03	5.87E-05

Table 4-8 Smooth Gob Model Scaled Residuals as reported by SC/Tetra

Steady State Check - Smooth Gob Model					
U	6.83E-06	V	3.59E-06	W	8.92E-06
P	6.48E-06	TK	7.61E-05	TE	4.95E-05
CN01	4.95E-05	CN02	5.15E-05	CN03	8.63E-03

The pressure distribution from the two gob models can be seen in Figure 4-19 and Figure 4-20. As expected, the pressure distribution demonstrates a discontinuity at the boundary between the two permeability values.

CRADLE

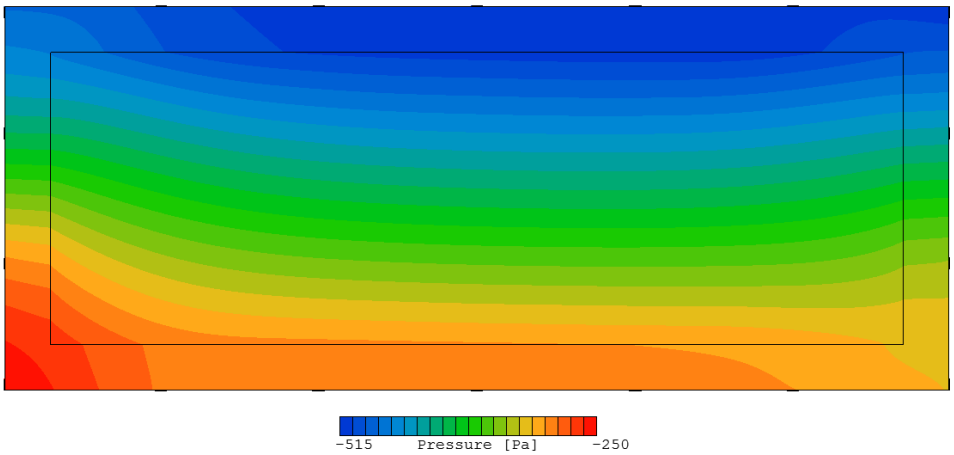

Figure 4-19 Two zone gob model pressure distribution at a plane 1 meter from the floor

CRADLE

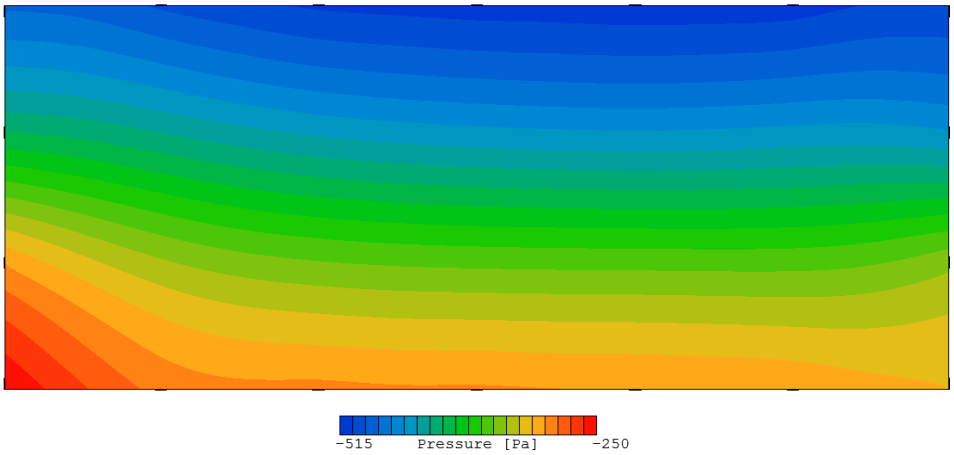

Figure 4-20 Smooth gob model pressure distribution at a plane 1 meter from the floor

The velocity distribution from the two gob models can be seen in Figure 4-21 and Figure 4-22. The discontinuity manifests as a concentration of flow around the perimeter of the gob, as one would expect. In the smooth gob model, the flow penetrates further into the gob from along both the longwall face and start up room. The velocity through the tailgate entries was more uniform in the smooth gob model, where the two zone model directed the air more to the corners.

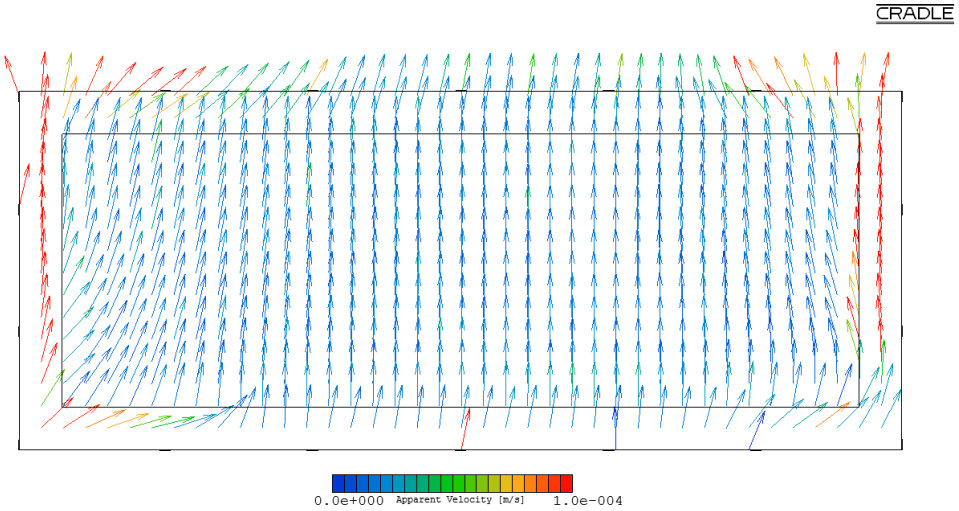

Figure 4-21 Two zone gob model velocity distribution at a plane 1 meter from the floor

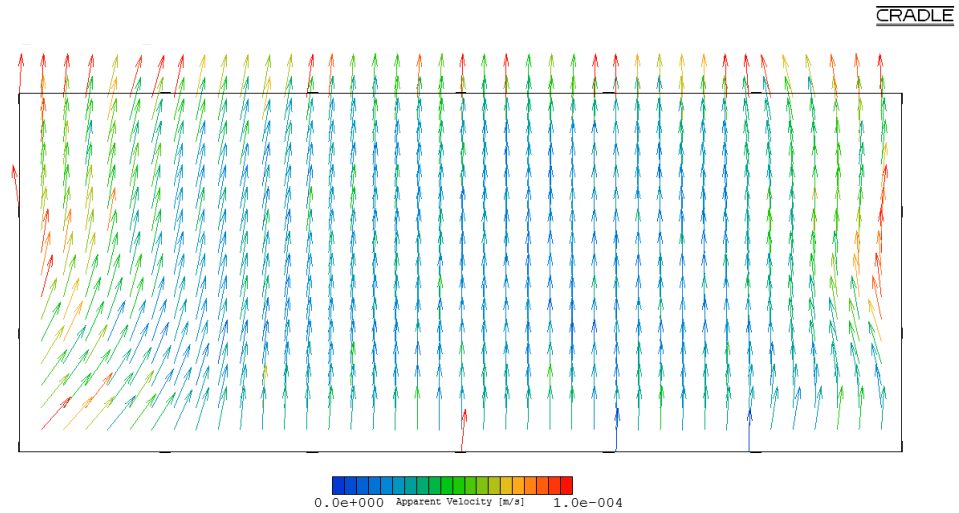

Figure 4-22 Smooth gob model velocity distribution at a plane 1 meter from the floor

Contours plots of oxygen concentration can be seen in Figure 4-23 and Figure 4-24. The modification to flow adversely affected the concentration of oxygen within the gob. With the flow of air concentrated at the corners in the two zone model, oxygen was depleted more rapidly in it when compared to the smooth gob model. An artifact from the limited number of coupling regions can be observed in each model, though it was more evident in the smooth gob model. Contours are observed radiating out from the connections to the headgate entries where air is entering to bleed the methane from the gob. In the two zone model, rapid gradients are observed trending along the boundary between the two permeability zones nearest the start-up room.

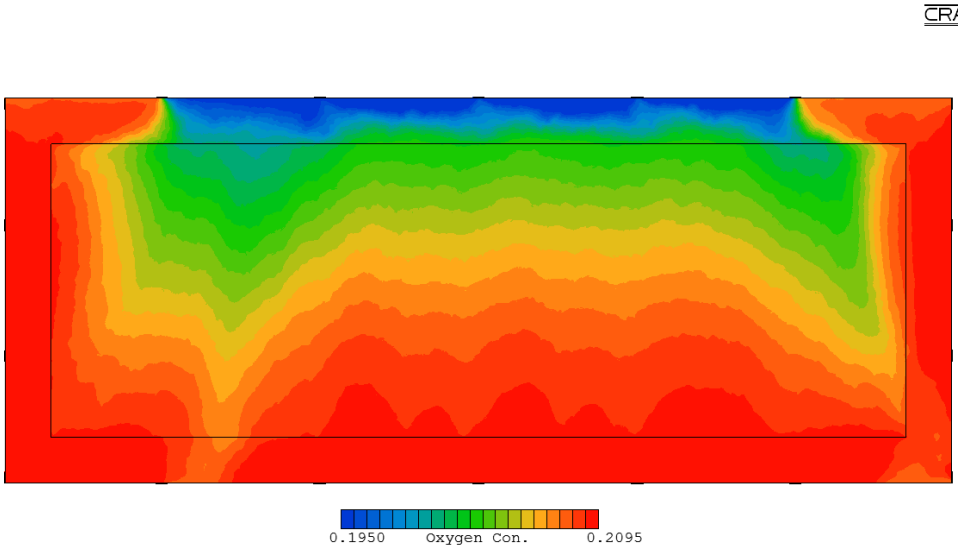

Figure 4-23 Two zone gob model oxygen concentration by volume distribution at a plane 1 meter from the floor

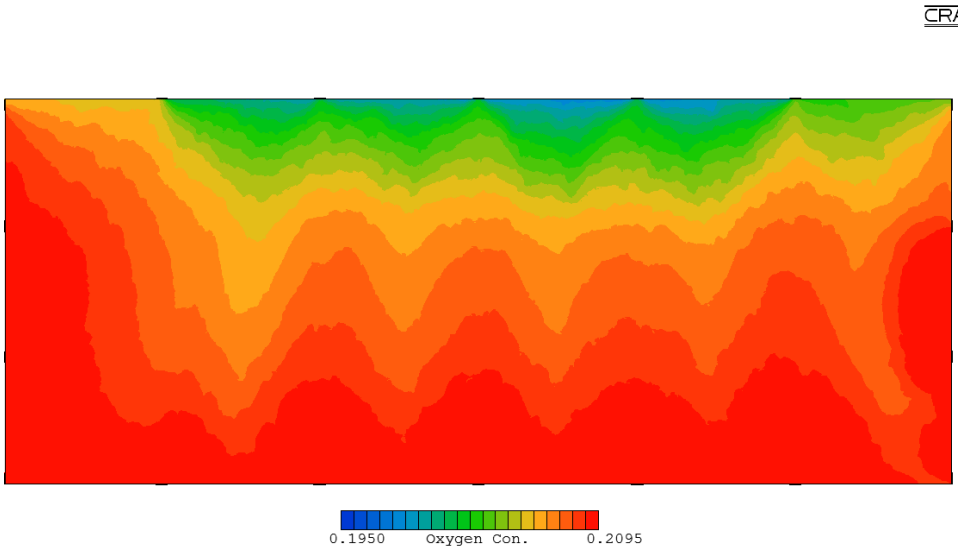

Figure 4-24 Smooth gob model oxygen concentration by volume distribution at a plane 1 meter from the floor

Contours of methane concentration are illustrated in Figure 4-25 and Figure 4-26. As with the oxygen concentration, the difference in distribution of flow causes elevated methane concentrations in the two zone gob model. Methane concentrations are roughly twice as high in the region adjacent to the tailgate entries. As with the plots of oxygen contours, artifacts from the number of coupling regions and the boundary between the two gob zones are readily observed.

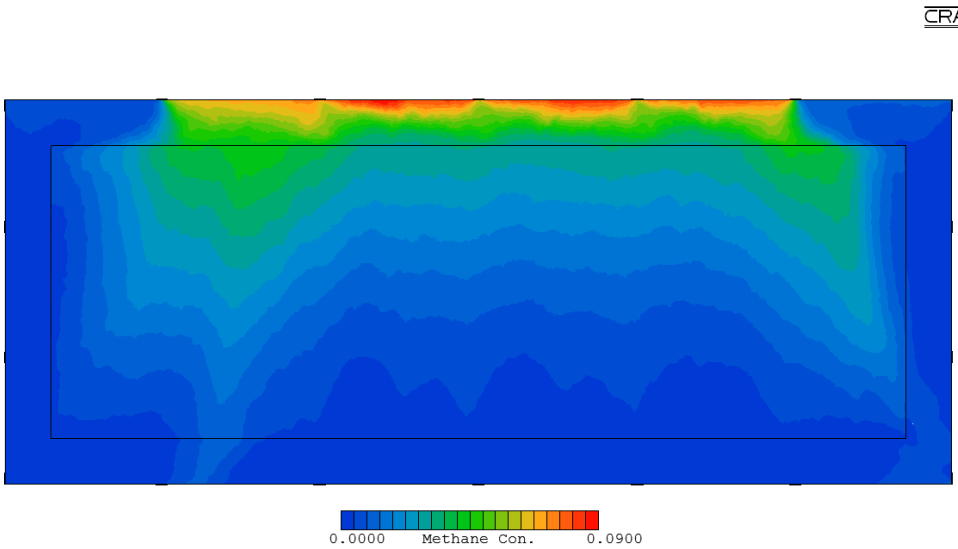

Figure 4-25 Two zone gob model methane concentration by volume distribution at a plane 1 meter from the floor

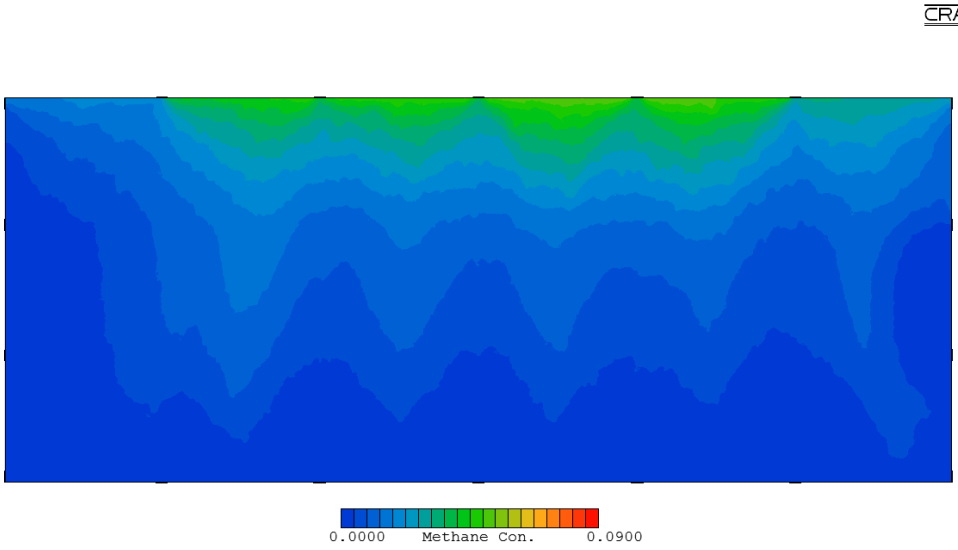

Figure 4-26 Smooth gob model methane concentration by volume distribution at a plane 1 meter from the floor

The explosibility contours are shown in Figure 4-27 and Figure 4-28. The effects of changing the permeability distribution had a dramatic impact on the size of the explosibility contours. The interior demonstrated an elevated potential for being at or near the explosive region of Coward's triangle. The contours clearly follow the border between the two zones. The smooth gob model demonstrated a thinner region

comprising an explosive mix which extended from the roof to the bleeder entries. A smaller region with a near explosive but lean mix is observed close to the walls along the tailgate entries.

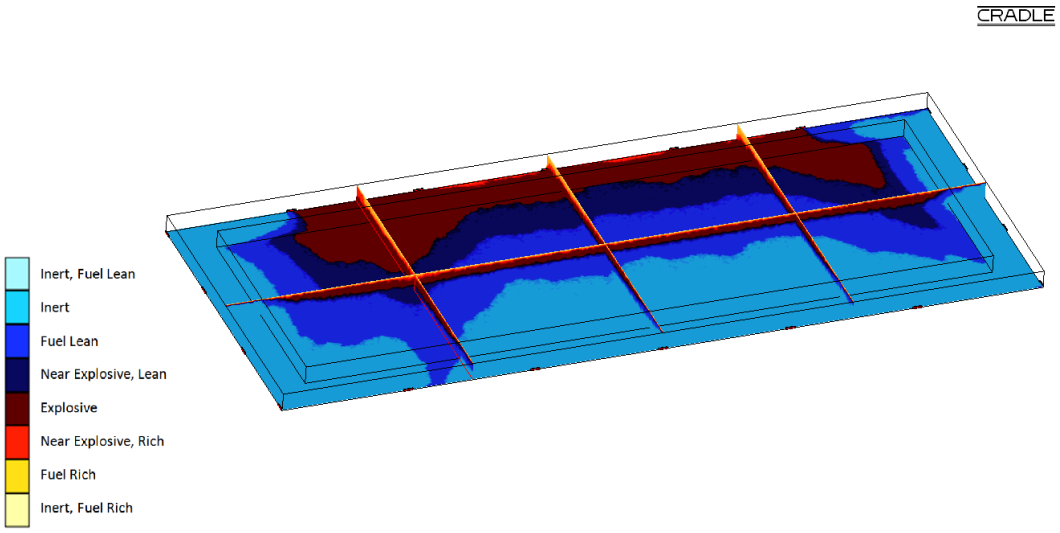

Figure 4-27 Two zone gob explosibility contours at a plane 1 meter from the floor and along four vertical planes

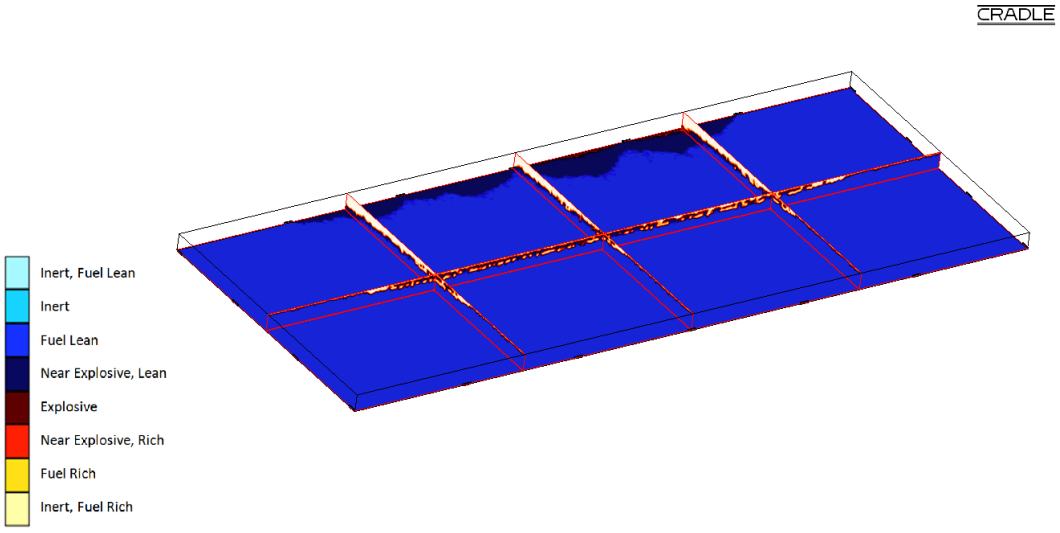

Figure 4-28 Smooth gob explosibility contours at a plane 1 meter from the floor and along four vertical planes

Gob models that include stepped distributions of permeability are insufficient for describing the conditions within the gob. While this in not wholly unexpected, the

results indicated that this would be inappropriate for even a first order approximation of the gob permeability. In each measure, the stepped discontinuity produced what were judged to be non-physical results, that is to say artifacts from the modeling process overwhelm the signal when compared to the smooth gob model.

The process also highlighted the subtlety of the composition of the gob. Despite the differences in gob models, the gob participation factor was within 2% of one another, meaning nearly identical quantities of air were flowing in and out of the gob portion of the MSVM. The resulting disparity between the two gob explosibility plots was remarkable. It is suggested that a first order approximation of the gob may be best met with a uniform value for permeability before switching to a smooth gob permeability model. It also highlights the possibility of marked changes in the distribution of the gob environment if a smooth gob permeability function is truncated to some maximum and minimum value. This may be enough to alter the flow distribution with an attendant change in gob composition.

The influence of the gob permeability was also examined by adjusted the values used for the smooth gob model. Gob permeability was both increased and decreased by a factor of 20%. With an increase in gob permeability, the resulting change in the gob participation factor was an increase to 4.18 m^3/s, or a 13.8% increase in air flowing through the gob over the baseline. Upon decreasing the permeability, the gob participation factor decreased to 3.03 m^3/s, for a 17.8% decrease from the baseline. The performance of the MSVM approach did indicate increasing flow with increasing permeability and decreasing flow with decreasing permeability. The influence of altering the permeability of the smooth gob model can be seen in Figure 4-29 and Figure 4-30, which demonstrates the enhanced methane dilution performance when increasing the gob permeability.

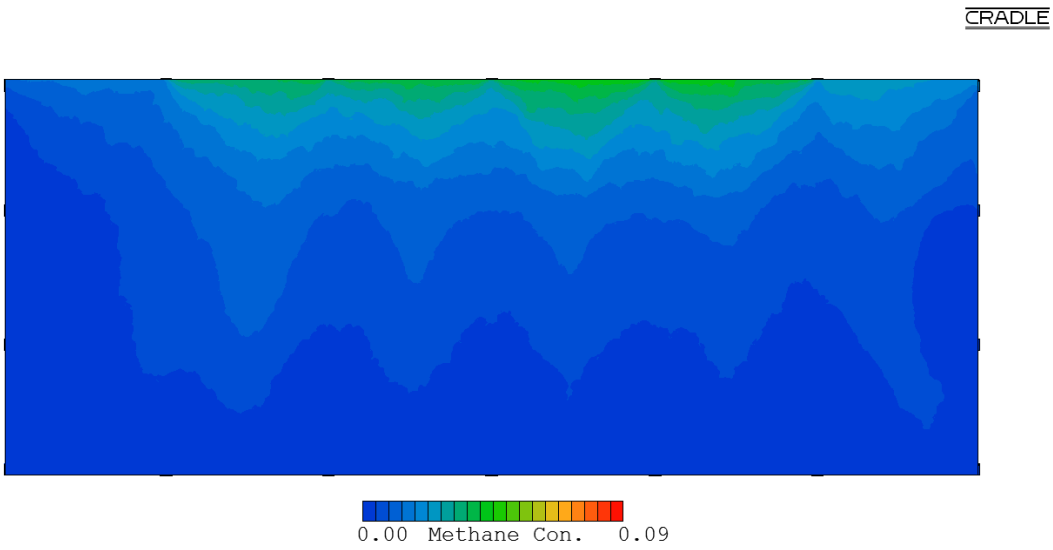

Figure 4-29 Influence of increased permeability upon methane concentrations in the gob at a plane 1 meter from the floor

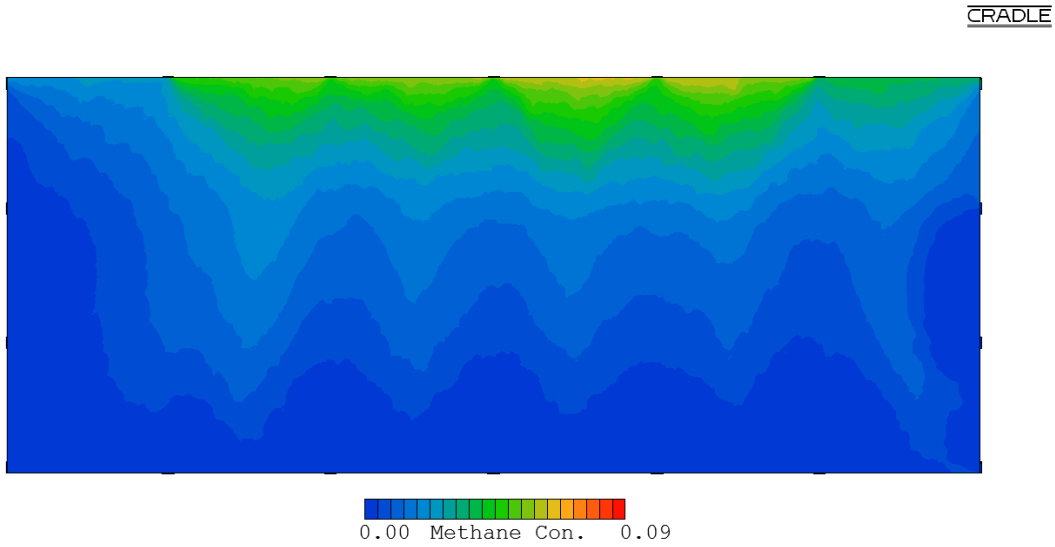

Figure 4-30 Influence of a 20% decrease in permeability upon methane concentrations in the gob at a plane 1 meter from the floor

The effect of gob permeability variations on velocity within the gob can be seen in Figure 4-31 and Figure 4-32. There was a subtle shift in the magnitude of the velocity in the gob as the permeability was varied. The direction of the flow did not appear to change with the permeability changes.

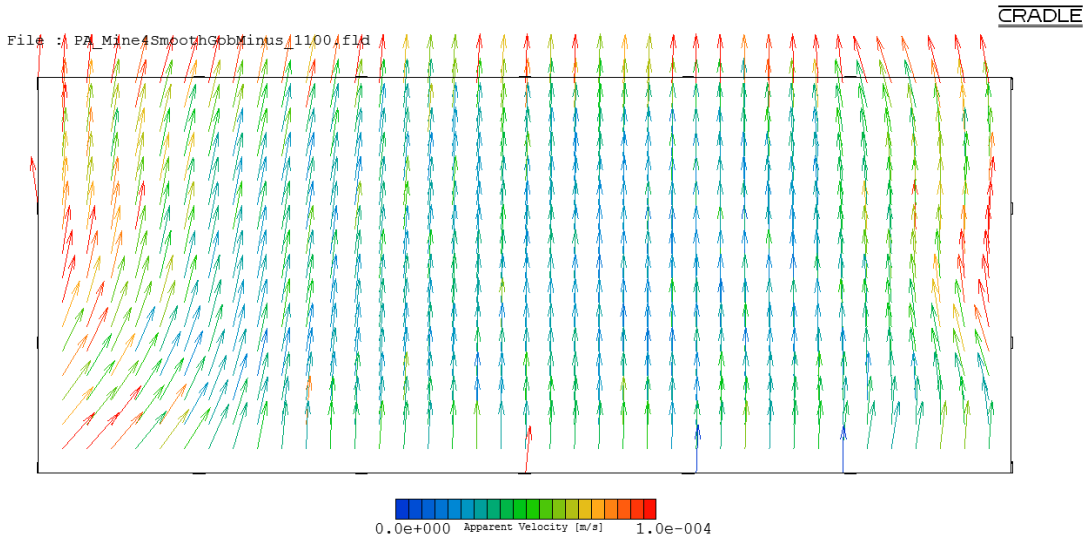

Figure 4-31 Influence of a 20% increase in permeability upon velocity in the gob at a plane 1 meter from the floor

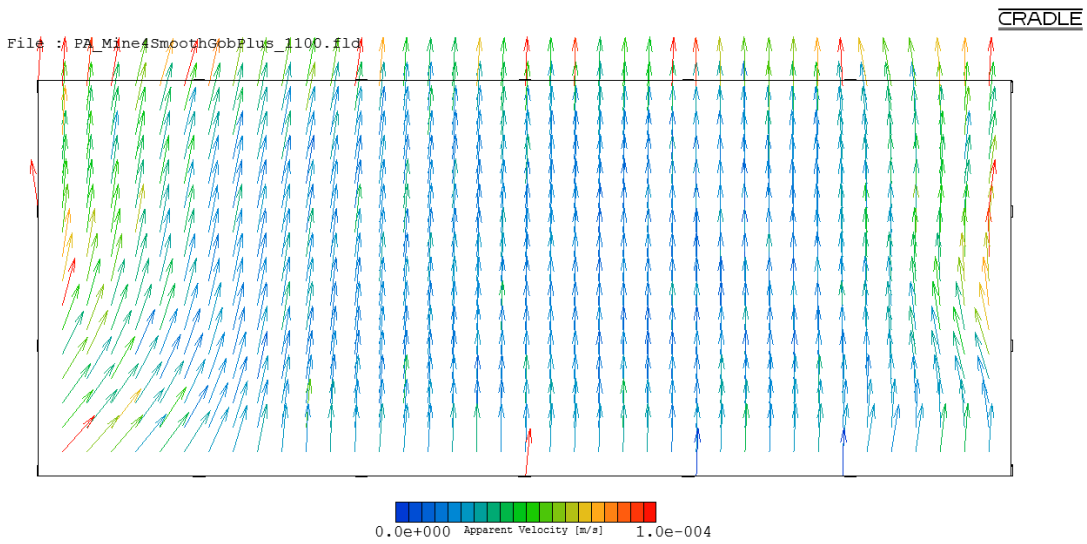

Figure 4-32 Influence of decreased permeability upon velocity in the gob at a plane 1 meter from the floor

4.3.6 Increased Coupling Regions

The original model included relatively sparse connections between the network model and the Gob model. A total of 18 connections were included, with 4 spread along the longwall face and start up room, and 5 along each of the gate entries. In reality, there is a near continuous connection along the longwall face, with air seeping around the longwall roof supports, and along the start-up room. Along the gate roads, the connections, which occur at every crosscut, are spaced 45 meters apart. There should be 23 connections between the network and the gob, if modeled one to one, along the gate entries.

In order to investigate the effect of increasing the coupling regions, the total number of regions was doubled. New geometry was generated with 7 connections along the longwall face and start-up room and 11 along the gate entries, for a total of 36 connections. The new geometry can be seen in Figure 4-33. The connections were distributed evenly around the perimeter of the gob. The width of the connections was reduced by half. No further changes were implemented in the geometry.

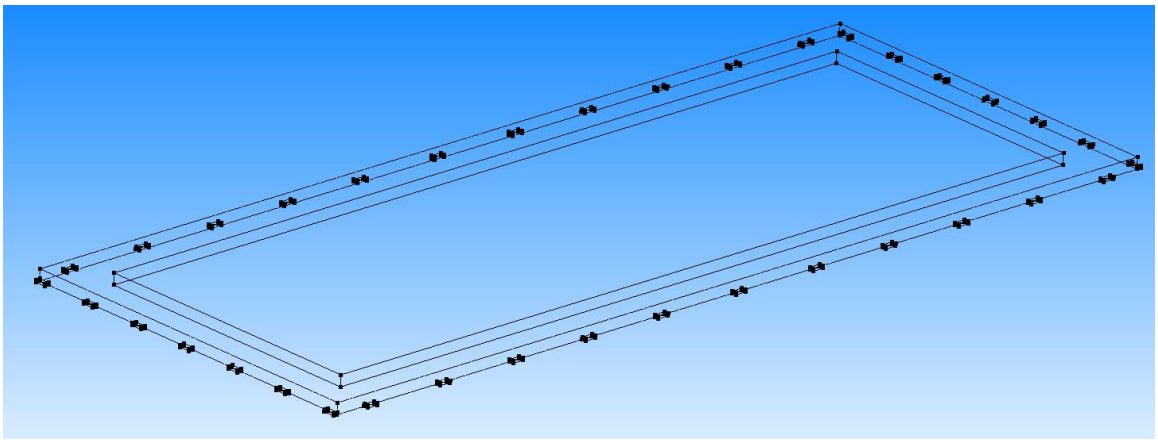

Figure 4-33 Geometry for the gob model with an increased number of coupling regions

To complement the added coupling regions in the Gob model, it was necessary to make a modification to the network model. New nodes were added to existing branch midpoints. Branch resistances were divided evenly between the resulting new branches. The locations for the added regions can be seen in Figure 4-34.

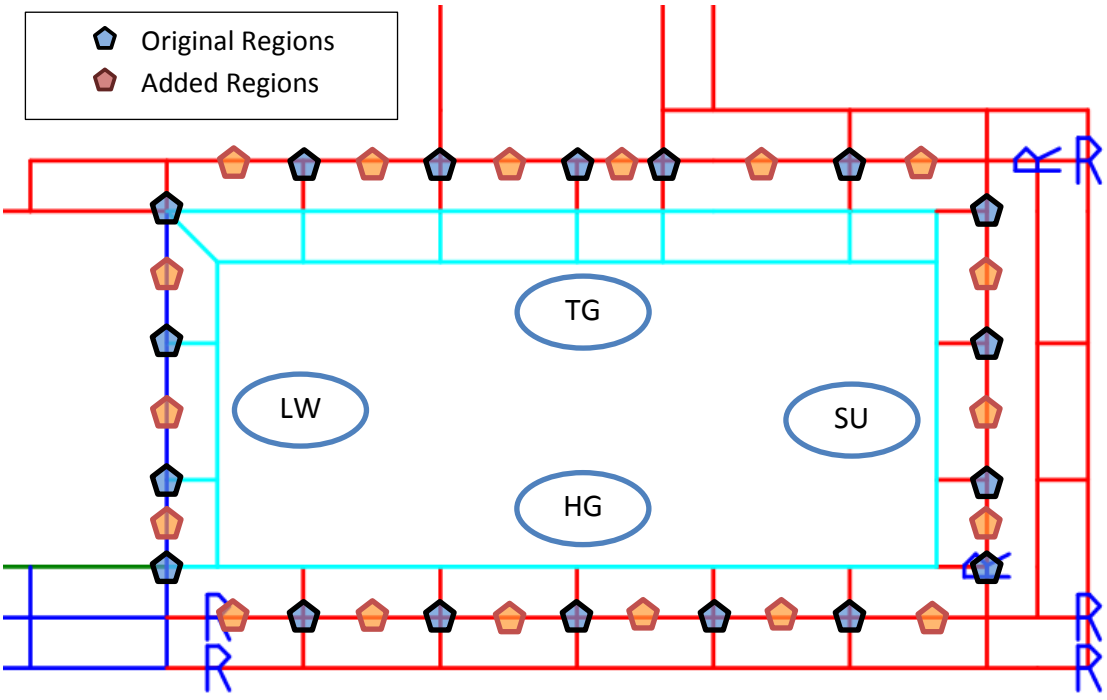

Figure 4-34 Locations for the added regions for coupling within the network model

The MSVM model was run with identical boundary conditions as previous models using the smooth gob permeability model. Gob participation was found to be within 0.9% of previous runs, with a total of 3.81 m^3/s of air flowing into the gob.

The MSVM model was also tested with the two zone gob model. This served to highlight one of the weaknesses of the approach. Elevated concentrations of oxygen were observed at the coupling regions near the tailgate entries, as shown in Figure 4-35. This was counter to expectations as those regions were outlets for the gob model. With no expected source of oxygen flowing in at that boundary, rising oxygen concentrations should not have been possible.

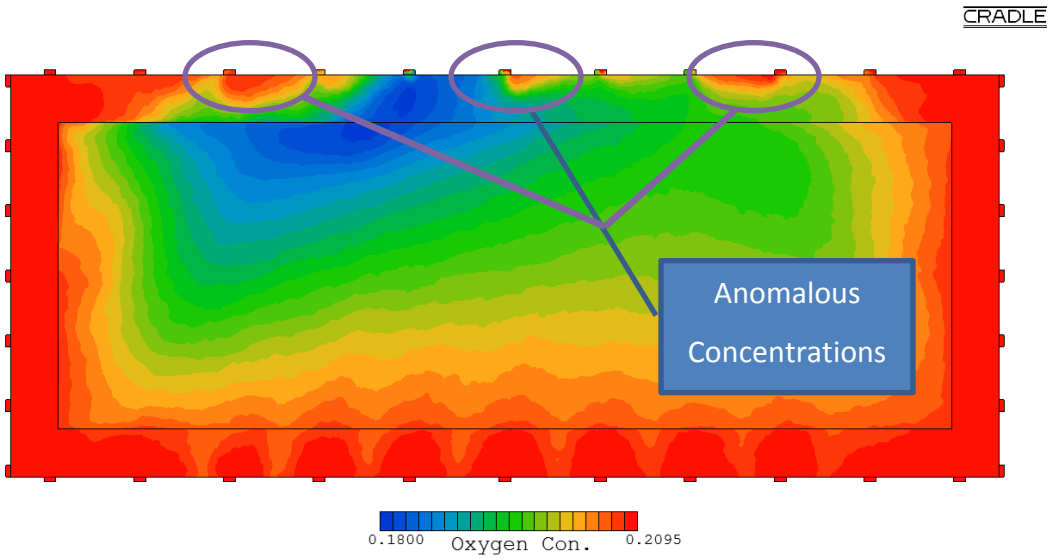

Figure 4-35 Anomalous oxygen concentrations observed in the gob model due to recirculating boundary conditions at a plane 1 meter from the floor

An examination of the coupling region conditions identified the issue as a poorly defined boundary. Direction of flow at a coupling boundary region is not established by the pressure boundary condition for the gob model. Air flow was entering and exiting the gob region on this surface, as illustrated in Figure 4-36. No ill effects to pressure or flow were observed in the network model, but the species concentrations were incorrect, just as they were incorrect in the Gob model. With air flowing into and out of the boundary, the species flux was treated in a non-conservative manner. It flowed

outward with one concentration, but flowed inward with the inflow settings established from the previous coupling iteration. Because this node is also associated with flow through the network, the concentration at the node would be lower than in the CFD domain because there is additional air moving through those tailgate network branches. This lowered the inflow concentration, effectively redistributing the concentration of species at these poorly defined boundary conditions.

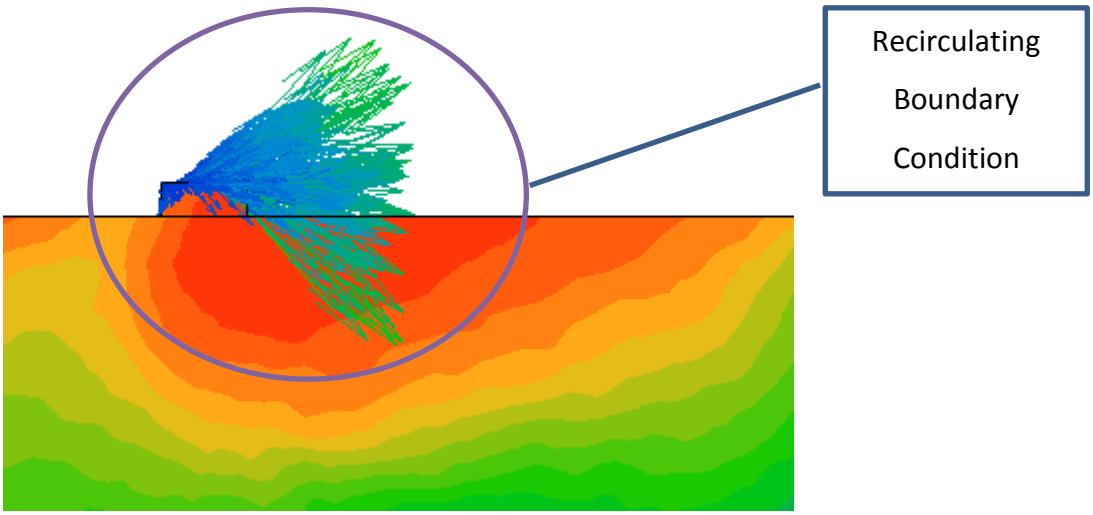

Figure 4-36 Poor performing coupled boundary condition at a plane 1 meter from the floor

While this defect was only observed in this one case with the abandoned 2 zone gob model, it clearly established that coupling regions could not be placed at will in the model. Care must be taken to ensure that the coupling boundaries are well formed and function entirely as either inlets or outlets to the model. A reexamination of previous results confirmed that this defect was absent from the models with fewer coupling regions. This may be due to the higher difference in pressure amongst adjacent coupling regions that the sparse connections would experience. However, it may only be an artifact from the stepped boundary condition which resulted in a non-physical distribution of pressure and flow in the gob, for this configuration. Additional examination of this problem was recommended; with a proposed solution discussed in the future work section.

4.3.7 Methane Emissions

The studies presented thus far have only included methane liberated into the gob from an assumed rider seam above it. A significant portion of the methane in the system would be released by the actions of the longwall shearer and from the freshly broken coal lying on the belt as it makes its way to the surface. It was assumed that a total of 0.262 m^3/s of methane would be generated at the longwall face. This methane was introduced into the network portion of the model as the node locations called out in Figure 4-37. The total methane was divided across these four locations, weighted by the length of the longwall face associated with each node.

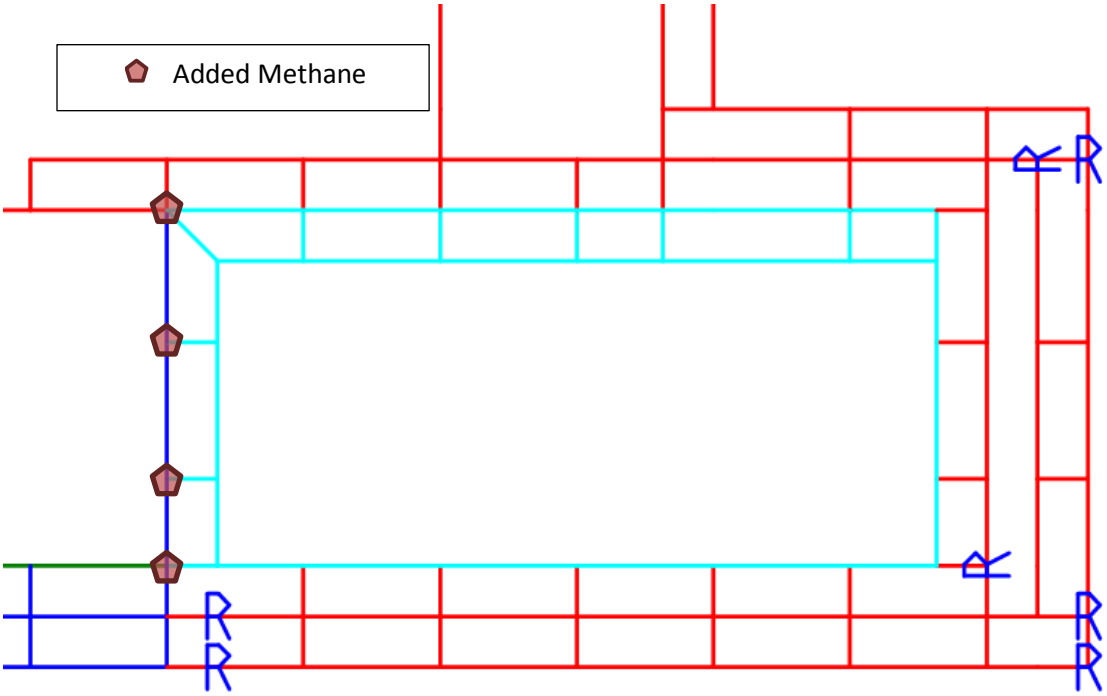

Figure 4-37 Location for methane addition due to longwall shearer action

The addition of methane along the longwall face primarily influenced the results in the network model. Little of the methane introduced at the longwall face entered the gob, with only 0.00269 m^3/s of methane entering from the two nodes closed to the headgate side. The remaining two nodes along the longwall face were flowing from gob to network model. The methane concentration at the end of the longwall face was 0.66%

by volume. This nearly matched the assumed concentration at the end of the longwall face of 0.7%. It seems that a small portion of the methane introduced along in this portion of the network model was transferred to the gob model, where it reported to the tailgate entries.

Figure 4-38 Network model response to methane addition at the longwall face

The methane concentration in the gob was only minimally effected. With only a limited quantity of methane entering from the longwall face, there was a mild shift in the contours of methane concentration when compared to the baseline case. The influence of the addition of methane due to the action of the longwall shearer can be more easily seen in Figure 4-40. With the range adjusted to display 0% to 2% methane concentration by volume, the modest rise in concentrations along the longwall face can be observed.

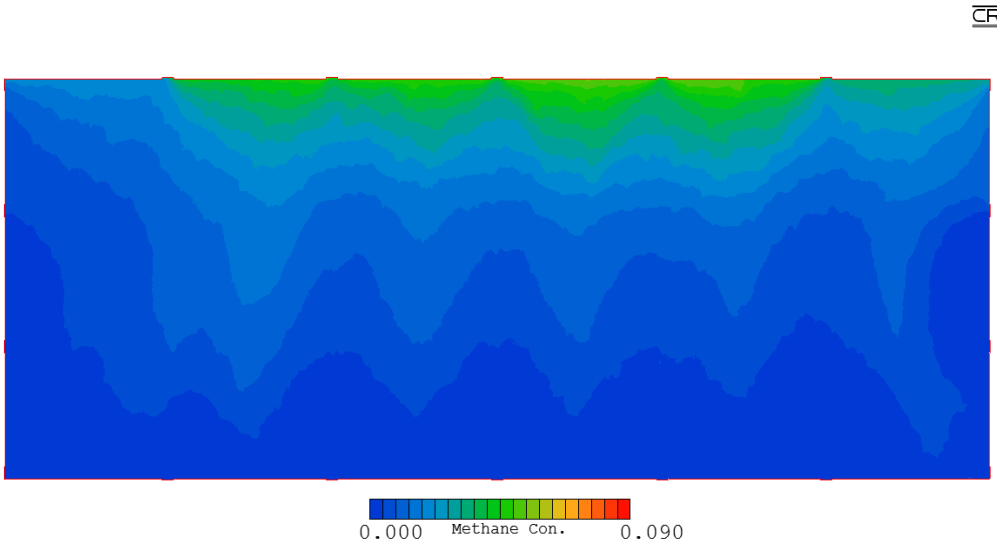

Figure 4-39 Gob model response to methane addition at the longwall face at a plane 1 meter from the floor

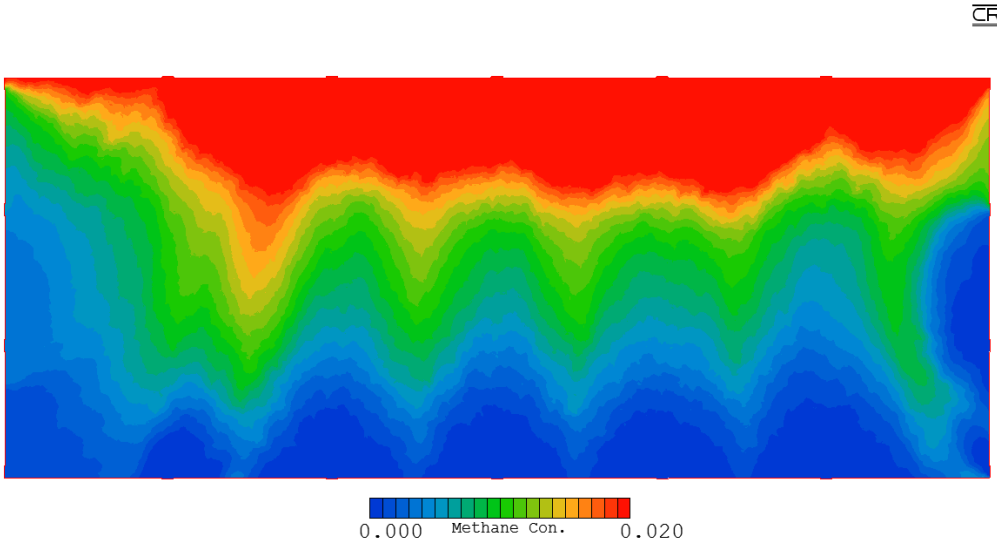

Figure 4-40 Gob model response to methane addition at the longwall face, contours from 0% to 2% at a plane 1 meter from the floor

5 Transient Modeling

Transient modeling began after completing the steady state scenarios. In each case, a steady state solution was used as the initial conditions for the gob Gob model as well as for the network model. With these conditions loaded, the transient scenario was initiated and the scenario was allowed to reach a new equilibrium point. This new equilibrium point was then compared to the original VNetPC model once the same change to the network was introduced.

5.1 Roof Fall in the Bleeder Entries

The first transient scenario investigated was a roof fall occurring in the bleeder entries. The bulk of the air flowing through the bleeder entries was concentrated in the outermost branch, as shown in Figure 5-1. A complete collapse of this entry was represented with an increase in resistance along branch number 455. The resistance was raised to 25,000 Ns^2/m^8. A roof fall in this area was expected to redirect air to the inner bleeder circuit. The quantity of air across the longwall face was expected to increase and more air would flow through the gob.

Coupling between the two models was initiated every 30 seconds. The time step for the Gob model was bounded by a 1 second maximum time step. The log files for the problem indicated that time steps as high as 70 seconds would have been possible, so this was well within the time step required for stability. The upper bound for the time step was established to ensure that race conditions between the two models would be avoided.

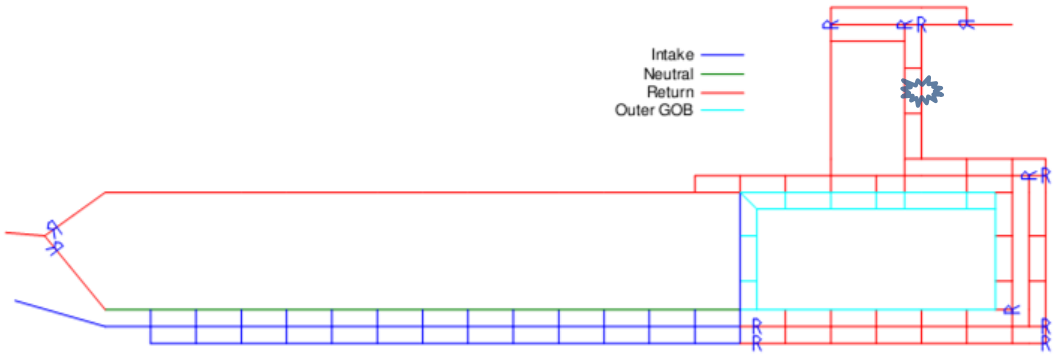

Figure 5-1 Location of roof fall, branch 455

The model completed running after an elapsed time of just under 18 minutes. Gob participation increased to 4.67 m^3/s, an increase of 27% over the baseline steady state case. A comparison between the MSVM results and the VNetPC model can be seen in Table 5-1. The percent difference for flow and pressure were 17.20% and 1.28% respectively. Two entries in the tailgate region accounted for the majority of the difference between the models. As with the steady state comparison, these branches had low flows across them and had an absolute difference of 0.6 m^3/s. In general, there was excellent agreement between the two models, once the new equilibrium condition was achieved.

Table 5-1 Comparison between MSVM and original VNetPC model, for the roof fall in bleeder entry scenario

Comparison Between MSVM Network Results and Original VNetPC Results								
Roof Fall in Bleeder Entry Scenario								
		Flow (m^3/s)				***Pressure (Pa)***		
Region	ID	MSVM	Original	% diff	ID	MSVM	Original	% diff
Intake	43	48.46	48.65	-0.40%	42	-81.0	-81.7	-0.85%
	23	39.80	39.95	-0.39%	22	-81.6	-82.3	-0.85%
	51	40.88	41.03	-0.38%	50	-200.0	-201.7	-0.83%
	31	39.12	39.27	-0.38%	30	-194.2	-195.8	-0.83%
Longwall	510	43.32	43.76	-1.02%	183	-303.4	-306.9	-1.14%
	632	42.28	42.99	-1.68%	160	-440.9	-449.3	-1.88%
	629	42.60	42.37	0.53%	94	-525.3	-532.9	-1.44%
Headgate	57	14.11	12.52	11.96%	56	-285.8	-281.2	1.61%
	37	8.25	8.06	2.30%	36	-267.2	-268.2	-0.37%
	61	11.48	11.69	-1.79%	60	-291.9	-286.1	2.00%
	41	7.60	7.57	0.45%	40	-284.4	-285.0	-0.21%
Bleeder	430	8.32	8.67	-4.18%	332	-292.0	-286.3	1.98%
	420	7.49	7.53	-0.55%	2	-360.3	-361.7	-0.39%
	424	12.42	12.71	-2.33%	161	-400.4	-403.8	-0.84%
	501	3.39	3.49	-3.00%	7	-550.4	-561.1	-1.93%
	141	1.52	1.54	-1.13%	138	-401.5	-404.7	-0.80%
	120	14.61	14.04	4.01%	118	-562.9	-573.8	-1.92%
	455	0.29	0.29	-0.27%	171	-2492.9	-2502.9	-0.40%
	439	28.03	28.01	0.06%	167	-695.4	-705.5	-1.44%
	480	30.68	30.70	-0.06%	157	-764.6	-774.6	-1.30%
Tailgate	496	8.32	8.51	-2.27%	95	-551.2	-560.1	-1.60%
	116	27.15	27.79	-2.33%	115	-551.4	-560.3	-1.60%
	494	1.20	1.81	-40.82%	97	-567.9	-578.1	-1.79%
	119	7.17	7.36	-2.59%	169	-568.5	-578.8	-1.80%
	493	-0.44	0.17	449.42%	168	-567.8	-578.1	-1.79%
	492	4.94	4.64	6.36%	99	-558.6	-570.1	-2.04%
Return	115	5.37	5.66	-5.22%	113	-537.1	-545.1	-1.47%
	95	12.91	13.09	-1.36%	93	-537.0	-545.0	-1.47%
	94	7.54	7.43	1.49%	92	-541.1	-548.9	-1.43%
Belt	75	22.68	22.86	-0.81%	73	-240.8	-242.9	-0.88%
	71	13.82	13.87	-0.38%	69	-248.0	-250.4	-0.96%
	64	20.76	20.85	-0.42%	62	-271.5	-274.2	-1.01%

Residual values at the boundary conditions were examined for pressure and flow. Pressure residuals was normalized against the average pressure value in the gob, -424 Pa, while the flow residuals were normalized against the gob participation factor, 4.67 m^3/s. Normalized Pressure values rapidly settled below a threshold of 10^{-3} for all but

two of the shared boundaries after 330 seconds. The remaining two settled below a value of $2x10^{-3}$ after 1,050 seconds. Normalized total flow residuals never achieved the threshold of 10^{-3}, but instead settled below a value of $2x10^{-3}$ after 1,440 seconds.

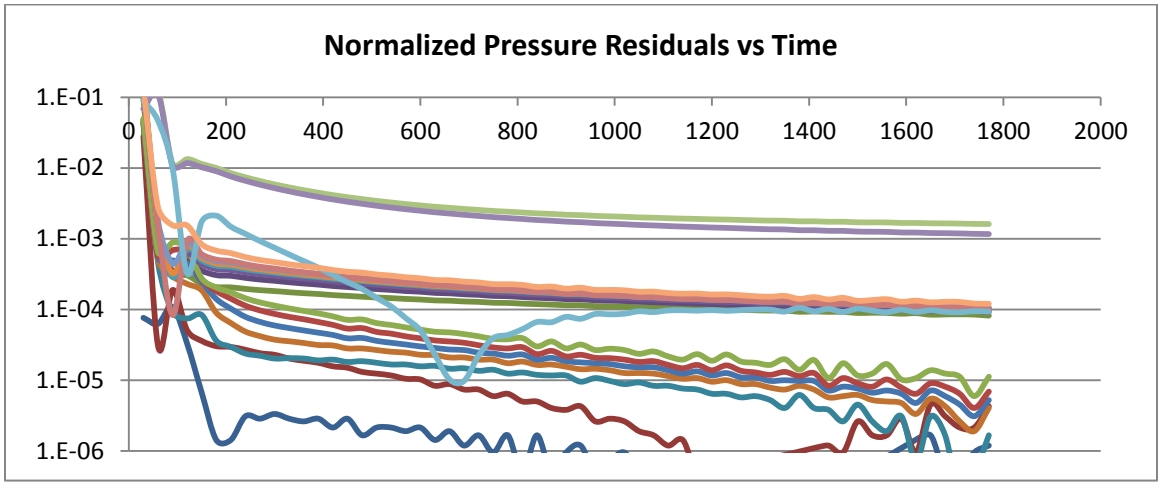

Figure 5-2 Normalized pressure residuals versus time in seconds for the roof fall in bleeder entry scenario

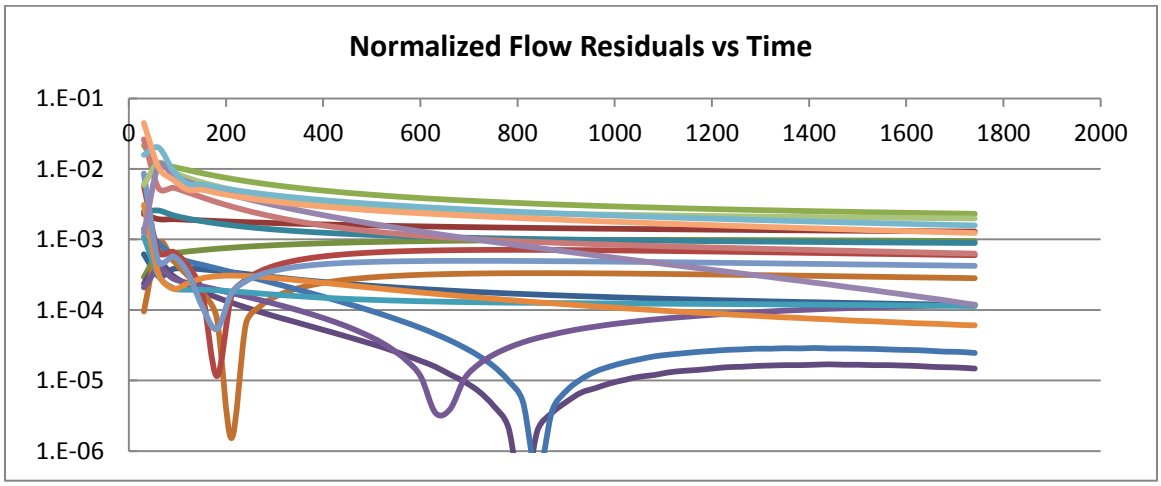

Figure 5-3 Normalized flow residuals versus time in seconds for the roof fall in bleeder entry scenario

The increase in gob participation was largely confined to the corner near the head gate and start up rooms. This was due to the air being redirected to across the start up room due to the obstruction in the bleeder entries. The evolution of the flow pattern through

the gob was where the transient response was most evident. It can be seen in Figure 5-4.

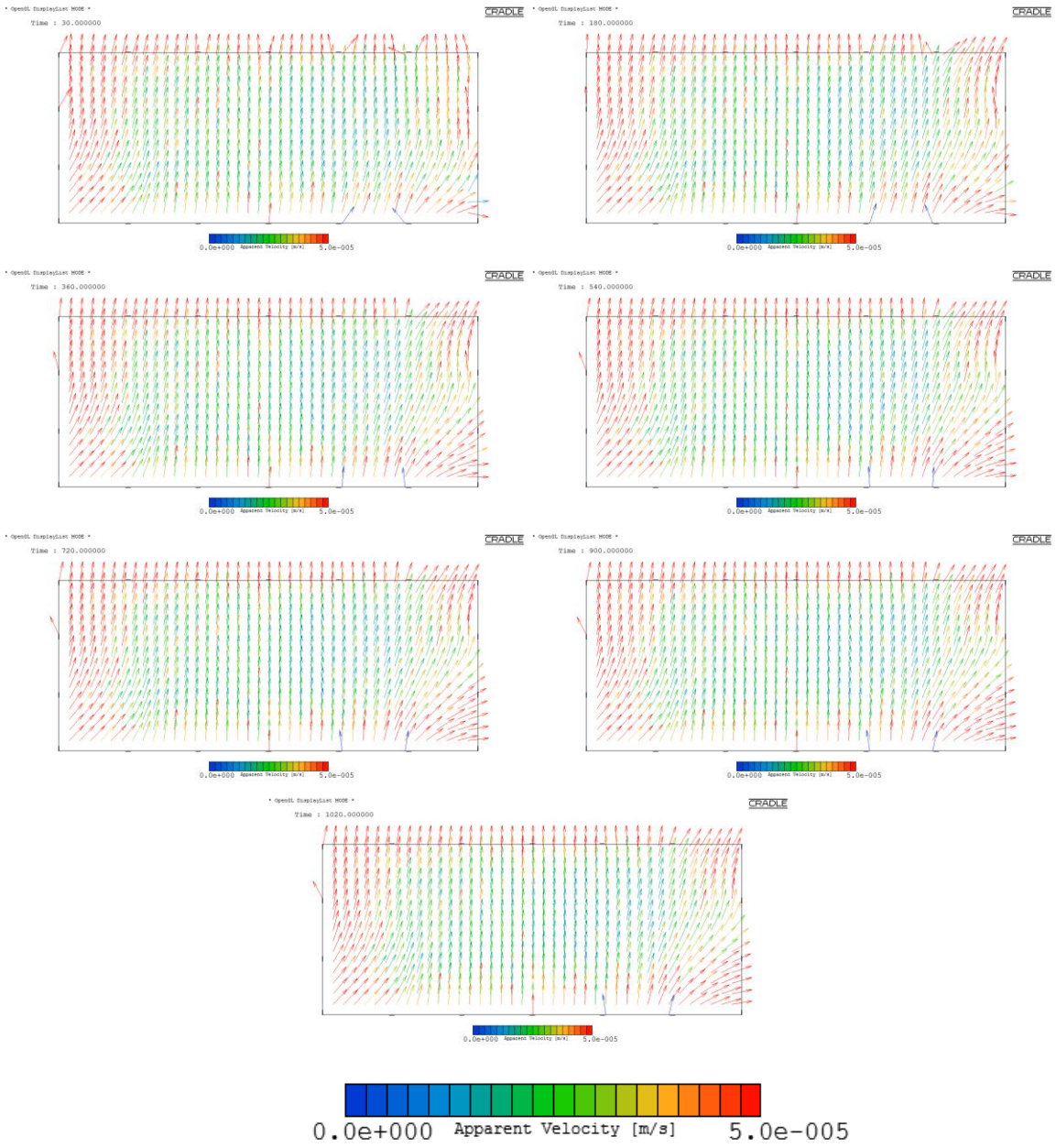

Figure 5-4 Transient response of flow due to a roof fall in branch in the bleeder entries at a plane 1 meter from the floor

No appreciable changes in methane levels or gob explosibility were observed within the gob. As seen in the previous images, the flow of air from the longwall face and through the tailgate entries remained consistent through the scenario.

5.2 Roof Fall in the Adjacent Panel Start Up Room

The start up room from the previous adjacent panel was open to carry air to the bleeder shaft. Nearly a fourth of the air reporting to the bleeder shaft was delivered through this entry. The roof fall scenario from the previous section was repeated for this branch, numbered 480, as shown in Figure 5-5.

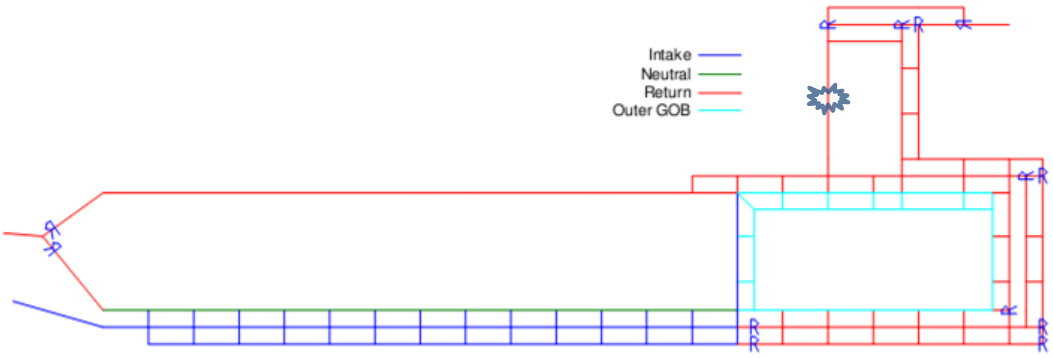

Figure 5-5 Location of roof fall, branch 480

A complete collapse of this entry was represented with an increase in resistance along branch number 480. The resistance was raised to 25,000 Ns^2/m^8. A roof fall in this area was expected to redirect air to the bleeder circuit. The quantity of air across the longwall face was expected to decrease and more air would again flow through the gob.

During this scenario, the MSVM model reached a new equilibrium point after just over 25 minutes had elapsed. The gob participation factor increased to 4.58 m3/s, a 24% increase in air delivered to the gob over the baseline steady state case. The comparison between the MSVM model and the VNetPC model, with the same change applied, can be seen in Table 5-2. As before, there is close agreement between the two models. The average percent difference in reported flow between the two models was 2.61% and the average percent difference in pressure was 1.38%.

Table 5-2 Comparison between MSVM and original VNetPC model for the roof fall in adjacent panel start up room scenario

Comparison Between MSVM Network Results and Original VNetPC Results								
Roof Fall in Adjacent Panel Start Up Room Scenario								
		Flow (m^3/s)				***Pressure (Pa)***		
Region	ID	MSVM	Original	% diff	ID	MSVM	Original	% diff
Intake	43	48.55	48.63	-0.17%	42	-81.4	-81.7	-0.39%
	23	39.93	39.99	-0.15%	22	-82.0	-82.3	-0.33%
	51	41.05	41.11	-0.14%	50	-201.2	-201.8	-0.31%
	31	39.26	39.32	-0.15%	30	-195.4	-196.0	-0.32%
Longwall	510	38.00	38.92	-2.39%	183	-291.7	-295.0	-1.12%
	632	36.98	37.69	-1.90%	160	-396.9	-404.5	-1.90%
	629	37.27	37.14	0.35%	94	-461.5	-468.8	-1.58%
Headgate	57	17.34	15.98	8.16%	56	-309.0	-297.4	3.84%
	37	12.00	11.60	3.37%	36	-293.6	-290.9	0.93%
	61	14.29	14.75	-3.14%	60	-317.8	-305.1	4.07%
	41	11.78	11.82	-0.36%	40	-332.5	-329.0	1.05%
Bleeder	430	11.50	11.90	-3.39%	332	-318.1	-305.5	4.05%
	420	11.94	12.03	-0.76%	2	-525.3	-524.6	0.14%
	424	20.52	20.85	-1.59%	161	-634.9	-637.6	-0.43%
	501	2.92	3.08	-5.31%	7	-510.9	-519.5	-1.67%
	141	30.73	30.83	-0.31%	138	-833.2	-837.6	-0.53%
	120	-1.97	-1.88	4.86%	118	-509.3	-518.0	-1.70%
	455	32.23	32.31	-0.24%	171	-976.2	-981.4	-0.53%
	439	26.67	26.59	0.31%	167	-633.2	-641.5	-1.31%
	480	0.10	0.09	5.68%	157	-717.3	-725.1	-1.08%
Tailgate	496	6.95	7.15	-2.87%	95	-479.6	-488.0	-1.75%
	116	21.71	22.33	-2.83%	115	-479.7	-488.1	-1.74%
	494	5.59	5.50	1.56%	97	-501.7	-511.0	-1.83%
	119	24.98	24.80	0.74%	169	-509.2	-518.3	-1.77%
	493	5.46	5.29	3.25%	168	-508.6	-517.6	-1.76%
	492	-0.78	-0.91	-16.02%	99	-508.6	-517.6	-1.76%
Return	115	2.60	2.85	-9.05%	113	-470.9	-478.5	-1.59%
	95	11.63	11.75	-1.03%	93	-470.9	-478.5	-1.59%
	94	9.03	8.91	1.31%	92	-476.7	-484.1	-1.54%
Belt	75	22.87	23.11	-1.03%	73	-242.0	-243.0	-0.40%
	71	12.44	12.52	-0.68%	69	-247.8	-249.0	-0.48%
	64	19.31	19.42	-0.59%	62	-267.6	-269.3	-0.65%

5.3 Bleeder Fan Loss of Power

The final transient scenario examined was a complete loss of power to the bleeder fan. With the bleeder fan coasting down, the pressure and flow within the network was significantly impacted, with flow reversals occurring in nearly all the branches along the tailgate and a portion of the bleeder entries. The flow through the bleeder shaft, a boundary condition for the network portion of the MSVM was modified to impart a logarithmic decay in flow that can be seen in Figure 5-6.

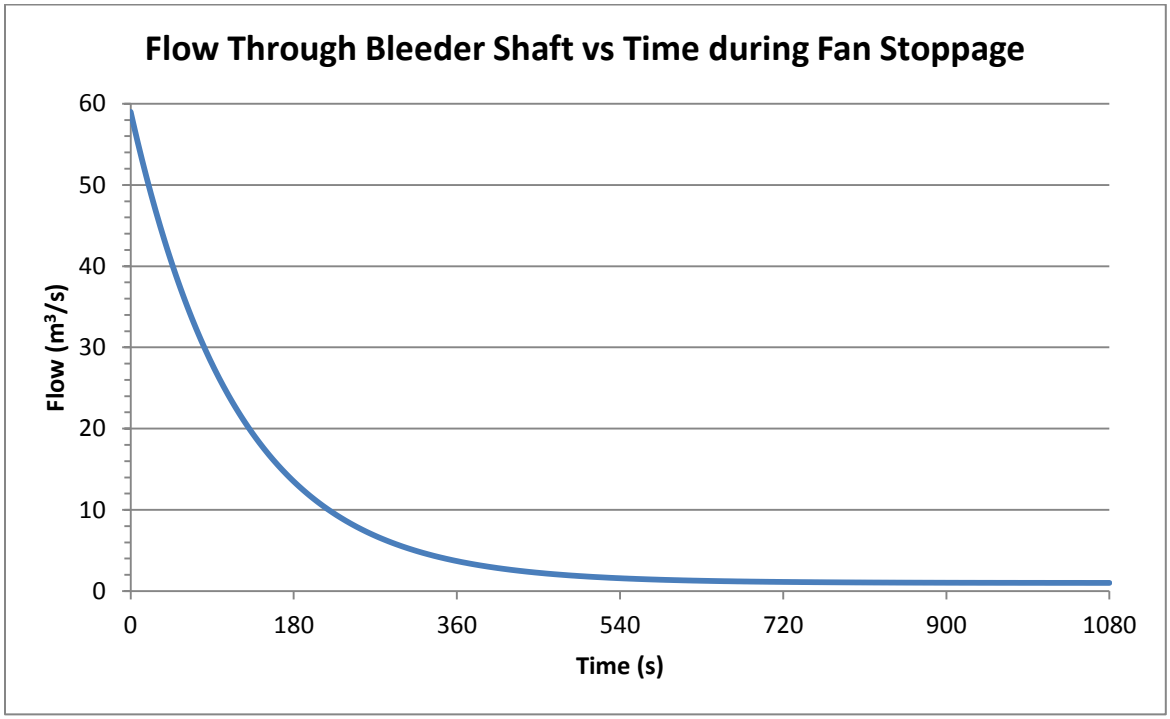

Figure 5-6 Boundary condition of flow through bleeder shaft for fan stoppage scenario

The change in pressure through the gob in response to the bleeder fan stoppage can be seen in 

Figure 5-7. The pressure gradient, oriented from headgate side to tailgate side, deteriorates as it was largely driven by the action of the bleeder fan. Mild ringing around the coupling regions can be seen, which in turn influences the flow patterns through the gob.

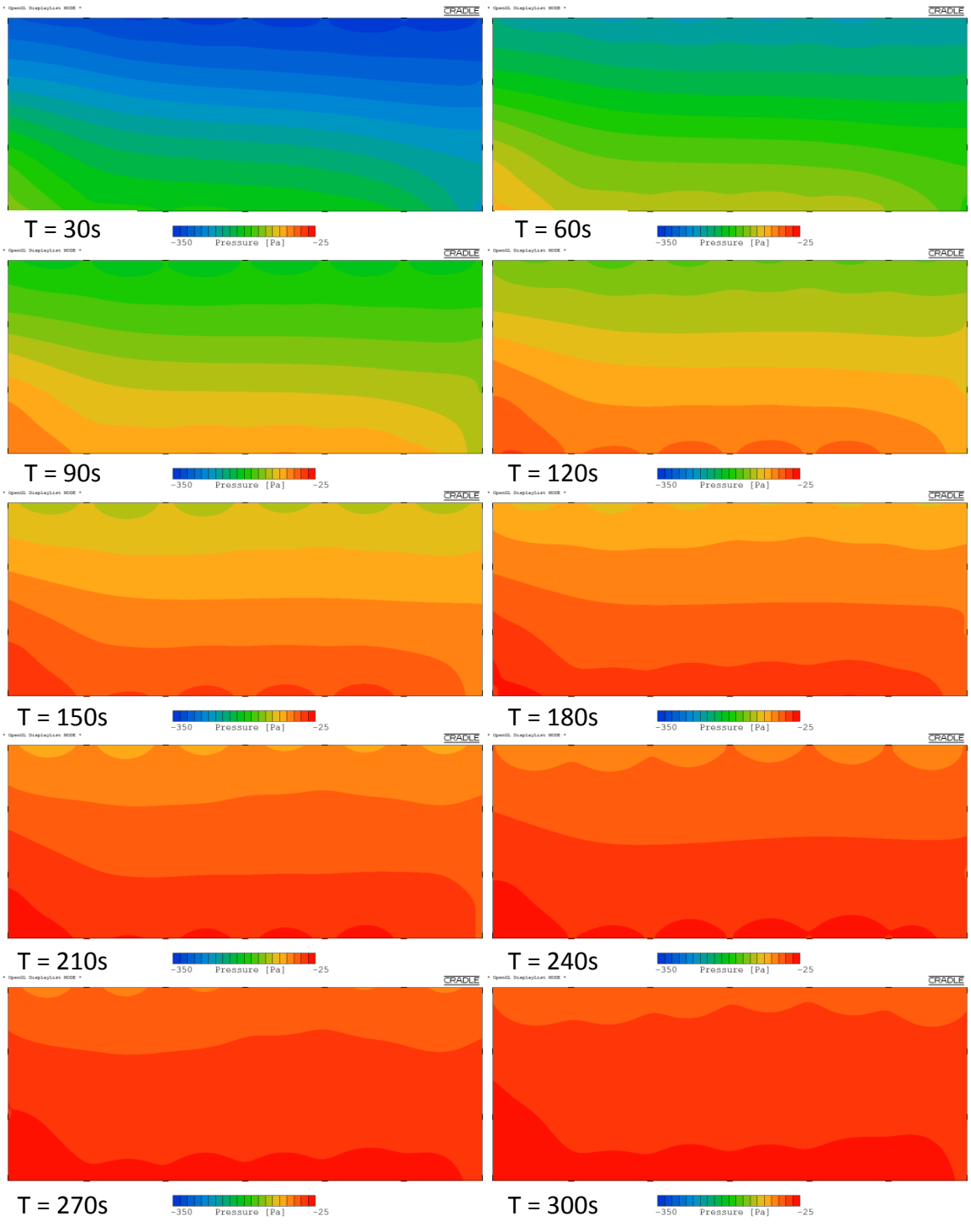
CRADLE
T = 30s
T = 60s
T = 90s
T = 120s
T = 150s
T = 180s
T = 210s
T = 240s
T = 270s
T = 300s
-350 Pressure [Pa] -25

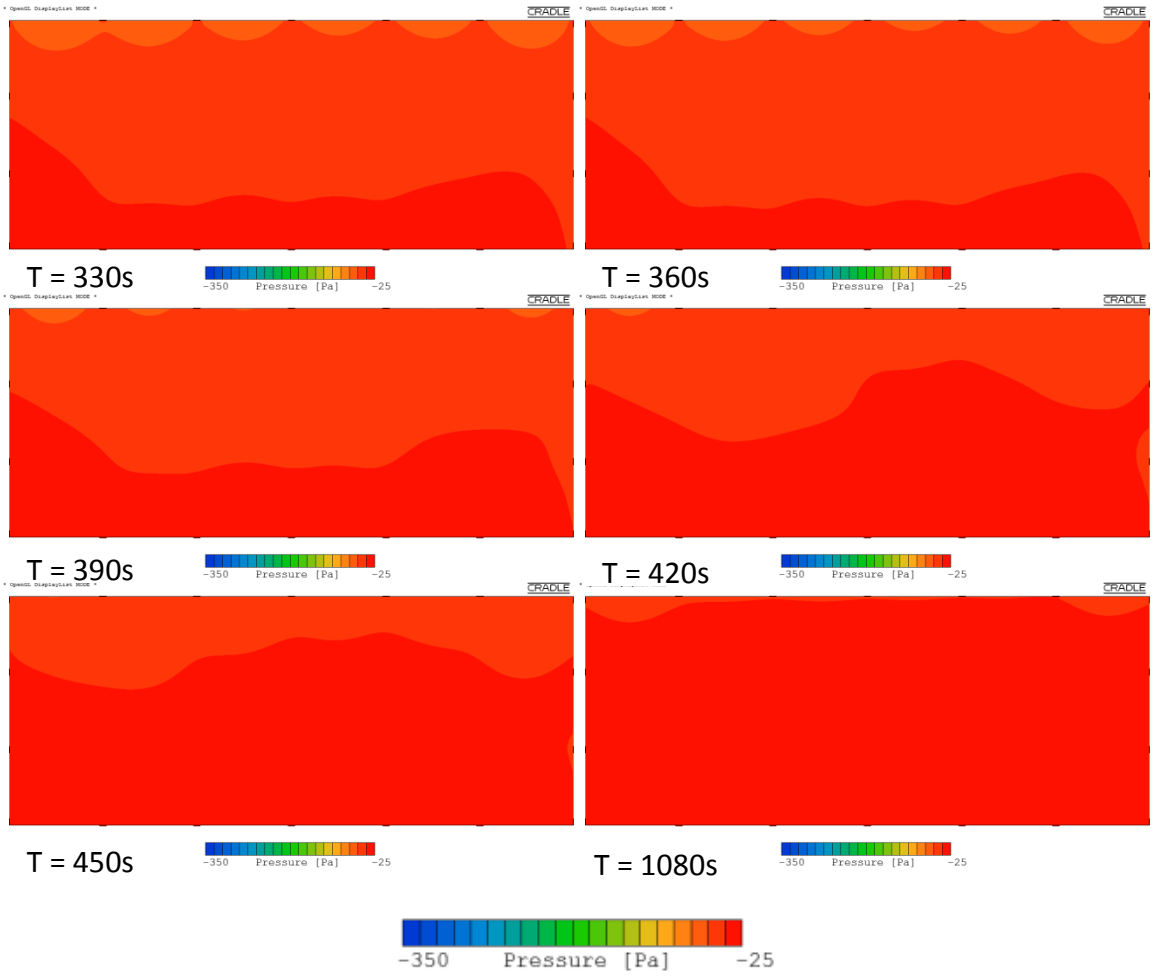

Figure 5-7 Transient pressure response within the gob due to a stoppage of the bleeder fan at a plane 1 meter from the floor

The evolution of the flow pattern within the gob is shown in Figure 5-8. The pattern within the gob was well structured in the beginning. The boundary conditions were changing rapidly and the ringing around the headgate and tailgate coupled regions was evident in the flow patterns as well. By the end of the 18 minute duration, the pattern within the gob from headgate side to tailgate side was largely disrupted. The gob participation factor dropped to 1.75 m^3/s, a decline of over 50%. The flow through the gob was being driven, in all likelihood, by the main fan, where previously it was largely influenced by the actions of the bleeder fan.

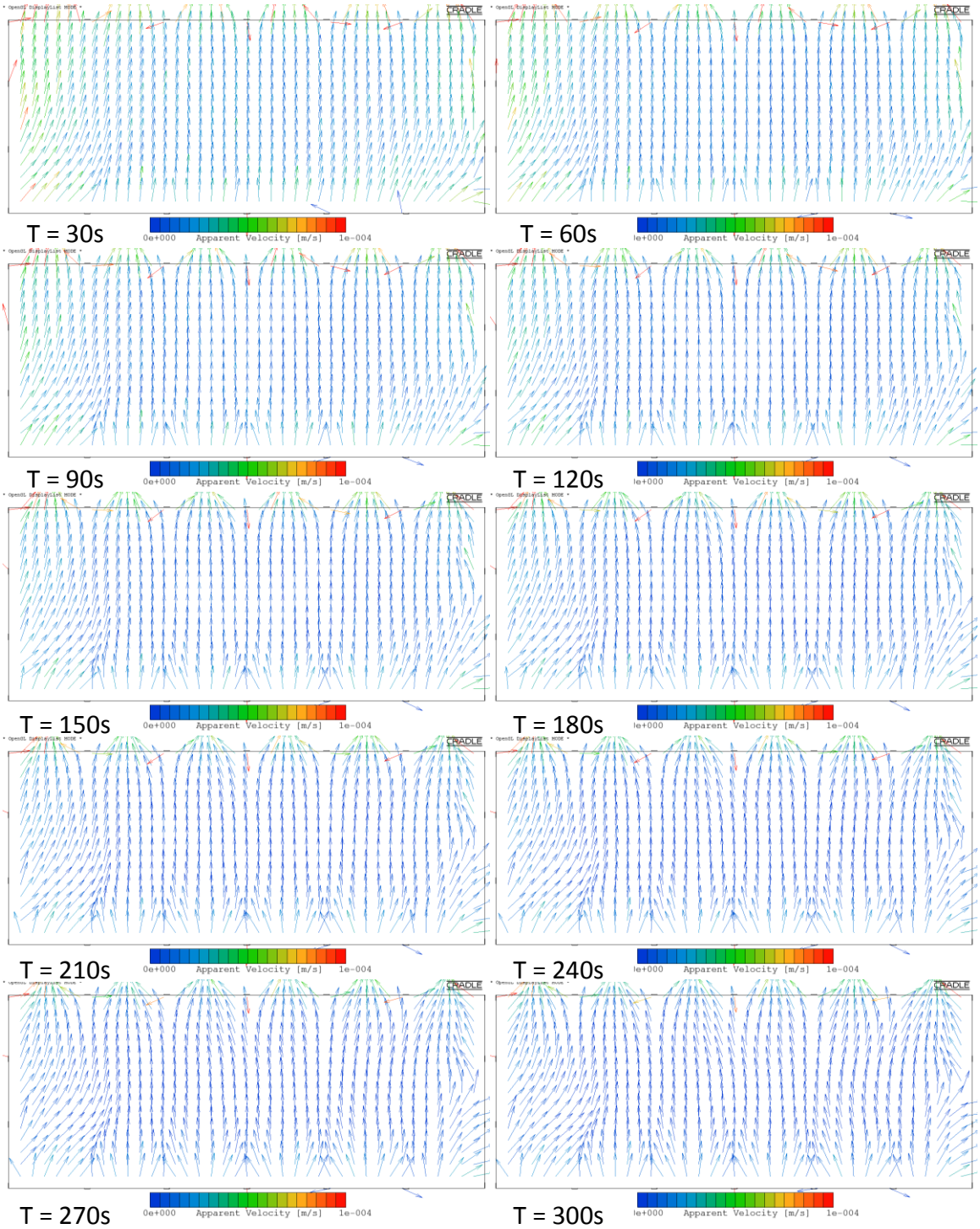
CRADLE
0e+000 Apparent Velocity [m/s] 1e-004
T = 30s
T = 60s
T = 90s
T = 120s
T = 150s
T = 180s
T = 210s
T = 240s
T = 270s
T = 300s

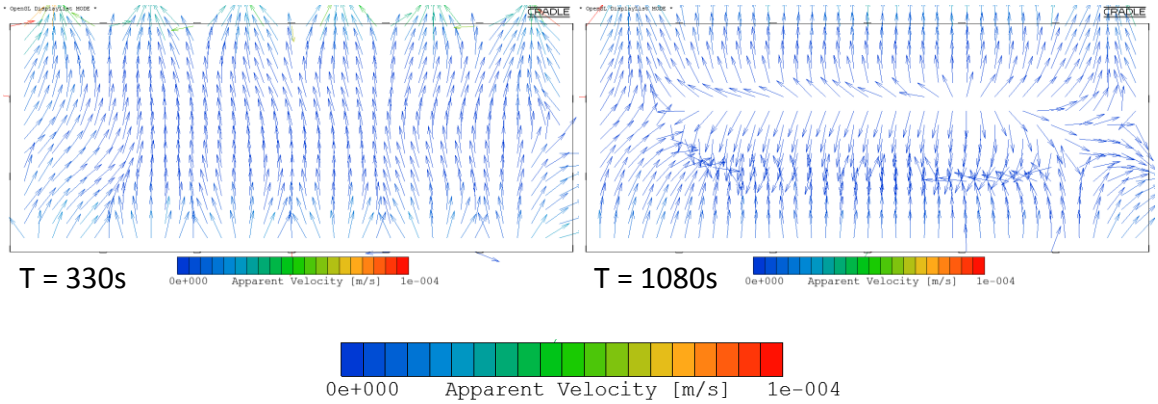

Figure 5-8 Transient flow response within the gob due to a stoppage of the bleeder fan at a plane 1 meter from the floor

The response of the gob methane concentration can be seen in Figure 5-9. There was little observable change in methane concentrations. The inflow of methane at 0.1229 m^3/s was too small relative to the gob volume of 10 million cubic meters to have an appreciable change over the 18 minute duration.

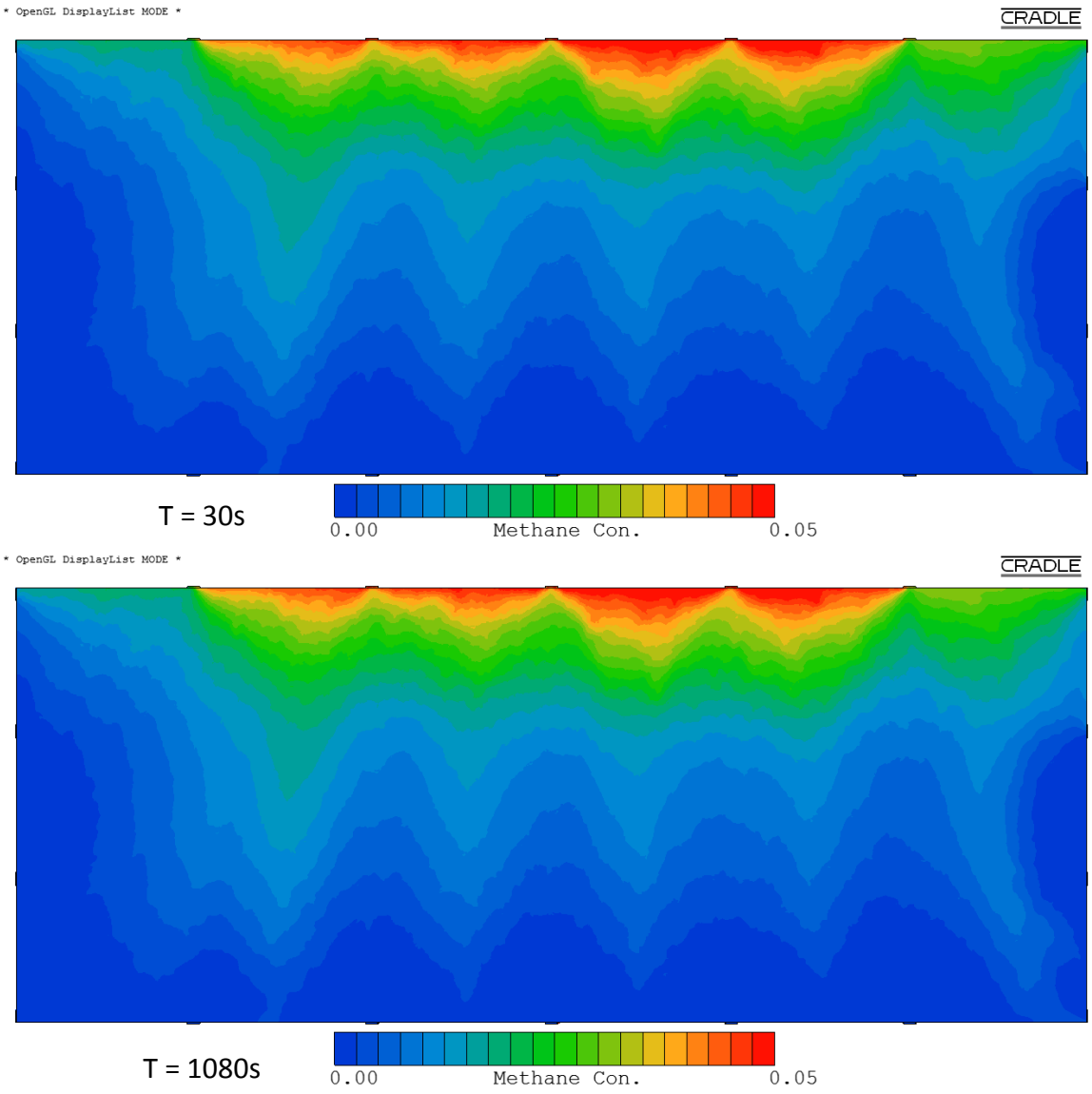

Figure 5-9 Transient methane concentration response within the gob due to a stoppage of the bleeder fan at a plane 1 meter from the floor

The results from MSVM network model were compared with the VNetPC results with the same reduction in flow at the bleeder fan as shown in Table 5-3. The final results of the MSVM network model closely match the VNetPC model. Flow and pressure were within 6.53% and 2.10% respectively.

Table 5-3 Comparison between MSVM and original VNetPC model for the fan stoppage scenario

Comparison Between MSVM Network Results and Original VNetPC Results								
Stoppage of Bleeder Fan								
		Flow (m^3/s)				***Pressure (Pa)***		
Region	ID	MSVM	Original	% diff	ID	MSVM	Original	% diff
Intake	43	17.38	17.46	-0.45%	42	-10.3	-10.4	-1.45%
	23	13.84	13.89	-0.37%	22	-10.1	-10.3	-1.71%
	51	13.95	13.92	0.19%	50	-24.0	-24.8	-3.32%
	31	13.52	13.57	-0.38%	30	-23.0	-23.8	-3.26%
Longwall	510	9.76	9.46	3.12%	183	-31.4	-32.5	-3.50%
	632	9.62	9.28	3.59%	160	-38.4	-36.1	6.13%
	629	10.02	9.16	8.92%	94	-42.9	-43.0	-0.17%
Headgate	57	2.92	2.91	0.27%	56	-30.1	-31.5	-4.55%
	37	1.99	2.01	-0.97%	36	-29.8	-31.0	-4.04%
	61	2.87	2.72	5.35%	60	-30.4	-31.9	-4.96%
	41	1.99	1.95	2.27%	40	-30.9	-32.2	-4.12%
Bleeder	430	2.18	2.10	3.87%	332	-30.4	-31.9	-4.87%
	420	2.03	1.98	2.30%	2	-36.5	-37.5	-2.84%
	424	3.49	3.39	2.99%	161	-39.6	-40.5	-2.13%
	501	0.72	0.69	3.70%	7	-42.0	-42.5	-1.08%
	141	2.13	2.12	0.35%	138	-40.6	-41.2	-1.40%
	120	1.97	2.06	-4.32%	118	-42.4	-42.9	-1.07%
	455	2.01	2.02	-0.28%	171	-41.3	-41.8	-1.25%
	439	0.06	0.09	-45.99%	167	-42.6	-42.6	-0.05%
	480	-1.06	-0.93	13.37%	157	-42.4	-42.6	-0.53%
Tailgate	496	0.22	0.27	-18.22%	95	-43.0	-43.0	-0.09%
	116	-4.32	-4.42	-2.35%	115	-43.0	-43.0	-0.03%
	494	-0.75	-0.54	32.26%	97	-42.6	-42.7	-0.21%
	119	-2.08	-2.42	-15.27%	169	-42.6	-42.6	-0.12%
	493	-0.72	-0.55	27.35%	168	-42.5	-42.6	-0.15%
	492	0.69	0.71	-2.70%	99	-42.4	-42.8	-1.03%
Return	115	-8.44	-8.49	-0.55%	113	-44.7	-44.8	-0.25%
	95	5.36	5.33	0.58%	93	-44.9	-45.0	-0.24%
	94	13.81	13.82	-0.11%	92	-58.3	-58.5	-0.42%
Belt	75	2.94	2.79	5.18%	73	-28.5	-29.7	-4.03%
	71	12.80	12.68	0.97%	69	-34.9	-36.4	-4.25%
	64	15.96	15.91	0.28%	62	-50.4	-52.4	-3.88%

6 Conclusions

6.1 Conclusions

The objective of this dissertation was to adapt the multi-scale technique practiced in other fields to the mining engineering discipline. Mine ventilation systems are especially suited to this technique, as they are networks, by their very nature, with high aspect ratio elements in the form of entries, slopes, and shafts. This affords one the ability to model the bulk of the network with a simplified model, while the area local to the problem of interest can be represented with greater complexity. The challenge of modeling the gob environment was the problem of interest in this dissertation. The gob is an important source of coalbed methane which presents a hazard to those working in the mine. Because the gob tends to be massive, with numerous connections to the ventilation network, it is a natural candidate for the MSVM approach.

The Gob model was developed with guidance provided by the literature review. The essential nature of modeling the gob is encapsulated within the chosen porous media model. In this dissertation, two formulations of the gob model were examined. One was a simple two zone gob model while the other was a continuously variable fit of permeability. The former model was available with the standard settings of SC/Tetra, while the continuously variable fit required a user defined function to implement. The permeability for this work was drawn from geotechnical modeling literature. The geotechnical model predicts the porosity of the gob which then predicts permeability through the use of the Kozeny-Carman equation.

The necessity of the MSVM approach was established through an exhaustive study of mine entry meshing parameters. The momentum sink at the walls due to friction is handled by the rough log law of the wall in SC/Tetra. It is expected that there is a mesh of minimum element count that can accurately predict pressure and flow in an entry represented in CFD. There is a practical limit to the range of velocities that one will encounter in the mining environment, generally ranging from 0.05 to 15 m/s and all turbulent. The correlation between mine entry friction factors and the Moody friction

factor was established, which served as the theoretical expected value for the CFD study. The testing was automated using a sequence of PERL scripts that generated new meshes, input files, and extracted data from the log files. A clear rubric for meshing coal mine entries was established that could accurately depict a range of relative roughness values from smooth walls up to 5%. This encompassed the range of friction factors expected in the mine. The conclusion was that it took roughly 1,000 elements per meter of entry to capture pressure and flow distributions within the mine. The scenario modeled with the MSVM technique had 22 km of entries, and was only a portion of the mine. It was represented with a little over 200 elements, as compared to 22 million elements. It was clearly established that the mine ventilations systems are excellent candidates for the multi-scale approach.

The network portion of the MSVM was developed in Matlab using an explicit, finite difference approach. A number of simplifying assumptions were necessary to accomplish this task, including the decision to implement an incompressible model. The continuity equations were reduced to a just four essential equations used to recursively calculate the pressure, flow, and species concentration within the system. Comparisons between the calibrated VNetPC model and the network portion of the MSVM yielded identical results, for steady state cases.

The first coupling exercise was an asynchronous scheme that required manual intervention to progress to steady state. Both the network and gob portion of the model were allowed to progress to steady state before exchanging boundary conditions. It was found that just thirteen coupling iterations were needed to achieve convergence at a 10-3 m^3/s level. This was an encouraging result as it demonstrated how quickly this technique could progress to convergence. Despite the large change in exchanged boundary conditions early in the testing, the process did not diverge and no need for under relaxation of the coupled data was identified. With these results the user defined function for the coupling algorithm was developed.

Complementary portions of code in SC/Tetra and Matlab were developed to handle the coupling scheme. The key challenges were preventing race conditions at the boundary condition, and dealing with the nuances of MPI enabled code running on a linux platform with 16 nodes and locally on a Windows platform. Boundary conditions were passed with flat text files which was the most straightforward method considering the two platforms used. It also served as a log file for information passed at the coupled boundaries. There was a fair amount of overhead with reading and writing to the disk, so synchronous coupling was deemed too costly to implement. Instead, the system was set up to exchange boundary information at every *nth* cycle, or at some prescribed time interval. With the model in this study, a minimum of twenty cycles were required to prevent race conditions from occurring. This provided the Matlab and SC/Tetra portions sufficient time to complete their respective calculations and generate new boundary conditions. It was desired to implement synchronous coupling, but this would require implement the entirety of the Matlab code within the SC/Tetra user defined code library. This was identified as a candidate for future work.

The MSVM scenario was based upon the work of NIOSH researchers. They conducted a tracer gas study and ventilation survey of a longwall mine in south western Pennsylvania. The use of a tube bundle sampling system allowed the researchers to characterize portions of the mine which would be otherwise inaccessible. The work culminated in a calibrated VNetPC model of the mine, which included branches representing the gob. This was considered to be my baseline case for comparison with the present MSVM approach.

The MSVM modeling process began with a mesh independence study. This provided the necessary guidance for choosing appropriate meshing parameters for the subsequent models. The importance of having a grid independent solution is self-evident. Mesh independence was judged by the amount of air entering and exiting the gob and the distribution of this exchange about the perimeter. A qualitative evaluation of the methane distribution was also performed. The final meshing guidelines yielded a base

octant size of 2.5 meters with significant refinement near the coupled boundaries. The total element count for the selected mesh was nearly 1.5 million elements, which was less than typically encountered in modern gob modeling studies. This was attributed to have no elements in the Gob model dedicated to entryways. Computation time for this MSVM model was just over forty minutes.

During the mesh independence study, the performance of the coupling scheme was also evaluated. Normalized residuals at the boundaries were tracked during the simulation, for pressure, flow, and methane concentration. The coupling scheme implemented included exchanging boundary information at 50 cycle intervals. This proved to be a modest decline over the previously run manual coupling exercise, with convergence achieved after 14 iterations.

The MSVM technique was validated against the original VNetPC model provided by NIOSH. A total of 32 locations spread around the network were compared across the two models. These included pressure and flow readings spread across all the regions in the mine ventilation system, including intake, longwall, headgate, bleeder, tailgate, return, and belt entries. The average percent difference for flow between the present MSVM study and the original calibrated VNetPC model was 1.92%, and 1.22% for pressure data points. The only significant difference was found in a branch in the tailgate entries, which had a percent difference of 27%, but an absolute difference of 0.054 m^3/s. In summary, there was excellent agreement between the two models for pressure and flow.

Sensitivity to the selected turbulence model was evaluated next. Six turbulence models were examined. The standard κ-ε model failed to converge, while the formulations that included low Reynolds number adaptations were able to converge. This was thought to be due to the treatment near the walls of the gob model. The AKN κ-ε model includes added damping that more accurately accounts for the effects of the wall. This AKN κ-ε model was used for subsequent studies.

The results of the gob model comparison demonstrated the advantage associated with using a smooth gob model. The two zone gob model demonstrated several obviously non-physical results. This had a great impact on the contours of gob explosibility. The two zone gob model was deemed inappropriate for even approximations. In other models, adjustments to the gob permeability values yielded the expected changes to the gob participation factor. With an increase in gob permeability, the resulting change in the gob participation factor was an increase to 4.18 m^3/s, or a 13.8% increase in air flowing through the gob over the baseline. Upon decreasing the permeability, the gob participation factor decreased to 3.03 m^3/s, for a 17.8% decrease from the baseline. The performance of the MSVM approach did indicate increasing flow with increasing permeability and decreasing flow with decreasing permeability.

An examination of increasing the number of coupling regions highlighted one of the drawbacks of this approach. Flow through the boundary was found to be recirculating at this region. This was judged to be due to the close proximity of the coupling regions which led to low difference in pressure between adjacent coupling regions. Care must be taken to ensure that the coupling boundaries are well formed and function entirely as either inlets or outlets to the model. A proposed solution to this problem is discussed in the future work section.

6.2 Novel Contribution to the Field of Mining Engineering

The principal aim of this research was to create a new and significant contribution to the study of flow through the mine ventilation system and the influence of the gob during longwall retreat mining. There are certainly difficulties associated with accurately modeling this region due to its relative inaccessibility. This research effort allows a more complete examination of the influence of the mine network on the flow patterns within the gob. There is no expectation of a complete and wholly accurate model of flow, but there is an expectation of an improved modeling through the use of the network as a boundary condition and with the additional benefit of adding transient simulations to the field.

Many researchers have examined the flow of gas through the gob for spontaneous combustion studies and to maximize the effect of inertization and gob borehole venting strategies using computational fluid dynamics, but none have included the mine network. The fan or fans and the rubbing surfaces of the entries are the key source and sink for momentum in the system. Including these features within the computational domain of a three dimensional model had been previously out of reach. Simplifying these features as one dimensional elements offers a compromise of speed and accuracy, while retaining these key momentum exchanges. This has been accomplished in other fields. Adapting these techniques to the mine ventilation system paves the way for new simulations in other mine ventilation problems, such as combustion modeling, the influence of gas outbursts, the ventilation of room and pillar mines with pillar extraction, and the examination of face ventilation scenarios that could potentially benefit from including the mine network in the computational domain.

6.3 Recommendations for Future Work

Combining the findings of the literature survey with the research conducted during the course of preparing this dissertation, leads to the following recommendations for future work.

- *Non-equilibrium Methane Desorption Model*
  The reservoir based modeling approach includes a sophisticated model for methane desorption that more has not been adapted to any CFD studies. This could be necessary for proper modeling of transient scenarios instead of using a fixed inflow condition. This is envisioned as a volume where this model could be implemented, more closely mimicking the physical phenomena
- *Recirculating Boundary Conditions*
  The problem of recirculating boundary conditions needs to be corrected to expand the applicability of the MSVM approach. A partial solution of adding artificial viscosity to the boundary conditions does ensure that the coupling regions operate as either inlets or outlets exclusively. The next step would be to measure the pressure slightly downstream and make an adjustment to compensate for the high shear stresses added which alters the flowrate through these highly viscous zones.
- *Synchronous Coupling*
  Due to the overhead with the method chosen for exchanging boundary conditions, synchronous coupling was not practical. By re-architecting the network code, this could

be implemented entirely within SC/Tetra user defined functions to enable fully synchronous coupling at any time or cycle interval chosen.

- *Scale Modeling of the Gob*
  Scale modeling of the gob environment could lead to fresh insight into the problem that would lead to better modeling in CFD. The inhospitable nature of the gob prevents direct study, so scale modeling would be the next logical course to take.
- *Other MSVM Scenarios*
  The multi-scale approach to ventilation modeling is new to the field of mine ventilation research. It could be applied to the study of mine fires, dust control technologies, and other problems of interest in mining.

Appendix I

1 Steady State MSVM Input Files

The following is a record of the s files used as input conditions to SC/Tetra.

1.1 Two Zone Gob Model with 18 Coupled Regions

The following is an example of the input file ('.s') for SC/Tetra for the steady state case with a 2 zone gob model.

```
SDAT
SC/Tetra
  10   0   0
PREI    PA_Mine1.pre
RO      PA_Mine1.r
POST    PA_Mine1
/
   1   1   0
PA_Mine1
   3   1
CHKC
   1
pLW1
pLW2
pLW3
pLW4
pHG1
pHG2
pHG3
pHG4
pHG5
pTG1
pTG2
pTG3
pTG4
pTG5
pSU1
pSU2
pSU3
pSU4
/
CHKF
   1
LW1
LW2
LW3
LW4
HG1
```

```
HG2
HG3
HG4
HG5
TG1
TG2
TG3
TG4
TG5
SU1
SU2
SU3
SU4
/
CHKL
       1        1        0        1        1
CYCS
       1    1100
EQUA
1101111
FLUX
%CNAM Flux_1
  -2   0 -100   0   2 -100
   3
1 50
PressMatlab2CradleM1.csv
MassCradle2MatlabM1.csv
                        5                        50
   7
   3
C1Matlab2CradleM1.csv
C2Matlab2CradleM1.csv
C3Matlab2CradleM1.csv
C1Cradle2MatlabM1.csv
C2Cradle2MatlabM1.csv
C3Cradle2MatlabM1.csv
LW1
/
%CNAM Flux_2
  -2   0 -101   0   2 -101
   3
1 50
PressMatlab2CradleM1.csv
MassCradle2MatlabM1.csv
                        5                        50
   7
   3
C1Matlab2CradleM1.csv
C2Matlab2CradleM1.csv
C3Matlab2CradleM1.csv
C1Cradle2MatlabM1.csv
C2Cradle2MatlabM1.csv
```

```
C3Cradle2MatlabM1.csv
LW2
/
%CNAM Flux_3
  -2   0 -102   0   2 -102
   3
1 50
PressMatlab2CradleM1.csv
MassCradle2MatlabM1.csv
                       5                       50
   7
   3
C1Matlab2CradleM1.csv
C2Matlab2CradleM1.csv
C3Matlab2CradleM1.csv
C1Cradle2MatlabM1.csv
C2Cradle2MatlabM1.csv
C3Cradle2MatlabM1.csv
LW3
/
%CNAM Flux_4
  -2   0 -103   0   2 -103
   3
1 50
PressMatlab2CradleM1.csv
MassCradle2MatlabM1.csv
                       5                       50
   7
   3
C1Matlab2CradleM1.csv
C2Matlab2CradleM1.csv
C3Matlab2CradleM1.csv
C1Cradle2MatlabM1.csv
C2Cradle2MatlabM1.csv
C3Cradle2MatlabM1.csv
LW4
/
%CNAM Flux_5
  -2   0 -104   0   2 -104
   3
1 50
PressMatlab2CradleM1.csv
MassCradle2MatlabM1.csv
                       5                       50
   7
   3
C1Matlab2CradleM1.csv
C2Matlab2CradleM1.csv
C3Matlab2CradleM1.csv
C1Cradle2MatlabM1.csv
C2Cradle2MatlabM1.csv
C3Cradle2MatlabM1.csv
```

```
HG1
/
%CNAM Flux_6
  -2   0 -105   0   2 -105
   3
1 50
PressMatlab2CradleM1.csv
MassCradle2MatlabM1.csv
                       5                       50
   7
   3
C1Matlab2CradleM1.csv
C2Matlab2CradleM1.csv
C3Matlab2CradleM1.csv
C1Cradle2MatlabM1.csv
C2Cradle2MatlabM1.csv
C3Cradle2MatlabM1.csv
HG2
/
%CNAM Flux_7
  -2   0 -106   0   2 -106
   3
1 50
PressMatlab2CradleM1.csv
MassCradle2MatlabM1.csv
                       5                       50
   7
   3
C1Matlab2CradleM1.csv
C2Matlab2CradleM1.csv
C3Matlab2CradleM1.csv
C1Cradle2MatlabM1.csv
C2Cradle2MatlabM1.csv
C3Cradle2MatlabM1.csv
HG3
/
%CNAM Flux_8
  -2   0 -107   0   2 -107
   3
1 50
PressMatlab2CradleM1.csv
MassCradle2MatlabM1.csv
                       5                       50
   7
   3
C1Matlab2CradleM1.csv
C2Matlab2CradleM1.csv
C3Matlab2CradleM1.csv
C1Cradle2MatlabM1.csv
C2Cradle2MatlabM1.csv
C3Cradle2MatlabM1.csv
HG4
```

```
/
%CNAM Flux_9
  -2   0 -108   0   2 -108
   3
1 50
PressMatlab2CradleM1.csv
MassCradle2MatlabM1.csv
                       5                       50
   7
   3
C1Matlab2CradleM1.csv
C2Matlab2CradleM1.csv
C3Matlab2CradleM1.csv
C1Cradle2MatlabM1.csv
C2Cradle2MatlabM1.csv
C3Cradle2MatlabM1.csv
HG5
/
%CNAM Flux_10
  -2   0 -109   0   2 -109
   3
1 50
PressMatlab2CradleM1.csv
MassCradle2MatlabM1.csv
                       5                       50
   7
   3
C1Matlab2CradleM1.csv
C2Matlab2CradleM1.csv
C3Matlab2CradleM1.csv
C1Cradle2MatlabM1.csv
C2Cradle2MatlabM1.csv
C3Cradle2MatlabM1.csv
TG1
/
%CNAM Flux_11
  -2   0 -110   0   2 -110
   3
1 50
PressMatlab2CradleM1.csv
MassCradle2MatlabM1.csv
                       5                       50
   7
   3
C1Matlab2CradleM1.csv
C2Matlab2CradleM1.csv
C3Matlab2CradleM1.csv
C1Cradle2MatlabM1.csv
C2Cradle2MatlabM1.csv
C3Cradle2MatlabM1.csv
TG2
/
```

```
%CNAM Flux_12
  -2   0 -111   0   2 -111
   3
1 50
PressMatlab2CradleM1.csv
MassCradle2MatlabM1.csv
                       5                       50
   7
   3
C1Matlab2CradleM1.csv
C2Matlab2CradleM1.csv
C3Matlab2CradleM1.csv
C1Cradle2MatlabM1.csv
C2Cradle2MatlabM1.csv
C3Cradle2MatlabM1.csv
TG3
/
%CNAM Flux_13
  -2   0 -112   0   2 -112
   3
1 50
PressMatlab2CradleM1.csv
MassCradle2MatlabM1.csv
                       5                       50
   7
   3
C1Matlab2CradleM1.csv
C2Matlab2CradleM1.csv
C3Matlab2CradleM1.csv
C1Cradle2MatlabM1.csv
C2Cradle2MatlabM1.csv
C3Cradle2MatlabM1.csv
TG4
/
%CNAM Flux_14
  -2   0 -113   0   2 -113
   3
1 50
PressMatlab2CradleM1.csv
MassCradle2MatlabM1.csv
                       5                       50
   7
   3
C1Matlab2CradleM1.csv
C2Matlab2CradleM1.csv
C3Matlab2CradleM1.csv
C1Cradle2MatlabM1.csv
C2Cradle2MatlabM1.csv
C3Cradle2MatlabM1.csv
TG5
/
%CNAM Flux_15
```

```
  -2   0 -114   0   2 -114
   3
1 50
PressMatlab2CradleM1.csv
MassCradle2MatlabM1.csv
                       5                       50
   7
   3
C1Matlab2CradleM1.csv
C2Matlab2CradleM1.csv
C3Matlab2CradleM1.csv
C1Cradle2MatlabM1.csv
C2Cradle2MatlabM1.csv
C3Cradle2MatlabM1.csv
SU1
/
%CNAM Flux_16
  -2   0 -115   0   2 -115
   3
1 50
PressMatlab2CradleM1.csv
MassCradle2MatlabM1.csv
                       5                       50
   7
   3
C1Matlab2CradleM1.csv
C2Matlab2CradleM1.csv
C3Matlab2CradleM1.csv
C1Cradle2MatlabM1.csv
C2Cradle2MatlabM1.csv
C3Cradle2MatlabM1.csv
SU2
/
%CNAM Flux_17
  -2   0 -116   0   2 -116
   3
1 50
PressMatlab2CradleM1.csv
MassCradle2MatlabM1.csv
                       5                       50
   7
   3
C1Matlab2CradleM1.csv
C2Matlab2CradleM1.csv
C3Matlab2CradleM1.csv
C1Cradle2MatlabM1.csv
C2Cradle2MatlabM1.csv
C3Cradle2MatlabM1.csv
SU3
/
%CNAM Flux_18
  -2   0 -117   0   2 -117
```

```
   3
1 50
PressMatlab2CradleM1.csv
MassCradle2MatlabM1.csv
                      5                       50
   7
   3
C1Matlab2CradleM1.csv
C2Matlab2CradleM1.csv
C3Matlab2CradleM1.csv
C1Cradle2MatlabM1.csv
C2Cradle2MatlabM1.csv
C3Cradle2MatlabM1.csv
SU4
/
%CNAM Methane_Inflow
  -1   7   0   0   0   1
                 0.1229   0
                      0                        1
0
Inflow
/
/
FORC
%CNAM Forc_1
   5                   1016                        0
1   1
OuterGob
/
%CNAM Forc_2
   5                   10600                       0
1   1
InnerGob
/
/
GWLN
   0
INIT
PRES
                   -300  -1
OuterGob
InnerGob
/
/
INIT
CN02
                      1  -1
InnerGob
OuterGob
/
/
PLGN
```

```
pLW1
                          1                          0
0                      -0.8
                        -0.8                        3.5
1
                        -0.8                        3.5
-13.5
                        -0.8                         -1
-13.5
                        -0.8                         -1
1
/
pLW2
                          1                          0
0                      -0.8
                        -0.8                        3.5
-131.5
                        -0.8                        3.5
-146
                        -0.8                         -1
-146
                        -0.8                         -1
-131.5
/
pLW3
                          1                          0
0                      -0.8
                        -0.8                        3.5
-274
                        -0.8                        3.5
-288.5
                        -0.8                         -1
-288.5
                        -0.8                         -1
-274
/
pLW4
                          1                          0
0                      -0.8
                        -0.8                        3.5
-406.5
                        -0.8                        3.5
-421
                        -0.8                         -1
-421
                        -0.8                         -1
-406.5
/
pHG1
                          0                          0
-1                     -0.8
```

```
                    164                     3.5
0.8
                  178.5                     3.5
0.8
                  178.5                      -1
0.8
                    164                      -1
0.8
/
pHG2
                      0                       0
-1                 -0.8
                  336.5                     3.5
0.8
                    351                     3.5
0.8
                    351                      -1
0.8
                  336.5                      -1
0.8
/
pHG3
                      0                       0
-1                 -0.8
                 510.25                     3.5
0.8
                 524.75                     3.5
0.8
                 524.75                      -1
0.8
                 510.25                      -1
0.8
/
pHG4
                      0                       0
-1                 -0.8
                    684                     3.5
0.8
                  698.5                     3.5
0.8
                  698.5                      -1
0.8
                    684                      -1
0.8
/
pHG5
                      0                       0
-1                 -0.8
                  856.5                     3.5
0.8
                    871                     3.5
0.8
```

```
                    871                    -1
0.8
                  856.5                    -1
0.8
/
pTG1
                      0                     0
1                 -420.8
                    164                   3.5
-420.8
                  178.5                   3.5
-420.8
                  178.5                    -1
-420.8
                    164                    -1
-420.8
/
pTG2
                      0                     0
1                 -420.8
                  336.5                   3.5
-420.8
                    351                   3.5
-420.8
                    351                    -1
-420.8
                  336.5                    -1
-420.8
/
pTG3
                      0                     0
1                 -420.8
                 510.25                   3.5
-420.8
                 524.75                   3.5
-420.8
                 524.75                    -1
-420.8
                 510.25                    -1
-420.8
/
pTG4
                      0                     0
1                 -420.8
                    684                   3.5
-420.8
                  698.5                   3.5
-420.8
                  698.5                    -1
-420.8
                    684                    -1
-420.8
```

```
/
pTG5
                      0                       0
1                  -420.8
                   856.5                     3.5
-420.8
                     871                     3.5
-420.8
                     871                      -1
-420.8
                   856.5                      -1
-420.8
/
pSU1
                      -1                       0
0                 -1035.8
                  1035.8                     3.5
1
                  1035.8                     3.5
-13.5
                  1035.8                      -1
-13.5
                  1035.8                      -1
1
/
pSU2
                      -1                       0
0                 -1035.8
                  1035.8                     3.5
-131.5
                  1035.8                     3.5
-146
                  1035.8                      -1
-146
                  1035.8                      -1
-131.5
/
pSU3
                      -1                       0
0                 -1035.8
                  1035.8                     3.5
-274
                  1035.8                     3.5
-288.5
                  1035.8                      -1
-288.5
                  1035.8                      -1
-274
/
pSU4
                      -1                       0
0                 -1035.8
```

```
                  1035.8                      3.5
-406.5
                  1035.8                      3.5
-421
                  1035.8                       -1
-421
                  1035.8                       -1
-406.5
/
/
PROP
%CNAM air(incompressible/20C)
   1   1                   1.206               1.83e-005
1007                  0.0256   0
/
                1.9e-005                      0
0                       0                      0
0
                1.6e-005                      0
0                       0                      0
0
                      0                       0
0                       0                      0
0
STED
   9  -1                  0.0001
/
TBTY
   4
WL02
   0   0
/
   1
@UNDEFINEDMOM
/
/
WPUT
   0
ZGWV
   0
GOGO
```

1.2 Two Zone Gob Model with 36 Coupled Regions

The following is an example of the input file ('.s') for SC/Tetra for the steady state case with a 2 zone gob mode and the expanded number of coupled regions.

```
SDAT
SC/Tetra
  10   0   0
PREI    PA_MineXLinks.pre
RO      PA_MineXLinks.r
POST    PA_MineXLinks
/
   1   1   0
PA_MineXLinks
   3   1
CHKC
   1
pLW1
pLW2
pLW3
pLW4
pLW5
pLW6
pLW7
pHG1
pHG2
pHG3
pHG4
pHG5
pHG6
pHG7
pHG8
pHG9
pHG10
pHG11
pTG1
pTG2
pTG3
pTG4
pTG5
pTG6
pTG7
pTG8
pTG9
pTG10
pTG11
pSU1
pSU2
```

```
pSU3
pSU4
pSU5
pSU6
pSU7
/
CHKF
   1
LW1
LW2
LW3
LW4
LW5
LW6
LW7
HG1
HG2
HG3
HG4
HG5
HG6
HG7
HG8
HG9
HG10
HG11
TG1
TG2
TG3
TG4
TG5
TG6
TG7
TG8
TG9
TG10
TG11
SU1
SU2
SU3
SU4
SU5
SU6
SU7
/
CHKL
       1        1        0        1        1
CYCS
       1    1100
EQUA
1101111
FLUX
```

```
%CNAM Flux_1
  -2   0   -100   0   2   -100
   3
1 50
PressMatlab2CradleXL.csv
MassCradle2MatlabXL.csv
                      5                      50
   7
   3
C1Matlab2CradleXL.csv
C2Matlab2CradleXL.csv
C3Matlab2CradleXL.csv
C1Cradle2MatlabXL.csv
C2Cradle2MatlabXL.csv
C3Cradle2MatlabXL.csv
LW1
/
%CNAM Flux_2
  -2   0   -101   0   2   -101
   3
1 50
PressMatlab2CradleXL.csv
MassCradle2MatlabXL.csv
                      5                      50
   7
   3
C1Matlab2CradleXL.csv
C2Matlab2CradleXL.csv
C3Matlab2CradleXL.csv
C1Cradle2MatlabXL.csv
C2Cradle2MatlabXL.csv
C3Cradle2MatlabXL.csv
LW2
/
%CNAM Flux_3
  -2   0   -102   0   2   -102
   3
1 50
PressMatlab2CradleXL.csv
MassCradle2MatlabXL.csv
                      5                      50
   7
   3
C1Matlab2CradleXL.csv
C2Matlab2CradleXL.csv
C3Matlab2CradleXL.csv
C1Cradle2MatlabXL.csv
C2Cradle2MatlabXL.csv
C3Cradle2MatlabXL.csv
LW3
/
%CNAM Flux_4
```

```
  -2   0   -103   0   2   -103
   3
1 50
PressMatlab2CradleXL.csv
MassCradle2MatlabXL.csv
                       5                       50
   7
   3
C1Matlab2CradleXL.csv
C2Matlab2CradleXL.csv
C3Matlab2CradleXL.csv
C1Cradle2MatlabXL.csv
C2Cradle2MatlabXL.csv
C3Cradle2MatlabXL.csv
LW4
/
%CNAM Flux_5
  -2   0   -104   0   2   -104
   3
1 50
PressMatlab2CradleXL.csv
MassCradle2MatlabXL.csv
                       5                       50
   7
   3
C1Matlab2CradleXL.csv
C2Matlab2CradleXL.csv
C3Matlab2CradleXL.csv
C1Cradle2MatlabXL.csv
C2Cradle2MatlabXL.csv
C3Cradle2MatlabXL.csv
LW5
/
%CNAM Flux_6
  -2   0   -105   0   2   -105
   3
1 50
PressMatlab2CradleXL.csv
MassCradle2MatlabXL.csv
                       5                       50
   7
   3
C1Matlab2CradleXL.csv
C2Matlab2CradleXL.csv
C3Matlab2CradleXL.csv
C1Cradle2MatlabXL.csv
C2Cradle2MatlabXL.csv
C3Cradle2MatlabXL.csv
LW6
/
%CNAM Flux_7
  -2   0   -106   0   2   -106
```

```
   3
1 50
PressMatlab2CradleXL.csv
MassCradle2MatlabXL.csv
                       5                       50
   7
   3
C1Matlab2CradleXL.csv
C2Matlab2CradleXL.csv
C3Matlab2CradleXL.csv
C1Cradle2MatlabXL.csv
C2Cradle2MatlabXL.csv
C3Cradle2MatlabXL.csv
LW7
/
%CNAM Flux_8
  -2   0   -107   0   2   -107
   3
1 50
PressMatlab2CradleXL.csv
MassCradle2MatlabXL.csv
                       5                       50
   7
   3
C1Matlab2CradleXL.csv
C2Matlab2CradleXL.csv
C3Matlab2CradleXL.csv
C1Cradle2MatlabXL.csv
C2Cradle2MatlabXL.csv
C3Cradle2MatlabXL.csv
HG1
/
%CNAM Flux_9
  -2   0   -108   0   2   -108
   3
1 50
PressMatlab2CradleXL.csv
MassCradle2MatlabXL.csv
                       5                       50
   7
   3
C1Matlab2CradleXL.csv
C2Matlab2CradleXL.csv
C3Matlab2CradleXL.csv
C1Cradle2MatlabXL.csv
C2Cradle2MatlabXL.csv
C3Cradle2MatlabXL.csv
HG2
/
%CNAM Flux_10
  -2   0   -109   0   2   -109
   3
```

```
1 50
PressMatlab2CradleXL.csv
MassCradle2MatlabXL.csv
                      5                     50
   7
   3
C1Matlab2CradleXL.csv
C2Matlab2CradleXL.csv
C3Matlab2CradleXL.csv
C1Cradle2MatlabXL.csv
C2Cradle2MatlabXL.csv
C3Cradle2MatlabXL.csv
HG3
/
%CNAM Flux_11
  -2   0   -110   0   2   -110
   3
1 50
PressMatlab2CradleXL.csv
MassCradle2MatlabXL.csv
                      5                     50
   7
   3
C1Matlab2CradleXL.csv
C2Matlab2CradleXL.csv
C3Matlab2CradleXL.csv
C1Cradle2MatlabXL.csv
C2Cradle2MatlabXL.csv
C3Cradle2MatlabXL.csv
HG4
/
%CNAM Flux_12
  -2   0   -111   0   2   -111
   3
1 50
PressMatlab2CradleXL.csv
MassCradle2MatlabXL.csv
                      5                     50
   7
   3
C1Matlab2CradleXL.csv
C2Matlab2CradleXL.csv
C3Matlab2CradleXL.csv
C1Cradle2MatlabXL.csv
C2Cradle2MatlabXL.csv
C3Cradle2MatlabXL.csv
HG5
/
%CNAM Flux_13
  -2   0   -112   0   2   -112
   3
1 50
```

```
PressMatlab2CradleXL.csv
MassCradle2MatlabXL.csv
                      5                      50
   7
   3
C1Matlab2CradleXL.csv
C2Matlab2CradleXL.csv
C3Matlab2CradleXL.csv
C1Cradle2MatlabXL.csv
C2Cradle2MatlabXL.csv
C3Cradle2MatlabXL.csv
HG6
/
%CNAM Flux_14
  -2   0   -113   0   2   -113
   3
1 50
PressMatlab2CradleXL.csv
MassCradle2MatlabXL.csv
                      5                      50
   7
   3
C1Matlab2CradleXL.csv
C2Matlab2CradleXL.csv
C3Matlab2CradleXL.csv
C1Cradle2MatlabXL.csv
C2Cradle2MatlabXL.csv
C3Cradle2MatlabXL.csv
HG7
/
%CNAM Flux_15
  -2   0   -114   0   2   -114
   3
1 50
PressMatlab2CradleXL.csv
MassCradle2MatlabXL.csv
                      5                      50
   7
   3
C1Matlab2CradleXL.csv
C2Matlab2CradleXL.csv
C3Matlab2CradleXL.csv
C1Cradle2MatlabXL.csv
C2Cradle2MatlabXL.csv
C3Cradle2MatlabXL.csv
HG8
/
%CNAM Flux_16
  -2   0   -115   0   2   -115
   3
1 50
PressMatlab2CradleXL.csv
```

```
MassCradle2MatlabXL.csv
                      5                      50
   7
   3
C1Matlab2CradleXL.csv
C2Matlab2CradleXL.csv
C3Matlab2CradleXL.csv
C1Cradle2MatlabXL.csv
C2Cradle2MatlabXL.csv
C3Cradle2MatlabXL.csv
HG9
/
%CNAM Flux_17
  -2   0   -116   0   2   -116
   3
1 50
PressMatlab2CradleXL.csv
MassCradle2MatlabXL.csv
                      5                      50
   7
   3
C1Matlab2CradleXL.csv
C2Matlab2CradleXL.csv
C3Matlab2CradleXL.csv
C1Cradle2MatlabXL.csv
C2Cradle2MatlabXL.csv
C3Cradle2MatlabXL.csv
HG10
/
%CNAM Flux_18
  -2   0   -117   0   2   -117
   3
1 50
PressMatlab2CradleXL.csv
MassCradle2MatlabXL.csv
                      5                      50
   7
   3
C1Matlab2CradleXL.csv
C2Matlab2CradleXL.csv
C3Matlab2CradleXL.csv
C1Cradle2MatlabXL.csv
C2Cradle2MatlabXL.csv
C3Cradle2MatlabXL.csv
HG11
/
%CNAM Flux_19
  -2   0   -118   0   2   -118
   3
1 50
PressMatlab2CradleXL.csv
MassCradle2MatlabXL.csv
```

```
                      5                      50
   7
   3
C1Matlab2CradleXL.csv
C2Matlab2CradleXL.csv
C3Matlab2CradleXL.csv
C1Cradle2MatlabXL.csv
C2Cradle2MatlabXL.csv
C3Cradle2MatlabXL.csv
TG1
/
%CNAM Flux_20
  -2   0   -119   0   2   -119
   3
1 50
PressMatlab2CradleXL.csv
MassCradle2MatlabXL.csv
                      5                      50
   7
   3
C1Matlab2CradleXL.csv
C2Matlab2CradleXL.csv
C3Matlab2CradleXL.csv
C1Cradle2MatlabXL.csv
C2Cradle2MatlabXL.csv
C3Cradle2MatlabXL.csv
TG2
/
%CNAM Flux_21
  -2   0   -120   0   2   -120
   3
1 50
PressMatlab2CradleXL.csv
MassCradle2MatlabXL.csv
                      5                      50
   7
   3
C1Matlab2CradleXL.csv
C2Matlab2CradleXL.csv
C3Matlab2CradleXL.csv
C1Cradle2MatlabXL.csv
C2Cradle2MatlabXL.csv
C3Cradle2MatlabXL.csv
TG3
/
%CNAM Flux_22
  -2   0   -121   0   2   -121
   3
1 50
PressMatlab2CradleXL.csv
MassCradle2MatlabXL.csv
                      5                      50
```

```
   7
   3
C1Matlab2CradleXL.csv
C2Matlab2CradleXL.csv
C3Matlab2CradleXL.csv
C1Cradle2MatlabXL.csv
C2Cradle2MatlabXL.csv
C3Cradle2MatlabXL.csv
TG4
/
%CNAM Flux_23
  -2   0   -122   0   2   -122
   3
1 50
PressMatlab2CradleXL.csv
MassCradle2MatlabXL.csv
                       5                       50
   7
   3
C1Matlab2CradleXL.csv
C2Matlab2CradleXL.csv
C3Matlab2CradleXL.csv
C1Cradle2MatlabXL.csv
C2Cradle2MatlabXL.csv
C3Cradle2MatlabXL.csv
TG5
/
%CNAM Flux_24
  -2   0   -123   0   2   -123
   3
1 50
PressMatlab2CradleXL.csv
MassCradle2MatlabXL.csv
                       5                       50
   7
   3
C1Matlab2CradleXL.csv
C2Matlab2CradleXL.csv
C3Matlab2CradleXL.csv
C1Cradle2MatlabXL.csv
C2Cradle2MatlabXL.csv
C3Cradle2MatlabXL.csv
TG6
/
%CNAM Flux_25
  -2   0   -124   0   2   -124
   3
1 50
PressMatlab2CradleXL.csv
MassCradle2MatlabXL.csv
                       5                       50
   7
```

```
   3
C1Matlab2CradleXL.csv
C2Matlab2CradleXL.csv
C3Matlab2CradleXL.csv
C1Cradle2MatlabXL.csv
C2Cradle2MatlabXL.csv
C3Cradle2MatlabXL.csv
TG7
/
%CNAM Flux_26
  -2   0   -125   0   2   -125
   3
1 50
PressMatlab2CradleXL.csv
MassCradle2MatlabXL.csv
                       5                       50
   7
   3
C1Matlab2CradleXL.csv
C2Matlab2CradleXL.csv
C3Matlab2CradleXL.csv
C1Cradle2MatlabXL.csv
C2Cradle2MatlabXL.csv
C3Cradle2MatlabXL.csv
TG8
/
%CNAM Flux_27
  -2   0   -126   0   2   -126
   3
1 50
PressMatlab2CradleXL.csv
MassCradle2MatlabXL.csv
                       5                       50
   7
   3
C1Matlab2CradleXL.csv
C2Matlab2CradleXL.csv
C3Matlab2CradleXL.csv
C1Cradle2MatlabXL.csv
C2Cradle2MatlabXL.csv
C3Cradle2MatlabXL.csv
TG9
/
%CNAM Flux_28
  -2   0   -127   0   2   -127
   3
1 50
PressMatlab2CradleXL.csv
MassCradle2MatlabXL.csv
                       5                       50
   7
   3
```

```
C1Matlab2CradleXL.csv
C2Matlab2CradleXL.csv
C3Matlab2CradleXL.csv
C1Cradle2MatlabXL.csv
C2Cradle2MatlabXL.csv
C3Cradle2MatlabXL.csv
TG10
/
%CNAM Flux_29
  -2   0   -128   0   2   -128
   3
1 50
PressMatlab2CradleXL.csv
MassCradle2MatlabXL.csv
                       5                       50
   7
   3
C1Matlab2CradleXL.csv
C2Matlab2CradleXL.csv
C3Matlab2CradleXL.csv
C1Cradle2MatlabXL.csv
C2Cradle2MatlabXL.csv
C3Cradle2MatlabXL.csv
TG11
/
%CNAM Flux_30
  -2   0   -129   0   2   -129
   3
1 50
PressMatlab2CradleXL.csv
MassCradle2MatlabXL.csv
                       5                       50
   7
   3
C1Matlab2CradleXL.csv
C2Matlab2CradleXL.csv
C3Matlab2CradleXL.csv
C1Cradle2MatlabXL.csv
C2Cradle2MatlabXL.csv
C3Cradle2MatlabXL.csv
SU1
/
%CNAM Flux_31
  -2   0   -130   0   2   -130
   3
1 50
PressMatlab2CradleXL.csv
MassCradle2MatlabXL.csv
                       5                       50
   7
   3
C1Matlab2CradleXL.csv
```

```
C2Matlab2CradleXL.csv
C3Matlab2CradleXL.csv
C1Cradle2MatlabXL.csv
C2Cradle2MatlabXL.csv
C3Cradle2MatlabXL.csv
SU2
/
%CNAM Flux_32
  -2   0   -131   0   2   -131
   3
1 50
PressMatlab2CradleXL.csv
MassCradle2MatlabXL.csv
                       5                       50
   7
   3
C1Matlab2CradleXL.csv
C2Matlab2CradleXL.csv
C3Matlab2CradleXL.csv
C1Cradle2MatlabXL.csv
C2Cradle2MatlabXL.csv
C3Cradle2MatlabXL.csv
SU3
/
%CNAM Flux_33
  -2   0   -132   0   2   -132
   3
1 50
PressMatlab2CradleXL.csv
MassCradle2MatlabXL.csv
                       5                       50
   7
   3
C1Matlab2CradleXL.csv
C2Matlab2CradleXL.csv
C3Matlab2CradleXL.csv
C1Cradle2MatlabXL.csv
C2Cradle2MatlabXL.csv
C3Cradle2MatlabXL.csv
SU4
/
%CNAM Flux_34
  -2   0   -133   0   2   -133
   3
1 50
PressMatlab2CradleXL.csv
MassCradle2MatlabXL.csv
                       5                       50
   7
   3
C1Matlab2CradleXL.csv
C2Matlab2CradleXL.csv
```

```
C3Matlab2CradleXL.csv
C1Cradle2MatlabXL.csv
C2Cradle2MatlabXL.csv
C3Cradle2MatlabXL.csv
SU5
/
%CNAM Flux_35
  -2   0   -134   0   2   -134
   3
1 50
PressMatlab2CradleXL.csv
MassCradle2MatlabXL.csv
                      5                      50
   7
   3
C1Matlab2CradleXL.csv
C2Matlab2CradleXL.csv
C3Matlab2CradleXL.csv
C1Cradle2MatlabXL.csv
C2Cradle2MatlabXL.csv
C3Cradle2MatlabXL.csv
SU6
/
%CNAM Flux_36
  -2   0   -135   0   2   -135
   3
1 50
PressMatlab2CradleXL.csv
MassCradle2MatlabXL.csv
                      5                      50
   7
   3
C1Matlab2CradleXL.csv
C2Matlab2CradleXL.csv
C3Matlab2CradleXL.csv
C1Cradle2MatlabXL.csv
C2Cradle2MatlabXL.csv
C3Cradle2MatlabXL.csv
SU7
/
%CNAM Methane_Inflow
  -1   7   0   0   0   1
                 0.1229   0
                      0                        1
0
Inflow
/
/
FORC
%CNAM Forc_1
   5                  1016                       0
1   1
```

```
OuterGob
/
%CNAM Forc_2
   5                  10600                        0
1   1
InnerGob
/
/
GWLN
   0
INIT
PRES
                    -300  -1
OuterGob
InnerGob
/
/
INIT
CN02
                       1  -1
InnerGob
OuterGob
/
/
PLGN
pLW1
      1     0     0     -0.8
      -0.8  3.5   5
      -0.8  3.5   -25
      -0.8  -1    -25
      -0.8  -1    5
/
pLW2
      1     0     0     -0.8
      -0.8  3.5   -60
      -0.8  3.5   -90
      -0.8  -1    -90
      -0.8  -1    -60
/
pLW3
      1     0     0     -0.8
      -0.8  3.5   -130
      -0.8  3.5   -160
      -0.8  -1    -160
      -0.8  -1    -130
/
pLW4
      1     0     0     -0.8
      -0.8  3.5   -190
      -0.8  3.5   -220
      -0.8  -1    -220
      -0.8  -1    -190
```

```
/
pLW5
      1     0     0     -0.8
      -0.8  3.5   -260
      -0.8  3.5   -290
      -0.8  -1    -290
      -0.8  -1    -260
/
pLW6
      1     0     0     -0.8
      -0.8  3.5   -330
      -0.8  3.5   -360
      -0.8  -1    -360
      -0.8  -1    -330
/
pLW7
      1     0     0     -0.8
      -0.8  3.5   -400
      -0.8  3.5   -430
      -0.8  -1    -430
      -0.8  -1    -400
/
pHG1
      0     0     -1    -0.8
      30    3.5   0.8
      60    3.5   0.8
      60    -1    0.8
      30    -1    0.8
/
pHG2
      0     0     -1    -0.8
      120   3.5   0.8
      150   3.5   0.8
      150   -1    0.8
      120   -1    0.8
/
pHG3
      0     0     -1    -0.8
      220   3.5   0.8
      250   3.5   0.8
      250   -1    0.8
      220   -1    0.8
/
pHG4
      0     0     -1    -0.8
      310   3.5   0.8
      340   3.5   0.8
      340   -1    0.8
      310   -1    0.8
/
pHG5
      0     0     -1    -0.8
```

```
      400   3.5   0.8
      430   3.5   0.8
      430   -1    0.8
      400   -1    0.8
/
pHG6
      0     0     -1    -0.8
      500   3.5   0.8
      530   3.5   0.8
      530   -1    0.8
      500   -1    0.8
/
pHG7
      0     0     -1    -0.8
      600   3.5   0.8
      630   3.5   0.8
      630   -1    0.8
      600   -1    0.8
/
pHG8
      0     0     -1    -0.8
      695   3.5   0.8
      725   3.5   0.8
      725   -1    0.8
      695   -1    0.8
/
pHG9
      0     0     -1    -0.8
      790   3.5   0.8
      820   3.5   0.8
      820   -1    0.8
      790   -1    0.8
/
pHG10
      0     0     -1    -0.8
      885   3.5   0.8
      915   3.5   0.8
      915   -1    0.8
      885   -1    0.8
/
pHG11
      0     0     -1    -0.8
      980   3.5   0.8
      1010  3.5   0.8
      1010  -1    0.8
      980   -1    0.8
/
pTG1
      0     0     1     -420.8
      30    3.5   -420.8
      60    3.5   -420.8
      60    -1    -420.8
```

```
      30    -1    -420.8
/
pTG2
      0     0     1     -420.8
      120   3.5   -420.8
      150   3.5   -420.8
      150   -1    -420.8
      120   -1    -420.8
/
pTG3
      0     0     1     -420.8
      220   3.5   -420.8
      250   3.5   -420.8
      250   -1    -420.8
      220   -1    -420.8
/
pTG4
      0     0     1     -420.8
      310   3.5   -420.8
      340   3.5   -420.8
      340   -1    -420.8
      310   -1    -420.8
/
pTG5
      0     0     1     -420.8
      400   3.5   -420.8
      430   3.5   -420.8
      430   -1    -420.8
      400   -1    -420.8
/
pTG6
      0     0     1     -420.8
      500   3.5   -420.8
      530   3.5   -420.8
      530   -1    -420.8
      500   -1    -420.8
/
pTG7
      0     0     1     -420.8
      600   3.5   -420.8
      630   3.5   -420.8
      630   -1    -420.8
      600   -1    -420.8
/
pTG8
      0     0     1     -420.8
      695   3.5   -420.8
      725   3.5   -420.8
      725   -1    -420.8
      695   -1    -420.8
/
pTG9
```

```
      0     0     1     -420.8
      790   3.5   -420.8
      820   3.5   -420.8
      820   -1    -420.8
      790   -1    -420.8
/
pTG10
      0     0     1     -420.8
      885   3.5   -420.8
      915   3.5   -420.8
      915   -1    -420.8
      885   -1    -420.8
/
pTG11
      0     0     1     -420.8
      980   3.5   -420.8
      1010  3.5   -420.8
      1010  -1    -420.8
      980   -1    -420.8
/
pSU1
      -1    0     0     -1035.8
      1035.8      3.5   5
      1035.8      3.5   -25
      1035.8      -1    -25
      1035.8      -1    5
/
pSU2
      -1    0     0     -1035.8
      1035.8      3.5   -60
      1035.8      3.5   -90
      1035.8      -1    -90
      1035.8      -1    -60
/
pSU3
      -1    0     0     -1035.8
      1035.8      3.5   -130
      1035.8      3.5   -160
      1035.8      -1    -160
      1035.8      -1    -130
/
pSU4
      -1    0     0     -1035.8
      1035.8      3.5   -190
      1035.8      3.5   -220
      1035.8      -1    -220
      1035.8      -1    -190
/
pSU5
      -1    0     0     -1035.8
      1035.8      3.5   -260
      1035.8      3.5   -290
```

```
      1035.8     -1    -290
      1035.8     -1    -260
/
pSU6
      -1    0     0     -1035.8
      1035.8     3.5   -330
      1035.8     3.5   -360
      1035.8     -1    -360
      1035.8     -1    -330
/
pSU7
      -1    0     0     -1035.8
      1035.8     3.5   -400
      1035.8     3.5   -430
      1035.8     -1    -430
      1035.8     -1    -400
/
/
PROP
%CNAM air(incompressible/20C)
   1   1                    1.206               1.83e-005
1007                  0.0256   0
/
                1.9e-005                        0
0                        0                       0
0
                1.6e-005                        0
0                        0                       0
0
                       0                        0
0                        0                       0
0
STED
   9   -1                   0.0001
/
TBTY
   8
WL02
   0   0
/
   1
@UNDEFINEDMOM
/
/
WPUT
   0
ZGWV
   0
GOGO
```

1.3 Smooth Gob Model with 18 Coupled Regions

```
SDAT
SC/Tetra
  10   0   0
PREI    PA_Mine4SmoothGob.pre
RO      PA_Mine4SmoothGob.r
POST    PA_Mine4SmoothGob
/
   1   1   0
PA_Mine4SmoothGob
   3   1
CHKC
   1
pLW1
pLW2
pLW3
pLW4
pHG1
pHG2
pHG3
pHG4
pHG5
pTG1
pTG2
pTG3
pTG4
pTG5
pSU1
pSU2
pSU3
pSU4
/
CHKF
   1
LW1
LW2
LW3
LW4
HG1
HG2
HG3
HG4
HG5
TG1
TG2
TG3
TG4
TG5
SU1
SU2
SU3
```

```
SU4
/
CHKL
       1       1       0       1       1
CYCS
       1    1100
EQUA
1101111
FLUX
%CNAM Flux_1
  -2   0 -100   0   2 -100
   3
1 50
PressMatlab2CradleM4.csv
MassCradle2MatlabM4.csv
                        5                       50
   7
   3
C1Matlab2CradleM4.csv
C2Matlab2CradleM4.csv
C3Matlab2CradleM4.csv
C1Cradle2MatlabM4.csv
C2Cradle2MatlabM4.csv
C3Cradle2MatlabM4.csv
LW1
/
%CNAM Flux_2
  -2   0 -101   0   2 -101
   3
1 50
PressMatlab2CradleM4.csv
MassCradle2MatlabM4.csv
                        5                       50
   7
   3
C1Matlab2CradleM4.csv
C2Matlab2CradleM4.csv
C3Matlab2CradleM4.csv
C1Cradle2MatlabM4.csv
C2Cradle2MatlabM4.csv
C3Cradle2MatlabM4.csv
LW2
/
%CNAM Flux_3
  -2   0 -102   0   2 -102
   3
1 50
PressMatlab2CradleM4.csv
MassCradle2MatlabM4.csv
                        5                       50
   7
   3
```

```
C1Matlab2CradleM4.csv
C2Matlab2CradleM4.csv
C3Matlab2CradleM4.csv
C1Cradle2MatlabM4.csv
C2Cradle2MatlabM4.csv
C3Cradle2MatlabM4.csv
LW3
/
%CNAM Flux_4
  -2   0 -103   0   2 -103
   3
1 50
PressMatlab2CradleM4.csv
MassCradle2MatlabM4.csv
                       5                       50
   7
   3
C1Matlab2CradleM4.csv
C2Matlab2CradleM4.csv
C3Matlab2CradleM4.csv
C1Cradle2MatlabM4.csv
C2Cradle2MatlabM4.csv
C3Cradle2MatlabM4.csv
LW4
/
%CNAM Flux_5
  -2   0 -104   0   2 -104
   3
1 50
PressMatlab2CradleM4.csv
MassCradle2MatlabM4.csv
                       5                       50
   7
   3
C1Matlab2CradleM4.csv
C2Matlab2CradleM4.csv
C3Matlab2CradleM4.csv
C1Cradle2MatlabM4.csv
C2Cradle2MatlabM4.csv
C3Cradle2MatlabM4.csv
HG1
/
%CNAM Flux_6
  -2   0 -105   0   2 -105
   3
1 50
PressMatlab2CradleM4.csv
MassCradle2MatlabM4.csv
                       5                       50
   7
   3
C1Matlab2CradleM4.csv
```

```
C2Matlab2CradleM4.csv
C3Matlab2CradleM4.csv
C1Cradle2MatlabM4.csv
C2Cradle2MatlabM4.csv
C3Cradle2MatlabM4.csv
HG2
/
%CNAM Flux_7
  -2   0 -106   0   2 -106
   3
1 50
PressMatlab2CradleM4.csv
MassCradle2MatlabM4.csv
                       5                       50
   7
   3
C1Matlab2CradleM4.csv
C2Matlab2CradleM4.csv
C3Matlab2CradleM4.csv
C1Cradle2MatlabM4.csv
C2Cradle2MatlabM4.csv
C3Cradle2MatlabM4.csv
HG3
/
%CNAM Flux_8
  -2   0 -107   0   2 -107
   3
1 50
PressMatlab2CradleM4.csv
MassCradle2MatlabM4.csv
                       5                       50
   7
   3
C1Matlab2CradleM4.csv
C2Matlab2CradleM4.csv
C3Matlab2CradleM4.csv
C1Cradle2MatlabM4.csv
C2Cradle2MatlabM4.csv
C3Cradle2MatlabM4.csv
HG4
/
%CNAM Flux_9
  -2   0 -108   0   2 -108
   3
1 50
PressMatlab2CradleM4.csv
MassCradle2MatlabM4.csv
                       5                       50
   7
   3
C1Matlab2CradleM4.csv
C2Matlab2CradleM4.csv
```

```
C3Matlab2CradleM4.csv
C1Cradle2MatlabM4.csv
C2Cradle2MatlabM4.csv
C3Cradle2MatlabM4.csv
HG5
/
%CNAM Flux_10
  -2   0 -109   0   2 -109
   3
1 50
PressMatlab2CradleM4.csv
MassCradle2MatlabM4.csv
                       5                       50
   7
   3
C1Matlab2CradleM4.csv
C2Matlab2CradleM4.csv
C3Matlab2CradleM4.csv
C1Cradle2MatlabM4.csv
C2Cradle2MatlabM4.csv
C3Cradle2MatlabM4.csv
TG1
/
%CNAM Flux_11
  -2   0 -110   0   2 -110
   3
1 50
PressMatlab2CradleM4.csv
MassCradle2MatlabM4.csv
                       5                       50
   7
   3
C1Matlab2CradleM4.csv
C2Matlab2CradleM4.csv
C3Matlab2CradleM4.csv
C1Cradle2MatlabM4.csv
C2Cradle2MatlabM4.csv
C3Cradle2MatlabM4.csv
TG2
/
%CNAM Flux_12
  -2   0 -111   0   2 -111
   3
1 50
PressMatlab2CradleM4.csv
MassCradle2MatlabM4.csv
                       5                       50
   7
   3
C1Matlab2CradleM4.csv
C2Matlab2CradleM4.csv
C3Matlab2CradleM4.csv
```

```
C1Cradle2MatlabM4.csv
C2Cradle2MatlabM4.csv
C3Cradle2MatlabM4.csv
TG3
/
%CNAM Flux_13
  -2   0 -112   0   2 -112
   3
1 50
PressMatlab2CradleM4.csv
MassCradle2MatlabM4.csv
                       5                       50
   7
   3
C1Matlab2CradleM4.csv
C2Matlab2CradleM4.csv
C3Matlab2CradleM4.csv
C1Cradle2MatlabM4.csv
C2Cradle2MatlabM4.csv
C3Cradle2MatlabM4.csv
TG4
/
%CNAM Flux_14
  -2   0 -113   0   2 -113
   3
1 50
PressMatlab2CradleM4.csv
MassCradle2MatlabM4.csv
                       5                       50
   7
   3
C1Matlab2CradleM4.csv
C2Matlab2CradleM4.csv
C3Matlab2CradleM4.csv
C1Cradle2MatlabM4.csv
C2Cradle2MatlabM4.csv
C3Cradle2MatlabM4.csv
TG5
/
%CNAM Flux_15
  -2   0 -114   0   2 -114
   3
1 50
PressMatlab2CradleM4.csv
MassCradle2MatlabM4.csv
                       5                       50
   7
   3
C1Matlab2CradleM4.csv
C2Matlab2CradleM4.csv
C3Matlab2CradleM4.csv
C1Cradle2MatlabM4.csv
```

```
C2Cradle2MatlabM4.csv
C3Cradle2MatlabM4.csv
SU1
/
%CNAM Flux_16
  -2   0 -115   0   2 -115
   3
1 50
PressMatlab2CradleM4.csv
MassCradle2MatlabM4.csv
                       5                       50
   7
   3
C1Matlab2CradleM4.csv
C2Matlab2CradleM4.csv
C3Matlab2CradleM4.csv
C1Cradle2MatlabM4.csv
C2Cradle2MatlabM4.csv
C3Cradle2MatlabM4.csv
SU2
/
%CNAM Flux_17
  -2   0 -116   0   2 -116
   3
1 50
PressMatlab2CradleM4.csv
MassCradle2MatlabM4.csv
                       5                       50
   7
   3
C1Matlab2CradleM4.csv
C2Matlab2CradleM4.csv
C3Matlab2CradleM4.csv
C1Cradle2MatlabM4.csv
C2Cradle2MatlabM4.csv
C3Cradle2MatlabM4.csv
SU3
/
%CNAM Flux_18
  -2   0 -117   0   2 -117
   3
1 50
PressMatlab2CradleM4.csv
MassCradle2MatlabM4.csv
                       5                       50
   7
   3
C1Matlab2CradleM4.csv
C2Matlab2CradleM4.csv
C3Matlab2CradleM4.csv
C1Cradle2MatlabM4.csv
C2Cradle2MatlabM4.csv
```

```
C3Cradle2MatlabM4.csv
SU4
/
%CNAM Methane_Inflow
  -1   7   0   0   0   1
                 0.1229   0
                      0                        1
0
Inflow
/
/
FORC
%CNAM Forc_1
  -5                      0                        0
0   1
  28
-5000
  55
   -205.6
    162.3
    485.3
    379.3
      9.75e-07
   1.3697e-10
   8.6755e-12
  -3.9617e-11
   2.7287e-11
   1.1096e-12
  -5.5804e-11
   3.2365e-12
   4.2817e-11
  -3.7495e-12
   2.1402e-11
   1.1268e-10
   6.1561e-13
   1.6338e-11
  -1.4478e-12
    1.208e-10
   3.3733e-12
  -4.1614e-12
   4.0156e-12
  -3.4939e-11
    -1.55e-12
  -1.4678e-11
SmoothGob
/
/
GWLN
   0
INIT
PRES
                   -300  -1
```

```
SmoothGob
/
/
INIT
CN02
                        1  -1
SmoothGob
/
/
PLGN
pLW1
                          1                          0
0                       -0.8
                       -0.8                        3.5
1
                       -0.8                        3.5
-13.5
                       -0.8                         -1
-13.5
                       -0.8                         -1
1
/
pLW2
                          1                          0
0                       -0.8
                       -0.8                        3.5
-131.5
                       -0.8                        3.5
-146
                       -0.8                         -1
-146
                       -0.8                         -1
-131.5
/
pLW3
                          1                          0
0                       -0.8
                       -0.8                        3.5
-274
                       -0.8                        3.5
-288.5
                       -0.8                         -1
-288.5
                       -0.8                         -1
-274
/
pLW4
                          1                          0
0                       -0.8
                       -0.8                        3.5
-406.5
```

```
                    -0.8                      3.5
-421
                    -0.8                       -1
-421
                    -0.8                       -1
-406.5
/
pHG1
                       0                       0
-1                   -0.8
                     164                       3.5
0.8
                   178.5                       3.5
0.8
                   178.5                       -1
0.8
                     164                       -1
0.8
/
pHG2
                       0                       0
-1                   -0.8
                   336.5                       3.5
0.8
                     351                       3.5
0.8
                     351                       -1
0.8
                   336.5                       -1
0.8
/
pHG3
                       0                       0
-1                   -0.8
                  510.25                       3.5
0.8
                  524.75                       3.5
0.8
                  524.75                       -1
0.8
                  510.25                       -1
0.8
/
pHG4
                       0                       0
-1                   -0.8
                     684                       3.5
0.8
                   698.5                       3.5
0.8
                   698.5                       -1
0.8
```

```
                    684                    -1
0.8
/
pHG5
                      0                     0
-1                 -0.8
                  856.5                   3.5
0.8
                    871                   3.5
0.8
                    871                    -1
0.8
                  856.5                    -1
0.8
/
pTG1
                      0                     0
1                 -420.8
                    164                   3.5
-420.8
                  178.5                   3.5
-420.8
                  178.5                    -1
-420.8
                    164                    -1
-420.8
/
pTG2
                      0                     0
1                 -420.8
                  336.5                   3.5
-420.8
                    351                   3.5
-420.8
                    351                    -1
-420.8
                  336.5                    -1
-420.8
/
pTG3
                      0                     0
1                 -420.8
                 510.25                   3.5
-420.8
                 524.75                   3.5
-420.8
                 524.75                    -1
-420.8
                 510.25                    -1
-420.8
/
pTG4
```

```
                    0                     0
1                -420.8
                  684                   3.5
-420.8
                698.5                   3.5
-420.8
                698.5                    -1
-420.8
                  684                    -1
-420.8
/
pTG5
                    0                     0
1                -420.8
                856.5                   3.5
-420.8
                  871                   3.5
-420.8
                  871                    -1
-420.8
                856.5                    -1
-420.8
/
pSU1
                   -1                     0
0              -1035.8
               1035.8                   3.5
1
               1035.8                   3.5
-13.5
               1035.8                    -1
-13.5
               1035.8                    -1
1
/
pSU2
                   -1                     0
0              -1035.8
               1035.8                   3.5
-131.5
               1035.8                   3.5
-146
               1035.8                    -1
-146
               1035.8                    -1
-131.5
/
pSU3
                   -1                     0
0              -1035.8
               1035.8                   3.5
-274
```

```
                  1035.8                        3.5
-288.5
                  1035.8                         -1
-288.5
                  1035.8                         -1
-274
/
pSU4
                      -1                          0
0                 -1035.8
                  1035.8                        3.5
-406.5
                  1035.8                        3.5
-421
                  1035.8                         -1
-421
                  1035.8                         -1
-406.5
/
/
PROP
%CNAM air(incompressible/20C)
   1   1                    1.206                1.83e-005
1007                  0.0256   0
/
                1.9e-005                         0
0                        0                        0
0
                1.6e-005                         0
0                        0                        0
0
                        0                        0
0                        0                        0
0
STED
   9  -1                   0.0001
/
TBTY
   4
WL02
   0   0
/
   1
@UNDEFINEDMOM
/
/
WPUT
   0
ZGWV
   0
GOGO
```

1.4 Smooth Gob Model with 36 Coupled Regions

```
SDAT
SC/Tetra
  10   0   0
PREI    SmoothGobFinal.pre
RO      SmoothGobFinal2.r
POST    SmoothGobFinal2
/
   1   1   0
SmoothGobFinal2
   3   1
CHKC
   1
pLW1
pLW2
pLW3
pLW4
pLW5
pLW6
pLW7
pHG1
pHG2
pHG3
pHG4
pHG5
pHG6
pHG7
pHG8
pHG9
pHG10
pHG11
pTG1
pTG2
pTG3
pTG4
pTG5
pTG6
pTG7
pTG8
pTG9
pTG10
pTG11
pSU1
pSU2
pSU3
pSU4
pSU5
pSU6
pSU7
/
CHKF
```

```
   1
LW1
LW2
LW3
LW4
LW5
LW6
LW7
HG1
HG2
HG3
HG4
HG5
HG6
HG7
HG8
HG9
HG10
HG11
TG1
TG2
TG3
TG4
TG5
TG6
TG7
TG8
TG9
TG10
TG11
SU1
SU2
SU3
SU4
SU5
SU6
SU7
/
CHKL
       1       1       0       1       1
CYCS
       1    1100
EQUA
1101111
FLUX
%CNAM Flux_1
  -2   0 -100   0   2 -100
   3
1 50
PressMatlab2CradleXL.csv
MassCradle2MatlabXL.csv
                      5                     50
```

```
   7
   3
C1Matlab2CradleXL.csv
C2Matlab2CradleXL.csv
C3Matlab2CradleXL.csv
C1Cradle2MatlabXL.csv
C2Cradle2MatlabXL.csv
C3Cradle2MatlabXL.csv
LW1
/
%CNAM Flux_2
  -2   0 -101   0   2 -101
   3
1 50
PressMatlab2CradleXL.csv
MassCradle2MatlabXL.csv
                       5                       50
   7
   3
C1Matlab2CradleXL.csv
C2Matlab2CradleXL.csv
C3Matlab2CradleXL.csv
C1Cradle2MatlabXL.csv
C2Cradle2MatlabXL.csv
C3Cradle2MatlabXL.csv
LW2
/
%CNAM Flux_3
  -2   0 -102   0   2 -102
   3
1 50
PressMatlab2CradleXL.csv
MassCradle2MatlabXL.csv
                       5                       50
   7
   3
C1Matlab2CradleXL.csv
C2Matlab2CradleXL.csv
C3Matlab2CradleXL.csv
C1Cradle2MatlabXL.csv
C2Cradle2MatlabXL.csv
C3Cradle2MatlabXL.csv
LW3
/
%CNAM Flux_4
  -2   0 -103   0   2 -103
   3
1 50
PressMatlab2CradleXL.csv
MassCradle2MatlabXL.csv
                       5                       50
   7
```

```
   3
C1Matlab2CradleXL.csv
C2Matlab2CradleXL.csv
C3Matlab2CradleXL.csv
C1Cradle2MatlabXL.csv
C2Cradle2MatlabXL.csv
C3Cradle2MatlabXL.csv
LW4
/
%CNAM Flux_5
  -2   0 -104   0   2 -104
   3
1 50
PressMatlab2CradleXL.csv
MassCradle2MatlabXL.csv
                       5                       50
   7
   3
C1Matlab2CradleXL.csv
C2Matlab2CradleXL.csv
C3Matlab2CradleXL.csv
C1Cradle2MatlabXL.csv
C2Cradle2MatlabXL.csv
C3Cradle2MatlabXL.csv
LW5
/
%CNAM Flux_6
  -2   0 -105   0   2 -105
   3
1 50
PressMatlab2CradleXL.csv
MassCradle2MatlabXL.csv
                       5                       50
   7
   3
C1Matlab2CradleXL.csv
C2Matlab2CradleXL.csv
C3Matlab2CradleXL.csv
C1Cradle2MatlabXL.csv
C2Cradle2MatlabXL.csv
C3Cradle2MatlabXL.csv
LW6
/
%CNAM Flux_7
  -2   0 -106   0   2 -106
   3
1 50
PressMatlab2CradleXL.csv
MassCradle2MatlabXL.csv
                       5                       50
   7
   3
```

```
C1Matlab2CradleXL.csv
C2Matlab2CradleXL.csv
C3Matlab2CradleXL.csv
C1Cradle2MatlabXL.csv
C2Cradle2MatlabXL.csv
C3Cradle2MatlabXL.csv
LW7
/
%CNAM Flux_8
  -2   0 -107   0   2 -107
   3
1 50
PressMatlab2CradleXL.csv
MassCradle2MatlabXL.csv
                       5                       50
   7
   3
C1Matlab2CradleXL.csv
C2Matlab2CradleXL.csv
C3Matlab2CradleXL.csv
C1Cradle2MatlabXL.csv
C2Cradle2MatlabXL.csv
C3Cradle2MatlabXL.csv
HG1
/
%CNAM Flux_9
  -2   0 -108   0   2 -108
   3
1 50
PressMatlab2CradleXL.csv
MassCradle2MatlabXL.csv
                       5                       50
   7
   3
C1Matlab2CradleXL.csv
C2Matlab2CradleXL.csv
C3Matlab2CradleXL.csv
C1Cradle2MatlabXL.csv
C2Cradle2MatlabXL.csv
C3Cradle2MatlabXL.csv
HG2
/
%CNAM Flux_10
  -2   0 -109   0   2 -109
   3
1 50
PressMatlab2CradleXL.csv
MassCradle2MatlabXL.csv
                       5                       50
   7
   3
C1Matlab2CradleXL.csv
```

```
C2Matlab2CradleXL.csv
C3Matlab2CradleXL.csv
C1Cradle2MatlabXL.csv
C2Cradle2MatlabXL.csv
C3Cradle2MatlabXL.csv
HG3
/
%CNAM Flux_11
  -2   0 -110   0   2 -110
   3
1 50
PressMatlab2CradleXL.csv
MassCradle2MatlabXL.csv
                       5                       50
   7
   3
C1Matlab2CradleXL.csv
C2Matlab2CradleXL.csv
C3Matlab2CradleXL.csv
C1Cradle2MatlabXL.csv
C2Cradle2MatlabXL.csv
C3Cradle2MatlabXL.csv
HG4
/
%CNAM Flux_12
  -2   0 -111   0   2 -111
   3
1 50
PressMatlab2CradleXL.csv
MassCradle2MatlabXL.csv
                       5                       50
   7
   3
C1Matlab2CradleXL.csv
C2Matlab2CradleXL.csv
C3Matlab2CradleXL.csv
C1Cradle2MatlabXL.csv
C2Cradle2MatlabXL.csv
C3Cradle2MatlabXL.csv
HG5
/
%CNAM Flux_13
  -2   0 -112   0   2 -112
   3
1 50
PressMatlab2CradleXL.csv
MassCradle2MatlabXL.csv
                       5                       50
   7
   3
C1Matlab2CradleXL.csv
C2Matlab2CradleXL.csv
```

```
C3Matlab2CradleXL.csv
C1Cradle2MatlabXL.csv
C2Cradle2MatlabXL.csv
C3Cradle2MatlabXL.csv
HG6
/
%CNAM Flux_14
  -2   0 -113   0   2 -113
   3
1 50
PressMatlab2CradleXL.csv
MassCradle2MatlabXL.csv
                       5                       50
   7
   3
C1Matlab2CradleXL.csv
C2Matlab2CradleXL.csv
C3Matlab2CradleXL.csv
C1Cradle2MatlabXL.csv
C2Cradle2MatlabXL.csv
C3Cradle2MatlabXL.csv
HG7
/
%CNAM Flux_15
  -2   0 -114   0   2 -114
   3
1 50
PressMatlab2CradleXL.csv
MassCradle2MatlabXL.csv
                       5                       50
   7
   3
C1Matlab2CradleXL.csv
C2Matlab2CradleXL.csv
C3Matlab2CradleXL.csv
C1Cradle2MatlabXL.csv
C2Cradle2MatlabXL.csv
C3Cradle2MatlabXL.csv
HG8
/
%CNAM Flux_16
  -2   0 -115   0   2 -115
   3
1 50
PressMatlab2CradleXL.csv
MassCradle2MatlabXL.csv
                       5                       50
   7
   3
C1Matlab2CradleXL.csv
C2Matlab2CradleXL.csv
C3Matlab2CradleXL.csv
```

```
C1Cradle2MatlabXL.csv
C2Cradle2MatlabXL.csv
C3Cradle2MatlabXL.csv
HG9
/
%CNAM Flux_17
  -2   0 -116   0   2 -116
   3
1 50
PressMatlab2CradleXL.csv
MassCradle2MatlabXL.csv
                       5                       50
   7
   3
C1Matlab2CradleXL.csv
C2Matlab2CradleXL.csv
C3Matlab2CradleXL.csv
C1Cradle2MatlabXL.csv
C2Cradle2MatlabXL.csv
C3Cradle2MatlabXL.csv
HG10
/
%CNAM Flux_18
  -2   0 -117   0   2 -117
   3
1 50
PressMatlab2CradleXL.csv
MassCradle2MatlabXL.csv
                       5                       50
   7
   3
C1Matlab2CradleXL.csv
C2Matlab2CradleXL.csv
C3Matlab2CradleXL.csv
C1Cradle2MatlabXL.csv
C2Cradle2MatlabXL.csv
C3Cradle2MatlabXL.csv
HG11
/
%CNAM Flux_19
  -2   0 -118   0   2 -118
   3
1 50
PressMatlab2CradleXL.csv
MassCradle2MatlabXL.csv
                       5                       50
   7
   3
C1Matlab2CradleXL.csv
C2Matlab2CradleXL.csv
C3Matlab2CradleXL.csv
C1Cradle2MatlabXL.csv
```

```
C2Cradle2MatlabXL.csv
C3Cradle2MatlabXL.csv
TG1
/
%CNAM Flux_20
  -2   0 -119   0   2 -119
   3
1 50
PressMatlab2CradleXL.csv
MassCradle2MatlabXL.csv
                       5                       50
   7
   3
C1Matlab2CradleXL.csv
C2Matlab2CradleXL.csv
C3Matlab2CradleXL.csv
C1Cradle2MatlabXL.csv
C2Cradle2MatlabXL.csv
C3Cradle2MatlabXL.csv
TG2
/
%CNAM Flux_21
  -2   0 -120   0   2 -120
   3
1 50
PressMatlab2CradleXL.csv
MassCradle2MatlabXL.csv
                       5                       50
   7
   3
C1Matlab2CradleXL.csv
C2Matlab2CradleXL.csv
C3Matlab2CradleXL.csv
C1Cradle2MatlabXL.csv
C2Cradle2MatlabXL.csv
C3Cradle2MatlabXL.csv
TG3
/
%CNAM Flux_22
  -2   0 -121   0   2 -121
   3
1 50
PressMatlab2CradleXL.csv
MassCradle2MatlabXL.csv
                       5                       50
   7
   3
C1Matlab2CradleXL.csv
C2Matlab2CradleXL.csv
C3Matlab2CradleXL.csv
C1Cradle2MatlabXL.csv
C2Cradle2MatlabXL.csv
```

```
C3Cradle2MatlabXL.csv
TG4
/
%CNAM Flux_23
  -2   0 -122   0   2 -122
   3
1 50
PressMatlab2CradleXL.csv
MassCradle2MatlabXL.csv
                       5                       50
   7
   3
C1Matlab2CradleXL.csv
C2Matlab2CradleXL.csv
C3Matlab2CradleXL.csv
C1Cradle2MatlabXL.csv
C2Cradle2MatlabXL.csv
C3Cradle2MatlabXL.csv
TG5
/
%CNAM Flux_24
  -2   0 -123   0   2 -123
   3
1 50
PressMatlab2CradleXL.csv
MassCradle2MatlabXL.csv
                       5                       50
   7
   3
C1Matlab2CradleXL.csv
C2Matlab2CradleXL.csv
C3Matlab2CradleXL.csv
C1Cradle2MatlabXL.csv
C2Cradle2MatlabXL.csv
C3Cradle2MatlabXL.csv
TG6
/
%CNAM Flux_25
  -2   0 -124   0   2 -124
   3
1 50
PressMatlab2CradleXL.csv
MassCradle2MatlabXL.csv
                       5                       50
   7
   3
C1Matlab2CradleXL.csv
C2Matlab2CradleXL.csv
C3Matlab2CradleXL.csv
C1Cradle2MatlabXL.csv
C2Cradle2MatlabXL.csv
C3Cradle2MatlabXL.csv
```

```
TG7
/
%CNAM Flux_26
  -2   0 -125   0   2 -125
   3
1 50
PressMatlab2CradleXL.csv
MassCradle2MatlabXL.csv
                       5                       50
   7
   3
C1Matlab2CradleXL.csv
C2Matlab2CradleXL.csv
C3Matlab2CradleXL.csv
C1Cradle2MatlabXL.csv
C2Cradle2MatlabXL.csv
C3Cradle2MatlabXL.csv
TG8
/
%CNAM Flux_27
  -2   0 -126   0   2 -126
   3
1 50
PressMatlab2CradleXL.csv
MassCradle2MatlabXL.csv
                       5                       50
   7
   3
C1Matlab2CradleXL.csv
C2Matlab2CradleXL.csv
C3Matlab2CradleXL.csv
C1Cradle2MatlabXL.csv
C2Cradle2MatlabXL.csv
C3Cradle2MatlabXL.csv
TG9
/
%CNAM Flux_28
  -2   0 -127   0   2 -127
   3
1 50
PressMatlab2CradleXL.csv
MassCradle2MatlabXL.csv
                       5                       50
   7
   3
C1Matlab2CradleXL.csv
C2Matlab2CradleXL.csv
C3Matlab2CradleXL.csv
C1Cradle2MatlabXL.csv
C2Cradle2MatlabXL.csv
C3Cradle2MatlabXL.csv
TG10
```

```
/
%CNAM Flux_29
  -2   0 -128   0   2 -128
   3
1 50
PressMatlab2CradleXL.csv
MassCradle2MatlabXL.csv
                       5                       50
   7
   3
C1Matlab2CradleXL.csv
C2Matlab2CradleXL.csv
C3Matlab2CradleXL.csv
C1Cradle2MatlabXL.csv
C2Cradle2MatlabXL.csv
C3Cradle2MatlabXL.csv
TG11
/
%CNAM Flux_30
  -2   0 -129   0   2 -129
   3
1 50
PressMatlab2CradleXL.csv
MassCradle2MatlabXL.csv
                       5                       50
   7
   3
C1Matlab2CradleXL.csv
C2Matlab2CradleXL.csv
C3Matlab2CradleXL.csv
C1Cradle2MatlabXL.csv
C2Cradle2MatlabXL.csv
C3Cradle2MatlabXL.csv
SU1
/
%CNAM Flux_31
  -2   0 -130   0   2 -130
   3
1 50
PressMatlab2CradleXL.csv
MassCradle2MatlabXL.csv
                       5                       50
   7
   3
C1Matlab2CradleXL.csv
C2Matlab2CradleXL.csv
C3Matlab2CradleXL.csv
C1Cradle2MatlabXL.csv
C2Cradle2MatlabXL.csv
C3Cradle2MatlabXL.csv
SU2
/
```

```
%CNAM Flux_32
  -2   0 -131   0   2 -131
   3
1 50
PressMatlab2CradleXL.csv
MassCradle2MatlabXL.csv
                       5                       50
   7
   3
C1Matlab2CradleXL.csv
C2Matlab2CradleXL.csv
C3Matlab2CradleXL.csv
C1Cradle2MatlabXL.csv
C2Cradle2MatlabXL.csv
C3Cradle2MatlabXL.csv
SU3
/
%CNAM Flux_33
  -2   0 -132   0   2 -132
   3
1 50
PressMatlab2CradleXL.csv
MassCradle2MatlabXL.csv
                       5                       50
   7
   3
C1Matlab2CradleXL.csv
C2Matlab2CradleXL.csv
C3Matlab2CradleXL.csv
C1Cradle2MatlabXL.csv
C2Cradle2MatlabXL.csv
C3Cradle2MatlabXL.csv
SU4
/
%CNAM Flux_34
  -2   0 -133   0   2 -133
   3
1 50
PressMatlab2CradleXL.csv
MassCradle2MatlabXL.csv
                       5                       50
   7
   3
C1Matlab2CradleXL.csv
C2Matlab2CradleXL.csv
C3Matlab2CradleXL.csv
C1Cradle2MatlabXL.csv
C2Cradle2MatlabXL.csv
C3Cradle2MatlabXL.csv
SU5
/
%CNAM Flux_35
```

```
  -2   0 -134   0   2 -134
   3
1 50
PressMatlab2CradleXL.csv
MassCradle2MatlabXL.csv
                        5                        50
   7
   3
C1Matlab2CradleXL.csv
C2Matlab2CradleXL.csv
C3Matlab2CradleXL.csv
C1Cradle2MatlabXL.csv
C2Cradle2MatlabXL.csv
C3Cradle2MatlabXL.csv
SU6
/
%CNAM Flux_36
  -2   0 -135   0   2 -135
   3
1 50
PressMatlab2CradleXL.csv
MassCradle2MatlabXL.csv
                        5                        50
   7
   3
C1Matlab2CradleXL.csv
C2Matlab2CradleXL.csv
C3Matlab2CradleXL.csv
C1Cradle2MatlabXL.csv
C2Cradle2MatlabXL.csv
C3Cradle2MatlabXL.csv
SU7
/
%CNAM Methane_Inflow
  -1   7   0   0   0   1
                   0.1229      0
                        0                         1
0
Inflow
/
/
FORC
%CNAM Forc_1
  -5                       0                         0
0   1
  28
-5000
  55
   -205.6
    162.3
    485.3
    379.3
```

```
      9.75e-7
   1.3697e-10
   8.6755e-12
  -3.9617e-11
   2.7287e-11
   1.1096e-12
  -5.5804e-11
   3.2365e-12
   4.2817e-11
  -3.7495e-12
   2.1402e-11
   1.1268e-10
   6.1561e-13
   1.6338e-11
  -1.4478e-12
    1.208e-10
   3.3733e-12
  -4.1614e-12
   4.0156e-12
  -3.4939e-11
    -1.55e-12
  -1.4678e-11
SmoothGob
CoupledBoundaries
/
/
GWLN
   0
INIT
PRES
                    -300   1
/
INIT
CN02
                       1  -1
SmoothGob
/
/
PLGN
pLW1
                       1                         0
0                    -0.8
                    -0.8                      3.5
5
                    -0.8                      3.5
-25
                    -0.8                       -1
-25
                    -0.8                       -1
5
/
pLW2
```

```
                    1                    0
0                  -0.8
                  -0.8                 3.5
-60
                  -0.8                 3.5
-90
                  -0.8                  -1
-90
                  -0.8                  -1
-60
/
pLW3
                    1                    0
0                  -0.8
                  -0.8                 3.5
-130
                  -0.8                 3.5
-160
                  -0.8                  -1
-160
                  -0.8                  -1
-130
/
pLW4
                    1                    0
0                  -0.8
                  -0.8                 3.5
-190
                  -0.8                 3.5
-220
                  -0.8                  -1
-220
                  -0.8                  -1
-190
/
pLW5
                    1                    0
0                  -0.8
                  -0.8                 3.5
-260
                  -0.8                 3.5
-290
                  -0.8                  -1
-290
                  -0.8                  -1
-260
/
pLW6
                    1                    0
0                  -0.8
                  -0.8                 3.5
-330
```

```
                    -0.8                    3.5
-360
                    -0.8                     -1
-360
                    -0.8                     -1
-330
/
pLW7
                       1                     0
0                   -0.8
                    -0.8                    3.5
-400
                    -0.8                    3.5
-430
                    -0.8                     -1
-430
                    -0.8                     -1
-400
/
pHG1
                       0                     0
-1                  -0.8
                      30                    3.5
0.8
                      60                    3.5
0.8
                      60                     -1
0.8
                      30                     -1
0.8
/
pHG2
                       0                     0
-1                  -0.8
                     120                    3.5
0.8
                     150                    3.5
0.8
                     150                     -1
0.8
                     120                     -1
0.8
/
pHG3
                       0                     0
-1                  -0.8
                     220                    3.5
0.8
                     250                    3.5
0.8
                     250                     -1
0.8
```

```
                    220                     -1
0.8
/
pHG4
                      0                      0
-1                   -0.8
                    310                    3.5
0.8
                    340                    3.5
0.8
                    340                     -1
0.8
                    310                     -1
0.8
/
pHG5
                      0                      0
-1                   -0.8
                    400                    3.5
0.8
                    430                    3.5
0.8
                    430                     -1
0.8
                    400                     -1
0.8
/
pHG6
                      0                      0
-1                   -0.8
                    500                    3.5
0.8
                    530                    3.5
0.8
                    530                     -1
0.8
                    500                     -1
0.8
/
pHG7
                      0                      0
-1                   -0.8
                    600                    3.5
0.8
                    630                    3.5
0.8
                    630                     -1
0.8
                    600                     -1
0.8
/
pHG8
```

```
                    0                    0
-1                 -0.8
                  695                  3.5
0.8
                  725                  3.5
0.8
                  725                   -1
0.8
                  695                   -1
0.8
/
pHG9
                    0                    0
-1                 -0.8
                  790                  3.5
0.8
                  820                  3.5
0.8
                  820                   -1
0.8
                  790                   -1
0.8
/
pHG10
                    0                    0
-1                 -0.8
                  885                  3.5
0.8
                  915                  3.5
0.8
                  915                   -1
0.8
                  885                   -1
0.8
/
pHG11
                    0                    0
-1                 -0.8
                  980                  3.5
0.8
                 1010                  3.5
0.8
                 1010                   -1
0.8
                  980                   -1
0.8
/
pTG1
                    0                    0
1                -420.8
                   30                  3.5
-420.8
```

```
                    60                    3.5
-420.8
                    60                     -1
-420.8
                    30                     -1
-420.8
/
pTG2
                     0                      0
1                -420.8
                   120                    3.5
-420.8
                   150                    3.5
-420.8
                   150                     -1
-420.8
                   120                     -1
-420.8
/
pTG3
                     0                      0
1                -420.8
                   220                    3.5
-420.8
                   250                    3.5
-420.8
                   250                     -1
-420.8
                   220                     -1
-420.8
/
pTG4
                     0                      0
1                -420.8
                   310                    3.5
-420.8
                   340                    3.5
-420.8
                   340                     -1
-420.8
                   310                     -1
-420.8
/
pTG5
                     0                      0
1                -420.8
                   400                    3.5
-420.8
                   430                    3.5
-420.8
                   430                     -1
-420.8
```

```
                    400                     -1
-420.8
/
pTG6
                      0                      0
1                 -420.8
                    500                    3.5
-420.8
                    530                    3.5
-420.8
                    530                     -1
-420.8
                    500                     -1
-420.8
/
pTG7
                      0                      0
1                 -420.8
                    600                    3.5
-420.8
                    630                    3.5
-420.8
                    630                     -1
-420.8
                    600                     -1
-420.8
/
pTG8
                      0                      0
1                 -420.8
                    695                    3.5
-420.8
                    725                    3.5
-420.8
                    725                     -1
-420.8
                    695                     -1
-420.8
/
pTG9
                      0                      0
1                 -420.8
                    790                    3.5
-420.8
                    820                    3.5
-420.8
                    820                     -1
-420.8
                    790                     -1
-420.8
/
pTG10
```

```
                    0                    0
1                -420.8
                  885                  3.5
-420.8
                  915                  3.5
-420.8
                  915                   -1
-420.8
                  885                   -1
-420.8
/
pTG11
                    0                    0
1                -420.8
                  980                  3.5
-420.8
                 1010                  3.5
-420.8
                 1010                   -1
-420.8
                  980                   -1
-420.8
/
pSU1
                   -1                    0
0              -1035.8
               1035.8                  3.5
5
               1035.8                  3.5
-25
               1035.8                   -1
-25
               1035.8                   -1
5
/
pSU2
                   -1                    0
0              -1035.8
               1035.8                  3.5
-60
               1035.8                  3.5
-90
               1035.8                   -1
-90
               1035.8                   -1
-60
/
pSU3
                   -1                    0
0              -1035.8
               1035.8                  3.5
-130
```

```
                1035.8                      3.5
-160
                1035.8                       -1
-160
                1035.8                       -1
-130
/
pSU4
                    -1                       0
0              -1035.8
                1035.8                      3.5
-190
                1035.8                      3.5
-220
                1035.8                       -1
-220
                1035.8                       -1
-190
/
pSU5
                    -1                       0
0              -1035.8
                1035.8                      3.5
-260
                1035.8                      3.5
-290
                1035.8                       -1
-290
                1035.8                       -1
-260
/
pSU6
                    -1                       0
0              -1035.8
                1035.8                      3.5
-330
                1035.8                      3.5
-360
                1035.8                       -1
-360
                1035.8                       -1
-330
/
pSU7
                    -1                       0
0              -1035.8
                1035.8                      3.5
-400
                1035.8                      3.5
-430
                1035.8                       -1
-430
```

```
                  1035.8                          -1
-400
/
/
PROP
%CNAM air(incompressible/20C)
   1   1                    1.206               1.83e-005
1007                   0.0256   0
/
                1.9e-005                         0
0                        0                        0
0
                1.6e-005                         0
0                        0                        0
0
                       0                         0
0                        0                        0
0
STED
   9  -1                   0.0001
/
TBTY
   4
WL02
   0   0
/
   1
@UNDEFINEDMOM
/
/
WPUT
   0
ZGWV
   0
GOGO
```

Appendix II

2.1 Friction Factor from SC /Tetra Results

Inputs to model:

- Equivalent roughness for the wall shear stress condition, e [m]
- Pressure difference at intake and exhaust surface boundaries, ΔP [N/m^2]

Output from model:

- Volumetric Flow Rate, Q [m^3/s]

Frictional Pressure Drop through Atkinson's Square Law

$$P = RQ^2 \quad \left[{}^{N}/_{m^2} \right]$$

which becomes

$$R = \frac{P}{Q^2} \quad \left[{}^{Ns^2}/_{m^8} \right]$$

Where R is the Atkinson's resistance, a combination of density and rational turbulent resistance which is the product of the following

$$R = k\, L\, \frac{per}{A^3} \quad \left[{}^{Ns^2}/_{m^8} \right]$$

where

- k is the Atkinson's Friction Factor [Ns^2/m^4] or [kg/m^3]
- L is length [m]
- per is the perimeter length [m]
- A^3 is the cube of the cross sectional area [m^6]

Factoring

$$k = \frac{R\, A^3}{L\, per} \quad \left[{}^{Ns^2}/_{m^4} \right]$$

Atkinson's work predates Darcy, Reynolds, Stanton, Prandtl, and Nikuradse. He never realized the dependence on density because he only worked in mines that were relatively shallow. Density, for his purposes, was effectively a constant. It later was shown that:

$$k = \frac{f\,\rho}{8} \quad \left[Ns^2/_{m^4}\right]$$

where

- f is the coefficient of friction [dimensionless]
- ρ is the density, assuming standard 1.2 [kg/m^3]

2.2 Theoretical Flow from Roughness

Colebrook Approximation, simplified for wholly turbulent flow

$$f_t = \frac{1}{\left(2\,\log\left(\frac{3.7}{\varepsilon_t}\right)\right)^2}$$

where ε_t is the relative roughness for the tunnel

$$\varepsilon_t = \frac{\mathrm{e_t}}{D_h} \quad [\text{dimensionless}]$$

- e_t is the equivalent roughness for the tunnel [m]
- D_h is the hydraulic diameter

$$D_h = \frac{4\,A_t}{per_t} \quad [m]$$

Darcy-Weisbach equation used to determine Velocity and consequently Q

$$\Delta P = \left(\sum K + f_t \frac{L_t}{D_h}\right)\frac{\rho v^2}{2} \quad \left[N/_{m^2}\right]$$

where

- ΔP is the pressure gradient, the same used for the previous work [N/m^2]
- $\sum K$ is the sum of the pressures losses in the tunnel, zero in this case
- L_t is the length of the tunnel [m]
- v is the air velocity [m/s]

Realizing that the air velocity is related to the volumetric flow rate by the cross sectional area and the hydraulic diameter is a function of cross sectional area and perimeter, the above simplifies to

$$\Delta P = \frac{f_t\,\rho_t}{8}\,\frac{L_t\,per_t}{{A_t}^3}\,Q^2 \quad \left[N/_{m^2}\right]$$

or

$$\Delta P = k \frac{L_t \, per_t}{{A_t}^3} Q^2 \quad \left[{N}/{m^2}\right]$$

or

$$\Delta P = RQ^2 \quad \left[{N}/{m^2}\right]$$

Thus

$$Q = \sqrt{\frac{\Delta P}{\frac{f_t \, \rho_t}{8} \frac{L_t \, per_t}{{A_t}^3}}} \quad [m^3]$$

Appendix III

3.1 SC/Tetra User Defined Functions

```
#ifndef SCT10_US_C  /*only sct10_us.c defined*/
#define SCT10_US_C
#endif

#include "sct10_us.h"
#include <stdio.h>
#include <string.h>
#include <direct.h>
#include <stdlib.h>

/*****************************************
**  CONSTANTS DEFINED FOR Gob Modeling  **
*****************************************/

#define MAXREGIONNUMBER           500           //     This is the maximum
expected number of regions for use in coupling to Matlab
#define MAXREGIONNAME             40            //     This is the maximum length
of name of regions, limited by CRADLE UI to 36
#define MAXLINELENGTH             2048   //     This is the maximum expected line
length
#define MAXFILENAME               200           //  This is the maximum expected
file name length
#define REGIONSFIELD       4             //     This is the index where the names
of regions start in the coupling files
#define ISWOFFSET                 100           //  In Cradle, ISW begins at 100
#define FILEREADATTEMPTS    1             //  This is the number of attempts to
read in a file for importing data
#define FILERETRYWAIT             10000  //  This is the delay introduced between
successive read attempts in milliseconds
#define GOBEXPONENT               1             //  This is the exponent from
ploss = RQ^n
#define ITHELEMENT                120000        //  ith element to be used for
debug
#define SPECIESO2                 1             //  This is the expected order for
species concentration of oxygen
#define SPECIESCH4                2             //     This is the expected order
for species concentration of methane
#define CFDTOKEN                  "cfdtoken.txt"
#define MATLABTOKEN               "matlabtoken.txt"
#define DEBUG                     0

/***********************************
**  VARIABLES DEFINED FOR COUPLING  **
***********************************/
int regionNumber =0;
int couplingMethod;
int couplingCFD2MatlabFlag = 0;                 // Rais flag to output CFD data to
Matlab
int couplingMatlab2CFDFlag = 0;                 // Raise flag to say look for
MATLABTOKEN
int couplingMatlab2CFDFlagKillNext = 0;   // Cycle in which coupling did occur,
remove MATLABTOKEN at +1
```

```
int couplingCycle = 0;                                  // Cycle where coupling
should occur
int gobElem = -1;
int coupleElem = -1;

fprec couplingInterval;
fprec couplingTime = 100000000;                  // Arbitrary large value to
prevent false coupling signal
fprec previousMatlabTime =0;
fprec *pressure;
fprec *species1;
fprec *species2;
fprec *species3;
fprec *species4;
fprec *species5;

fprec normXeMean=0;
fprec normXeStd=0;
fprec normYeMean=0;
fprec normYeStd=0;
fprec kFactor = 0;
fprec p00;
fprec p10 =0;
fprec p01 =0;
fprec p20 =0;
fprec p11 =0;
fprec p02 =0;
fprec p30 =0;
fprec p21 =0;
fprec p12 =0;
fprec p03 =0;
fprec p40 =0;
fprec p31 =0;
fprec p22 =0;
fprec p13 =0;
fprec p04 =0;
fprec p50 =0;
fprec p41 =0;
fprec p32 =0;
fprec p23 =0;
fprec p14 =0;
fprec p05 =0;
fprec   highViscosity;
fprec normalViscosity;
fprec viscXmax;
fprec viscXmin;
fprec viscYmax;
fprec viscYmin;
fprec viscZmax;
fprec viscZmin;


fprec *coef0Forc;

char pressureInputFile[MAXFILENAME]={"\0"};
char species1InputFile[MAXFILENAME]={"\0"};
char species2InputFile[MAXFILENAME]={"\0"};
char species3InputFile[MAXFILENAME]={"\0"};
```

```
char species4InputFile[MAXFILENAME]={"\0"};
char species5InputFile[MAXFILENAME]={"\0"};

char massFlowOutputFile[MAXFILENAME]={"\0"};
char species1OutputFile[MAXFILENAME]={"\0"};
char species2OutputFile[MAXFILENAME]={"\0"};
char species3OutputFile[MAXFILENAME]={"\0"};
char species4OutputFile[MAXFILENAME]={"\0"};
char species5OutputFile[MAXFILENAME]={"\0"};

/************************************
*** SYSTEM ***************************
************************************/
void usu_versioninfo(int *id1,int *id2,int *id3,char *text)
{
       MAPUSERFUNC
              /* please do not change next five lines ! */
              *id1 =  _MAJOR_VER;
       *id2 =  1000*_FPREC_NUM + 100*_ARCH_NUM + _RELEASE;
       *id3 = _VER_DATE;
       /* user specified string (< 1000 chars) */
       strcpy(text,"compiled at " __TIME__ " " __DATE__);
}
int usu_fprecinfo()
{
       return sizeof(fprec);
}


/************************************
*** FLUXES ***************************
************************************/

void usr_pres(int isw,int nlines)
{
       char line[MAXLINELENGTH];
       char msg[MAXLINELENGTH];

       regionNumber++;
       usf_getline(line, MAXLINELENGTH);
       sscanf(line, "%i %lg", &couplingMethod, &couplingInterval);
       usf_getline(line, MAXLINELENGTH);
       sscanf(line, "%s", &pressureInputFile);
       usf_getline(line, MAXLINELENGTH);
       sscanf(line, "%s", &massFlowOutputFile);


       if (regionNumber ==1){
              sprintf(msg, "    Coupling Method: = %d Interval: %f \n",
couplingMethod, couplingInterval); usf_sout(msg);
              sprintf(msg, "    File for Pressure Coupling Input: %s RegionISW: %d
\n", pressureInputFile, isw); usf_sout(msg);
              sprintf(msg, "    File for Mass Flow Coupling Output: %s RegionISW:
%d \n", massFlowOutputFile, isw); usf_sout(msg);
       }
       else if (regionNumber>1 && DEBUG ==1){
              sprintf(msg, "    Coupling Method: = %d Interval: %f \n",
couplingMethod, couplingInterval); usf_sout(msg);
```

```
		sprintf(msg, "    File for Pressure Coupling Input: %s RegionISW: %d
\n", pressureInputFile, isw); usf_sout(msg);
		sprintf(msg, "    File for Mass Flow Coupling Output: %s RegionISW:
%d \n", massFlowOutputFile, isw); usf_sout(msg);
	}
}
fprec use_pres(int isw,int nnd)
{

	return pressure[isw-ISWOFFSET];
}

void usr_cc(int isw,int nlines)
{
	char line[MAXLINELENGTH];
	char msg[MAXLINELENGTH];

	int numSpecies;

	// Three possible scenarios, with either 3, 4, or 5 diffusive species,
using the Mixing Option within Cradle
	// Case 3:  O2, CH4 (or dust), N2
	// Case 4:  O2, CH4, CO2, N2
	// Case 5:  O2, CH4, CO2, CO, N2

	usf_getline(line, MAXLINELENGTH);
	sscanf(line, "%i", &numSpecies);
	if (DEBUG==1){
		sprintf(msg, "    Number of Species for Coupling Input: %d \n",
numSpecies); usf_sout(msg);
	}
	switch (numSpecies){
	case 3:
		usf_getline(line, MAXLINELENGTH);
		sscanf(line, "%s", &species1InputFile);
		sprintf(msg, "    File for Species 1 Coupling Input: %s RegionISW:
%d \n", species1InputFile, isw); usf_sout(msg);
		usf_getline(line, MAXLINELENGTH);
		sscanf(line, "%s", &species2InputFile);
		sprintf(msg, "    File for Species 2 Coupling Input: %s RegionISW:
%d \n", species2InputFile, isw); usf_sout(msg);
		usf_getline(line, MAXLINELENGTH);
		sscanf(line, "%s", &species3InputFile);
		sprintf(msg, "    File for Species 3 Coupling Input: %s RegionISW:
%d \n", species3InputFile, isw); usf_sout(msg);

		usf_getline(line, MAXLINELENGTH);
		sscanf(line, "%s", &species1OutputFile);
		sprintf(msg, "    File for Species 1 Coupling Output: %s RegionISW:
%d \n", species1OutputFile, isw); usf_sout(msg);
		usf_getline(line, MAXLINELENGTH);
		sscanf(line, "%s", &species2OutputFile);
		sprintf(msg, "    File for Species 2 Coupling Output: %s RegionISW:
%d \n", species2OutputFile, isw); usf_sout(msg);
		usf_getline(line, MAXLINELENGTH);
		sscanf(line, "%s", &species3OutputFile);
		sprintf(msg, "    File for Species 3 Coupling Output: %s RegionISW:
%d \n", species3OutputFile, isw); usf_sout(msg);
```

```
                break;
        case 4:
                usf_getline(line, MAXLINELENGTH);
                sscanf(line, "%s", &species1InputFile);
                sprintf(msg, "    File for Species 1 Coupling Input: %s RegionISW:
%d \n", species1InputFile, isw); usf_sout(msg);
                usf_getline(line, MAXLINELENGTH);
                sscanf(line, "%s", &species2InputFile);
                sprintf(msg, "    File for Species 2 Coupling Input: %s RegionISW:
%d \n", species2InputFile, isw); usf_sout(msg);
                usf_getline(line, MAXLINELENGTH);
                sscanf(line, "%s", &species3InputFile);
                sprintf(msg, "    File for Species 3 Coupling Input: %s RegionISW:
%d \n", species3InputFile, isw); usf_sout(msg);
                usf_getline(line, MAXLINELENGTH);
                sscanf(line, "%s", &species4InputFile);
                sprintf(msg, "    File for Species 4 Coupling Input: %s RegionISW:
%d \n", species4InputFile, isw); usf_sout(msg);

                usf_getline(line, MAXLINELENGTH);
                sscanf(line, "%s", &species1OutputFile);
                sprintf(msg, "    File for Species 1 Coupling Output: %s RegionISW:
%d \n", species1OutputFile, isw); usf_sout(msg);
                usf_getline(line, MAXLINELENGTH);
                sscanf(line, "%s", &species2OutputFile);
                sprintf(msg, "    File for Species 2 Coupling Output: %s RegionISW:
%d \n", species2OutputFile, isw); usf_sout(msg);
                usf_getline(line, MAXLINELENGTH);
                sscanf(line, "%s", &species3OutputFile);
                sprintf(msg, "    File for Species 3 Coupling Output: %s RegionISW:
%d \n", species3OutputFile, isw); usf_sout(msg);
                usf_getline(line, MAXLINELENGTH);
                sscanf(line, "%s", &species4OutputFile);
                sprintf(msg, "    File for Species 4 Coupling Output: %s RegionISW:
%d \n", species4OutputFile, isw); usf_sout(msg);
                break;
        case 5:
                usf_getline(line, MAXLINELENGTH);
                sscanf(line, "%s", &species1InputFile);
                sprintf(msg, "    File for Species 1 Coupling Input: %s RegionISW:
%d \n", species1InputFile, isw); usf_sout(msg);
                usf_getline(line, MAXLINELENGTH);
                sscanf(line, "%s", &species2InputFile);
                sprintf(msg, "    File for Species 2 Coupling Input: %s RegionISW:
%d \n", species2InputFile, isw); usf_sout(msg);
                usf_getline(line, MAXLINELENGTH);
                sscanf(line, "%s", &species3InputFile);
                sprintf(msg, "    File for Species 3 Coupling Input: %s RegionISW:
%d \n", species3InputFile, isw); usf_sout(msg);
                usf_getline(line, MAXLINELENGTH);
                sscanf(line, "%s", &species4InputFile);
                sprintf(msg, "    File for Species 4 Coupling Input: %s RegionISW:
%d \n", species4InputFile, isw); usf_sout(msg);
                usf_getline(line, MAXLINELENGTH);
                sscanf(line, "%s", &species5InputFile);
                sprintf(msg, "    File for Species 5 Coupling Input: %s RegionISW:
%d \n", species5InputFile, isw); usf_sout(msg);
```

```
                usf_getline(line, MAXLINELENGTH);
                sscanf(line, "%s", &species1OutputFile);
                sprintf(msg, "    File for Species 1 Coupling Output: %s RegionISW:
%d \n", species1OutputFile, isw); usf_sout(msg);
                usf_getline(line, MAXLINELENGTH);
                sscanf(line, "%s", &species2OutputFile);
                sprintf(msg, "    File for Species 2 Coupling Output: %s RegionISW:
%d \n", species2OutputFile, isw); usf_sout(msg);
                usf_getline(line, MAXLINELENGTH);
                sscanf(line, "%s", &species3OutputFile);
                sprintf(msg, "    File for Species 3 Coupling Output: %s RegionISW:
%d \n", species3OutputFile, isw); usf_sout(msg);
                usf_getline(line, MAXLINELENGTH);
                sscanf(line, "%s", &species4OutputFile);
                sprintf(msg, "    File for Species 4 Coupling Output: %s RegionISW:
%d \n", species4OutputFile, isw); usf_sout(msg);
                usf_getline(line, MAXLINELENGTH);
                sscanf(line, "%s", &species5OutputFile);
                sprintf(msg, "    File for Species 5 Coupling Output: %s RegionISW:
%d \n", species5OutputFile, isw); usf_sout(msg);
                break;
        }
}
fprec use_cc(int isw,int iii,int nnd)
{
        switch(iii){
        case 1:
                return species1[isw-ISWOFFSET];
                break;
        case 2:
                return species2[isw-ISWOFFSET];
                break;
        case 3:
                return species3[isw-ISWOFFSET];
                break;
        case 4:
                return species4[isw-ISWOFFSET];
                break;
        case 5:
                return species5[isw-ISWOFFSET];
                break;
        default:
                return 0.0;
                break;
        }
}

/************************************
*** FORCE CONDITIONS *****************
************************************/
void usr_forc(int isw,int nlines)
{
        char line[MAXLINELENGTH];
        char msg[MAXLINELENGTH];

        int polyFitType;

        usf_getline(line, MAXLINELENGTH);
```

```
	sscanf(line, "%i", &gobElem);
	usf_getline(line, MAXLINELENGTH);
	sscanf(line, "%i", &polyFitType);


	switch(polyFitType){
	case 55:
		usf_sout("\n===== Gob Resistance Function Initialization
=====\r\n");
		sprintf(msg, "\nGob Resistance mapped to CFD using Matlab Curve
Fitting Tool\n", polyFitType); usf_sout(msg);
		sprintf(msg, "Linear model Poly55:\n");usf_sout(msg);
		sprintf(msg, "   f(x,y) = p00 + p10*x + p01*y + p20*x^2 + p11*x*y +
p02*y^2 + p30*x^3 + p21*x^2*y\n"); usf_sout(msg);
		sprintf(msg, "      + p12*x*y^2 + p03*y^3 + p40*x^4 + p31*x^3*y +
p22*x^2*y^2\n");  usf_sout(msg);
		sprintf(msg, "      + p13*x*y^3 + p04*y^4 + p50*x^5 + p41*x^4*y +
p32*x^3*y^2\n");  usf_sout(msg);
		sprintf(msg, "      + p23*x^2*y^3 + p14*x*y^4 + p05*y^5\n\n");
usf_sout(msg);
		sprintf(msg, "   Where x and y are normalized\n");usf_sout(msg);
		usf_getline(line, MAXLINELENGTH);
		sscanf(line, "%lg", &normXeMean);
		usf_getline(line, MAXLINELENGTH);
		sscanf(line, "%lg", &normXeStd); sprintf(msg,"      X Mean:  % 6.2f
STD:  % 6.2f\n",normXeMean, normXeStd);usf_sout(msg);
		usf_getline(line, MAXLINELENGTH);
		sscanf(line, "%lg", &normYeMean);
		usf_getline(line, MAXLINELENGTH);
		sscanf(line, "%lg", &normYeStd); sprintf(msg,"      Y Mean:  % 6.2f
STD:  % 6.2f\n\n",normYeMean, normYeStd);usf_sout(msg);
		usf_getline(line, MAXLINELENGTH);
		sscanf(line, "%lg", &kFactor); sprintf(msg,"      K factor:  % 5.4e
\n\n", kFactor);usf_sout(msg);
		sprintf(msg,"      Test Element:  %d \n\n", gobElem);usf_sout(msg);
		usf_getline(line, MAXLINELENGTH);
		sscanf(line, "%lg", &p00); sprintf(msg,"      p00:  %
5.4e\n",p00);usf_sout(msg);
		usf_getline(line, MAXLINELENGTH);
		sscanf(line, "%lg", &p10); sprintf(msg,"      p10:  %
5.4e\n",p10);usf_sout(msg);
		usf_getline(line, MAXLINELENGTH);
		sscanf(line, "%lg", &p01); sprintf(msg,"      p01:  %
5.4e\n",p01);usf_sout(msg);
		usf_getline(line, MAXLINELENGTH);
		sscanf(line, "%lg", &p20); sprintf(msg,"      p20:  %
5.4e\n",p20);usf_sout(msg);
		usf_getline(line, MAXLINELENGTH);
		sscanf(line, "%lg", &p11); sprintf(msg,"      p11:  %
5.4e\n",p11);usf_sout(msg);
		usf_getline(line, MAXLINELENGTH);
		sscanf(line, "%lg", &p02); sprintf(msg,"      p02:  %
5.4e\n",p02);usf_sout(msg);
		usf_getline(line, MAXLINELENGTH);
		sscanf(line, "%lg", &p30); sprintf(msg,"      p30:  %
5.4e\n",p30);usf_sout(msg);
		usf_getline(line, MAXLINELENGTH);
```

```
                sscanf(line, "%lg", &p21); sprintf(msg,"      p21:  %
5.4e\n",p21);usf_sout(msg);
                usf_getline(line, MAXLINELENGTH);
                sscanf(line, "%lg", &p12); sprintf(msg,"      p12:  %
5.4e\n",p12);usf_sout(msg);
                usf_getline(line, MAXLINELENGTH);
                sscanf(line, "%lg", &p03); sprintf(msg,"      p03:  %
5.4e\n",p03);usf_sout(msg);
                usf_getline(line, MAXLINELENGTH);
                sscanf(line, "%lg", &p40); sprintf(msg,"      p40:  %
5.4e\n",p40);usf_sout(msg);
                usf_getline(line, MAXLINELENGTH);
                sscanf(line, "%lg", &p31); sprintf(msg,"      p31:  %
5.4e\n",p31);usf_sout(msg);
                usf_getline(line, MAXLINELENGTH);
                sscanf(line, "%lg", &p22); sprintf(msg,"      p22:  %
5.4e\n",p22);usf_sout(msg);
                usf_getline(line, MAXLINELENGTH);
                sscanf(line, "%lg", &p13); sprintf(msg,"      p13:  %
5.4e\n",p13);usf_sout(msg);
                usf_getline(line, MAXLINELENGTH);
                sscanf(line, "%lg", &p04); sprintf(msg,"      p04:  %
5.4e\n",p04);usf_sout(msg);
                usf_getline(line, MAXLINELENGTH);
                sscanf(line, "%lg", &p50); sprintf(msg,"      p50:  %
5.4e\n",p50);usf_sout(msg);
                usf_getline(line, MAXLINELENGTH);
                sscanf(line, "%lg", &p41); sprintf(msg,"      p41:  %
5.4e\n",p41);usf_sout(msg);
                usf_getline(line, MAXLINELENGTH);
                sscanf(line, "%lg", &p32); sprintf(msg,"      p32:  %
5.4e\n",p32);usf_sout(msg);
                usf_getline(line, MAXLINELENGTH);
                sscanf(line, "%lg", &p23); sprintf(msg,"      p23:  %
5.4e\n",p23);usf_sout(msg);
                usf_getline(line, MAXLINELENGTH);
                sscanf(line, "%lg", &p14); sprintf(msg,"      p14:  %
5.4e\n",p14);usf_sout(msg);
                usf_getline(line, MAXLINELENGTH);
                sscanf(line, "%lg", &p05); sprintf(msg,"      p05:  %
5.4e\n",p05);usf_sout(msg);
                break;
        }
        sprintf(msg,"\nApplied to region(s):\n");usf_sout(msg);
}
void use_forc(int isw,int ie,int ifa,fprec *coef)
{
        char msg[MAXLINELENGTH];
        int numCycle;
        int numFirstCycle;
        int prl_rank, prl_root=0;
        fprec xe;
        fprec ye;
        fprec xen;
        fprec yen;
        fprec cValue=0;

        MPI_Comm_rank(MPI_COMM_WORLD, &prl_rank);
```

```
	numCycle = usf_ncyc();
	numFirstCycle = usf_ncyc1();

	xe = usf_ze(ie);
	ye = usf_xe(ie);

	xen = (xe-normXeMean)/normXeStd;
	yen = (ye-normYeMean)/normYeStd;

	if (numCycle == numFirstCycle){
		cValue = p00 + p10*xen+p01*yen;
		if (ie == ITHELEMENT){sprintf(msg,"cValue1 is:
%e\n",cValue);usf_sout(msg);}
		cValue = cValue + p20*pow(xen,2)+p11*xen*yen+p02*pow(yen,2);
		if (ie == ITHELEMENT){sprintf(msg,"cValue2 is:
%e\n",cValue);usf_sout(msg);}
		cValue = cValue +
p30*pow(xen,3)+p21*pow(xen,2)*yen+p12*xen*pow(yen,2)+p03*pow(yen,3);
		if (ie == ITHELEMENT){sprintf(msg,"cValue3 is:
%e\n",cValue);usf_sout(msg);}
		cValue = cValue +
p40*pow(xen,4)+p31*pow(xen,3)*yen+p22*pow(xen,2)*pow(yen,2);
		if (ie == ITHELEMENT){sprintf(msg,"cValue4 is:
%e\n",cValue);usf_sout(msg);}
		cValue = cValue + p13*xen*pow(yen,3)+p04*pow(yen,4);
		if (ie == ITHELEMENT){sprintf(msg,"cValue5 is:
%e\n",cValue);usf_sout(msg);}
		cValue = cValue +
p50*pow(xen,5)+p41*pow(xen,4)*yen+p32*pow(xen,3)*pow(yen,2);
		if (ie == ITHELEMENT){sprintf(msg,"cValue6 is:
%e\n",cValue);usf_sout(msg);}
		cValue = cValue +
p23*pow(xen,2)*pow(yen,3)+p14*xen*pow(yen,4)+p05*pow(yen,5);
		if (ie == ITHELEMENT){sprintf(msg,"cValue7 is:
%e\n",cValue);usf_sout(msg);}
		coef0Forc[ie]= kFactor/cValue;
		if (ie == gobElem&&prl_rank==prl_root){
			sprintf(msg,"Element number is:  %i\n",ie);usf_sout(msg);
			sprintf(msg,"Element coordinate is:
(%f,%f)\n",xe,ye);usf_sout(msg);
			sprintf(msg,"Normalized Element coordinate is:
(%f,%f)\n",xen,yen);usf_sout(msg);
			sprintf(msg,"Calculated permeability is:
%e\n",cValue);usf_sout(msg);
			sprintf(msg,"Value resistance is:
%e\n",coef0Forc[ie]);usf_sout(msg);
		}
	}
	if (numCycle == numFirstCycle+5&&prl_rank==prl_root){
		if (ie == gobElem){
			sprintf(msg,"Value resistance is:
%e\n",coef0Forc[ie]);usf_sout(msg);
		}
	}
	coef[0]=coef0Forc[ie];
	coef[1]= 0.0f;
	coef[2]= GOBEXPONENT;
```

```
}

/************************************
*** REPORT FUNCTIONS *****************
************************************/
void usl_chkf_flxio(char *name,fprec area,fprec mflx,fprec flx)
{
	FILE *fp;

	int prl_rank, prl_root=0;


	MPI_Comm_rank(MPI_COMM_WORLD, &prl_rank);
	if(strcmp(massFlowOutputFile,"\0")!=0&&prl_rank==prl_root&&couplingCFD2Matl
abFlag==1){
		fp = fopen(massFlowOutputFile, "a");
		fprintf(fp,", %s, %lg",name, mflx);
		fclose(fp);
	}
}

void usl_chkc_flxio(char *name,int iii,fprec mflx)
{
	FILE *fp;
	char msg[MAXLINELENGTH];
	int prl_rank, prl_root=0;

	MPI_Comm_rank(MPI_COMM_WORLD, &prl_rank);

	switch (iii){
	case 1:

	if(strcmp(species1OutputFile,"\0")!=0&&prl_rank==prl_root&&couplingCFD2Matl
abFlag==1){
			fp = fopen(species1OutputFile, "a");
			fprintf(fp,", %s, %lg",name, mflx);
			fclose(fp);
		}
		break;
	case 2:

	if(strcmp(species2OutputFile,"\0")!=0&&prl_rank==prl_root&&couplingCFD2Matl
abFlag==1){
			fp = fopen(species2OutputFile, "a");
			fprintf(fp,", %s, %lg",name, mflx);
			fclose(fp);
		}
		break;
	case 3:

	if(strcmp(species3OutputFile,"\0")!=0&&prl_rank==prl_root&&couplingCFD2Matl
abFlag==1){
			fp = fopen(species3OutputFile, "a");
			fprintf(fp,", %s, %lg",name, mflx);
			fclose(fp);
		}
		break;
	case 4:
```

```
	if(strcmp(species4OutputFile,"\0")!=0&&prl_rank==prl_root&&couplingCFD2Matl
abFlag==1){
			fp = fopen(species4OutputFile, "a");
			fprintf(fp,", %s, %lg",name, mflx);
			fclose(fp);
		}
		break;
	case 5:

	if(strcmp(species5OutputFile,"\0")!=0&&prl_rank==prl_root&&couplingCFD2Matl
abFlag==1){
			fp = fopen(species5OutputFile, "a");
			fprintf(fp,", %s, %lg",name, mflx);
			fclose(fp);
		}
		break;
	}
}

/*************************************
*** TIMING FUNCTIONS *****************
*************************************/
void usu_init()
{
	FILE *fp;
	char msg[MAXLINELENGTH];
	int prl_rank, prl_root=0;
	int elemNumber, numNodes;

	elemNumber = usf_nelem();
	numNodes = usf_nnods();

	pressure =  (fprec *)malloc(regionNumber*sizeof(fprec));
	species1 =  (fprec *)malloc(regionNumber*sizeof(fprec));
	species2 =  (fprec *)malloc(regionNumber*sizeof(fprec));
	species3 =  (fprec *)malloc(regionNumber*sizeof(fprec));
	species4 =  (fprec *)malloc(regionNumber*sizeof(fprec));
	species5 =  (fprec *)malloc(regionNumber*sizeof(fprec));
	coef0Forc = (fprec *)malloc(elemNumber*sizeof(fprec));

	MPI_Comm_rank(MPI_COMM_WORLD, &prl_rank);

	if (DEBUG ==1){
		sprintf(msg, "(DEBUG)  ====== Begin of usu_init() =====\n");
usf_sout(msg);
	}

	if(strcmp(massFlowOutputFile,"\0")!=0&&prl_rank==prl_root){
		fp = fopen(massFlowOutputFile, "a");
		fprintf(fp,
"*************************************************************************
****\n");
		fprintf(fp, "***                    Begin MassFlowCradle2Matlab
Output                         ***\n");
		fprintf(fp,
"*************************************************************************
****\n");
```

```
		fclose(fp);
	}
	if(strcmp(species1OutputFile,"\0")!=0&&prl_rank==prl_root){
		fp = fopen(species1OutputFile, "a");

	fprintf(fp,"**********************************************************************
**********\n");
		fprintf(fp,"***                    Begin Species1Cradle2Matlab
Output                         ***\n");

	fprintf(fp,"**********************************************************************
**********\n");
		fclose(fp);
	}
	if(strcmp(species2OutputFile,"\0")!=0&&prl_rank==prl_root){
		fp = fopen(species2OutputFile, "a");

	fprintf(fp,"**********************************************************************
**********\n");
		fprintf(fp,"***                    Begin Species2Cradle2Matlab
Output                         ***\n");

	fprintf(fp,"**********************************************************************
**********\n");
		fclose(fp);
	}
	if(strcmp(species3OutputFile,"\0")!=0&&prl_rank==prl_root){
		fp = fopen(species3OutputFile, "a");

	fprintf(fp,"**********************************************************************
**********\n");
		fprintf(fp,"***                    Begin Species3Cradle2Matlab
Output                         ***\n");

	fprintf(fp,"**********************************************************************
**********\n");
		fclose(fp);
	}
	if(strcmp(species4OutputFile,"\0")!=0&&prl_rank==prl_root){
		fp = fopen(species4OutputFile, "a");

	fprintf(fp,"**********************************************************************
**********\n");
		fprintf(fp,"***                    Begin Species4Cradle2Matlab
Output                         ***\n");

	fprintf(fp,"**********************************************************************
**********\n");
		fclose(fp);
	}
	if(strcmp(species5OutputFile,"\0")!=0&&prl_rank==prl_root){
		fp = fopen(species5OutputFile, "a");

	fprintf(fp,"**********************************************************************
**********\n");
		fprintf(fp,"***                    Begin Species5Cradle2Matlab
Output                         ***\n");
```

```
	fprintf(fp,"**********************************************************************
**********************\n");
		fclose(fp);
	}
	if (DEBUG ==1){
		sprintf(msg, "(DEBUG)  ====== End of usu_init() =====\n");
usf_sout(msg);
	}
}
void usu_cycle_start()
{
	FILE *fp, *mToken;
	char msg[MAXLINELENGTH];
	char line[MAXLINELENGTH];
	char lastLine[MAXLINELENGTH];
	char *tokens;
	int numCycle, matlabCycle, j, errorFlag=0;
	fprec time, timeStep, matlabTime;
	int prl_rank, prl_root=0;
	int numFirstCycle;

	if (DEBUG==1){
		sprintf(msg, "(DEBUG)  ====== Begin of usu_cycle_start() =====\n");
usf_sout(msg);
	}
	numCycle = usf_ncyc();
	numFirstCycle = usf_ncyc1();
	time = usf_time();
	timeStep = usf_dt();

	// Beginning of Coupling UDF portion
	if (numCycle==numFirstCycle){
		couplingMatlab2CFDFlag = 1;
		usf_sout("\n=== Multi-Scale Ventilation Modeling Initialization
===\r\n");
		switch(couplingMethod){
		case 1:
			couplingCycle = numCycle + (int)(couplingInterval);
			sprintf(msg, "   Coupling Interval by Cycle:  %i\n",
(int)(couplingInterval)); usf_sout(msg);
			break;
		case 2:
			couplingTime = time + couplingInterval;
			sprintf(msg, "   Coupling Interval by Time:  %lg sec\n",
couplingInterval); usf_sout(msg);
			break;
		}
	}
	if (numCycle>=couplingCycle || time >= couplingTime){
		if (DEBUG==1){
			sprintf(msg, "(DEBUG)        Raise couplingCFD2MatlabFlag due
to cycle or time condition met\n"); usf_sout(msg);
		}
		couplingCFD2MatlabFlag = 1;
	}

	mToken = fopen(MATLABTOKEN, "r");
```

```
	if (DEBUG==1){
		sprintf(msg, "(DEBUG)  Attempting to Open Matlab Token\n");
usf_sout(msg);
		if (mToken!=NULL && ferror(mToken)){
			sprintf(msg, "(DEBUG)     ****  Problem with Matlab Token
Error code:  %i  **** \n", ferror(mToken)); usf_sout(msg);
		}
		else if (mToken == NULL){
			sprintf(msg, "(DEBUG)     ****  Matlab Token not found
****\n"); usf_sout(msg);
		}
	}
	if (mToken == NULL && numCycle == numFirstCycle){
		sprintf(msg, "MSVM ERROR:  Pressure at Coupling Boundaries
Uninitiliazed\n");
		usf_stop(msg);
	}
	MPI_Comm_rank(MPI_COMM_WORLD, &prl_rank);
	if (couplingMatlab2CFDFlagKillNext==1){
		if (prl_rank==prl_root){
			remove(MATLABTOKEN);
		}
		couplingMatlab2CFDFlagKillNext=0;
	}
	if
(couplingMatlab2CFDFlag==1&&mToken!=NULL&&strcmp(pressureInputFile,"\0")!=0){
		fclose(mToken);
		if (DEBUG==1){
			sprintf(msg, "(DEBUG)  CouplingMatlab2CFDFlag found true
\n(DEBUG)  Matlab Token closed\n"); usf_sout(msg);
		}
		fp = fopen(pressureInputFile, "rt");
		if (DEBUG==1){
			sprintf(msg, "(DEBUG)  Attempting to Open
pressureInputFile\n"); usf_sout(msg);
			if (fp != NULL && ferror(fp)){
				sprintf(msg, "(DEBUG)     ****  Problem with
pressureInputFile Error code:  %i  **** \n", ferror(mToken)); usf_sout(msg);
			}
			else if (fp == NULL){
				sprintf(msg, "(DEBUG)     ****  pressureInputFile not
found  ****\n"); usf_sout(msg);
			}
		}
		if (fp!=NULL && ferror(fp)){
			sprintf(msg,
"********************************************************** \n"); usf_sout(msg);
			sprintf(msg, "****  Error opening input file for pressure
coupling  **** \n"); usf_sout(msg);
			sprintf(msg,
"********************************************************** \n \n");
usf_sout(msg);
			sprintf(msg, "      Error code:  %i \n", ferror(fp));
usf_sout(msg);
			fclose(fp);
		}
		else if (fp==NULL){
```

```
                    sprintf(msg,
"******************************************************** \n"); usf_sout(msg);
                    sprintf(msg, "****  Error opening input file for pressure
coupling  **** \n"); usf_sout(msg);
                    sprintf(msg,
"******************************************************** \n \n");
usf_sout(msg);
                    sprintf(msg, "      Unable to find input file for pressure
coupling:  %s ****\n", pressureInputFile); usf_sout(msg);
             }
             else{
                    usf_sout("\n=== Multi-Scale Ventilation Modeling Coupled
Boundary Conditions ===\r\n");
                    sprintf(msg, "   Coupling initiated Cycle:  %i, Time:
%lg\n",numCycle, time); usf_sout(msg);
                    sprintf(msg, "   REGION        PRESSURE\n"); usf_sout(msg);
                    fgets(line,MAXLINELENGTH,fp);
                    while (fgets(line,MAXLINELENGTH, fp)!=NULL){
                           strcpy(lastLine, line);
                    }
                    tokens=strtok(line," ,\n");
                    sscanf(tokens,"%i",&matlabCycle);
                    tokens=strtok(NULL," ,\n");
                    tokens=strtok(NULL," ,\n");
                    sscanf(tokens,"%lg",&matlabTime);
                    for(j=0;j<regionNumber;j++){
                           tokens=strtok(NULL," ,\n");
                           if (tokens!=NULL){
                                  sscanf(tokens,"%lg",&pressure[j]);
                                  sprintf(msg, "   %6i%16lg\n",j+100,pressure[j]);
usf_sout(msg);
                           }
                    }
                    couplingMatlab2CFDFlag = 0;
                    couplingMatlab2CFDFlagKillNext=1;
                    fclose(fp);

                    if (strcmp(species1InputFile,"\0")!=0){
                           fp = fopen(species1InputFile, "r");
                           if (fp==NULL){
                                  sprintf(msg, "**** Unable to open input file for
species coupling:  %s ****\n", species1InputFile); usf_sout(msg);
                           }
                           else{
                                  sprintf(msg, "      Species 1 Input File
Found\n"); usf_sout(msg);
                                  fgets(line,MAXLINELENGTH,fp);
                                  while (fgets(line,MAXLINELENGTH, fp)!=NULL){
                                         strcpy(lastLine, line);
                                  }
                                  tokens=strtok(line," ,\n");
                                  tokens=strtok(NULL," ,\n");
                                  tokens=strtok(NULL," ,\n");
                                  for(j=0;j<regionNumber;j++){
                                         tokens=strtok(NULL," ,\n");
                                         if (tokens!=NULL){
                                                sscanf(tokens,"%lg",&species1[j]);
```

```
                                                sprintf(msg, "
%6i%16lg\n",j+100,species1[j]); usf_sout(msg);
                                        }
                                }
                                fclose(fp);
                        }
                }

                if (strcmp(species2InputFile,"\0")!=0){
                        fp = fopen(species2InputFile, "r");
                        if (fp==NULL){
                                sprintf(msg, "**** Unable to open input file for
species coupling:  %s ****\n", species2InputFile); usf_sout(msg);
                        }
                        else{
                                sprintf(msg, "      Species 2 Input File
Found\n"); usf_sout(msg);
                                fgets(line,MAXLINELENGTH,fp);
                                while (fgets(line,MAXLINELENGTH, fp)!=NULL){
                                        strcpy(lastLine, line);
                                }
                                tokens=strtok(line," ,\n");
                                tokens=strtok(NULL," ,\n");
                                tokens=strtok(NULL," ,\n");
                                for(j=0;j<regionNumber;j++){
                                        tokens=strtok(NULL," ,\n");
                                        if (tokens!=NULL){
                                                sscanf(tokens,"%lg",&species2[j]);
                                                sprintf(msg, "
%6i%16lg\n",j+100,species2[j]); usf_sout(msg);
                                        }
                                }
                                fclose(fp);
                        }
                }

                if (strcmp(species3InputFile,"\0")!=0){
                        fp = fopen(species3InputFile, "r");
                        if (fp==NULL){
                                sprintf(msg, "**** Unable to open input file for
species coupling:  %s ****\n", species3InputFile); usf_sout(msg);
                        }
                        else{
                                sprintf(msg, "      Species 3 Input File
Found\n"); usf_sout(msg);
                                fgets(line,MAXLINELENGTH,fp);
                                while (fgets(line,MAXLINELENGTH, fp)!=NULL){
                                        strcpy(lastLine, line);
                                }
                                tokens=strtok(line," ,\n");
                                tokens=strtok(NULL," ,\n");
                                tokens=strtok(NULL," ,\n");
                                for(j=0;j<regionNumber;j++){
                                        tokens=strtok(NULL," ,\n");
                                        if (tokens!=NULL){
                                                sscanf(tokens,"%lg",&species3[j]);
                                                sprintf(msg, "
%6i%16lg\n",j+100,species3[j]); usf_sout(msg);
```

```
                                        }
                                }
                                fclose(fp);
                        }
                }

                if (strcmp(species4InputFile,"\0")!=0){
                        fp = fopen(species4InputFile, "r");
                        if (fp==NULL){
                                sprintf(msg, "**** Unable to open input file for
species coupling:  %s ****\n", species4InputFile); usf_sout(msg);
                        }
                        else{
                                sprintf(msg, "      Species 4 Input File
Found\n"); usf_sout(msg);
                                fgets(line,MAXLINELENGTH,fp);
                                while (fgets(line,MAXLINELENGTH, fp)!=NULL){
                                        strcpy(lastLine, line);
                                }
                                tokens=strtok(line," ,\n");
                                tokens=strtok(NULL," ,\n");
                                tokens=strtok(NULL," ,\n");
                                for(j=0;j<regionNumber;j++){
                                        tokens=strtok(NULL," ,\n");
                                        if (tokens!=NULL){
                                                sscanf(tokens,"%lg",&species4[j]);
                                                sprintf(msg, "
%6i%16lg\n",j+100,species4[j]); usf_sout(msg);
                                        }
                                }
                                fclose(fp);
                        }
                }

                if (strcmp(species5InputFile,"\0")!=0){
                        fp = fopen(species5InputFile, "r");
                        if (fp==NULL){
                                sprintf(msg, "**** Unable to open input file for
species coupling:  %s ****\n", species5InputFile); usf_sout(msg);
                        }
                        else{
                                sprintf(msg, "      Species 5 Input File
Found\n"); usf_sout(msg);
                                fgets(line,MAXLINELENGTH,fp);
                                while (fgets(line,MAXLINELENGTH, fp)!=NULL){
                                        strcpy(lastLine, line);
                                }
                                tokens=strtok(line," ,\n");
                                tokens=strtok(NULL," ,\n");
                                tokens=strtok(NULL," ,\n");
                                for(j=0;j<regionNumber;j++){
                                        tokens=strtok(NULL," ,\n");
                                        if (tokens!=NULL){
                                                sscanf(tokens,"%lg",&species5[j]);
                                                sprintf(msg, "
%6i%16lg\n",j+100,species5[j]); usf_sout(msg);
                                        }
                                }
```

```
                                        fclose(fp);
                                }
                        }
                }
        }

        if(strcmp(massFlowOutputFile,"\0")!=0&&prl_rank==prl_root&&couplingCFD2Matl
abFlag==1){
                fp = fopen(massFlowOutputFile, "a");
                fprintf(fp,"%i, %lg, %lg",numCycle, timeStep, time);
                fclose(fp);
        }
        if(strcmp(species1OutputFile,"\0")!=0&&prl_rank==prl_root&&couplingCFD2Matl
abFlag==1){
                fp = fopen(species1OutputFile, "a");
                fprintf(fp,"%i, %lg, %lg",numCycle, timeStep, time);
                fclose(fp);
        }
        if(strcmp(species2OutputFile,"\0")!=0&&prl_rank==prl_root&&couplingCFD2Matl
abFlag==1){
                fp = fopen(species2OutputFile, "a");
                fprintf(fp,"%i, %lg, %lg",numCycle, timeStep, time);
                fclose(fp);
        }
        if(strcmp(species3OutputFile,"\0")!=0&&prl_rank==prl_root&&couplingCFD2Matl
abFlag==1){
                fp = fopen(species3OutputFile, "a");
                fprintf(fp,"%i, %lg, %lg",numCycle, timeStep, time);
                fclose(fp);
        }
        if(strcmp(species4OutputFile,"\0")!=0&&prl_rank==prl_root&&couplingCFD2Matl
abFlag==1){
                fp = fopen(species4OutputFile, "a");
                fprintf(fp,"%i, %lg, %lg",numCycle, timeStep, time);
                fclose(fp);
        }
        if(strcmp(species5OutputFile,"\0")!=0&&prl_rank==prl_root&&couplingCFD2Matl
abFlag==1){
                fp = fopen(species5OutputFile, "a");
                fprintf(fp,"%i, %lg, %lg",numCycle, timeStep, time);
                fclose(fp);
        }
        if (DEBUG==1){
                sprintf(msg, "(DEBUG)  ====== End of usu_cycle_start() =====\n");
usf_sout(msg);
        }
}


void usu_cycle_end()
{
        FILE *fp;
        FILE *cfdToken;
        char msg[MAXLINELENGTH];
        int prl_rank, numCycle, prl_root=0;
        fprec time;

        numCycle = usf_ncyc();
```

```
	time = usf_time();

	if (DEBUG == 1){
		sprintf(msg, "(DEBUG)  ====== Begin of usu_cycle_end() =====\n");
usf_sout(msg);
	}

	MPI_Comm_rank(MPI_COMM_WORLD, &prl_rank);
	if(strcmp(massFlowOutputFile,"\0")!=0&&prl_rank==prl_root&&couplingCFD2Matl
abFlag==1){
		fp = fopen(massFlowOutputFile, "a");
		fprintf(fp,"\n");
		fclose(fp);
	}
	if(strcmp(species1OutputFile,"\0")!=0&&prl_rank==prl_root&&couplingCFD2Matl
abFlag==1){
		fp = fopen(species1OutputFile, "a");
		fprintf(fp,"\n");
		fclose(fp);
	}
	if(strcmp(species2OutputFile,"\0")!=0&&prl_rank==prl_root&&couplingCFD2Matl
abFlag==1){
		fp = fopen(species2OutputFile, "a");
		fprintf(fp,"\n");
		fclose(fp);
	}
	if(strcmp(species3OutputFile,"\0")!=0&&prl_rank==prl_root&&couplingCFD2Matl
abFlag==1){
		fp = fopen(species3OutputFile, "a");
		fprintf(fp,"\n");
		fclose(fp);
	}
	if(strcmp(species4OutputFile,"\0")!=0&&prl_rank==prl_root&&couplingCFD2Matl
abFlag==1){
		fp = fopen(species4OutputFile, "a");
		fprintf(fp,"\n");
		fclose(fp);
	}
	if(strcmp(species5OutputFile,"\0")!=0&&prl_rank==prl_root&&couplingCFD2Matl
abFlag==1){
		fp = fopen(species5OutputFile, "a");
		fprintf(fp,"\n");
		fclose(fp);
	}
	if (couplingCFD2MatlabFlag==1){
		if (prl_rank==prl_root){
			cfdToken = fopen(CFDTOKEN, "w");
			fprintf(cfdToken,"Marco\n");
			fclose(cfdToken);
		}
		couplingCFD2MatlabFlag = 0;
		couplingMatlab2CFDFlag = 1;
		if (DEBUG==1){
				sprintf(msg, "(DEBUG)  CFDTOKEN created to signal
Matlab\n"); usf_sout(msg);
				sprintf(msg, "(DEBUG)  Flag couplingCFD2MatlabFlag
lowered\n"); usf_sout(msg);
```

```
                        sprintf(msg, "(DEBUG)  Flag couplingMatlab2CFDFlag
raised\n"); usf_sout(msg);
                }
                switch(couplingMethod){
                case 1:
                        couplingCycle = numCycle + (int)(couplingInterval+0.5);
                        if (DEBUG==1){
                                sprintf(msg, "(DEBUG)  Coupling Cycle updated:  %i \n",
couplingCycle); usf_sout(msg);
                        }
                        break;
                case 2:
                        couplingTime = time + couplingInterval;
                        if (DEBUG==1){
                                sprintf(msg, "(DEBUG)  Coupling Time updated:  %lg \n",
couplingTime); usf_sout(msg);
                        }
                        break;
                }
        }
        if (DEBUG==1){
                sprintf(msg, "(DEBUG)  ====== End of usu_cycle_end() =====\n");
usf_sout(msg);
        }
}
void usu_final()
{
        char msg[MAXLINELENGTH];

        if (DEBUG ==1){
                sprintf(msg, "(DEBUG)  ====== Begin of usu_final() =====\n");
usf_sout(msg);
        }
        free(pressure);
        free(species1);
        free(species2);
        free(species3);
        free(species4);
        free(species5);
        free(coef0Forc);

        if (DEBUG ==1){
                sprintf(msg, "(DEBUG)  Completed memory clean up\n"); usf_sout(msg);
        }
        if (DEBUG ==1){
                sprintf(msg, "(DEBUG)  ====== End of usu_final() =====\n");
usf_sout(msg);
        }
}

/************************************
*** FIELD FILE OUTPUT ***************
************************************/
void usu_fld_scalar_out(int n,USU_FLDOUT *fldout)
{
        static fprec *gob;
        int nnods, nnd, nspecies;
```

```
	fprec cOxygen, cMethane, cNitrogen, thresh1, thresh2, thresh3, thresh4,
thresh5;

	nnods = usf_nnods();
	nspecies = usf_icono();

	if (n==1) {
		gob = (fprec*)malloc(nnods*sizeof(fprec));
	}
	if (n==1 && nspecies >=3){
		for (nnd=0;nnd<nnods; nnd++){
			cOxygen = usf_c(SPECIESO2,nnd)*100;
			cMethane = usf_c(SPECIESCH4,nnd)*100;
			cNitrogen = 100 - cOxygen - cMethane;
			// usf_c reports mass concentration of species
			// converting mass concentration to volume concentration,
assuming ideal gas law applies
			//mTotal = cOxygen*32+cMethane*16+cNitrogen*28;

			//cOxygen = 100*cOxygen*mTotal/32;
			//cMethane = 100*cMethane*mTotal/16;
			gob[nnd]=0;

			if (cMethane > 0.0000 && cMethane <= 4.0732){
				thresh1 = 8;
				thresh2 = -1.4831*cMethane+20.95;
				thresh3 = -8.5588*cMethane+49.771;
				thresh4 = -.2095*cMethane +20.95;
				if (cOxygen >= 0.0000 && cOxygen <= thresh1){
					gob[nnd] = 0.9375;
				}
				else if (cOxygen > thresh1 && cOxygen <= thresh2){
					gob[nnd] = 0.8125;
				}
				else if (cOxygen > thresh2 && cOxygen <= thresh3){
					gob[nnd] = 0.6875;
				}
				else if (cOxygen > thresh3 && cOxygen <= thresh4){
					gob[nnd] = 0.5625;
				}
				else{
					gob[nnd] = 0;
				}
			}
			else if (cMethane > 4.0732 && cMethane <= 5.9000){
				thresh1 = 8;
				thresh2 = -1.4831*cMethane+20.95;
				thresh3 = -8.5588*cMethane+62.694;
				thresh4 = -.2095*cMethane +20.95;
				if (cOxygen >= 0.0000 && cOxygen <= thresh1){
					gob[nnd] = 0.9375;
				}
				else if (cOxygen > thresh1 && cOxygen <= thresh2){
					gob[nnd] = 0.8125;
				}
				else if (cOxygen > thresh2 && cOxygen <= thresh3){
					gob[nnd] = 0.5625;
				}
```

```
        else if (cOxygen > thresh3 && cOxygen <= thresh4){
                gob[nnd] = 0.4375;
        }
        else{
                gob[nnd] = 0;
        }
}
else if (cMethane > 5.9000 && cMethane <= 6.7393){
        thresh1 = 8;
        thresh2 = -1.4831*cMethane+20.95;
        thresh3 = 0.6162*cMethane + 8.5644;
        thresh4 = -.2095*cMethane +20.95;
        if (cOxygen >= 0.0000 && cOxygen <= thresh1){
                gob[nnd] = 0.9375;
        }
        else if (cOxygen > thresh1 && cOxygen <= thresh2){
                gob[nnd] = 0.8125;
        }
        else if (cOxygen > thresh2 && cOxygen <= thresh3){
                gob[nnd] = 0.3125;
        }
        else if (cOxygen > thresh3 && cOxygen <= thresh4){
                gob[nnd] = 0.4375;
        }
        else{
                gob[nnd] = 0;
        }
}
else if (cMethane > 6.7393 && cMethane <= 8.7320){
        thresh1 = 8;
        thresh2 = -1.4831*cMethane+20.95;
        thresh3 = 0.6162*cMethane + 6.8025;
        thresh4 = 0.6162*cMethane + 8.5644;
        thresh5 = -.2095*cMethane +20.95;
        if (cOxygen >= 0.0000 && cOxygen <= thresh1){
                gob[nnd] = 0.9375;
        }
        else if (cOxygen > thresh1 && cOxygen <= thresh2){
                gob[nnd] = 0.8125;
        }
        else if (cOxygen > thresh2 && cOxygen <= thresh3){
                gob[nnd] = 0.1875;
        }
        else if (cOxygen > thresh3 && cOxygen <= thresh4){
                gob[nnd] = 0.3125;
        }
        else if (cOxygen > thresh4 && cOxygen <= thresh5){
                gob[nnd] = 0.4375;
        }
        else{
                gob[nnd] = 0;
        }
}
else if (cMethane > 8.7320){
        thresh1 = 8;
        thresh2 = 0.6162*cMethane + 6.8025;
        thresh3 = 0.6162*cMethane + 8.5644;
        thresh4 = -.2095*cMethane +20.95;
```

```
                        if (cOxygen >= 0.0000 && cOxygen <= thresh1){
                                gob[nnd] = 0.0625;
                        }
                        else if (cOxygen > thresh1 && cOxygen <= thresh2){
                                gob[nnd] = 0.1875;
                        }
                        else if (cOxygen > thresh2 && cOxygen <= thresh3){
                                gob[nnd] = 0.3125;
                        }
                        else if (cOxygen > thresh3 && cOxygen <= thresh4){
                                gob[nnd] = 0.4375;
                        }
                        else{
                                gob[nnd] = 0;
                        }
                }
        }

        fldout->ptr=gob;
        strcpy(fldout->title, "Methane Explosibility");
        strcpy(fldout->name, "CH4Boom");
    }
    else {
        free (gob);
    }
}
```

BIBLIOGRAPHY

American Society of Heating, R. and A.-C. E. S. *2009 ASHRAE Handbook Fundamentals.*; American Society of Heating, Refrigerating & Air Conditioning Engineers: Atlanta, 2010.

ASTM D388-12 Classification of Coals by Rank; ASTM International: West Conshohocken, PA, 2012.

ASTM D7569-10 Determination of Gas Content in Coal - Direct Desorption Method; ASTM International: West Conshohocken, PA, 2010.

Bertard, C.; Bruyet, B.; Gunther, J. Determination of desorbable gas concentration of coal (direct method). International Journal of Rock Mechanics and Mining Sciences & Geomechanics Abstracts 1970, 7, 43–65.

Bluestein, G.; Smith, V. Mine rescue effort turns to recovery http://www.nbcnews.com/id/36183425/ns/us_news-life/t/mine-rescue-effort-turns-recovery/ (accessed Mar 28, 2013).

Choi, J.; Lin, C.-L. Multiscale numerical analysis of airflow in CT-based subject specific breathing human lungs http://ir.uiowa.edu/etd/2685 (accessed Nov 21, 2012).

Cienski, J. Poland Mine Disaster | Coal Mining Safety http://www.globalpost.com/dispatch/poland/090930/coal-mining-safety-mines (accessed Nov 14, 2012).

Clayton, J. . Geochemistry of coalbed gas – A review. International Journal of Coal Geology 1998, 35, 159–173.

Colella, F.; Rein, G.; Verda, V.; Borchiellini, R. Multiscale modeling of transient flows from fire and ventilation in long tunnels. Computers & Fluids 2011, 51, 16–29.

Coward, H. F. Explosivity of atmospheres behind stoppings. Transactions of the Institute of Mining Engineers 1928, 77, 94–115.

Diamond, W. P.; Levine, J. R. Direct method determination of the gas content of coal procedures and results http://purl.access.gpo.gov/GPO/LPS97469 (accessed Nov 20, 2012).

Diamond, W. P.; Murrie, G. W.; McCulloch, C. M. Methane gas content of the Mary Lee group of coalbeds, Jefferson, Tuscaloosa, and Walker Counties, Ala http://books.google.com/books?id=F0C3-VJ-BLAC (accessed Nov 15, 2012).

Diamond, W. P.; Schatzel, S. J. Measuring the gas content of coal: A review. International Journal of Coal Geology 1998, 35, 311–331.

Dziurzynski, W.; Wasilewski, S. Model and experimental studies in the longwall goaf under methane inflow conditions. In 14th U.S./North American Mine Ventilation Symposium, University of Utah, Salt Lake City, UT, June 17-20, 2012; Calizaya, F.; Nelson, M. G., Eds.; University of Utah: Salt Lake City, 2012; pp. 111–120.

Energy Information Administration (EIA) US coalbed methane http://purl.access.gpo.gov/GPO/LPS106949 (accessed Nov 20, 2012).

Esterhuizen, G. S.; Karacan, C. O. Development of Numerical Models to InvestigatePermeability Changes and Gas Emission around Longwall Mining Panel. In Alaska Rocks 2005, The 40th US Symposium on Rock Mechanics (USRMS); 2005.

Esterhuizen, G. S.; Karacan, C. A methodology for determining gob permeability distributions and its application to reservoir modeling of coal mine longwalls. In 2007 SME Annual Meeting, Denver, CO; 2007.

Forster, I.; Enever, J. R. Hydrogeological response of overburden strata to underground mining, Central Coast, New South Wales; Office of Energy: Sydney, 1992.

Galvin, J. M. Surface subsidence mechanisms–theory and practice. Part I–Theory. Coal J (16) 1987, 31–41.

Green, M. S.; Flanegan, K. C.; Gilcrease, P. C. Characterization of a methanogenic consortium enriched from a coalbed methane well in the Powder River Basin, U.S.A. International Journal of Coal Geology 2008, 76, 34–45.

Guo, H.; Adhikary, D. P.; Craig, M. S. Simulation of mine water inflow and gas emission during longwall mining. Rock Mechanics and Rock Engineering 2008, 42, 25–51.

Hartman, H. L. Mine ventilation and air conditioning; Wiley: New York, 1997.

Kapp, W. A.; Williams, R. C. Extraction of coal in the Sydney Basin from beneath large bodies of water. In Proceedings of the Aust IMM Conference. Newcastle; 1972; pp. 77–88.

Karacan, C. Ö. Modeling and prediction of ventilation methane emissions of U.S. longwall mines using supervised artificial neural networks. International Journal of Coal Geology 2008, 73, 371–387.

Karacan, C. Ö. Reconciling longwall gob gas reservoirs and venthole production performances using multiple rate drawdown well test analysis. International Journal of Coal Geology 2009, 80, 181–195.

Karacan, C. Ö.; Esterhuizen, G. S.; Schatzel, S. J.; Diamond, W. P. Reservoir simulation-based modeling for characterizing longwall methane emissions and gob gas venthole production. International Journal of Coal Geology 2007, 71, 225–245.

Kim, A. G. The composition of coalbed gas http://purl.access.gpo.gov/GPO/LPS97511 (accessed Nov 15, 2012).

Kim, A. G. Estimating methane content of bituminous coalbeds from adsorption data; Dept. of the Interior, Bureau of Mines: [Washington], 1977.

Kissell, F. N. Handbook for methane control in mining; Dept. of Health and Human Services, Public Health Service, Centers for Disease Control and Prevention, National Institute for Occupational Safety and Health, Pittsburgh Research Laboratory: Pittsburgh, PA, 2006.

Kuprat, A. P.; Kabilan, S.; Carson, J. P.; Corley, R. A.; Einstein, D. R. A Bidirectional Coupling Procedure Applied to Multiscale Respiratory Modeling. Journal of Computational Physics.

Levine, J. R. Coalification: the evolution of coal as source rock and reservoir rock for oil and gas. Hydrocarbons from coal: AAPG Studies in Geology 1993, 38, 39–77.

McFall, K. S.; Wicks, D. E.; Kuuskraa, V. A.; Gas Research Institute; Lewin and Associates A geologic assessment of natural gas from coal seams in the Warrior Basin, Alabama : topical report (September 1985 - September 1986); Gas Research Institute: Chicago, Ill., 1986.

McPherson, M. J. Subsurface ventilation and environmental engineering; Chapman & Hall: London; New York, 2009.

Moore, T. A. Coalbed methane: A review. International Journal of Coal Geology 2012, 101, 36–81.

MSHA MSHA - Statistics - Fatal Charts http://www.msha.gov/stats/charts/chartshome.htm (accessed Nov 14, 2012).

MSHA MSHA - Performance Coal - Upper Big Branch Mine-South Disaster Information Single Source Page

http://www.msha.gov/PerformanceCoal/PerformanceCoal.asp (accessed Nov 14, 2012).

National Mining Association (NMA) US Coal Production and Number of Mines by State and Coal Type, 2011 http://www.nma.org/pdf/c_production_mines_state_type.pdf (accessed Mar 28, 2013).

Patankar, S. V. Numerical heat transfer and fluid flow; Hemisphere Pub. Corp. ; McGraw-Hill: Washington; New York, 1980.

Ravi, S. BBC NEWS | South Asia | No survivors in India mine blast http://news.bbc.co.uk/2/hi/south_asia/5322398.stm (accessed Nov 14, 2012).

Reid, P.; McNally, G. H.; Ward, C. R. Effects of mining on the permeability of rock strata in the Southern Coalfield. In Proceedings of the Symposium on Geology in Longwall Mining; 1996; pp. 273–280.

Ren, T. X.; Balusu, R. CFD Modelling of Goaf Gas Migration to Improve the Control of Spontaneous Combustion in Longwalls 2005.

Ren, T. X.; Edwards, J. S. Three-dimensional computational fluid dynamics modelling of methane flow through permeable strata around a longwall face. Mining Technology 2000, 109, 41–48.

Ren, T. X.; Balusu, R. Proactive goaf inertisation for controlling longwall goaf heatings. Procedia Earth and Planetary Science 2009, 1, 309–315.

Rice, D. Composition and Origins of Coalbed Gas: Chapter 7. 1993, 180, 159–184.

A Guide to coalbed methane reservoir engineering; Saulsberry, J.; Schafer, P.; Schraufnagel, R., Eds.; Gas Research Institute: Chicago, Ill., 1996.

Şenel, İ. G.; Gürüz, A. G.; Yücel, H.; Kandas, A. W.; Sarofim, A. F. Characterization of Pore Structure of Turkish Coals. Energy Fuels 2001, 15, 331–338.

Singh, M.; Kendorsky, F. Strata disturbance prediction for mining beneath surface water and waste impoundments Proc 1st conference on ground control in mining, Morgantown, 2729 July 1981, P7689. Publ Morgantown: West Virginia University, 1981. International Journal of Rock Mechanics and Mining Sciences & Geomechanics Abstracts International Journal of Rock Mechanics and Mining Sciences & Geomechanics Abstracts 1983, 20, A13–A13.

Strapoc D; Schimmelmann A; Mastalerz M; Drobniak A; Hedges S Variability of geochemical properties in a microbially dominated coalbed gas system from the eastern margin of the Illinois Basin, USA. Int. J. Coal Geol. International Journal of Coal Geology 2008, 76, 98–110.

Terry, S.; Simonin, L. 19th-century coal mining; 1868.

Versteeg, H. K.; Malalasekera, W. An introduction to computational fluid dynamics : the finite volume method; Second.; New York : Wiley: Harlow, Essex, England; Longman Scientific & Technical, 2007.

Wachel, E. W. Establishing longwall gob porosity from compaction in western US coal mines, 2012.

Worrall, D., Jr. Modeling Gas Glows in Longwall Coal Mines Using Computational Fluid Synamics, Coloardo School of Mines: Golden, Colorado, 2012.

Yinan, H.; Ke, C. Negligence blamed in mine blast http://www.chinadaily.com.cn/china/2009-02/25/content_7509920.htm (accessed Nov 14, 2012).

Yuan, L.; Smith, A. C. Computational fluid dynamics modeling of spontaneous heating in longwall gob areas. TRANSACTIONS-SOCIETY FOR MINING METALLURGY AND EXPLORATION INCORPORATED 2007, 322, 37.

Zhang, J. Investigations of water inrushes from aquifers under coal seams. International journal of rock mechanics and mining sciences. 2005, 42, 350.

Timeline of accidents at Russian mines http://newsvote.bbc.co.uk/hi/russian/international/newsid_6474000/6474365.stm (accessed Nov 14, 2012).

VITA

William Chad Wedding was born in Morganfield, Kentucky. He graduated from Union County High School in 1995 at the top of his class. He then enrolled in the University of Kentucky as a National Merit Finalist. In May of 2000, he graduated cum laude from UK with a Bachelor of Science Degree in Mechanical Engineering.

Chad began his professional career in August of 2000 with Lexmark International in Lexington, Kentucky. During his nine year stint, he rose to the rank of senior mechanical engineer.

He returned to the University of Kentucky in the spring of 2009 to pursue a Master's of Science in Mining Engineering. His focus was the development of an instrument to measure window response to blast loading. His Master's thesis, titled "Experimental Study of Blast Resistant Glazing System Response to Explosive Loading, was successfully defended in the fall of 2010. He then remained at the University of Kentucky to pursue a Doctor of Philosophy degree in Mining Engineering, focused on mine ventilation system modeling.